University of Tennessee, Knoxville

TRACE: Tennessee Research and Creative Exchange

Doctoral Dissertations

Graduate School

12-2005

The Effect of Ultrasonic Vibration on the Solidification of Light Alloys

Xiaogang Jian
University of Tennessee - Knoxville

Follow this and additional works at: https://trace.tennessee.edu/utk_graddiss

Part of the Materials Science and Engineering Commons

Recommended Citation

Jian, Xiaogang, "The Effect of Ultrasonic Vibration on the Solidification of Light Alloys. " PhD diss., University of Tennessee, 2005.
https://trace.tennessee.edu/utk_graddiss/2144

This Dissertation is brought to you for free and open access by the Graduate School at TRACE: Tennessee Research and Creative Exchange. It has been accepted for inclusion in Doctoral Dissertations by an authorized administrator of TRACE: Tennessee Research and Creative Exchange. For more information, please contact trace@utk.edu.

To the Graduate Council:

I am submitting herewith a dissertation written by Xiaogang Jian entitled "The Effect of Ultrasonic Vibration on the Solidification of Light Alloys." I have examined the final electronic copy of this dissertation for form and content and recommend that it be accepted in partial fulfillment of the requirements for the degree of Doctor of Philosophy, with a major in Materials Science and Engineering.

Thomas T. Meek, Major Professor

We have read this dissertation and recommend its acceptance:

Philip Rack, Peter Liaw, Qingyou Han, James R. Thompson

Accepted for the Council:

Carolyn R. Hodges

Vice Provost and Dean of the Graduate School

(Original signatures are on file with official student records.)

To the Graduate Council:

I am submitting herewith a dissertation written by Xiaogang Jian entitled "The Effect of Ultrasonic Vibration on the Solidification of Light Alloys." I have examined the final electronic copy of this dissertation for form and content and recommend that it be accepted in partial fulfillment of the requirements for the degree of Doctor of Philosophy, with a major in Materials Science and Engineering.

Thomas T. Meek
Major Professor

We have read this dissertation
and recommend its acceptance:

Philip Rack

Peter Liaw

Qingyou Han

James R. Thompson

Acceptance for the Council:

Anne Mayhew
Vice Chancellor and Dean of
Graduate Studies

(Original signatures are on file with official student records.)

THE EFFECT OF ULTRASONIC VIBRATION ON THE SOLIDIFICATION OF LIGHT ALLOYS

A Dissertation

Presented for the

Doctor of Philosophy

Degree

The University of Tennessee, Knoxville

Xiaogang Jian

December, 2005

Copyright © 2005 by Xiaogang Jian.
All rights reserved.

DEDICATION

This dissertation is dedicated to my wife, Xiaofeng Li, and son, Noen Lee Jian, for always believing in me, inspiring me, and encouraging me to reach higher in order to achieve my goals.

Acknowledgements

Firstly, I would like to thank my advisor Dr. Thomas Meek for his kindness, wisdom and patience over the years. His support, advice and counsel have allowed me to develop my skills as a researcher within a supportive team environment. For his amazing insight, knowledge, kindness, and encouragement in many areas, I would be remiss if I did not extend deep thanks to my lab mentor Dr. Qingyou Han. His willingness to support my work and his guidance throughout my studies have been of equal importance. For the remaining members of my committee: Dr. Raymond A. Buchanan, Dr. Peter K. Liaw, and Dr. James R. Thompson, I extend my appreciation and gratitude for their input both directly and indirectly.

Within the MPG at ORNL, I owe many thanks to both students and staff. Specially, I thank Dr. Srinath Viswanathan, Dr. Vinod Sikka, and Dr. Craig Blue for their guidance and kindly help. I also owe a deep debt of gratitude to Mr. Larry Walker, Mr. Larry Allard, Edward Hatfield, and Mr. Tom Geer for technical support, valuable comments and suggestions. To my fellow graduate students, I express my gratitude for the many conversations that have had a tremendous impact on my research, Puja Kadolkar, Shengjun Zhang, Sherman McElroy, Cailu Xu, Teodora Nedkova, Shravan Indrakanti, and Yogesh Bhambri thank you so much. For fear of forgetting someone by name, I wish to thank the office staff of the Materials Science and Engineering Department for all their contributions great and small.

This dissertation is based on the work done for a project entitled *Ultrasonic Processing of Materials,* which is supported by the U.S. Department of Energy, Office of Energy Efficiency, Industrial Technologies Program, Industrial Materials for the Future (IMF) Program, under Award No. DE-FC07-01ID14256 and DE-AC05-00OR22725.

On a more personal level, there are many people who deserve mention. For their unwavering love and support over the years, my parents Wendao and Gouxiu deserve all the thanks and appreciation that I can express. I am indebted to my closest friend Yulin Lu. Lastly, I want to thank, from the depth of my being, my soul mate and wife, Xiaofeng for keeping me motivated through all times.

Abstract

This exposition presents the novel thermodynamical and microstructural modification to light alloys, such as aluminum alloys and magnesium alloys, by ultrasonic vibrations during their solidification processes. Ultrasonic vibration has proven to be effective in controlling columnar dendritic structure, reducing the size of equiaxed grains, and under some conditions, producing globular non-dendritic grains. Despite this, the solidification process under the effect of ultrasonic vibration was not clear. Not only was there no such research on how ultrasonic vibration affected its solidification thermodynamically, but also its effects on the as-cast microstructure, including the primary fcc phase, the eutectics, and the secondary phases, were not systematically studied. In addition, most studies had been empirical and phenomenological rather than quantitative.

Prior to the experiments, thermodynamic simulations were carried out using the Scheil model to determine the temperature versus solid fraction curve of the alloys. The starting temperature for ultrasonic processing and the casting temperature were predetermined according to the simulation result. An experimental apparatus which supplied a powerful 1500 Watts at 20 KHz of ultrasonic power was designed and built.

Thermal analysis experiments were performed. The result shows that, with ultrasonic vibration, the steady growth temperature and the minimum supercooling temperature have been elevated; while the recalescence time decreased, which indicates a much slower growth rate of primary fcc aluminum grains. The difference between dendrites nucleation/growth and thickening is not significant in the casting with ultrasonic vibration, which might suggest dendrites formation might not present in this solidification process.

The mechanisms for ultrasonic influence on solidification have been discussed. Two types of ultrasonic processing techniques were developed and attempted. The first one related to introducing the vibration into the solidifying specimen through the liquid, while the second through the formally solidified part. For the first ultrasonic processing technique, the treatment was employed isothermally, intermittently, and continuously. In contrast to the fully developed dendrites up to several millimeters in length in untreated

A356 alloy, fine globular primary fcc Al grains sized less than 200 μm were obtained in the specimen treated with 5 second intermittent ultrasonic vibrations. However, dendrites were not completely broken down into fine grains in the isothermally or continuously processed specimens. It may imply that there is limited effect of dendrite fragmentation on the formation of globular/non-dendrite microstructure in the acoustically processed melt, and acoustically induced heterogeneous nucleation seems to be the dominant mechanism for the formation of a globular microstructure. For the second approach, ultrasonic treatment was performed continuously. During the treatment, grain refinement reached an unprecedented level. The average grains were globular with size ranges from 20 to 40 μm. Superfine globular grains of size less than 20 μm were obtained in the area near the ultrasonic radiator. Similar grain refinement could only be reached by using a quenching method with a much faster cooling rate.

The main parameters of ultrasonic processing, such as casting temperature, ultrasonic intensity, and the distance from the radiator, have been investigated. It is concluded that high acoustic amplitude/intensity favors the formation of small, spherical primary aluminum grains. The casting temperature of 630°C brings about best grain refinement result. The primary aluminum grain size in a casting increases with the increasing distance from the acoustic radiator.

In order to examine the feasibility of ultrasonic vibration for SSM processing, high intensity ultrasonic vibration has been applied during the casting of A356 alloy at high volume. Non-dendritic/globular grains have been obtained. Grain refiner can further refine A356 alloy structure, with the combination of ultrasonic vibration.

Experiments on the grain refinement of other aluminum alloys have been carried out. Fine globular grains were obtained in various aluminum alloys, including A354, 319, 6063, 6061, 2618 alloys. It was found that 670 °C is the optimum casting temperature for grain refinement of 2618 with the aid of ultrasonic vibration.

The effect of ultrasonic vibration on the modification of eutectic silicon in aluminum-silicon alloys has been studied. The introduction of ultrasonic vibration into A356 alloy modified the morphology of eutectic silicon from a coarse acicular plate-like form to a finely dispersed rosette-like form. The length, width, and aspect ratio of

eutectic silicon all reduced significantly. This modification is beneficial to the mechanical properties.

Ultrasonic grain refinement and secondary phases modification to magnesium AM60B alloy have been examined. With ultrasonic vibration, alloy experienced a reduction in size of primary α-Mg grains from 760 μm to about 25~48 μm in diameter, which is much better than other traditional grain refinement methods. The morphology of eutectic phases was modified from a mainly fully divorced blocky morphology dispersed among dendrite arms, to a mainly lamellar/script morphology across the grain boundaries. Furthermore, the volume fraction of the eutectic morphology is less.

Ultrasonic processing of solidifying metals can have a number of applications. Incorporating ultrasonic vibration into a die casting machine would dramatically increase the integrity and properties of die castings. Ultrasonic vibration may be used for producing semisolid feedstock directly from molten metal. Ultrasonic techniques can also find applications in forging industries for processing alloys that are difficult to cast.

Ultrasonic treatment has the advantages of being environmentally favorable, cost effective, and ready to be combined with other known physical processing technologies for liquid and solidifying metal. It is expected that the results of this study will impact a wide range of alloy processing including DC casting, continuous casting, vacuum arc remelting, and foundry processing in the areas of grain refinement, semi-solid metalcasting (SSM), and the production of new and novel microstructures.

It is highly recommended to continue both the research reported in this study and the application and commercialization of this technology.

CONTENTS

CHAPTER 1 INTRODUCTION 1
1.1 Solidification and microstructure of light metals 2
1.2 Ultrasonic processing of materials 5
1.3 Dissertation goals and scope 6
CHAPTER 2 LITERATURE REVIEW 8
2.1 A brief history of ultrasonic processing in the field of metallurgy 8
2.2 Phenomena induced by the propagation of ultrasound 11
2.2.1. Ultrasonic streaming 11
2.2.2. Ultrasonic atomization 12
2.2.3. Ultrasonic homogenization 12
2.2.4. Cavitation 12
2.2.4.1 Origin of cavitation in melt 13
2.2.4.2 Effects of cavitation in melts 15
2.3 Solidification of light alloys in an ultrasonic field 16
2.3.1. Effect of ultrasonic vibration on nucleation of solids 17
2.3.2. Effect of ultrasonic vibration on the growth of solids 18
2.4 Challenges 19
CHAPTER 3 EXPERIMENTAL METHODOLOGY 21
3.1 Materials 21
3.2 Experiments 22
3.2.1. Thermal analysis 22
3.2.2. Solidification of aluminum alloys 25
3.2.3. Solidification of AM60B alloys 26
3.3 Experimental setups 26
3.4 Chemical etch of samples 27
3.5 Quantitative metallography 27
3.6 Thermodynamic simulations 30
3.7 Technical approach 37
CHAPTER 4 RESULTS AND DISCUSSIONS 39
4.1 Thermal analysis of the solidification of A356 alloy 39

4.1.1. Introduction 39
4.1.2. Experimental conditions 40
4.1.3. Results and discussion 42
4.2 Mechanisms for the effect of ultrasonic vibration on solidification 55
4.2.1. Heterogeneous nucleation vs. dendrite fragmentation 55
4.2.1.1 Introduction 56
4.2.1.2 Experiments 56
4.2.1.3 Results and discussion 57
4.2.2. Ultrasonic intensity 64
4.2.3. Casting temperature 65
4.2.4. Distance from the radiator 72
4.3 Grain refinement of A356 alloy for SSM processing 78
4.3.1. Introduction 79
4.3.2. Experimental conditions 79
4.3.3. Results and discussion 81
4.3.3.1 Ultrasonic processing of billet suit for SSM 81
4.3.3.2 Ultrasonic processing of billet suitable for SSM with the addition of grain refiner 85
4.4 Grain refinement in other aluminum alloys 88
4.4.1. 6061 alloy 88
4.4.2. 6063 alloy 91
4.4.3. 319 alloy 91
4.4.4. A354 alloy 91
4.4.5. 2618 alloy 97
4.5 Eutectic modification of an Al – Si based alloy 103
4.5.1. Introduction 103
4.5.2. Experimental conditions 106
4.5.3. Results and discussion 106
4.6 Microstructure modification in the magnesium AM60B alloy 112
4.6.1. Introduction 114
4.6.2. Experiment 116
4.6.3. Results and discussion 116
4.6.3.1 Effect of ultrasonic treatment on primary α-Mg grain size 116
4.6.3.2 Effect of ultrasonic treatment on eutectic morphology 122
CHAPTER 5 SUMMARY 131

5.1 Conclusions 131
5.2 Suggestions for future work 132
BIBLIOGRAPHY 133
APPENDICES 146
APPENDIX A ULTRASONIC PROCESSING SYSTEM 147
A.1 Ultrasonic vibration unit 147
A.2 Measurement of acoustic parameters 149
A.3 Elastic wave and ultrasound 150
APPENDIX B GRAIN REFINEMENT OF 4340 STEEL 155
APPENDIX C GRAIN REFINEMENT OF BISMUTH-TIN ALLOY USING HIGH FREQUENCY ULTRASONIC VIBRATION 158
VITA 161

LIST OF TABLES

Table 2.1 Methods of applying acoustic vibrations during casting 10
Table 2.2: Effects of ultrasound on the nucleation of crystals..... 17
Table 2.3: Crystal geometry and ultrasound intensity necessary for crystal dispersion... 19
Table 3.1: Composition of aluminum alloys..... 21
Table 3.2: The nominal composition (in wt %) of AB60B alloy..... 21
Table 4.1: The three parameters observed in the first part of a cooling curve 46
Table 4.2: The reactions during solidification of A356 alloy without ultrasonic vibration 51
Table 4.3: The reactions during solidification of A356 alloy with ultrasonic vibration... 54
Table 4.4: Quantitative analysis of effect of grain refiner on average grain size (µm).... 85
Table 4.5: Quantitative analysis of effect of grain refiner on average grain roundness ... 85
Table 4.6: Comparison of existing grain refining technologies of Mg-Al alloys..... 115
Table A.1: Classification of elastic wave 150
Table A.2: Sounds and their intensity..... 152
Table A.3: Acoustic impedance of some materials 152

LIST OF FIGURES

Figure 3.1: Equilibrium aluminum – silicon phase diagram..... 23
Figure 3.2: Equilibrium magnesium – aluminum phase diagram showing the liquidus and solidus of AM60B and its solid phases..... 24
Figure 3.3: The experimental apparatus for the ultrasonic vibrator/metal injection assembly at the top of the melts..... 28
Figure 3.4: Schematic experimental setup for the ultrasonic vibrator/metal injection assembly at the bottom of the melts..... 29
Figure 3.5: Schematic illustration of the positions of the sample in Figure 3.4 29
Figure 3.6: The temperature versus solid fraction curve of A356 alloy.. 31
Figure 3.7: The temperature versus solid fraction curve of 3004 alloy.. 32
Figure 3.8: The temperature versus solid fraction curve of A354 alloy.. 33
Figure 3.9: The temperature versus solid fraction curve of 6061 alloy.. 34
Figure 3.10: The temperature versus solid fraction curve of 6063 alloy.. 35
Figure 3.11: The temperature versus solid fraction curve of AM60B alloy.. 36
Figure 4.1: Location of thermocouples at the wall and center of sample crucible 41
Figure 4.2: Cooling curve collected from the thermocouple placed in the center of an A356 alloy casting (a) without and (b) with ultrasonic vibration. 43
Figure 4.3: The first derivative of the curve shown in Figure 4.2 (a) without and (b) with ultrasonic vibration..... 45
Figure 4.4: First part of a cooling curve and its derivative collected from the thermocouple placed in the center of an A356 alloy casting (a) without and (b) with ultrasonic vibration 47
Figure 4.5: Cooling curve collected from the thermocouple placed in the center and the wall of an A356 alloy casting (a) without and (b) with ultrasonic vibration. 50
Figure 4.6: The measured temperature difference between the wall and center of the casting (a) Tw – Tc without and (b) Tc – Tw with ultrasonic vibration. 52
Figure 4.7: The thermal analysis shows the duration of various reactions (1, 2, 3, 4) between the casting (a) without and (b) with ultrasonic vibration. 53

Figure 4.8: A comparison of microstructures obtained without (a) and with (b) the application of continuous acoustic power. 58
Figure 4.9: A comparison of microstructures obtained with the application of intermittent acoustic power for (a) 10 s (b) 20 s at each isothermal temperature step. 59
Figure 4.10: A comparison of microstructures obtained without (a) and with isothermal processing for 5 s at 614 °C (b), at 610 °C (c) and at 605 °C (d) 61
Figure 4.11: The microstructures of specimens subject to ultrasonic vibration for 20 s under isothermal processing conditions at (a) 614 °C and (b) 610 °C. 63
Figure 4.12: Microstructure of aluminum alloy A356 processed with varying ultrasonic amplitudes (a) 0% (No vibration), (b) 30%, (c) 50%, and (d) 70%. The casting temperature was 640°C. The specimens were vibrated for 60 s during solidification at ultrasonic amplitude of 0–70%..... 66
Figure 4.13: Quantitative analysis of the effect of ultrasonic amplitude on (a) primary grain area and (b) primary grain size. The casting temperature was 640°C. 68
Figure 4.14: Effect of casting temperature on as-cast microstructure of A356 alloy with ultrasonic vibration at 70% amplitude for 60 s (a) 620 °C, (b) 630 °C, (c) 640 °C, and (d) 650 °C..... 69
Figure 4.15: Quantitative analysis of the effect of casting temperature with ultrasonic vibration of 70% amplitude, (a) average area and (b) average size..... 71
Figure 4.16: Primary fcc aluminum grains present in the three zones and their transitions of the sample with ultrasonic treatment, at position (a) Zone I; (b) Transition between zone I and II; (c) Zone II; (d) Transition between zone II and III; (e) Zone III. as illustrated in Figure 3.5 73
Figure 4.17: Comparison of primary fcc aluminum grain size of the samples without and with ultrasonic treatment..... 76
Figure 4.18: Size distribution of primary fcc aluminum grain in the three zones of the sample with ultrasonic treatment. 77
Figure 4.19 Experimental apparatus for ultrasonic processing of molten aluminum alloy billet suitable for industrial scale SSM processing 80

Figure 4.20: Casting of 2 kg billet of A356 alloy without (a) and with ultrasonic vibration at different location in the casting (b~d). The casting temperature was 630 ^{o}C, and amplitude 100%, vibration time 60 seconds. The ultrasonic radiator is located at the bottom in the center of the billet 82
Figure 4.21: Quantitative analysis results showing the resultant 3-dimensional distribution of (a) average fcc grain size and (b) average roundness on the 2 kg billet with ultrasonic vibration. The ultrasonic radiator is located at (0, 0), where x is the distance from the center, and y is the distance from the bottom of the billet. 84
Figure 4.22: The effect of grain refiner on the 2 kg billet as-cast microstructure of A356 alloy without (a, b) and with (c, d) ultrasonic vibration under condition of 630 ^{o}C casting temperature, 100% amplitude, and 60 seconds vibration time. 86
Figure 4.23: Microstructure of 6061 alloy without ultrasonic vibration at a casting temperature of 690 ºC. 89
Figure 4.24: Microstructure of 6061 alloy with ultrasonic vibration at a casting temperature of (a) 700 ºC and (a) 720 ºC. 90
Figure 4.25: Microstructure of 6063 alloy without ultrasonic vibration at a casting temperature of 690 ºC. 92
Figure 4.26: Microstructure of 6063 alloy with ultrasonic vibration at a casting temperature of (a) 700 ºC and (a) 730 ºC. 93
Figure 4.27: Microstructure of 319 alloy without ultrasonic vibration at a casting temperature of 650 ºC. 94
Figure 4.28: Microstructure of 319 alloy with ultrasonic vibration at a casting temperature of (a) 640 ºC and (a) 650 ºC. 95
Figure 4.29: Microstructure of A354 alloy (a) without and (b) with ultrasonic processing. 96
Figure 4.30: Microstructure of 2618 alloy casting without ultrasonic vibration at the magnifications (a) 50 x and (b) 400 x. 98

Figure 4.31: Microstructure of 2618 alloy casting at the casting temperature of 680 °C with ultrasonic vibration at the magnifications (a) 50 x and (b) 400 x..... 99
Figure 4.32: Microstructure of 2618 alloy casting at the casting temperature of 670 °C with ultrasonic vibration at the magnifications (a) 50 x and (b) 400 x..... 100
Figure 4.33: Microstructure of 2618 alloy casting at the casting temperature of 660 °C with ultrasonic vibration at the magnifications (a) 50 x and (b) 400 x..... 101
Figure 4.34: Microstructure of 2618 alloy casting at the casting temperature of 650 °C with ultrasonic vibration at the magnifications (a) 50 x and (b) 400 x..... 102
Figure 4.35: Grain size calculation for 2618 alloy with and without ultrasonic vibration. 104
Figure 4.36: Eutectic modification observed by optical metallurgical microscopy at low magnification, (a) without ultrasonic treatment and (b) with ultrasonic treatment. 107
Figure 4.37: Eutectic modification observed by SEM at 2000X magnification, (a) without ultrasonic vibration and (b) with ultrasonic vibration..... 109
Figure 4.38: Silicon morphological analyses of A356 alloy without and with ultrasonic treatment. 110
Figure 4.39: Three-dimensional eutectic morphology observed using SEM at 2000X magnification, (a) without ultrasonic treatment and (b) with ultrasonic treatment. 111
Figure 4.40: Formation of eutectic cells among the aluminum grains (a) the eutectic cells form on the dendrite and grow in the remaining liquid in the mushy zone, (b) the eutectic cells nucleated independently in the liquid among the dendrites. 113
Figure 4.41: Dendritic microstructure in an AM60B alloy copper-mold casting without ultrasonic treatment. The casting temperature was 675 °C. 117
Figure 4.42: Fine globular grains in an AM60B alloy copper-mold casting with ultrasonic treatment, at position I as illustrated in Figure 3.5. The casting temperature was 675 °C. 118

Figure 4.43: Small grains in same sample as shown in Figure 4.42, from position II (5mm from the radiator). 119
Figure 4.44: Small grains in same sample as shown in Figure 4.42, from position III (a) 15mm from the radiator; (b) 30 mm from the radiator. 120
Figure 4.45: Small grains in same sample as shown in Figure 4.42, from position IV (top of the sample)..... 121
Figure 4.46: Comparison of primary magnesium grain size in an AM60B alloy copper-mold casting with and without ultrasonic treatment. 123
Figure 4.47: Secondary phase in the same sample shown in Figure 4.41. 124
Figure 4.48: Secondary phase from position I in the same sample shown in Figure 4.42, ... 126
Figure 4.49: Secondary phase from position II in the same sample shown in Figure 4.42 at different magnification (a) 400 X and (b) 1000 X 127
Figure 4.50: Secondary phase in position III in the same sample shown in Figure 4.42. a) 20 mm and (b) 30 mm from the radiator..... 128
Figure 4.51: Secondary phase in position IV (40 mm from the radiator) in the same sample shown in Figure 4.42 at a) 400 X and (b) 1000 X 129
Figure B.1: Microstructure of 4340 steel without ultrasonic vibration casting temperature, 1525°C. 156
Figure B.2: Microstructure of 4340 steel with 100% ultrasonic amplitude and 120 second exposure time (a) Casting temperature 1548°C (b) Casting temperature 1516°C. 157
Figure C.1: Microstructure of bismuth/tin alloy without ultrasonic vibration..... 159
Figure C.2: Microstructure of bismuth/tin alloy with 400-kHz vibration and varying ultrasonic amplitude. 160

LIST of EQUATIONS

Equation 1.1 2
Equation 1.2 3
Equation 1.3 3
Equation 2.1 13
Equation 2.2 13
Equation 2.3 13
Equation 2.4 14
Equation 2.5 14
Equation 2.6 14
Equation A.1 148
Equation A.2 148
Equation A.3 148
Equation A.4 148
Equation A.5 149
Equation A.6 150
Equation A.7 151
Equation A.8 151
Equation A.9 151
Equation A.10 151
Equation A.11 151
Equation A.12 151
Equation A.13 151
Equation A.14 151
Equation A.15 153
Equation A.16 153
Equation A.17 154
Equation A.18 154
Equation A.19 154

NOMENCLATURE

A/D	Analog/Digital
AFS	American Foundry Society
ASM	American Society of Metals
bcc	body-centered cubic
C_0	initial liquid composition
C_s^*	solid composition at the liquid –solid interface
DAS	dendrite arm spacing
D_L	liquid diffusion coefficient
DC	Direct Chill
DOE	U.S. Department of Energy
DSC	Differential Scanning Calorimetry
DTA	Differential Thermal Analysis
fcc	face-centered cubic
f_s	solid fraction
GM	General Motor Corporation
ΔH	molar change in enthalpy of the liquid
IMF	Industrial Materials for the Future
ITP	Industrial Technologies Program
k	Boltzmann's constant
k	equilibrium partition ratio
n	number of atoms per unit volume of liquid
n'_s	number of surface atoms on the substrate per unit volume of liquid
NADCA	North American Die Casting Association
ORNL	Oak Ridge National Laboratory
PZT	piezoelectric lead zirconate titanate
RPT	reduced-pressure test
SEM	scanning electron microscope/microscopy
T	temperature
T_G	steady state growth temperature
T_m	melting temperature

T_M	equilibrium melting point of the metal
T_{Min}	the lowest temperature during the supercooling, or the balance point when the latent heat released from the newly nucleated crystals catches up the heat exiting from the casting to the environment.
TMS	The Minerals, Metals, and Materials Society
t_{Rec}	the recalescence period
ΔT	undercooling of the liquid (T_M - T)
ΔT	the differential temperature between T_C and T_W in the melt
UT	University of Tennessee
UP	Ultrasonic processing
UV	ultrasonic vibration
V_s	molar volume of liquid
α	crystal constant
θ	contact angle of a cluster on a substrate
σ	solid/liquid interfacial free energy

Chapter 1

Introduction

The casting of metals evolved as a fabrication process approximately 5000 years ago. The industrial revolution in Europe and North America is synonymous historically with the development of the casting process [1]. Enormous expansion in the metal casting industry stemmed from the need to produce new machinery of all types for the growing manufacturing sector, food handling, energy, and transportation industries. The recent "energy crisis" of the 1970s triggered tremendous research into how to improve traditional metal casting technologies, and greater applications of light metals in many vehicles, ships and aircrafts.

Lighter, stronger, cheaper and cleaner - light metals such as aluminum and magnesium assure enormous economic and environmental benefits. One familiar light metal, aluminum, is so much a part of everyday life due to its excellence in strength-to-weight ratio, non-corrosiveness, lightness and recyclability. Magnesium, a common structural metal, is about one third lighter than aluminum. In the transportation area, light metals are already reducing the overall weight of cars, trucks, ships, and aircrafts and therefore their fuel consumption has decreased. For example, the amount of aluminum used in a typical United States family car increased from 44 kilograms in 1977 to 117 kilograms in 2001, while magnesium use increased from 0.5 kilograms to 3.9 kilograms in the same period [2].

On the other hand, the solidification process is basic to casting technologies such as die casting, direct chill casting, directionally solidified casting, continuous casting, foundry casting, single-crystal growth for semiconductors, rapidly solidified alloys and

glasses. The solidification process is the transformation from non-crystallographic (liquid) state to crystallographic (solid) state of a metal or alloy. The mechanism of solidification has been studied extensively during the past decades, along with the great demand of the applications in industries such as automotive, aerospace, manufacture, domestic food handling, and military. An understanding of the mechanism of solidification and how it is affected by such parameters as alloying, cooling conditions (mold types), casting temperature, is important in the control of mechanical properties of final products.

1.1 Solidification and microstructure of light metals

If a liquid is cooled below its equilibrium melting temperature (Tm), or supercooled, solidification begins by the formation of very small solid particles or nuclei (the nucleation process). When a solid particle (nuclei) forms within its own melt without aid of foreign materials, the process is called homogeneous nucleation. On the other hand, heterogeneous nucleation happens when nuclei start to form at solid impurity particles and/or the walls of the liquid container. The driving force for nucleation is the free energy change of the transformation. In practice heterogeneous nucleation is more likely because the energy barrier for heterogeneous nucleation is much smaller than for homogeneous nucleation. For metals, the nucleation rate for heterogeneous nucleation is derived by Turnbull and Fisher based on earlier work [3]. It is expressed as:

$$I_p = \frac{n'_s}{n} 10^{33} \exp\left[-\frac{4\pi\sigma^3 T_M{}^2 V_S{}^2}{3\Delta H^2 \Delta T^2 kT} (2+\cos\theta)(1-\cos\theta)^2 \right] \quad \text{Equation 1.1}$$

It can be seen that the higher ΔT, or the undercooling of the liquid (T_M - T), the higher the heterogeneous nucleation rate is.

The second stage of solidification is grain growth. Under certain conditions, nuclei may survive and continue to grow into grains. The growth mechanism for a pure metal is different from that for an alloy. For a pure metal, the grain growth of a diffuse solid/liquid is linearly in proportion to the undercooling. With some assumptions and simplifications, Turnbull calculated the growth rate in the following expression [4]:

$$R = \frac{D_L \Delta H_m}{\alpha k T_M^2} \Delta T = k_1 \Delta T \qquad \text{Equation 1.2}$$

On atomically smooth solid/liquid interfaces, there are three ways to achieve grain growth: (1) by repeated surface nucleation [5]; (2) by spiral growth [6]; and (3) growth from twin intersections [7,8]. The growth rates with those mechanisms are to some extent related to the supercooling of the solidifying liquid.

For the solidification of single-phase alloys with equilibrium at a liquid-solid interface, three mechanisms were proposed:

1) Equilibrium Solidification, which assumes complete diffusion in both the liquid and the solid state.
2) Scheil Model [9, 10], which assumes complete diffusion in the liquid and no diffusion in the solid state. With those assumptions, the composition of the solid at the liquid –solid interface C_s^* can be given as a function of solid fraction:

$$C_s^* = kC_0(1 - f_s)^{(k-1)} \qquad \text{Equation 1.3}$$

With this equation, the solid fraction vs. temperature curves can be determined by other known factors, i.e., the equilibrium partition ratio *k*, and initial liquid composition C_0.

3) Non-equilibrium Solidification which assumes limited diffusion with no convection in the liquid and no diffusion in the solid state [11].

To the light alloys, such as aluminum alloys and magnesium alloys, each grain contains a family of aluminum/magnesium dendrites which all originate from the same nucleus. The grain size of a casting is determined by a combination of both nucleation and grain growth conditions. During the nucleation process, in general, a larger number of nuclei allows more grains to form, bringing about a smaller grain size. So the grain size is inversely proportional to the number of effective nuclei present in the liquid. During the grain growth process, a higher cooling rate brings about a smaller value of DAS [12]. The dendrite arm spacing (DAS) bears an inverse relationship to the cooling rate through the mushy zone.

Grain refinement exerts a positive influence on several properties of cast aluminum and magnesium alloys, notably, hot tearing tendency [13], porosity [14], shrinkage distribution, intermetallic distribution, and certain mechanical properties such as tensile strength and elongation [15]. It is then of general interests to control the grain size and DAS through the management of both nucleation and grain growth.

In aluminum alloys, a grain refiner (Titanium or Titanium-Boron alloy) is usually added so that heterogeneous nucleation occurs. In general, embryos of the solid form on foreign particles such as TiB_2 added to the melt as a grain refiner. The solid embryos are initially globular. Then they grow into crystals of dendritic morphology. There are two ways to produce a fine microstructure. One is to provide a large quantity of nuclei so that there is no room for each grain to grow into a dendrite. The other is to break up the dendritic structure so that each secondary dendrite arm becomes a grain. The first method works during the nucleation stage and the second works during the growth stage of solidification.

For magnesium alloys, grain refinement is an important practice to improve the mechanical properties and the relevant research work dates back to the 1930s [16]. Several grain-refining techniques have been reported for magnesium – aluminum based alloys, namely superheating [17], carbon inoculation [18, 19], and the Elfinal process [20,21]. For magnesium alloys that do not contain aluminum, manganese, and silicon, zirconium is an extremely potent grain refiner [22,23].

However, for aluminum-silicon based alloys which contain a large fraction of eutectic, the properties are dependent on not only the grain sizes, but also the shape, size, and distribution of the eutectic silicon. Thus the process of eutectic modification becomes very important. For example, aluminum A356 alloy contains about 50 vol% eutectic phases. The final microstructure is largely determined by the eutectic reaction. Due to its diamond cubic crystal structure which predominantly grows in the <112> direction on the (111) plane, silicon is a faceted phase with strongly anisotropic growth, thus it is difficult to change the growth direction [24]. In unmodified A356 alloy, the main eutectic reaction occurs at 574 °C as a binary reaction, which results in coarse irregular plate-like silicon.

The modification of eutectic silicon is of general interest since fine eutectic silicon along with fine primary aluminum grains improve mechanical properties and ductility [25].

Three well known eutectic modification methods have been developed thus far, namely 1) chemical modification [26 - 28], which produces fine fibrous silicon structure through the addition with trace-levels of several elements, such as sodium, antimony, potassium, calcium, strontium, and barium; 2) quench modification [24, 29], which results in silicon forming an exceedingly fine form when compared to the unquenched silicon, through high cooling rates and rapid solidification in the growth rate ranging from 400 to 1000 μm per second; and 3) superheating modification, which requires the presence of magnesium in the alloy [30] to obtain fibrous silicon by heating up the melt from the usual pouring temperature to a temperature of 850 – 900 °C and held for about 15 – 30 minutes, then quickly cooled to the pouring temperature before casting. Chemical modification has been widely used in industry for producing A356 alloy with a fine and fibrous eutectic silicon phase, and thus improved mechanical properties.

1.2 Ultrasonic processing of materials

Ultrasonic processing of materials has been practiced for over a half century. It has been used in the generation of aerosols, the refinement of grain structure in crystallized solids and in the enhancement of diffusion in liquids and solids. It has also been employed to dry powders and other materials. In other areas it has been widely used in machining operations (drilling and cutting) and has also been used in welding and bonding. Ultrasonic bonding has been widely used in the integrated circuit industry for many years. Ultrasonic cleaning of materials and ultrasonic degassing of liquids has also found wide acceptance.

There have been a large number of investigations on the use of ultrasonic processing of light metals for the purpose of grain refinement and degassing. Ultrasonic vibration has proven to be a potentially new way of improving the quality of light metals. The introduction of high intensity ultrasonic vibration into the melt may control the columnar dendritic structure, reduce the size of equiaxed grains, and under some conditions, produce globular non-dendritic grains [31]. Attempts have also been made to

use ultrasonic vibrations for the production of SSM alloy stock [32]. Ultrasonic treatment possesses the advantages of being environmentally favorable, cost effective, and ready to be combined with other known physical processing technologies for liquid and solidified metal.

However, a closer survey of those previous works shows that grain refinement with ultrasonic treatment is still primarily empirical and phenomenological in nature, and with little systematic study of the mechanism for the modification of the solidification microstructure.

1.3 Dissertation goals and scope

This dissertation will be dedicated to determining the solidification mechanisms and establish a quantitative base for the ultrasonic processing of light metals. This study will focus on two classes of light metals, viz., aluminum alloys and magnesium alloys, and demonstrate the application of ultrasonic processing during ingot casting and foundry shape casting.

This investigation proposes to study the effect of acoustic energy of varying intensity introduced during the melting and solidification process. Variables will be input acoustic intensity and casting temperature. Studies have been carried out on many organic and metallic systems, which have verified the importance of this technique in influencing the final microstructure. The present study will carry out thermal analysis of the solidification reactions with ultrasonic vibration, and determine which mechanism, i.e. heterogeneous nucleation or dendrite fragmentation, is more important for grain refinement under ultrasonic vibrations. The study will further verify the formation mechanism of superfine grains and the eutectic modifications to light metals with ultrasonic treatment. Initial experiments will also be carried out to verify the effectiveness of ultrasonic vibration on the microstructure modification of magnesium alloys.

The results will provide core principles and establish quantitative bases for nucleation, growth, and fragmentation processes during solidification in an acoustic field, and provide tools for producing novel and fine-grained alloy microstructures. It is

expected that the results of the work will impact a wide range of alloy processing including DC casting, continuous casting, vacuum arc remelting, and foundry processing in the areas of degassing, grain refinement, semi-solid metalcasting (SSM), and the production of new and novel microstructures. Other applications include welding and brazing, metal atomization, processing of composites, and the possible use of pressure-induced phase transformations in the solid state to produce ultrafine or even nano-structures. Future applications could also involve the coupling of materials processing under an acoustic field with magnetic or electromagnetic fields or even microgravity to produce unique processes and microstructures.

Chapter 2

Literature Review

2.1 A brief history of ultrasonic processing in the field of metallurgy

Ultrasound is any acoustic wave above the normal range of human hearing, in other words, above 20,000 hertz. Humans cannot hear ultrasound, but many animals, such as bats, dolphins and whales, have long found ultrasound handy for probing (navigation).

The story of ultrasound and its effect on material dates back to1878, when Chernov proposed improving cast metals quality by elastic oscillations [33]. But after that, not until 1912 was there any applications of ultrasound in metallurgy. The tragedy of the Titanic spurred tremendous interest in the application of ultrasonic vibration. Pioneering experiments on the ultrasonic processing of materials started in the 1920s. Boyle [34] in 1922, and Taylor and Sproule [35] in 1929 proposed the potential of degassing metals by ultrasonic vibrations. In 1927 Wood and Loomis [36] reported the results of ultrasound affecting dispersion, emulsification and degassing. In 1936, Sokolov [37], for the first time, carried out experiments on sonication of molten zinc, tin, aluminum, and observed effects of ultrasound on the solidification of molten metals. Seeman [38] in 1936 and Schmid and Eret [39] in 1937 repeated Sokolov's experiments.

After World War Two, Russia (or the former USSR) published a tremendous number of papers on ultrasonic processing in the metallurgy area. In 1955 Danilov and his team of workers [40] proposed a mechanism of ultrasound affecting the formation and growth of crystal nuclei in supercooled melts of low melting point organic materials such

as betol, piperine, and salol. Also Danilov [41] published the result of the effect of impurities on the solidification of metals with ultrasonic treatment. In 1962, Kapustin and others [42] reported results on crystallization of some ultrasonically-treated organic substances and metals. In the 1960s, broad research was carried out on ultrasonic treatment of ferrous and nonferrous metals and alloys, such as Teumin [43], Abramov [44 - 47] (both authors dealt with ferrous metals and alloys), Polotskii [48] (about propagation and absorption of ultrasound in some molten nonferrous metals), and Eskin in [49, 50](about molten light alloys).

In recent years, Eskin [51, 52] and Abramov [53, 54] published their monographs on ultrasonic processing of materials.

In the United States, in 1960 Lane and Tiller [55] reported their work on ultrasonic energy affecting the melting of ferrous metals in electric arc furnaces with expendable electrodes. Grant [56] published in 1985 on ultrasonic atomization, ultrasonic brazing, and the ultrasonic effect of the mechanisms of crystallization.

In Japan, Furukawa [57] investigated continuous casting of aluminum alloys under ultrasonic vibration. Nakanishi and colleagues [58] reported the research done with Daihatsu Motor Co. on the feasibility of soaking aluminum oxide melt and its wetting powders and fibers using ultrasonic vibrations.

In Germany, in the 1950s in their books, Bergmann [59], Matauschek [60], and Herrmann [61] described a pilot plant for ultrasonic melting and casting. Many other investigations on ultrasonic applications on welding and atomization were carried out by Pohlmann and colleagues [62]. Seemann's group [38,63, 64] published experimental results on ultrasonic grain refinement of castings of aluminum alloys.

In England, the company Mullard [65] did most of the studies and developed industrial ultrasonic equipment. Mason [66-68] of Coventry University published work on improving casting quality and enhancing energy efficiency with power ultrasound.

Angelov of Bulgaria reported ultrasonic treatment of aluminum alloys with mold casting [69]. Kratky of the Solvak Republic conducted experiments on ultrasonic casting of aluminum alloys [70]. Also Lin Chun Mao [71] published initial results of ultrasonic treatment of aluminum alloy in 1979.

Many ultrasonic processing schemes suitable for industrial implementation only appeared in the late 1950s and early 1960s. For example, the Aluminum Company of America (Alcoa) attempted introducing ultrasonic vibrations into the mold walls during continuous casting of Al-Mg based alloys.

Detailed reviews of this subject were done by Eskin [50,51,72), Rozenberg [73, 74), Abramov [47, 53,54], and Balandin [75]. Campbell [76] summarized a variety of means in which acoustic vibrations could be applied during casting, as shown in Table 2.1:

In 2001, a project entitled "Ultrasonic Processing of Materials," was funded by the Industrial Technology Program (ITP) of the US Department of Energy. One of the research tasks involves the investigation of the effect of high-intensity ultrasonic vibration on the microstructure of wrought and foundry aluminum and magnesium alloys. This dissertation is based on the work done for the project.

Table 2.1 Methods of applying acoustic vibrations during casting

	Vibration of casting +mould	Vibration of casting	Vibration of liquid with an uncooled probe	Vibration of liquid with a cooled probe (separate nucleation source)
Casting+ vertical vibration	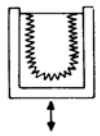	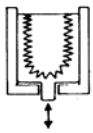	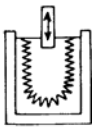	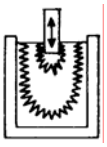
Casting+ horizontal vibration	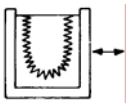	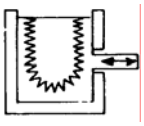	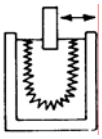	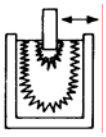
Casting+ rotational vibration	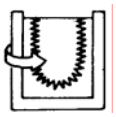	Not available	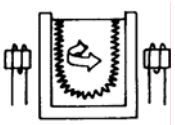	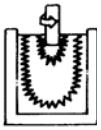

2.2 Phenomena induced by the propagation of ultrasound

Some phenomena, like acoustic streaming, cavitation, atomization, arise in the melt in which high intensity ultrasound propagates.

2.2.1. Ultrasonic streaming

Streaming is generated by the acoustic energy and momentum loss for overcoming the viscosity of the melt. It happens both in inhomogeneous sound fields and near various barriers like interfaces. Its scale and velocity are functions of properties of the treated melt, the shape and structure of external boundaries. It's noteworthy that the streaming velocity increases with acoustic intensity but is always far less than the driving ultrasonic velocity, no matter how high intensity it is [76].

Ultrasonic streaming is studied extensively in (1) small-scale vortices, which are developed in a viscous boundary layer near a barrier, (2) large scale streaming, (3) streaming developed in a medium restricted by rigid walls. Theory analyses are established by hydrodynamic equations for a viscous compressive liquid. Abramov studied streaming by using ultrasound 45 KHz and 100-250 KHz in frequency to treat melts of transparent organic substance. He found that ultrasonic intensity and melt temperature (which controls viscosity) mainly determine the nature, velocity and scale of streaming; at low ultrasonic intensity, streaming does not appear in a superheated melt. Other studies reveal that ultrasonic streaming never interacts with convective flows when ultrasonic intensity is low; by raising vibrational velocity amplitude (to 3~8cm/s), streaming and convective flows begin to interact and the steady state liquid velocity is 5~10 times larger than that of convective flows.

Ultrasonic streaming affects solidification through large-scale flows' equalizing the temperature of the liquid and increasing the transfer of fine nascent solidification sites and broken-down crystals.

2.2.2. Ultrasonic atomization

Ultrasonic atomization was first reported by Wood and Loomis [77] and developed by many others [78-80]. When the liquid is exposed to ultrasonic megahertz vibration, it is atomized as a result of turbulent flows and a spout appears on its surface.

Ultrasonic atomization is mainly controlled by liquid properties, ultrasonic parameters, and so on. For low frequency ultrasound, the atomization of liquid layers into drops may have these mechanisms:

- Cavitation hypothesis: action done by collapse of cavities near the liquid-gas interface.
- Destruction from bubbles pulsating near the liquid surface
- Bubble induced liquid splash
- Separation of liquid drops

Generally speaking, the status quo of ultrasonic atomization of liquid is such that its chief principles have been understood for cases of ultrasound feeding via a gas and a liquid developing in layer and in fountain.

2.2.3. Ultrasonic homogenization

Experiments for investigating ultrasonic degassing and filtration are also accompanied by a rapid transition of melt to a homogenous state. Baum first found this phenomenon by isothermally soaking the melts for a long time. Popel and Eskin continued the research and tried to find the optimal condition for ultrasonic homogenization, to make it an alternative to heat treatment.

2.2.4. Cavitation

Cavitation (of importance to structure modification) is the introduction of acoustic energy in the melt of sufficient amount to set up a pressure variation within the melt that initiates cavitation. In order to establish a condition where cavitation occurs and crystal dispersion takes place, an acoustic pressure of greater than 10 W/cm^2 at frequencies of 20 kHz is required. With sufficient acoustic pressure, the interfacial boundary that is the transition layer between the liquid and solid phases can be disrupted due to viscous

friction forces. A change of state of this layer will cause the crystal nucleation and growth conditions to change.

When cavitation occurs in a melt, the occurrence of pulsating cavitation bubbles can cause the dispersion of crystals and increase the nucleation rate of crystallization. Calculations have shown that the stresses created in the surface layer of metals by the implosion of a cavitation bubble immediately adjacent to the surface or separated from it by a distance of a few radii amount are approximately 13,000 atm. Such stresses can readily cause the dispersion of crystals at the crystallization front resulting in grain refinement.

The maximum and minimum pressures caused in the melt are given by the following equations [74]

$$p_{\max} = p_0 + \sqrt{2\rho c I} \qquad \text{Equation 2.1}$$

$$p_{\min} = p_0 - \sqrt{2\rho c I} \qquad \text{Equation 2.2}$$

where p_0 is the atmospheric pressure, ρ and c are the density and the wave velocity of the melt respectively, and I is the wave energy density in the melt. Thus, the application of ultrasonic energy to the melt results in the instantaneous variation in the local pressure from the minimum to the maximum.

2.2.4.1 Origin of cavitation in melt

When propagating in the melts, the acoustic wave in the rarefaction phase produces a tensile stress. It results in the forming of bubbles or discontinuities. Once being formed, the bubble can pulse, or increase its size to the maximum then collapse. This bubble behavior is called cavitation. Cavitation has been investigated by quite a few workers, both theoretically and experimentally. In his book Abramov quoted P_c^v, a critical value of sound pressure, to estimate the cavitational strength of a liquid containing vapor or gas nuclei (tiny bubbles). The bubble is stable when its peak sound pressure is less than P_c^v, or else it will grow and collapse [81] finally.

$$P_c^v = P_0 - P_v + \frac{2}{3\sqrt{3}}\sqrt{\frac{(2\sigma_L / R_0)^3}{P_0 - P_v + 2\sigma_L / R_0}} \qquad \text{Equation 2.3}$$

Where P_0 is the initial air pressure, P_v the saturation vapor pressure, R_0 initial radius.

When in the bubble the vapor pressure is not saturated and the sound pressure threshold becomes [82,83],

$$P_c^g = \sqrt{\frac{2}{3}} P_0 \sqrt{1 + \frac{2\sigma_L}{P_0 R_0} - \frac{c_\infty}{c_0}} \qquad \text{Equation 2.4}$$

Herring and Flinn [84] proposed a formula that sufficiently estimates the collapse velocity and minimum radius of the cavity.

$$R\left(1 - 2\frac{U}{c_0}\right)\frac{d^2R}{dt^2} + \frac{3}{2}\left(1 - \frac{4U}{3c_0}\right)\left(\frac{dR}{dt}\right)^2 + \frac{1}{\rho_L}$$
$$\left[P_0 - P_v - p_m \sin\omega t + \frac{2\sigma_L}{R} + \frac{4\eta U}{R} - \left(P_0 + \frac{2\sigma_L}{R_0}\right)\left(\frac{R_0}{R}\right)^{3\gamma}\right] + \frac{RU}{\rho_L c_0}\left(1 - \frac{U}{c_0}\right)\left(\frac{dP}{dR}\right) = 0$$

Equation 2.5

With a given velocity the motion of the cavity can be obtained by the Kirwood-Bethe-Gilmore equation [85]:

$$R\left(1 - \frac{U}{c}\right)\frac{d^2R}{dt^2} + \frac{3}{2}\left(1 - \frac{U}{3c}\right)\left(\frac{dR}{dt}\right)^2 - \left(1 + \frac{U}{c}\right)H - \frac{U}{c}\left(1 - \frac{U}{c}\right)R\frac{dH}{dR} = 0 \qquad \text{Equation 2.6}$$

Where U is the velocity of bubble boundary motion; R is the cavity radius; P_0 is the environment pressure; Pv is the vapor pressure; p_m is the amplitude; ω is the frequency; c is the sound velocity. H is the free enthalpy at the surface of a spherical cavity; γ=1 for isothermal pulsation and 4/3 for adiabatic pulsation.

The equation above was verified by experiment. It is found that the viscosity has a neglectable effect on cavitation bubble behavior, whereas the surface tension affects the bubble behavior in a complex way. Flinn [86] mentioned that bubble collapse can be stimulated by increasing the surface tension. Other results show that in the radiated wave the peak pressure increases with the decrease of density ρ_L, and the increase of nonlinear parameter n and sound velocity c_L.

The study of high temperature molten metals faces the experimental difficulties, such as high temperature, optical capacity, chemical reactivity and the contact

phenomena at the melt-horn interface. In order to avoid the high temperature and chemical reaction, Abramov et al. tested Ga (melting point 30 ^{o}C) and Wood's alloy (melting point 89 °C) with the radiation of ultrasound [87]. Results show that cavitation threshold is governed by the appearance of a subharmonic component (*f/2*).

Real liquid melts contains inclusions, i.e. solid or gaseous micro inhomogeneities. They can turn into cavities when in an ultrasonic field. Abramov studied the cavitation strength of some low-melting molten metals with bubbles [88]. It is revealed that at the acoustic pressure of several fractions of MPa and with the bubbles 10^{-4} m in radius, cavitation may arise in the melts. The effects on cavitation from particles and vessel walls are also studied with Sn, Al, Fe and water. Results show that, for a wettable solid, the nucleation energy and breaking pressure are larger for heterogeneous conditions than for homogeneous; for an unwettable solid, they are lower. The resonator surface condition also affects the cavitation threshold [89]. It should be noted that, in the ultrasonic treatment of Al, the cavitation threshold lowers with the increasing of hydrogen concentration. Alumina particles have a similar but stronger effect.

2.2.4.2 Effects of cavitation in melts

Quite a few investigations have been performed on the birth growth and consequences of cavitation. It is revealed that cavitation helps to change material structure and composition/phase distribution. The possible mechanism is related to:

- Mechanical shock.

Cavitation may happen when the stress at a point in liquid is high enough. Such a point can be gas bubble [90] or cavitation voids [91] by sharply beating the outside of the liquid container. Berger and Rostoker [92] are known as the first who successfully refined the grain of a cast by mechanical shock.

- Increase nucleation rate.

Hunt and Jackson [93] conducted experiments on ultrasonic treatment of low melting temperature metal. They found that the collapse of bubbles or cavities generated prodigious local pressure and increased nucleation rate. And the thermal spike associated

with the collapse can help the newly formed solid survive. It also gives reason for ultrasonic grain refinement.

- Damage to local solid interface.

Campbell [76]mentioned that the collapse near a solid might give the latter large shock induced mechanical damage, such as local brittle failure, phase change that might give rise to product failure.

- Melting corrosion solid interface.

Buxman and coworkers [94, 95] observed localized heating due to cavitation at high energies and cited cases of using the energy to remelt a whole cast or remelt grains in partial to give grain refinement. The cavitation with a large amount of bubbles finally collapsing can cause acoustic energy to be absorbed and dissipated as heat. From calculation, with the heat, even a small bubble of diameter 0.1mm could cause the remelting of a region 10 μm across.

- Droplet ejection

At some critical conditions of ultrasonic processing melts, metal is observed being ejected from the open surface of moulds. Theoretical predictions of the metal ejection and experiments have been carried out by many researchers [96 - 98]. The work shows that at low frequencies the metal ejection is not important.

2.3 Solidification of light alloys in an ultrasonic field

Accompanied with the development of modern industries, such as the automotive industry, aerospace engineering, construction engineering and oil production, higher quality products are required by improving alloy technologies, above all in melting and casting. Ultrasonic processing presents a new effective dynamic method for treating a molten and solidifying metal. Ultrasonic vibration may affect both stages of solidification to produce fine and globular grains. Since fragmentation promotes the formation of equiaxed grains, the formation of columnar structures during ingot casting and vacuum arc remelting will be restricted, resulting in the formation of fine equiaxed grains.

2.3.1. Effect of ultrasonic vibration on nucleation of solids

Ultrasonic vibration may affect nucleation in many ways. Obviously, the liquidus temperature of the alloy is a function of pressure. The liquidus temperature decreases with increasing pressure. By applying ultrasonic energy to a melt held close to its liquidus temperature, some regions in the melt might be superheated while others may be undercooled. Cibula[99] and Hunt and Jackson[100] estimated the bubble's temperature drops when it expands. A 10 Pa pressure drop from the expansion leads to a 20 °C temperature drop inside the bubble. At each location, the melt might undergo changes from undercooling to superheating at high frequencies. This may result in the formation of more solid embryos.

Danilov [40, 101], Berlaga, Gorskii [102], and Kapustin [42] conducted experiments with transparent organic substances, such as salol, thymol, betol and piperine, which were selected to have a clear metastability threshold so the waiting time of the first solidification site could be determined. In the case of betol, without vibration a given 42.5 °C undercooling results in a waiting time of 40 min; while with ultrasound of 100W•cm^{-2} in intensity, the waiting time drastically decreases to several minutes. Also the results indicated that the ultrasonic treatment increased the nucleation rate, as shown in Table 2.2.

Another possibility is that the grain refiners added to the melt might also be

Table 2.2: Effects of ultrasound on the nucleation of crystals

MATERIAL	CONTROL		ULTRASONIC	
	Metastability threshold (°C)	Minimal waiting time for the first solidification site (min)	Metastability threshold (°C)	Minimal waiting time for the first solidification site (min)
Betol	42.6	37	22.6	6
Naphthalene	8.0	6	2.0	0.1
Azonenzene	16.0	2	5.0	0.1
Salol	21	40	10	7
Bi	12	0.2	2	<0.05
Sb	25	10	2	<0.05

affected by ultrasonic vibrations since each foreign particle acting as nuclei is most effective under a certain undercooling and the undercooling of the melt is affected by Ultrasonic vibration. Nucleation may even occur in the melt at temperatures higher than the liquidus corresponding to atmospheric pressure. It has been reported that grain size was reduced when ultrasonic vibration was applied at temperatures higher than the liquidus temperature [73].

2.3.2. Effect of ultrasonic vibration on the growth of solids

Dendrite fragmentation is caused by melting at the dendrite root, where solutes are highly segregated. The melting at the dendrite roots may be due to the result of a local temperature increase. In an ultrasonic field, when cavitations happen, the diffusion in the liquid is almost complete; while in the absence of cavitations, acoustic streaming generates vibration pressure, viscous friction and forces of inertia which largely controls the crystal dispersion. The diffusion of solutes away from the dendrite roots reduces the solute concentration and increases the local melting temperature. This will also lead to melting at the dendrite roots. Stirring promotes dendrite fragmentation since it produces local temperature variations as well as promotes diffusion of solutes in the liquid. Like mechanical stirring, ultrasonic vibration also stirs the melt and should promote dendrite fragmentation. Furthermore, the local pressure fluctuations due to acoustic wave also lead to fluctuations in the melting temperature. These fluctuations should aid in the melting of the dendrite roots.

Campbell [76] predicted the vibration pressure at different displacement and frequency in the melt, tested ultrasonic solidifying Bi and Al and obtained the viscous forces and inertia forces vs. frequency and amplitude. The results indicated that ultrasonic vibration is capable of dendrite fragmentation. Using organic (thymol, naphthalene, naphthalene-axonezene) and metallic (Sn, Bi, Sn-Bi alloy, Sn-Zn alloy) crystals, Abramov [44] investigated ultrasonically induced crystal dispersion when there was no nucleation site at the solidification front resulting from a positive temperature gradient in the melt. He found out that, when the ultrasonic intensity was low without the presence of cavitation, ultrasound did not change the solidification front geometry but slightly

modified the temperature distribution in the melt. As the intensity increased until cavitational bubbles appeared, at first walls and roughness were produced at the solidification front by bubbles. Then they further break away some crystals and move them toward the liquid bulk. The resultant solidified products showed a finer structure. A further increase of acoustic intensity is accompanied by an extended dispersion zone length and resulted in better refined structure.

It is revealed that the acoustic intensity threshold for cavitation does not change with the crystal growth velocity or temperature gradient. Table 2.3 lists the relation between crystal geometry and ultrasound intensity necessary for crystal dispersion [103].

In general, a refined structure may be obtained even in the absence of cavitation. The wider the two phase zone, the better the refined results. Reduced refinement happens when the temperature gradient increases or solidification rate decreases.

2.4 Challenges

Thus, the challenges and hurdles to overcome can be listed bellow:

1) The thermal analysis and thermodynamic reaction process during solidification with the application of ultrasonic vibration are missing in all those investigations. Thermal analysis is an essential tool in determining the reactions and temperature point during solidification, thus decoding the mechanism of solidification under specific conditions, such as with the aid of ultrasonic treatment.

Table 2.3: Crystal geometry and ultrasound intensity necessary for crystal dispersion

Crystal growth velocity ($\mu m \cdot s^{-1}$)	Crystal length (mm)	Crystal radius (mm)	$\gamma, \times 10^{-2}$	Ultrasound intensity ($W \cdot cm^{-2}$)
5	0.2	0.05	6.25	30
16	0.4	0.06	2.25	20
25	0.6	0.08	1.78	15
50	1.0	0.12	1.44	10
100	1.6	0.20	1.55	10

Where $\gamma = \left(\frac{r}{l}\right)^2$, *r* is the crystal radius and *l* the crystal length

2) It is still unclear, with no convincing evidence in the literature as to which mechanism, i.e. heterogeneous nucleation or dendrite fragmentation, is more important for grain refinement under ultrasonic vibrations.

3) It is uncertain how superfine grains could be formed with the aid of ultrasonic treatment, and the primary mechanism for that.

4) It lacks publication on the eutectic modifications in light metals with the aid of ultrasonic treatment.

5) More quantitative information needs to be provided on modeling of ultrasonic processing. For example, the effectiveness of different processing methods, the function of processing parameters (intensity, duration time, etc), and how the casting conditions, like cooling rate, casting temperature, affects the formation of globular grains. Information is needed for eventual commercial implementation of ultrasonic processing technology.

6) There is not much information on the grain refinement of magnesium alloys with the aid of ultrasonic vibration. The effectiveness of ultrasonic vibration on the microstructure modification of magnesium alloys needs to be proven.

Therefore, this dissertation will focus on those challenges, and develop corresponding experimental assemblies, experimental techniques, and processing methods to overcome the above listed hurdles of the ultrasonic treatment of light metals.

Chapter 3

Experimental Methodology

3.1 Materials

For this investigation, the materials of interest were commercial magnesium – aluminum based AM60B alloy, aluminum – silicon based A356, A354, and 319 foundry alloys, aluminum – iron – magnesium based 3004, 6061, and 6063 wrought alloys. Composition of the above mentioned materials are listed in Tables 3.1 and 3.2.

Table 3.1: Composition of aluminum alloys

Alloy	**Si**	**Fe**	**Cu**	**Mn**	**Mg**	**Cr**	**Zn**	**Ti**	Ni	**Al**
A 356	7	0.1	0.15	0.08	0.4	-	0.08	0.15	-	91-93
A 354	8.6-9.4	0.15	1.6-2	0.1	0.5	-	0.1	0.2	-	87-89
319	5.5-6.5	<0.8	3-4	<0.5	<0.1	-	1	0.25	0.3	86-91
3004	0.6	0.7	0.05-0.20	1.0-1.5	0.8-1.5	0.08	0.10	0.04	-	95-98
6061	0.4-0.8	0.7	0.15-0.40	0.15	0.8-1.2	0.04-0.35	0.25	0.15	-	95-98
6063	0.3-0.6	0.35	0.10	0.10	0.45-0.9	0.10	0.10	0.10	-	97-99
2618	0.15-0.25	0.9-1.4	1.8-2.7	<0.25	1.2-1.8	-	<0.15	<0.2	0.8-1.4	91-95

Table 3.2: The nominal composition (in wt %) of AB60B alloy

Mg	Al	Mn	Zn	Si	Cu	Others
balance	5.7-6.3	0.27	<0.2	<0.5	<0.008	<0.01

Aluminum – silicon based alloys are known for their excellent fluidity, shrinkage tendency, pressure tightness, and resistance to tearing. Other minor elements are added to achieve special properties. For instance, the addition of Cu, Mg, or Ni improves tensile strength, machinability, and thermal conductivity. In general, the group of Al – Si alloys is characterized by excellent castability, good corrosion resistance, and can be machined and welded, and it constitute about 85 – 90 % of the total aluminum cast part produced.

The aluminum – silicon phase diagram [104] is shown in Figure 3.1. The equilibrium eutectic constitution is about 12.6 wt% silicon. The chosen aluminum alloys in this study fall into the hypoeutectic category. Their liquiduses are in the range of 610 – 660 °C. Their microstructure comprises both primary fcc aluminum containing 1.65 – 12.6 wt% silicon and eutectic containing silicon enriched aluminum and pure silicon.

On the other hand, magnesium-aluminum based alloys are the most commercially available magnesium alloy due to their relatively cheap price, readily castable, and good mechanical properties. AM60B alloy is magnesium – aluminum alloy with the addition of manganese to form ternary alloys with preferable corrosion resistance, ductility and impact strength.

From the equilibrium magnesium – aluminum phase diagram shown in Figure 3.2 [105], the equilibrium liquidus temperature of this alloy is about 617 °C. Its microstructure comprises both primary α-Mg containing 2% - 13% Al and eutectic containing Al enriched magnesium and β-$Mg_{17}Al_{12}$.

3.2 Experiments

3.2.1. Thermal analysis

Thermal analysis experiments were first carried out using A356 alloy, by introducing ultrasonic vibration during its solidification process. The alloy was melted in a graphite crucible inside a resistance furnace, and kept for half an hour at a temperature of 720 °C± 5 °C, about 100 °C higher than its liquidus temperature to allow the complete dissolution of silicon particles. The power of the furnace was cut off and its cover was then removed to allow a moderate cooling rate till solidification happens. Two thermocouples were

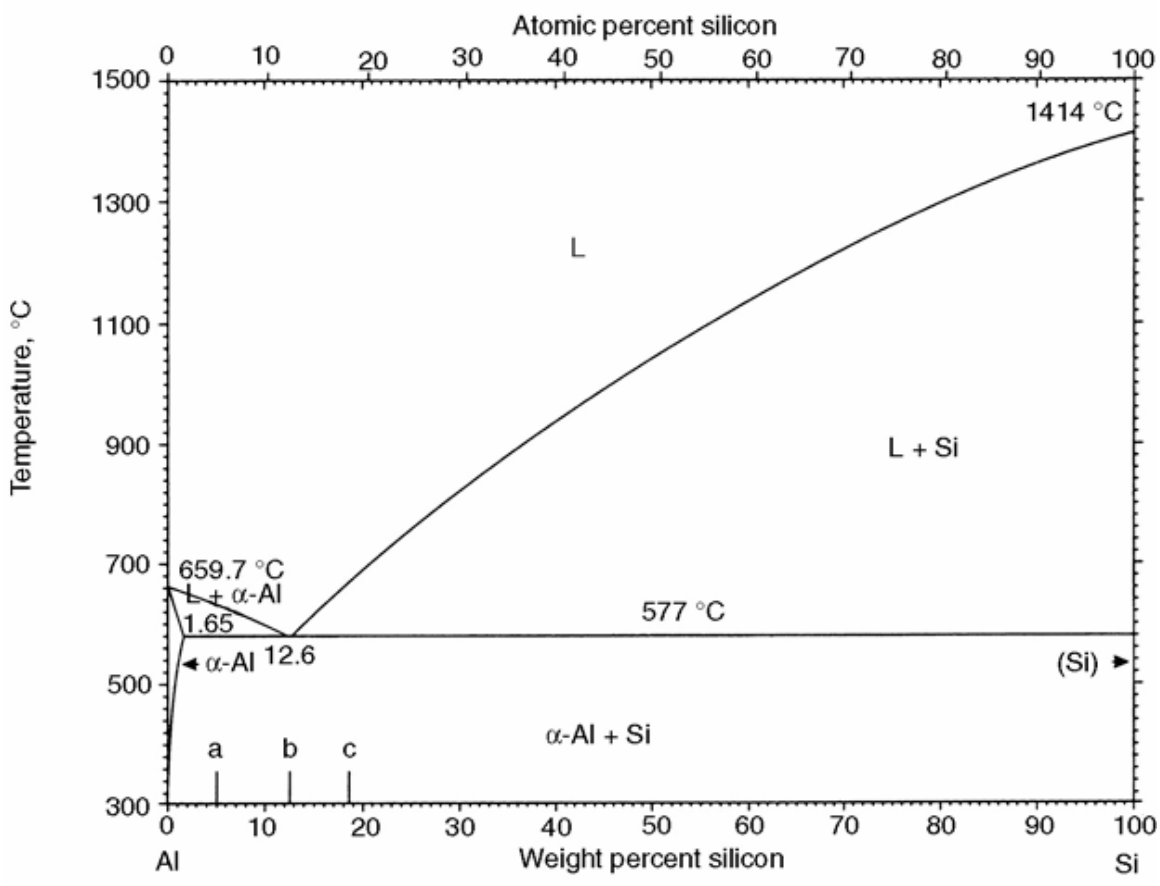

Figure 3.1: Equilibrium aluminum – silicon phase diagram

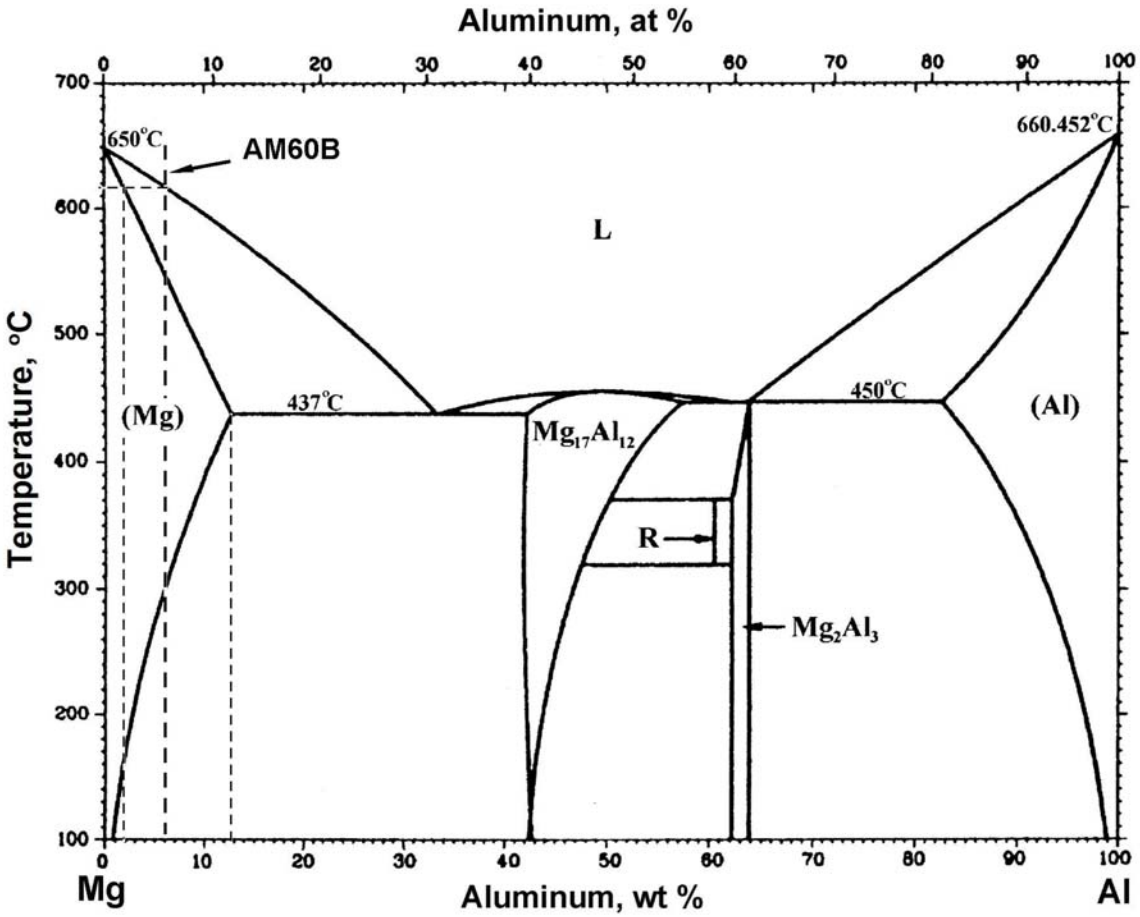

Figure 3.2: Equilibrium magnesium – aluminum phase diagram showing the liquidus and solidus of AM60B and its solid phases.

positioned inside the melt, one in contact with the inner wall of the crucible (T_w) and the other in the center of crucible (T_c). The outputs from the thermocouples were connected to a computer (via amplifiers and a multiple-channel A/D converter) where temperature / time data were recorded with a *Labview* program. The thermocouples used were calibrated before and after each series. When T_c reached 630 °C, ultrasonic vibration with an amplitude of 56.7 μm was started. For comparison reasons, experiments without ultrasonic vibration were also carried out.

The graphite crucible was in a bugle shape and held about 200 g of molten aluminum.

For each experiment, two cooling curves were constructed directly from the data collected from both thermal couples. The cooling curve of the center thermal couple shows the start of both the solidification process and the main eutectic reactions.

The first derivative of the curve of the center thermal couple was calculated. It gives the direct cooling rate at each temperature/time. The increase or decrease of the derivative indicates the change of cooling rate, or perhaps a formation of a new phase.

A third curve was calculated by subtracting T_w-T_c. This figure gives further detailed information on when the nucleation of each phase happens. The shaded area under the curve between each reaction indicates the duration of the reaction.

3.2.2. Solidification of aluminum alloys

These experiments were carried out in two groups: isothermal processing and intermittent processing. Before ultrasonic processing, the A356 alloy was melted to a temperature of 650 °C; while the ultrasonic radiator was preheated to this temperature then dipped into the melt. With the ultrasonic radiator inserted into the melt, the melt was kept at this temperature for 30 minutes. For the isothermal processing, the melt was then cooled down to a temperature near the liquidus (614 °C or 610 °C) and subjected to ultrasonic vibration for a given time (5, 10 and 20 sec). After processing, the melt was poured into a metal mold or clay-graphite crucible to solidify at two different cooling rates. For the intermittent processing, first the cover of the furnace was removed in order to cool down the melt with a rapid cooling rate. While the temperature was decreasing,

the melt was subjected to ultrasonic vibration for a certain time (5sec, 10sec, 20sec) at each temperature of 614°C, 610°C, 605°C, 600°C, 595°C, 590°C, 585°C, 580°C, 575°C or ultrasonically vibrated continuously from 614°C to 575°C. The ultrasonic system did not function when the melt reached 574°C since the solid fraction was too high.

Another method of application was investigated by vibrating the solid part of the solidifying sample. Accordingly ingots of tested material were melted in a 10 kg capacity SiC crucible using an electrical resistance furnace. The melt temperature was kept at a temperature about 50 to 150°C higher than the liquidus temperature of the alloy to allow for the complete dissolution of all elements during melting. The molten alloy was then poured into a copper or graphite mold which held up to 250 g of molten aluminum or 1 kg of steel 4340 alloy at various pouring temperatures. The ultrasonic vibration was started right before the melt was poured into the copper mold. In order to obtain the optimum condition for grain refinement, parameters such as vibration amplitude, vibration time, and pouring temperature of the melt were controlled. During the processing, the actual power output varied in the range of 5 to 75% of the nominal power capacity of the ultrasonic unit.

3.2.3. Solidification of AM60B alloys

The alloy was melted and held in a furnace for half an hour at 750 ± 5 °C, about 130 °C higher than its liquidus temperature. The molten alloy was then poured into a permanent copper mold at various pouring temperatures. During the melting and casting process, a sulfur hexafluoride gas was used for the protection of the magnesium alloy from igniting or oxidizing. Ultrasonic vibration with full amplitude was started right before the melt was poured into the mold. For comparison reasons, samples without subject to ultrasonic vibration were also made. The castings were hemispherical in shape with diameter of 5 cm and weight of 160 grams.

3.3 Experimental setups

An ultrasonic unit with high power capacity was used in this study. It consists of a 1500 watt electric power supply, a 20 kHz acoustic generator, an air cooled converter which was made of piezoelectric lead zirconate titanate crystals (PZT), a booster, a probe, and

an acoustic radiator made of titanium alloy Ti-6Al-4V. The ultrasonic amplitude can be continuously adjusted from 30% to 100% or 81 μm, which is the maximum amplitude of the unit.

Figure 3.3 is the setup for experiments when the ultrasonic vibrations were introduced into the melt from the top part. A pneumatically operated device moved the acoustic radiator up and down. The time to preheat the extender and to dip it into the melt can be precisely controlled.

Figure 3.4 is the setup for experiments when the ultrasonic vibrations were introduced into the melt from the bottom part. Fig 3.5 is the schematic of the sample.

3.4 Chemical etch of samples

Different etchants were used for different alloys.

For A356, 354, and 319 alloys, modified Keller's reagent, which is a solution of 95 ml H_2O, 2.5 ml HNO_3, 1.5 ml HF, and 1 ml HCl.

A356 was deeply etched with 0.5 % HF water solution to reveal the 3 – dimensional morphology of eutectic silicon.

For wrought aluminum alloys such as 3004, 6061, and 6063, the as-polished samples were mildly etched using a solution of 84 ml H_2O, 15.5 ml HNO_3, 0.5 ml HF, and 3 g CrO_3 so the grain size was revealed.

For AM60B alloy, the as-polished samples were slightly etched using a solution of 10 ml H_2O, 100 ml Ethyl Alcohol, 5 ml Acetic Acid, and 6 g Picric Acid.

3.5 Quantitative metallography

Quantitative metallographic analyses of aluminum rich primary α grains and eutectic Si particles were conducted using an image analysis software, Image-Pro Plus (version 5.0). For the characterization of primary α grains, the average area, particle size, and roundness were measured. The quantitative characterization of eutectic Si included particle area, length, and roundness. Furthermore scanning electron microscopy (SEM) was used for the observation of the three-dimensional eutectic Si morphology of the specimens deep-etched using a 0.5% HF- water solution.

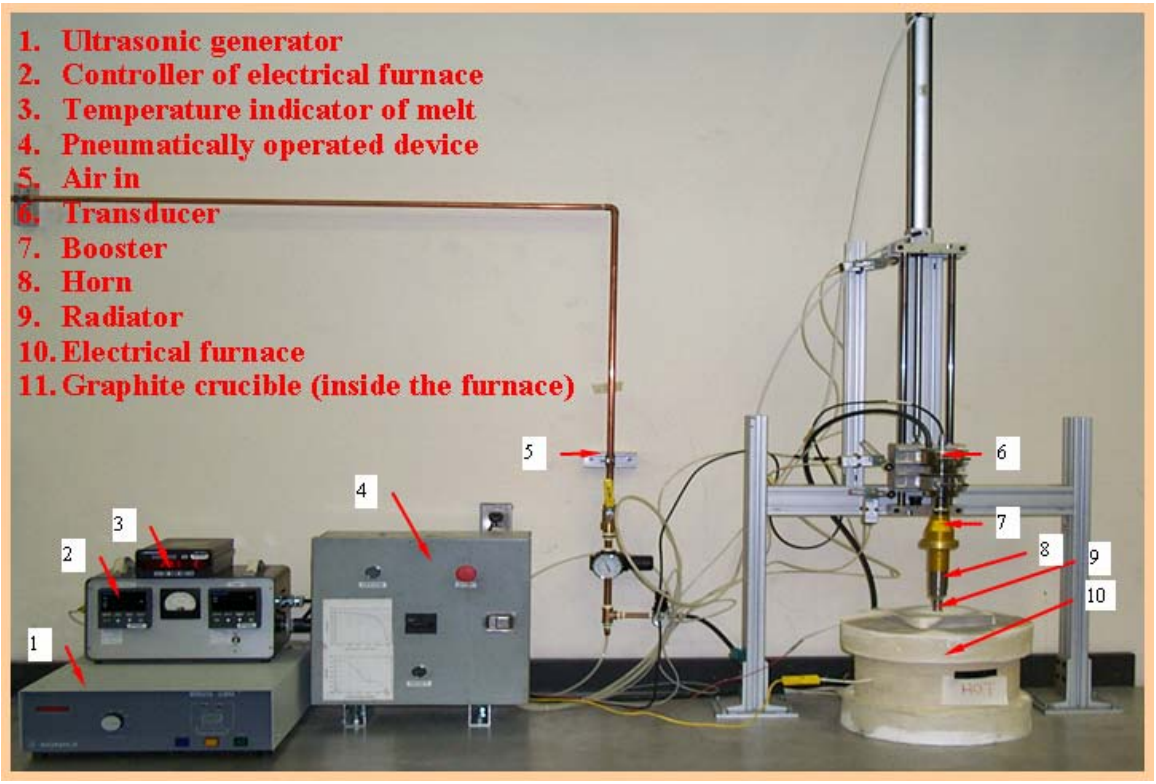

Figure 3.3: The experimental apparatus for the ultrasonic vibrator/metal injection assembly at the top of the melts.

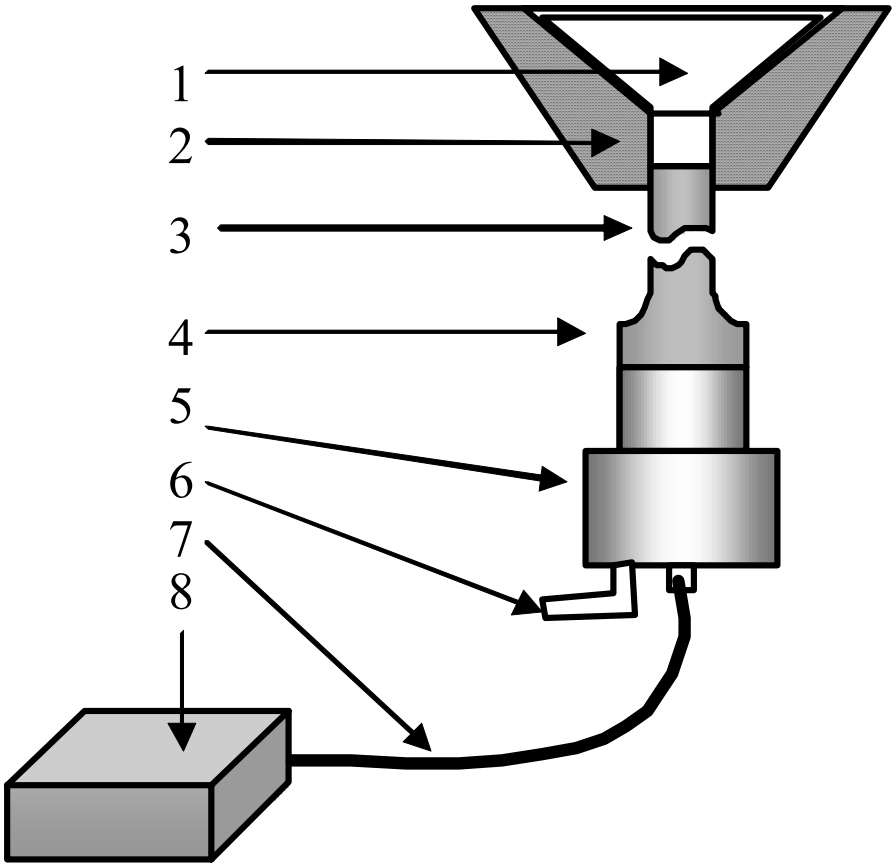

(1) Sample, (2) Copper mold, (3) Radiator, (4) Probe, (5) Transducer and Booster, (6) Inlet for compress cold air, (7) Ultrasonic power cable (8) Ultrasonic generator.

Figure 3.4: Schematic experimental setup for the ultrasonic vibrator/metal injection assembly at the bottom of the melts

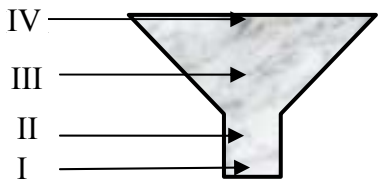

:I) near the radiator; II) an area between the radiator and the bulk area; III) the bulk area; IV) the top of the sample.

Figure 3.5: Schematic illustration of the positions of the sample in Figure 3.4

ASTM standard methods were used to determine grain size. Two parameters were measured to quantitatively characterize the primary fcc aluminum grain structure. These parameters are the average grain size (D) and the Roundness (Rn) of the grains. The average particle size is defined as:

$$D = 2 \times \sqrt{\frac{A}{\pi}} \tag{3}$$

where A is the area of a grain. The average grain size and its standard deviation were obtained based on the measurements over 2000 grains. The Roundness (Rn) is defined as:

$$Rn = \frac{4\pi A}{P^2} \tag{4}$$

where P is the perimeter of the particle. The maximum of Rn is 1 when the particle is a perfect sphere. Particles become less spherical at lower Rn values.

3.6 Thermodynamic simulations

In practice, the solidification process is basically a non-equilibrium process that can be simulated by Scheil Model [9, 10], which assumes local equilibrium at solid/liquid interface, no diffusion in the solid, and complete mixing in the liquid. With these assumptions, the thermodynamical simulation of the solidification of the alloys of interest were carried out. The results are demonstrated in Figure 3.6 - 11.

For A 356 alloy, Commercial A356 alloy was used for the experiments. Thermodynamic simulation results show that, as seen in Figure 3.6, the liquidus temperature of this alloy is 614 °C and the solidus temperature is 554 °C.

For AM60B alloy, as shown in Figure 3.11, at first, magnesium-rich dendrites form and grow (starts at 617 °C). As solidification progress, solutes build up in the liquid, resulting in the occurrence of some other reactions (i.e., eutectic reaction starts at 429 °C) and the formation of some intermetallic compounds (such as β-$Mg_{17}Al_{12}$) in the liquid among the dendrites arms and grains. The temperature of the last drop of liquid can be as low as 334 °C.

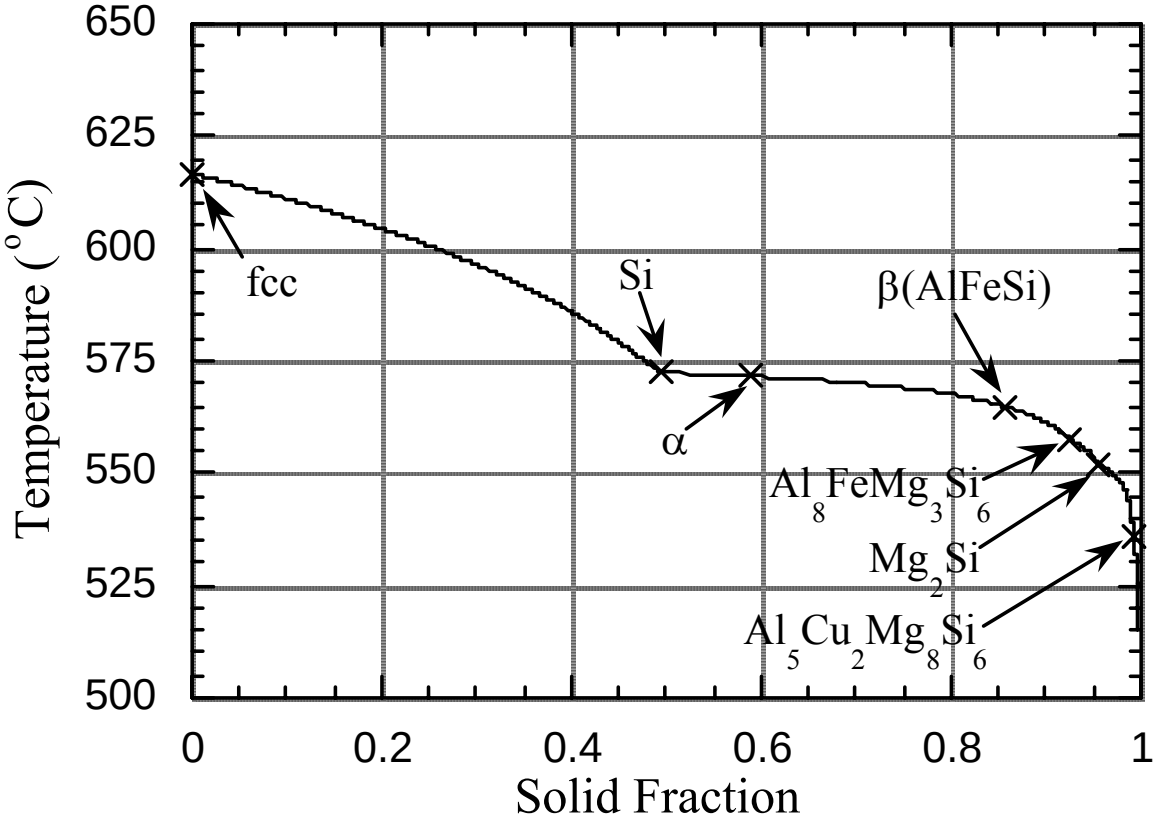

Figure 3.6: The temperature versus solid fraction curve of A356 alloy. The numbers and arrows indicate the solid fraction at which phases start to precipitate.

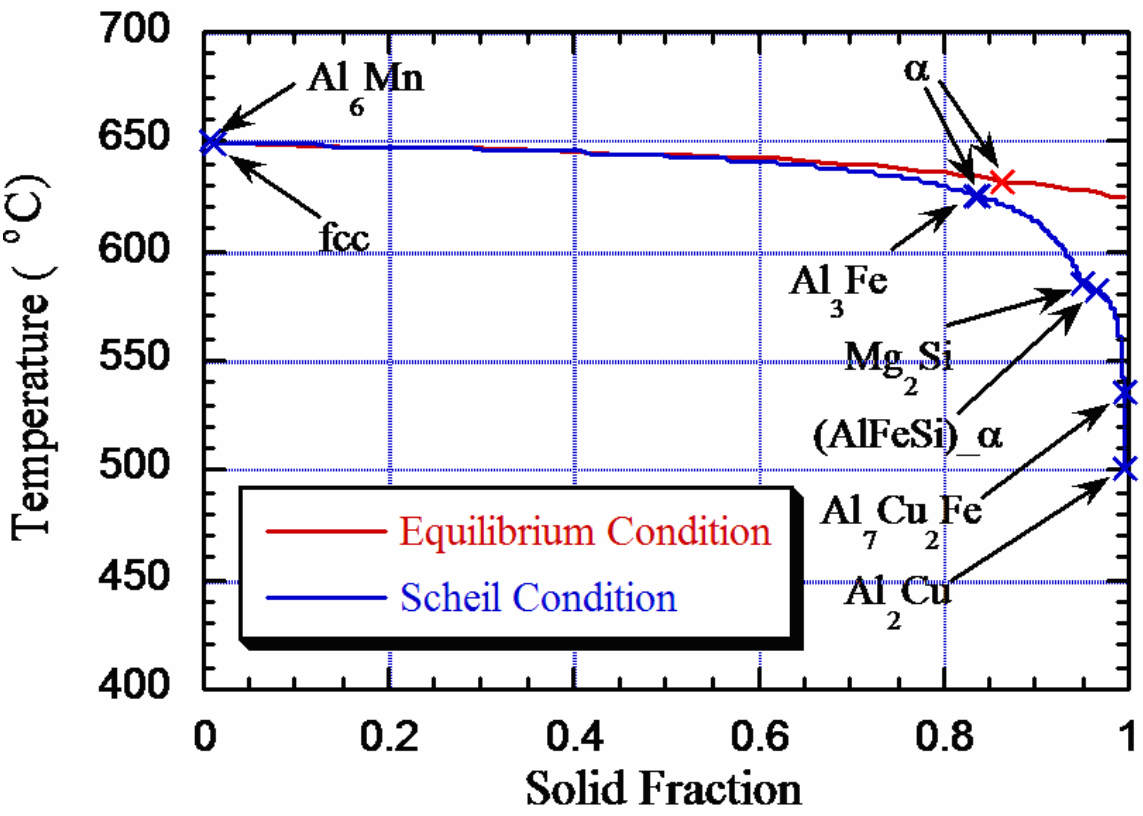

Figure 3.7: The temperature versus solid fraction curve of 3004 alloy. The numbers and arrows indicate the solid fraction at which phases start to precipitate.

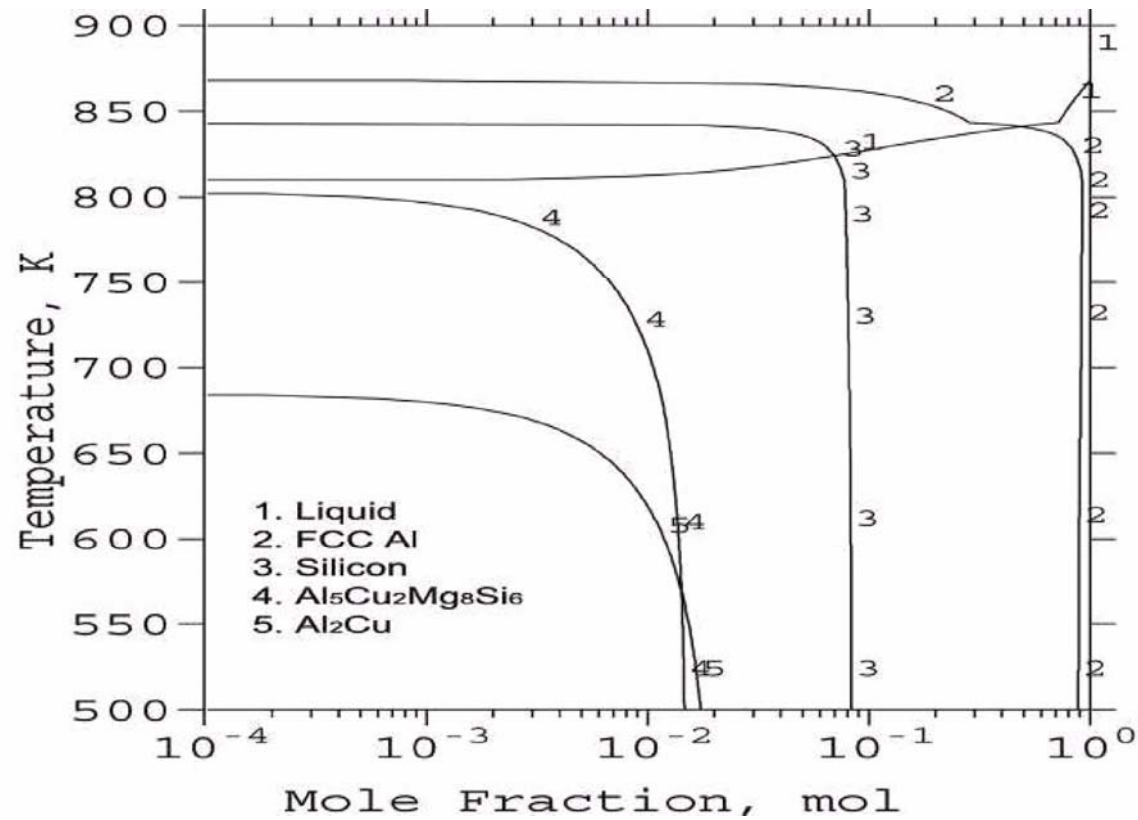

Figure 3.8: The temperature versus solid fraction curve of A354 alloy. The numbers and arrows indicate the solid fraction at which phases start to precipitate.

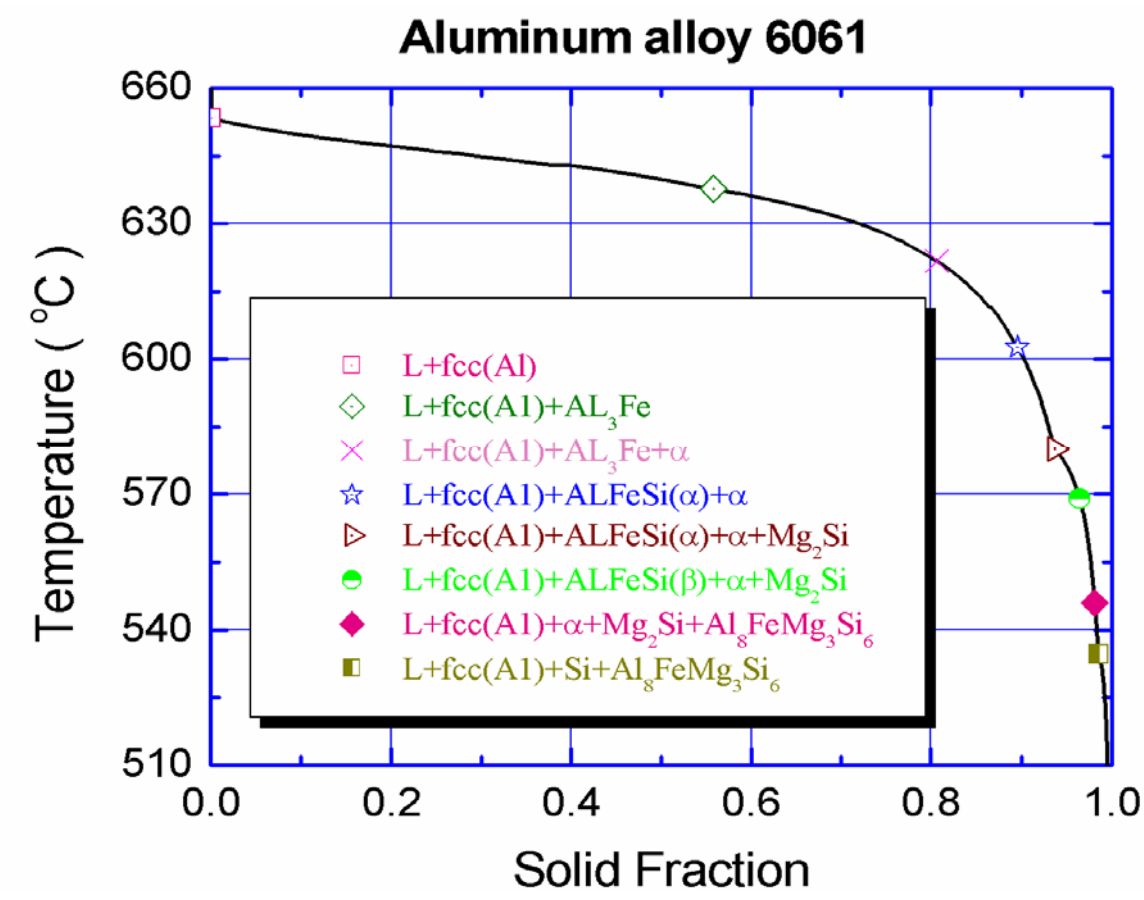

Figure 3.9: The temperature versus solid fraction curve of 6061 alloy. The numbers and arrows indicate the solid fraction at which phases start to precipitate.

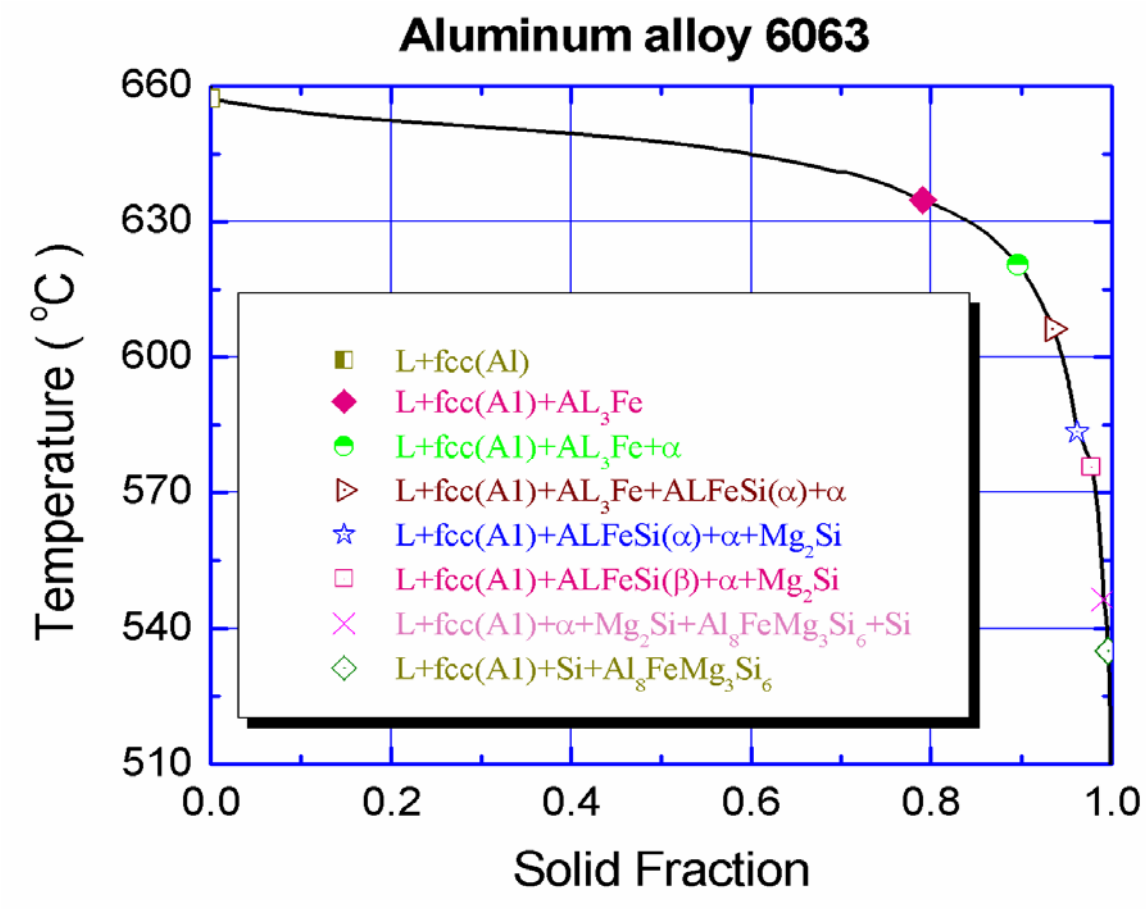

Figure 3.10: The temperature versus solid fraction curve of 6063 alloy. The numbers and arrows indicate the solid fraction at which phases start to precipitate.

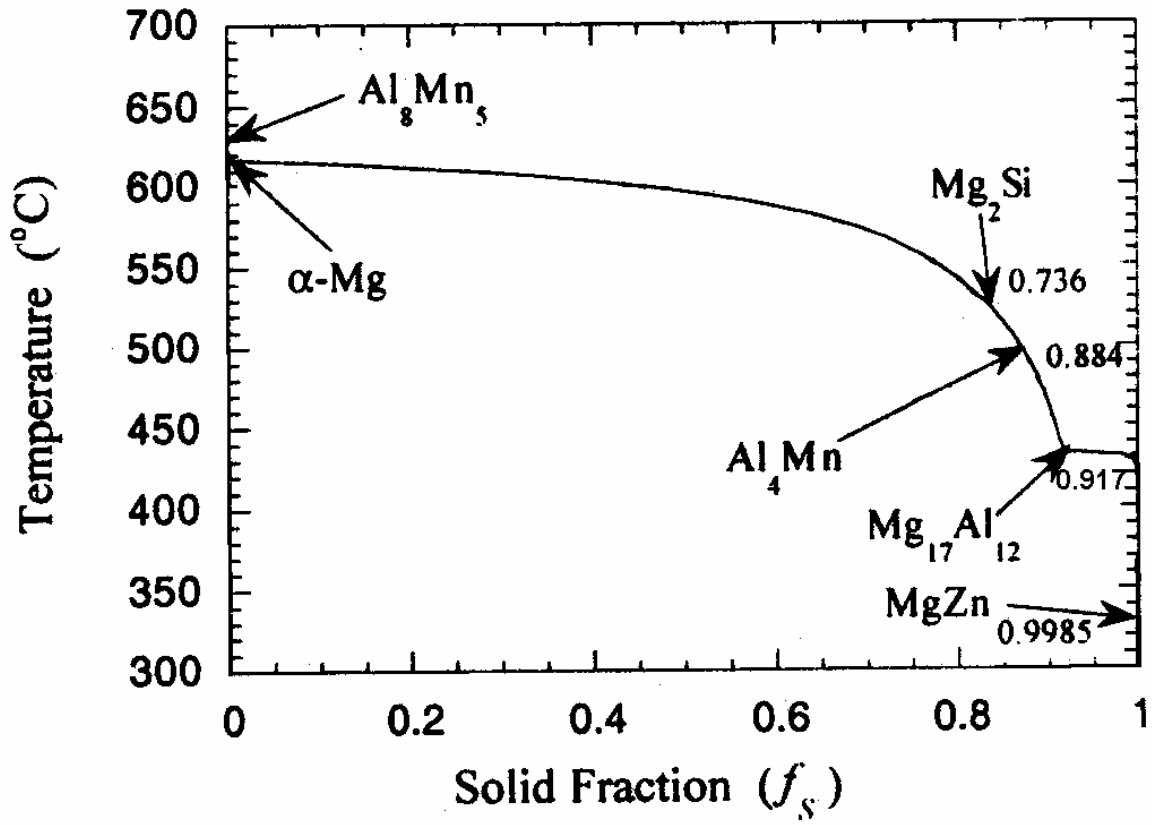

Figure 3.11: The temperature versus solid fraction curve of AM60B alloy. The numbers and arrows indicate the solid fraction at which phases start to precipitate.

3.7 Technical approach

It was hypothesized in this work that if acoustic energy were introduced into molten materials (aluminum alloys and magnesium alloy), the microstructure of the as-cooled material would be modified. Hopefully this modified microstructure would exhibit superior mechanical properties. This approach consisted of exposing molten metal samples to ultrasonic vibration of a certain intensity, amplitude, frequency and with a given exposure time. For the purpose of proof of principle, eight tasks were envisioned and carried out.

Task 1 Design of experimental apparatus

In this task, an experimental apparatus for various ultrasonic processing methods was designed and built. The critical task for the experimental apparatus was the design of the ultrasonic vibrator/metal injection assembly at the top or bottom of the metal mold. The assembly consists of an ultrasonic radiator/horn that injects ultrasonic energy into the molten metal, an ultrasonic transducer, a ram that connects to a piston to push the semi-solid billet out of the mold. The weight of the billet varied from 250 g to 2000 g. Work was carried out to develop a coating for the protection of the acoustic radiator from high temperature molten metals. Z-guard was selected since it was shown to provide the optimum protection.

Task 2 Thermodynamic simulations

In this task, thermodynamic simulation was done using the Scheil model to determine the solid fraction versus temperature curves of the aluminum alloys of interest, namely A 356, A354, 319, 6061, 6063, 3004, and a magnesium alloy, AM60B steel. The simulation assumes local equilibrium at the solid/liquid interface, no diffusion in the growing solid and complete mixing in the liquid. The developed relationship between solid fraction and temperature was used in the following tasks.

Task 3 Grain refinement of aluminum alloys

In this task, samples solidified under the influence of ultrasonic energy were sectioned for characterization. Grain morphology, grain size and size distribution were measured. The results showed that ultrasonic vibrations were very effective in production of fine globular grains.

Task 4 Secondary phase modification of aluminum alloys

In this task, the secondary phases modified by ultrasonic vibration were investigated. The morphologies of second phases were refined and modified in morphology. The measured results were correlated to the parameters such as ultrasonic frequency and power, solid fraction at which the ultrasonic energy is applied, and the cooling rates of the melt.

Task 5 Microstructure modification of AM60B alloy

In this task, the microstructural modification to AM60B alloy was demonstrated using ultrasonic energy. Results show a significant difference between the conventionally processed samples and those that had acoustic energy applied. Both primary α-magnesium grains and eutectic phases were refined and modified in a beneficial way.

Task 6 Parameters of ultrasonic processing

In this task, parameters for industrial applications of ultrasonic processing were developed, such as methods of introducing ultrasonic energy into the melt, amplitude and intensity of ultrasonic vibrations, ultrasonic exposure/time, sample cooling rates, and sample casting temperature.

Chapter 4

Results and Discussions

4.1 Thermal analysis of the solidification of A356 alloy

Thermal analysis is a handy tool for the investigation of the solidification process. This investigation employed thermal analysis for single-cooling and differential analysis of two-cooling curves. The results show elevated solidification temperatures T_G, T_N and T_{Min}, and all changed solidification reaction temperatures/durations in casting with ultrasonic vibration.

4.1.1. Introduction

Thermal analysis is a handy tool for the investigation of the solidification process, and has been use extensively [106 -119]. Various methods may be used to determine the solidification curve of the alloy. A direct method is to quench the solidifying samples at different temperatures (thus different solid fraction) then to determine the reactions at different stages of solidification [110, 111]. The difficulties involved in this method such as nonuniformity is a hindrance for its application. Another technique Differential Thermal Analysis (DTA) deals with the measurement of the temperature difference between the sample and an inert reference material by subjecting both of them to identical temperature-controlled heat-treatments. This method is applied to either detect the absorption or evolution of heat by comparing the temperatures of a sample and a reference that both are subjected to the identical conditions, or to study thermal properties and phase changes which do not lead to a change in enthalpy by subjecting two

references to heat-treatments that are not identical. A related technique, differential scanning calorimetry (DSC) has been developed by studying the differences in energy required to maintain the sample and reference at an identical temperature. DTA is often applied to study the solidification of Al-Si alloys [112-116].

In the study of the solidification process, a simple and traditional way is to just record the cooling curve of a location in a solidifying sample. Some major reaction temperatures can be projected from the plot of temperature against solidification time. In order to obtain the detailed information on the reactions during a solidification process, a technique based on this method and DTA has been develop, which is focused on the measurement of the temperatures of a solidifying sample at the locations of both the center (Tc) and the fringe (a common practice is the place near the wall of the crucible, or Tw). By comparing the plotted curves of Tc –Tw vs. t (solidification time), ΔT (the temperature differential between Tc and Tw) vs. t, and dT_C/dt vs. t, the reactions during the solidification process can thus be precisely determined [117-119]. This section employed these two methods to compare the solidification process without and with ultrasonic vibration.

4.1.2. Experimental conditions

Commercial aluminum A356 alloy and an ultrasonic unit described in Figure 3.4 were used in this study.

The material was melted in a clay-graphite crucible inside a resistance furnace, and kept at a temperature of 750 ºC for 30 minutes until it had attained thermal equilibrium. The clay-graphite is bugle shaped, as shown in Figure 4.1, and holds up to 250 g of molten aluminum alloy. Two thermocouples were positioned in the melt, one in contact with the inner wall and the other in the center of the crucible, as shown in Figure 4.1. The outputs from the thermocouples were connected to a notebook computer (via amplifiers, a multiple-channel A/D converter, and Labview programming). Thereafter the crucible with the thermocouples and the melt were taken out of the furnace to allow a moderate cooling rate. During the cooling and the subsequent solidification process, the

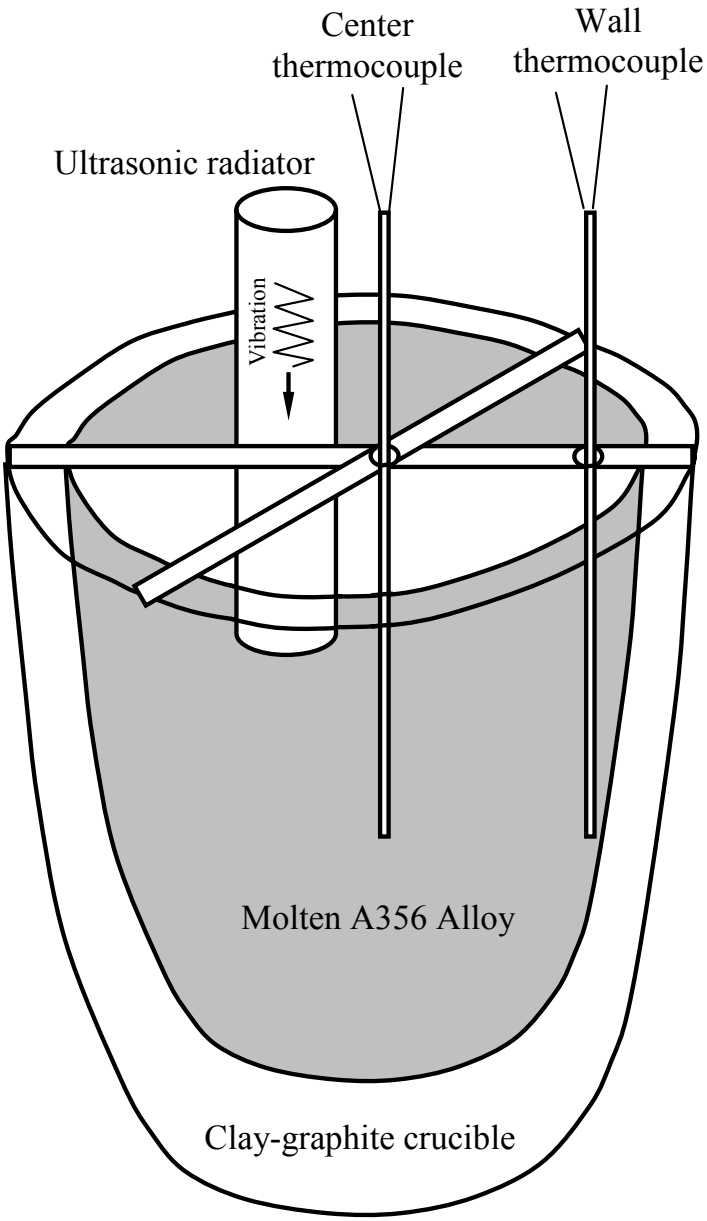

Figure 4.1: Location of thermocouples at the wall and center of sample crucible

temperature / time data were recorded and later processed in various ways. The thermocouples used were calibrated before each series of experiments.

In the experiments with ultrasonic vibration, the head of the ultrasonic radiator was preheated to 650 ºC in the furnace until temperature equilibrium was reached when the temperature of the melt reached 650 ºC, the radiator was inserted into the melt at the position shown in Figure 4.1 and ultrasonic vibration was turned on subsequently (when the melt temperature reached 630 ºC). An ultrasonic vibration with the amplitude of 100%, i.e. 56.7 μm (the maximum amplitude when the booster is not used in the ultrasonic system), was applied.

4.1.3. Results and discussion

The simple cooling curves of the center of the castings without and with ultrasonic vibration are shown in Figure 4.2. Without ultrasonic vibration, the solidification started at the point (30 second /~614 ºC), and the main eutectic reaction, i.e., the precipitation of eutectic aluminum, silicon, and some iron/manganese-containing particles, started at the point (280 second / 574 ºC), and finished at the point (500 second / 560 ºC). A simple calculation indicates that the precipitation of primary fcc aluminum lasted about 250 seconds, while the precipitation of the main eutectic lasted about 220 seconds. It took about 130 seconds (630 second minus 500 second) to cool down from 560 ºC to 500 ºC.

For the casting with ultrasonic vibration, the solidification started at the point (10 second /~618 ºC), and the main eutectic reaction, i.e., the precipitation of eutectic aluminum, silicon, and some iron/manganese-containing particles, started at the point (410 second / 574 ºC), and finished at the point (630 second / 560 ºC). The precipitation of primary fcc aluminum lasted about 400 seconds, while the precipitation of the main eutectic lasted about 220 seconds. It took about 140 second (770 second minus 630 second) to cool down from 560 ºC to 500 ºC.

Compared to the casting without ultrasonic vibration, it took a much longer time to finish the precipitation of primary fcc aluminum, and almost the same amount of time to finish the major eutectic reaction and the rest of the cooling process (from 560 ºC to 500 ºC). It implies that extra energy was involved in the solidification process of the

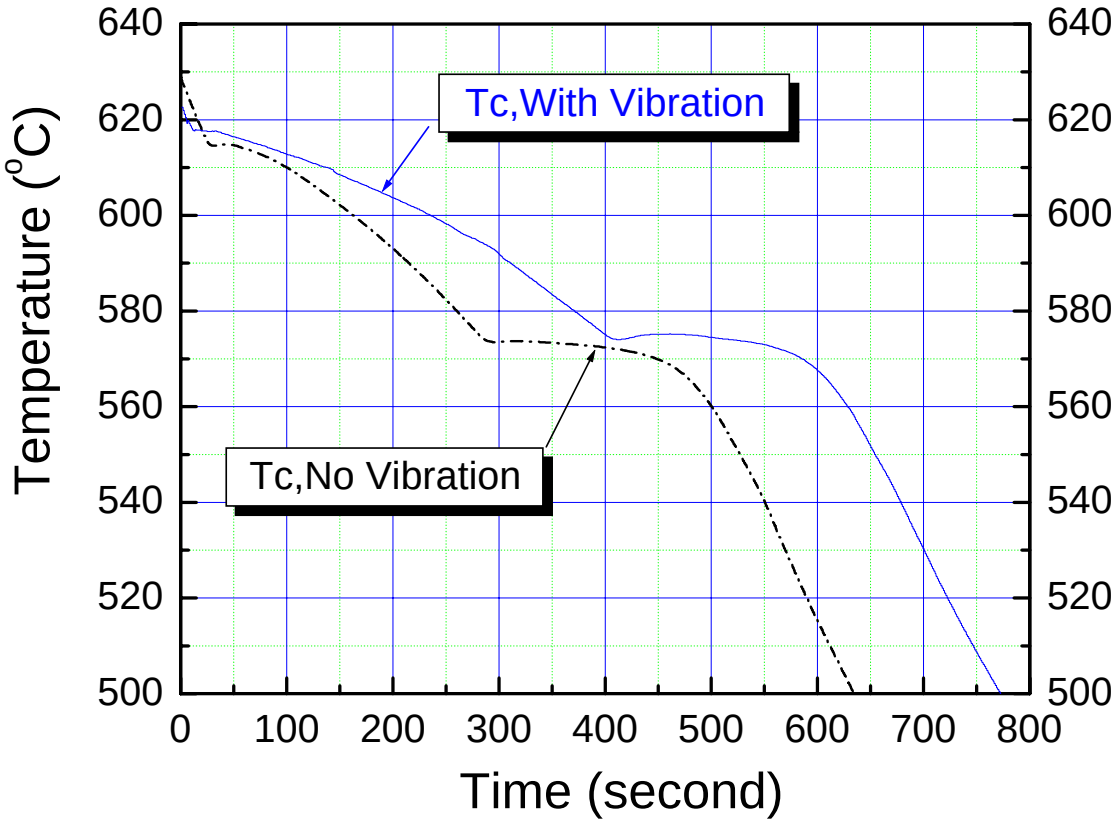

Figure 4.2: Cooling curve collected from the thermocouple placed in the center of an A356 alloy casting (a) without and (b) with ultrasonic vibration.

casting with ultrasonic vibration. It can be concluded that the extra energy is from ultrasonic vibration. Furthermore, the major eutectic reaction starts at about 50% solid fraction, when the primary fcc aluminum grains began to contact each other and form a network. Thereafter ultrasonic vibrational energy barely goes to the solidifying specimen. It is physically reasonable that the already-solidified part of the specimen which contacts the ultrasonic radiator gives greater acoustic impedance (than that in the liquid/semi solid state) for the ultrasonic energy to pass onto the specimen after that point.

The first derivatives of the cooling curves of both castings without and with ultrasonic vibration were calculated and are plotted in Figure 4.3. Detailed discussion of the meaning of this drawing may be found in references 112 and 118. The derivative at each point of the curve is numerically equal to the slope of the cooling curve, and corresponds to the cooling rate of the specimen. When the derivative increases, some reactions are in progress and are releasing heat from the specimen so the cooling rate decreases, like the appearance of a new phase.

For the casting without ultrasonic vibration, at section 1 of the curve, the derivative shoots rapidly up to a maximum then back down. This is because of a sudden nucleation of aluminum grains in the specimen. At the subsequent section 2, due to decrease of nucleation rate (lower temperature involved) and the frontal growth of aluminum dendrites occurs into the center of the sample from the slightly cooler walls, the derivative decrease. At section 3, the derivative differs from section 2 in that the dendrites thicken and fill the casting. At section 4, the sudden nucleation and growth of the silicon phase induces another rapid increase of the derivative. The continuing growth of the silicon phase slows down in section 5. At section 6, the formation of Mg_2Si brings about a miniature increase in the derivative. When the solidification ends, the cooling curve came back to the green line (the baseline when no nucleation/crystal growth is present, which goes nearer to zero as time elapses), which is shown in section 7.

By comparing the derivative curve to that of without ultrasonic vibration, it may be observed that in the casting with ultrasonic vibration, 1) a higher level of sections 2, 3, and 4, indicates the injection of ultrasonic energy into the system; 2) a less difference between section 2 and 3, implies the difference between dendrites nucleation/growth and

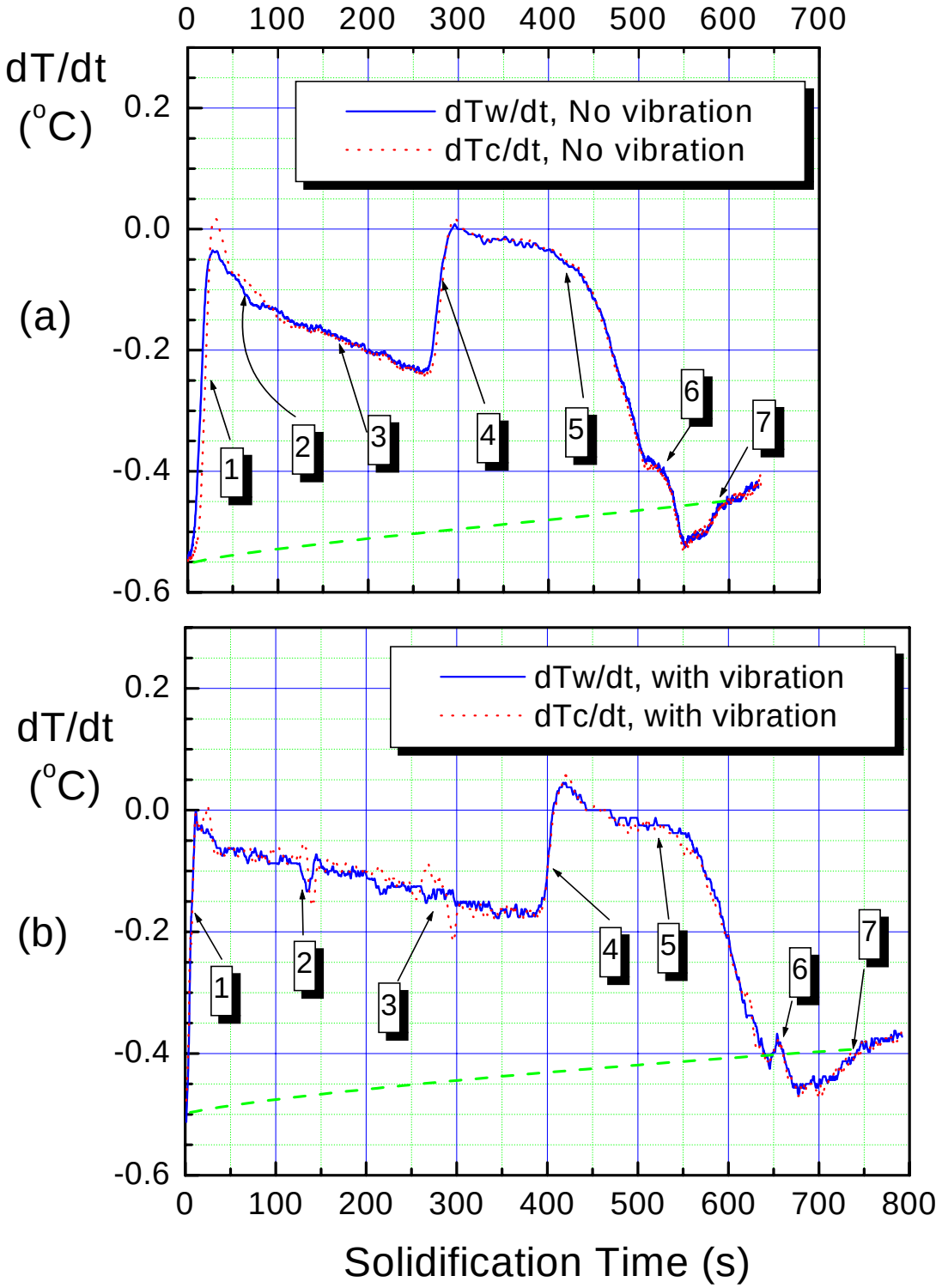

Figure 4.3: The first derivative of the curve shown in Figure 4.2 (a) without and (b) with ultrasonic vibration.

thickening is less significant, or even no dendritic grains formed. The microstructural observation in the later sections proves this point, that fine globular primary fcc grains were formed while ultrasonic vibration is present; 3) longer sections 2 and 3, which are also affected by the injection of ultrasonic energy; 4) a more significant section 6, might indicate more Mg_2Si has been formed.

The first part of a cooling curve encloses some noteworthy information, such as the three parameters:

T_G: steady state growth temperature of the melt under the cooling conditions prevailing;

T_{Min}: the lowest temperature during the supercooling, which is the balance point when the latent heat released from the newly nucleated crystals catches up to the heat exiting from the casting to the environment.

t_{Rec}: the recalescence period, i.e., the period between the T_{Min} and T_G, or the period when the casting is actually heating up because of the latent heat released.

In the casting without and with ultrasonic vibration, the first parts of the cooling curves are shown in Figure 4.4 (a) and (b), respectively. From both figures, the three parameters were read and listed in Table 4.1.

From Table 4.1, it is obvious that all three temperatures were significantly increased in the casting with ultrasonic vibration. It is understandable when connected to the ultrasonically induced cavitations, which cause a localized temperature drop (does not

Table 4.1: The three parameters observed in the first part of a cooling curve

PARAMETER	CASTING WITHOUT ULTRASONIC VIBRATION	CASTING WITH ULTRASONIC VIBRATION
T_G	615 ºC	620.2 ºC
T_{Min}	614 ºC	620
t_{Rec}	17 seconds	1 seconds

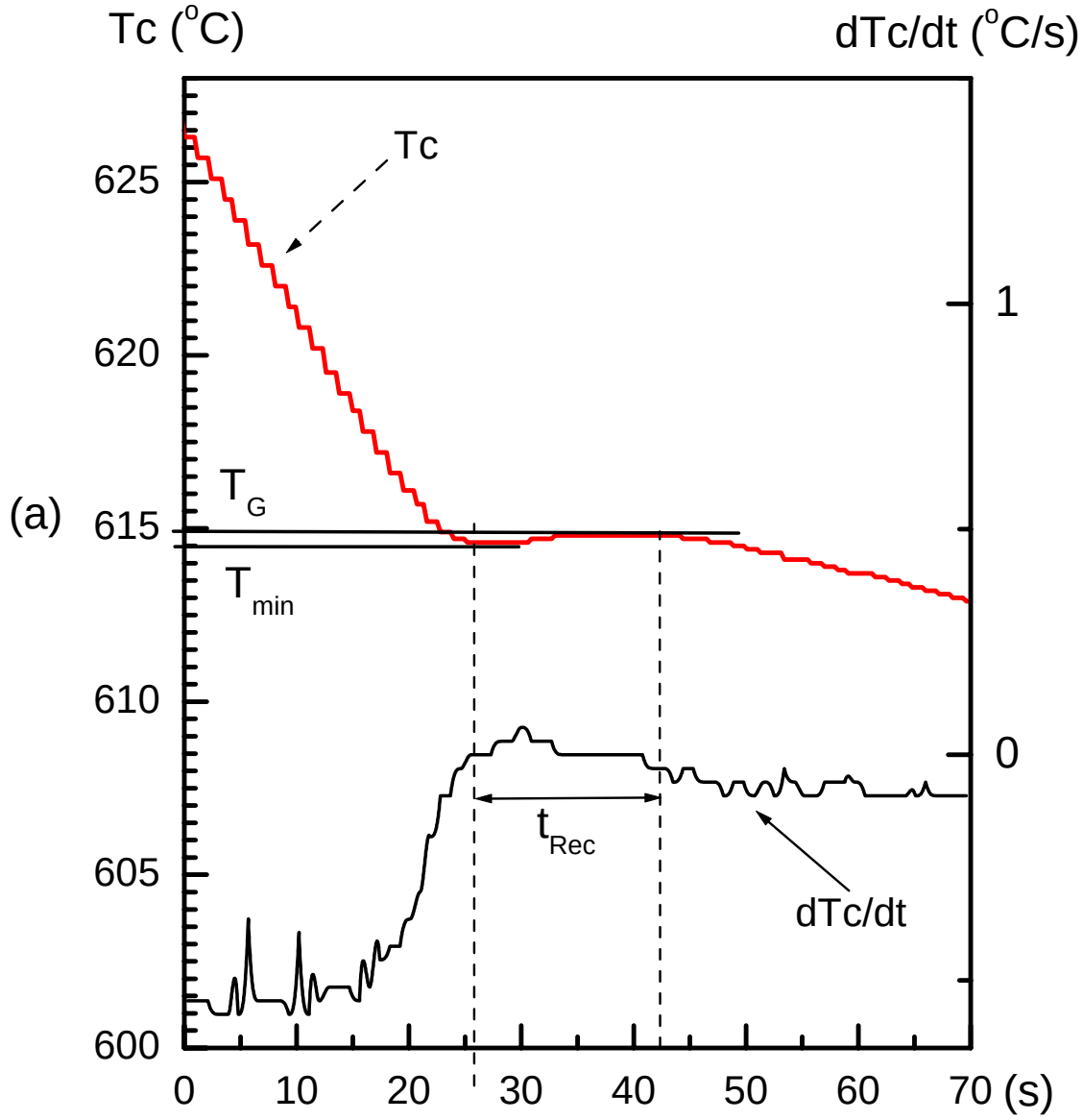

Figure 4.4: First part of a cooling curve and its derivative collected from the thermocouple placed in the center of an A356 alloy casting (a) without and (b) with ultrasonic vibration. (Continued on the next page)

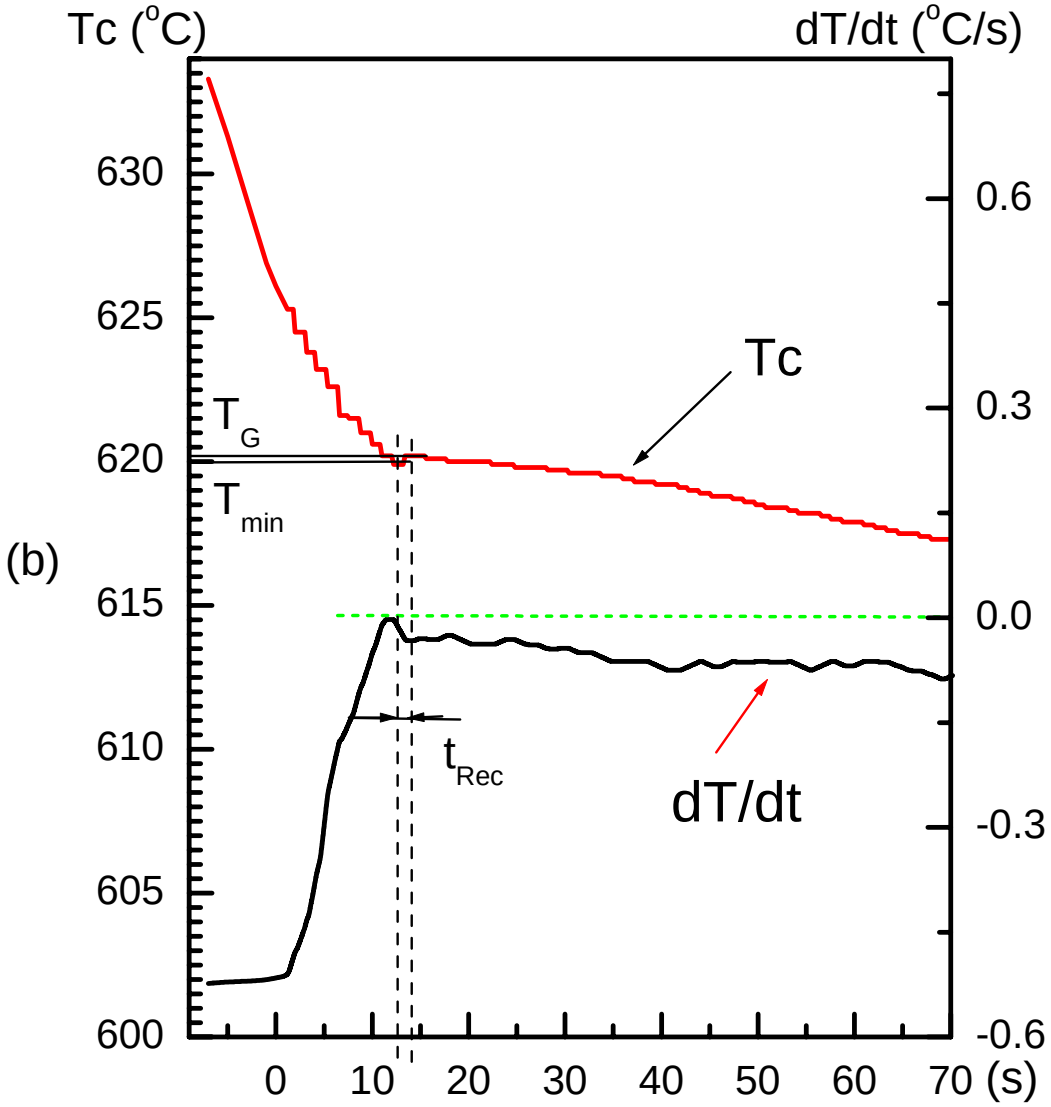

Figure 4.4 (continued)

affect the system measured temperature) and increase the nucleation rate at a higher temperature, so less supercooling is needed. However, a significantly shorter recalescence time t_{Rec} is also observed. It is possibly because both a lower nucleation rate (because of the higher temperature) and a primary fcc aluminum grain growth rate were involved at the beginning of the solidification process. On the other hand, from the discussion in the Chapter 2, it is known that with ultrasonic vibration, the nucleation rate increased considerably. So a much slower grain growth rate could be the only reason. The solid faction is a function of the solidifying temperature. With ultrasonic vibration, the injected ultrasonic energy slows down the cooling rate thus induces the decrease in the grain growth rate.

For casting without ultrasonic vibration, most of the heat is extracted from the system through the wall of a crucible. So the melt near the wall of the crucible first experiences the supercooling thus the nucleation and the grain growth. It is expected then that the temperature collected from the wall is always lower than that of the center. On the other hand, for the casting the ultrasonic vibration, most of the heat is extracted from the system through both the wall of a crucible and the ultrasonic radiator which is made of Ti6Al4V alloy, a far better heat conductor than the clay-graphite, i.e., the material for the crucible. So the melt near the center of the crucible (i.e., near the radiator, as shown in Figure 4.1) would experience a faster cooling than that near the wall of the crucible. Therefore it can be expected that the temperature collected from the center could be even lower than that near the wall.

Cooling curves collected from the center and wall of the crucibles without and with ultrasonic vibration are illustrated in Figure 4.5 (actually, the Tc is the same as that shown in Figure 4.2). As expected, in the casting without ultrasonic vibration, the temperature near the wall is lower than that of the center; while in the casting with ultrasonic vibration, the temperature at the center is lower than that near the wall. Another noteworthy phenomenon is that, as shown in the smaller figure in Figure 4.5, in the casting without ultrasonic vibration, both T_{Min} points are at the same temperature (about 614 ºC), which implies that the solidification process (reactions) is homogeneous in this casting; however in the casting with ultrasonic vibration, the T_{Min} point from the

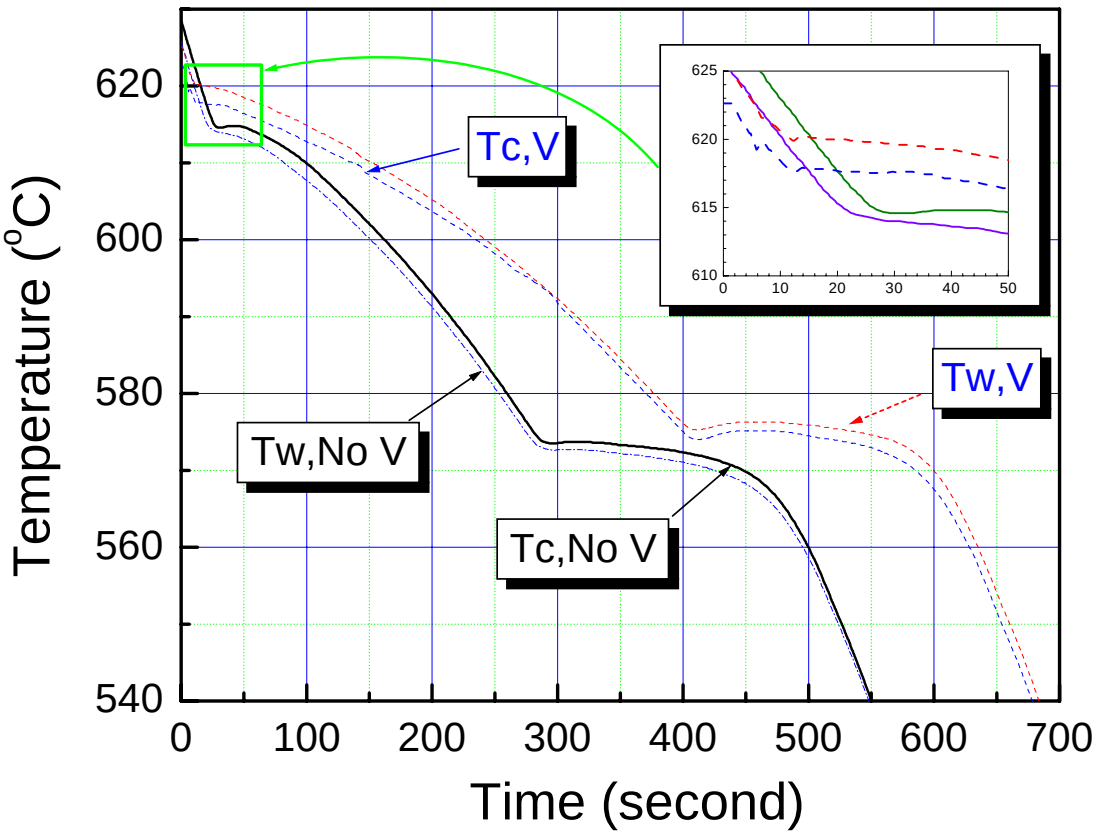

Figure 4.5: Cooling curve collected from the thermocouple placed in the center and the wall of an A356 alloy casting (a) without and (b) with ultrasonic vibration.

wall is higher (about 3 ºC) than that from the center. This significant difference suggests that ultrasonic vibration has produced an inhomogeneous solidification in the melt, in other words, that ultrasonic vibration has elevated the liquidus of the alloy. This effect is probably because ultrasonic vibration has an influence on the free energy necessary for the different phases in the alloy to solidify.

The magnitude of the temperature difference is plotted in Figure 4.6. In the casting without ultrasonic vibration (Figure 4.6a) of the ΔT curve, seven different regions may be distinguished. In region 1, the primary fcc aluminum starts to nucleate and the released heat causes the rise of the curve. In region 2, while the ΔT curve is going back down, a slight slope change can be seen which implies uneven grain growth of the dendrite network. In region 3, a rise in the curve indicates the formation of one or more new phase(s). In region 4, another sharper rise of the ΔT curve point to the formation of one or more new phase(s) that releases a large amount of energy. In the following regions 5~7, the solidification process has been discussed in the discussion of Figure 4.3. By combining the four curves in one figure, i.e. Figure 4.7, four regions have been identified for the reactions [118] throughout the solidification process, including the start temperature and the solid fraction data (from the thermodynamical simulation discussed previously in Chapter 2 section 3.6), as shown in Table 4.2.

Table 4.2: The reactions during solidification of A356 alloy without ultrasonic vibration

Region	Reaction	Simulation in Figure 3.6		Experiment in FIGURE 4.7a	
		T (ºC)	f_s (%)	T (ºC)	f_s (%)
1	L → Al(s)	614	0	614	0
2a	L → Al(s) + $Al1_5(FeMg)_3Si_2$	594	33	608	15
2b	L → Al(s) + Al_5FeSi	594	33	608	15
3a	L → Al(s) + Si + Al_5FeSi	575	50	574	51
3b	L + $Al1_5(FeMg)_3Si_2$ → Al(s) + Si + Al_5FeSi	566	87	568	72
4	L → Al(s) + Si + Mg_2Si	553	95	560	91
5*	L → Al(s) + Si + Mg_2Si + $Al_8FeMg_3Si_6$	550	99	N/A	N/A

*not observed in Figure 4.7 but reported in the reference 118

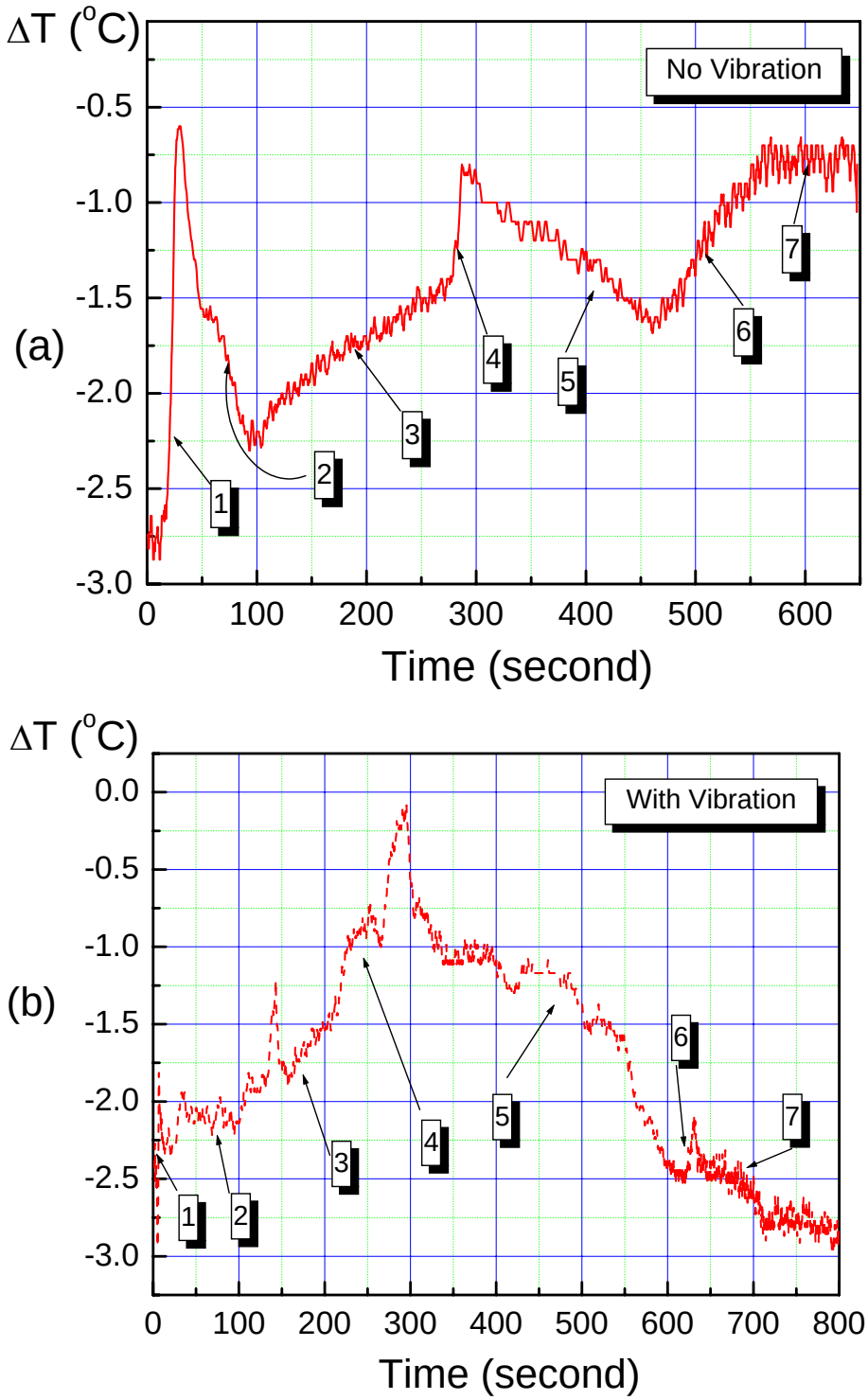

Figure 4.6: The measured temperature difference between the wall and center of the casting (a) Tw – Tc without and (b) Tc – Tw with ultrasonic vibration.

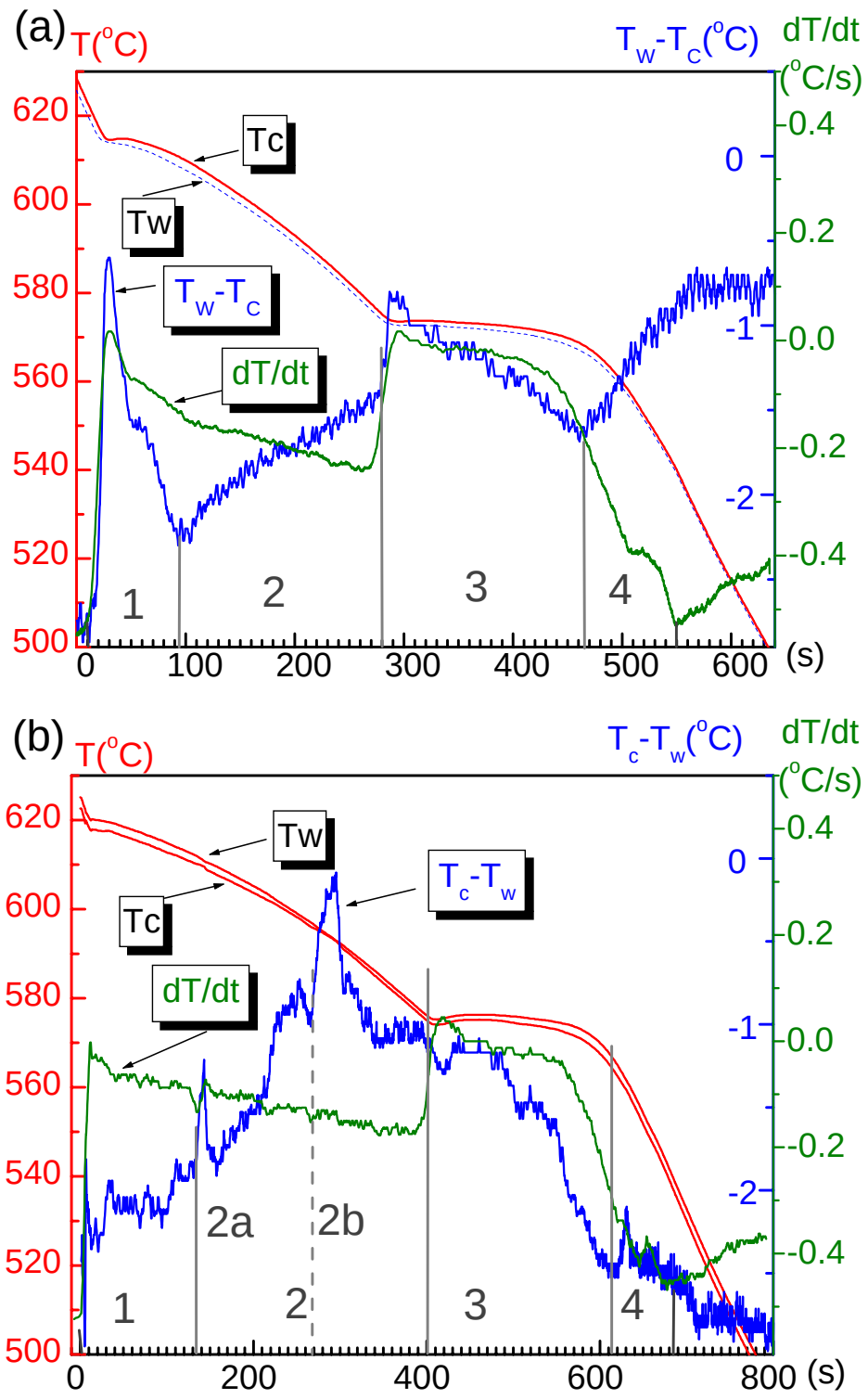

Figure 4.7: The thermal analysis shows the duration of various reactions (1, 2, 3, 4) between the casting (a) without and (b) with ultrasonic vibration.

In the casting with ultrasonic vibration (Figure 4.6b) of the ΔT curve, the regions are not as easily distinguished as that in the casting without ultrasonic vibration (Figure 4.6a). The peak in region 1 is far lower than that in Figure 4.6a; while another peak appears in region 3, which does not appear in Figure 4.6a. in Region 6 and 7, the absolute value of ΔT (about 2.5) is higher than that in Figure 4.6a (about 0.75). Those differences might suggest different reactions/phases has been involved, or the same reactions however at different temperature and different amount. From the combined Figure 4.7b, four different reaction regions have been identified. The start temperatures are picked and accordingly the solid fraction data are found in the thermodynamic simulation results shown in Figure 3.6, are shown in Table 4.3

The durations of each reaction without and with ultrasonic vibration is also worth noting. In the solidification without ultrasonic vibration, the durations of time for each reaction are (from region 1 to 4) 83 seconds, 187 seconds, 185 seconds, and 85 seconds. However, in the solidification with ultrasonic vibration, those durations become 120 seconds, 266 seconds, 210 seconds, and 69 seconds.

The duration of the formation of Mg_2Si is shorter however at a faster nucleation rate (in the previous discussion) in the solidification with ultrasonic vibration, so the total formed Mg_2Si could be the same in both solidifications.

Table 4.3: The reactions during solidification of A356 alloy with ultrasonic vibration

Region	Reaction	Experiment (Figure 4.7b)		Simulation f_S (%) (in Figure 3.6)
		T (ºC)	f_s (%)	
1	L → Al(s)	620	0	0
2a	L → Al(s) + $Al1_5(FeMg)_3Si_2$?	610	N/D*	12
2b	L → Al(s) + Al_5FeSi ?	595	N/D	32
3a	L → Al(s) + Si + Al_5FeSi ?	575	N/D	50
3b	L + $Al1_5(FeMg)_3Si_2$ → Al(s) + Si + Al_5FeSi ?	570	N/D	65
4	L → Al(s) + Si + Mg_2Si	564	N/D	86
5*	L → Al(s) + Si + Mg_2Si + $Al_8FeMg_3Si_6$?	N/A	N/A	N/A

*Not detected

From the table, it is noticed that all the reaction temperatures are elevated, that is to say, in the solidification with ultrasonic vibration, the nucleation of each phase starts at a higher temperature than that of without ultrasonic vibration. A conclusion from this is that less supercooling is needed when ultrasonic vibration is presented.

In summary, it is observed in the thermal analysis experiments that:

(1) It took a longer time to precipitate primary fcc aluminum but almost the same amount of time for the major eutectic reaction(s) and the cooling from 560 to 500 ºC in the casting with ultrasonic vibration. It implies a considerable amount of ultrasonic energy was introduced into the solidifying specimen before the major eutectic reaction(s).

(2) The difference between dendrites nucleation/growth and thickening is not significant in the casting with ultrasonic vibration. It suggests dendrites formation might not be present in this solidification process.

(3) In the casting with ultrasonic vibration, T_G and T_{Min} are elevated, while the recalescence time is much shorter. This might indicate a much slower growth rate of primary fcc aluminum grains.

(4) In the solidification with ultrasonic vibration, less supercooling is needed when ultrasonic vibration is present.

4.2 Mechanisms for the effect of ultrasonic vibration on solidification

Several researchers have proposed mechanisms by which refined globular grains are produced via ultrasonic vibrations [119]. These mechanisms are related to ultrasonically induced dendrite fragmentation and heterogeneous nucleation.

4.2.1. Heterogeneous nucleation vs. dendrite fragmentation

This section attempts to determine which mechanism, i.e., the ultrasonically induced dendrite fragmentation or heterogeneous nucleation, plays a major role in the solidification process. A356 melt was treated at various solid fractions isothermally with ultrasonic vibrations by dipping the acoustic radiator into the melt. Experimental results confirmed that globular grains could be effectively obtained when the melt was

ultrasonically treated at a temperature close to its liquidus and subsequently cooled quickly. It further illustrates the difficulty to form globular grains when the specimen is treated at isothermal temperatures in the mushy zone. It may imply that in the given experiments, cavitations-induced heterogeneous nucleation plays a more important role than dendrite fragmentation in the formation of globular grains.

4.2.1.1 Introduction

In previous sections, it has been shown that the introduction of high intensity ultrasonic vibration into the melt of aluminum alloys can eliminate columnar dendritic structure, refine the equiaxed grains, and under some conditions, produce globular non-dendritic grains [50, 119-139]. Mechanisms for grain refinement under ultrasonic vibrations have been proposed [136, 138, 139]. They are related to ultrasonically induced cavitations, which produce large instantaneous pressure and temperature fluctuations in the melt. These pressure and temperature fluctuations are likely to induce heterogeneous nucleation in the melt. They are also likely to promote dendrite fragmentation by enhancing solute diffusion through acoustic streaming. However, there is no convincing evidence in the literature as to which mechanism, i.e. heterogeneous nucleation or dendrite fragmentation, is more important for grain refinement under ultrasonic vibrations. This section describes some carefully designed experiments in which ultrasonic energy was injected in the melt at various stages of solidification for the purpose of solving this dilemma.

4.2.1.2 Experiments

The raw material used in this study was aluminum alloy A356. The experimental setup was described in Chapter 3.3, Figure 3.3.

Three types of experiments were carried out, namely continuous processing, intermittent processing, and isothermal processing. In the continuous processing, ultrasonic energy was injected into the molten aluminum over a range of temperature that covered from 634 °C to 574 °C as the alloy cooled in the furnace. The ultrasonic system was not able to function when the melt temperature was lower than 574 °C since the solid fraction was too high. The second approach, intermittent processing, was the stepwise

application of acoustic power coupled into the melt at different temperature intervals from 614 °C to 574 °C. Temperature intervals were 5 °C and the time of each isothermal treatment was varied over, 5, 10, and 20 s. The third approach consisted of isothermally applying acoustic energy into the melt at different solid fractions. The isothermal processing time varied from 5, 10, and 20 s. Experimental results reported in Reference [9] indicates that 20 s is enough to produce globular grains during solidification of aluminum alloys.

In the experiments, aluminum A356 alloys were heated up to 650℃ and cooled to pre-determined temperatures for ultrasonic processing. Meanwhile the ultrasonic radiator was also preheated to the same temperature as the aluminum melt. The radiator was then inserted into the melt. The specimens thus treated were cooled in the furnace to room temperature. The microstructure of the specimens was then characterized.

4.2.1.3 Results and discussion

Figure 4.8 shows the comparison of the obtained microstructure without (a) and with (b) the continuous application of acoustic power. Without acoustic vibration, the microstructure was dendritic and its average grain size was several millimeters. Upon the application of acoustic power, the dendritic structure was broken up into a somewhat globular grain structure. The average grain size was about 200 μm. This result is in accordance with previous work [136, 138, 139].

Microstructures corresponding to different intermittent time processing are presented in Figure 4.9. The comparison between Figure 4.8 (a) and Figure 4.9 reveals a very large difference in the resultant microstructure. In particular, the application of intermittent acoustic energy makes the microstructure more globular and destroys the dendritic microstructure. A comparison of Figure 4.8 (b) with Figure 4.9 shows little difference in terms of grain morphology between the application of intermittent and continuous acoustic power. However, the average grain size appears to be reduced by intermittent acoustic vibration. Figure 4.9 shows that the intermittent treatment is more efficient than the continuous treatment in terms of grain size reduction. This is due to the fact that the cooling rate in the specimen treated with intermittent vibration is faster than

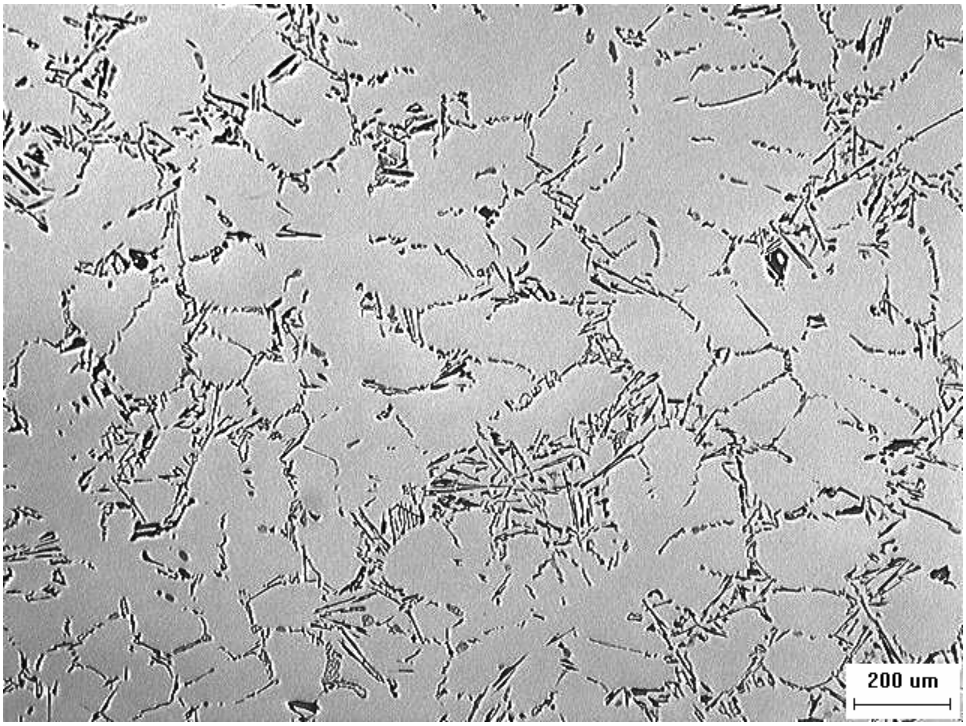

(a)

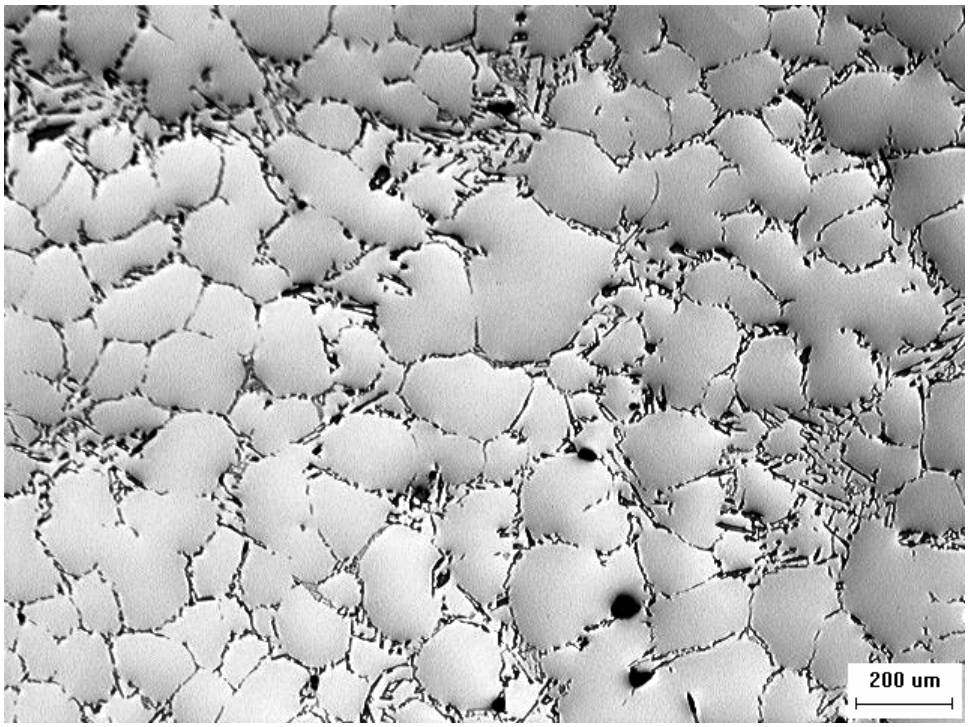

(b)

Figure 4.8: A comparison of microstructures obtained without (a) and with (b) the application of continuous acoustic power.

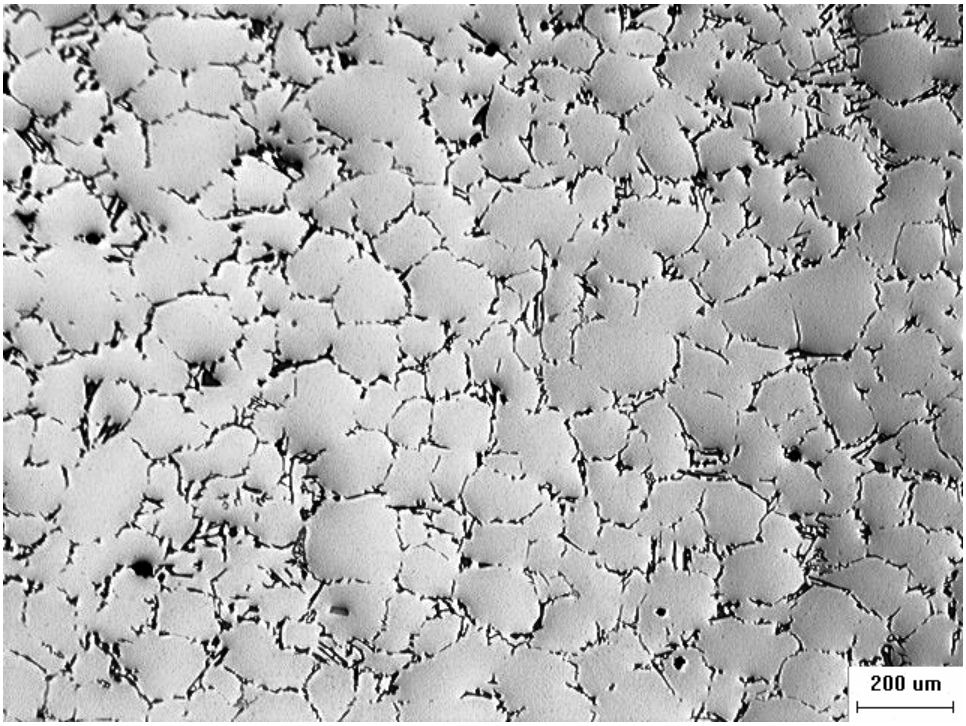

(a)

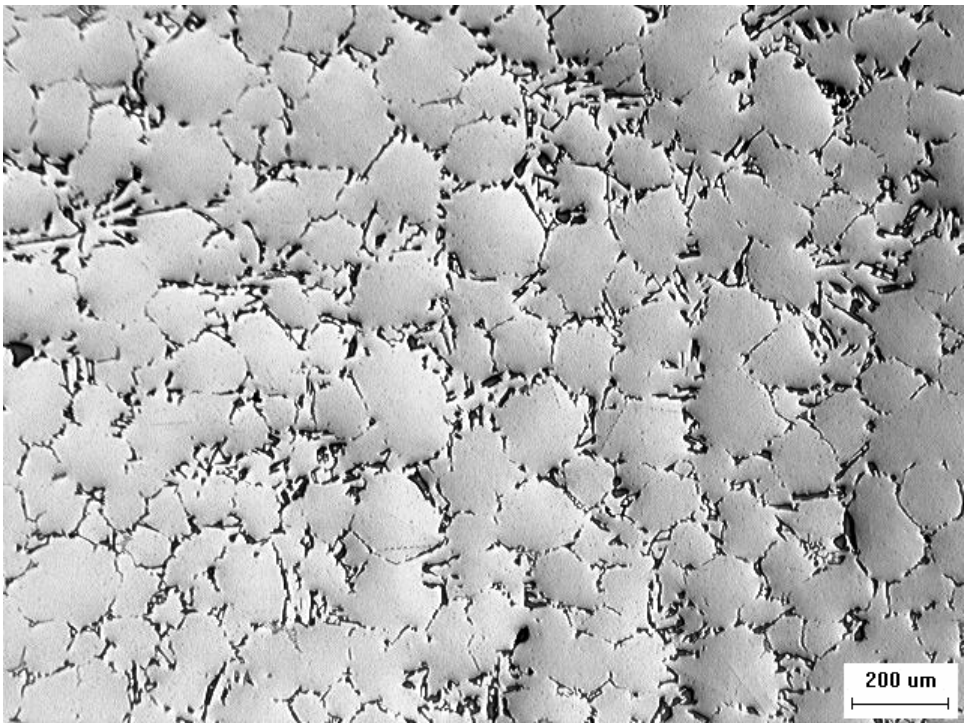

(b)

Figure 4.9: A comparison of microstructures obtained with the application of intermittent acoustic power for (a) 10 s (b) 20 s at each isothermal temperature step.

that treated with continuous vibration. Cooling rate has a major effect on the resultant grain size.

Isothermal processing was then carried out in the melt. Figure 4.10 shows the microstructure obtained for five conditions: without acoustic power applied (a); acoustic power applied for 10 s at 614 °C (b), at 610 °C (c), and at 605 °C (d). Isothermal processing reduces the average grain size compared with no applied acoustic vibrations. The comparison of Figure 4.10 (b) with (c) shows little effect of processing temperature on the average grain size using isothermal processing. No globular structures were obtained for isothermal processing for various times and temperatures in the range of 614 °C to 574 °C.

Note that 614 °C is the liquidus temperature of the alloy; 610 °C and 605 °C are the temperature where the corresponding solid fraction is about 0.1 and 0.18, respectively.

Finally the isothermal processing time was increased. Figure 4.11 shows the resultant microstructure of a specimen subjected to ultrasonic vibrations for 20 s at 614 °C (a) and at 610 °C (b). The extended isothermal vibration time seems to have little effect on breaking up dendritic structures further and forming globular structures.

It is well known that isothermal coarsening can be used to produce a globular microstructure in an aluminum alloy if the specimen is held at semisolid temperatures for an extended time [140]. Electromagnetic stirring can also be applied to a solidifying alloy to obtain globular grains at fairly short processing times [141]. In fact, both isothermal coarsening and electromagnetic stirring were successfully used for the production of globular, nondendritic microstructures. However, when ultrasonic energy is injected into aluminum alloy A356 at semisolid temperatures (mushy zone temperatures), as shown in Figure 4.10 and Figure 4.11, it is difficult to obtain globular grains in a short time frame. This may imply that the temperature and/or pressure fluctuations induced by ultrasonic vibration are not efficient in breaking up dendrites in the mushy zone. Dendrite fragmentation requires the remelting of the secondary dendrite at their roots [142]. Remelting of a solid is usually slow because latent heat and solute have to be removed from the roots of the secondary dendrites. The temperature and pressure fluctuations

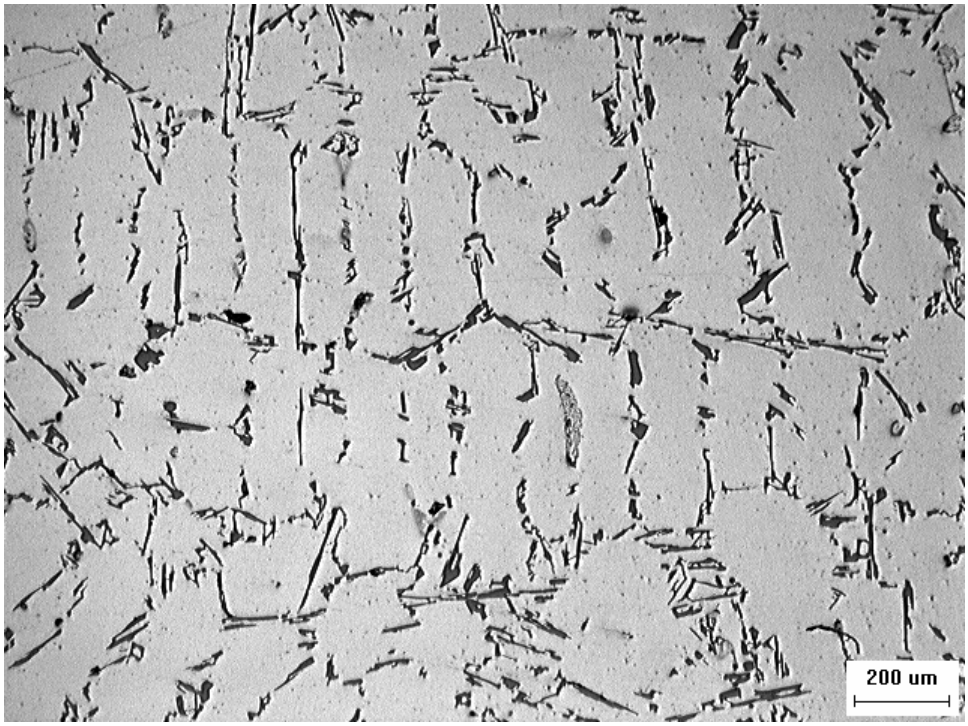

(a)

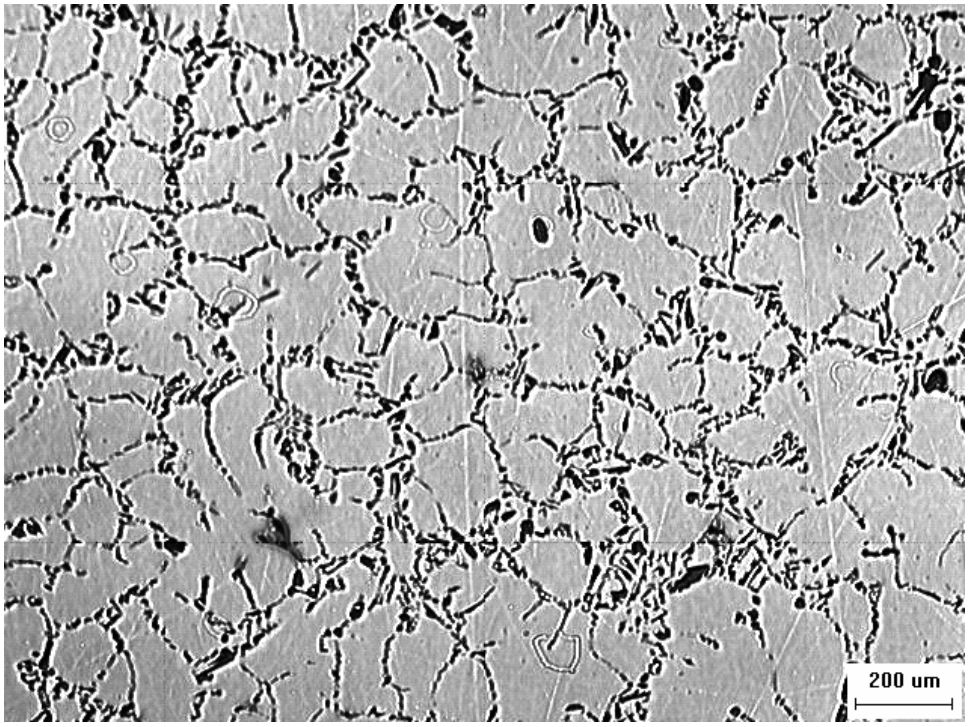

(b)

Figure 4.10:A comparison of microstructures obtained without (a) and with isothermal processing for 5 s at 614 °C (b), at 610 °C (c) and at 605 °C (d) (Continued on the next page)

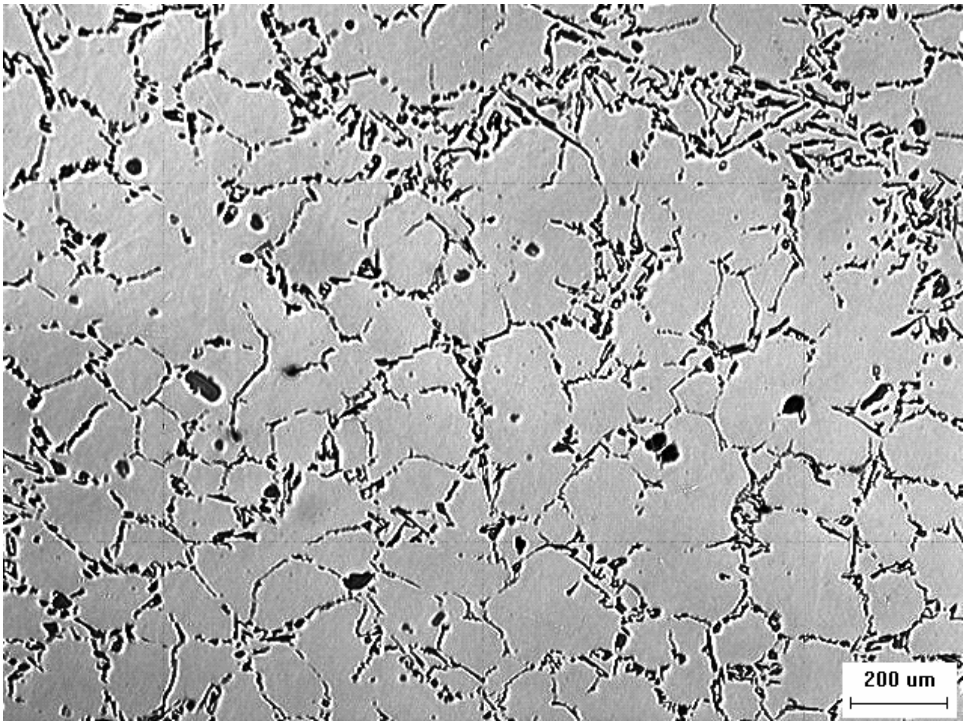

(c)

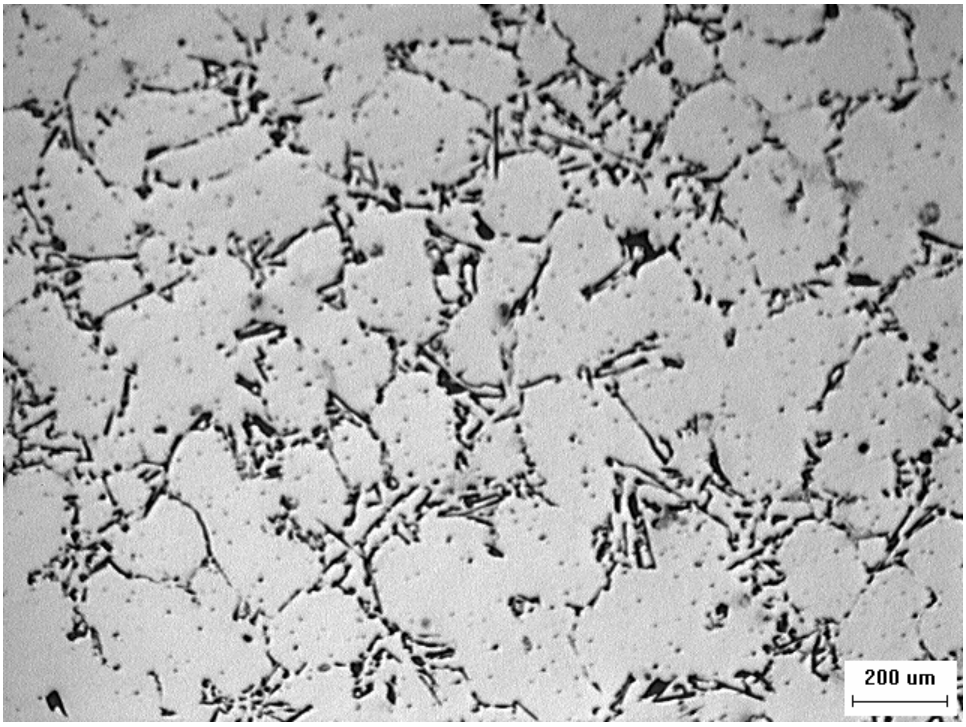

(d)

Figure 4.10: (continued).

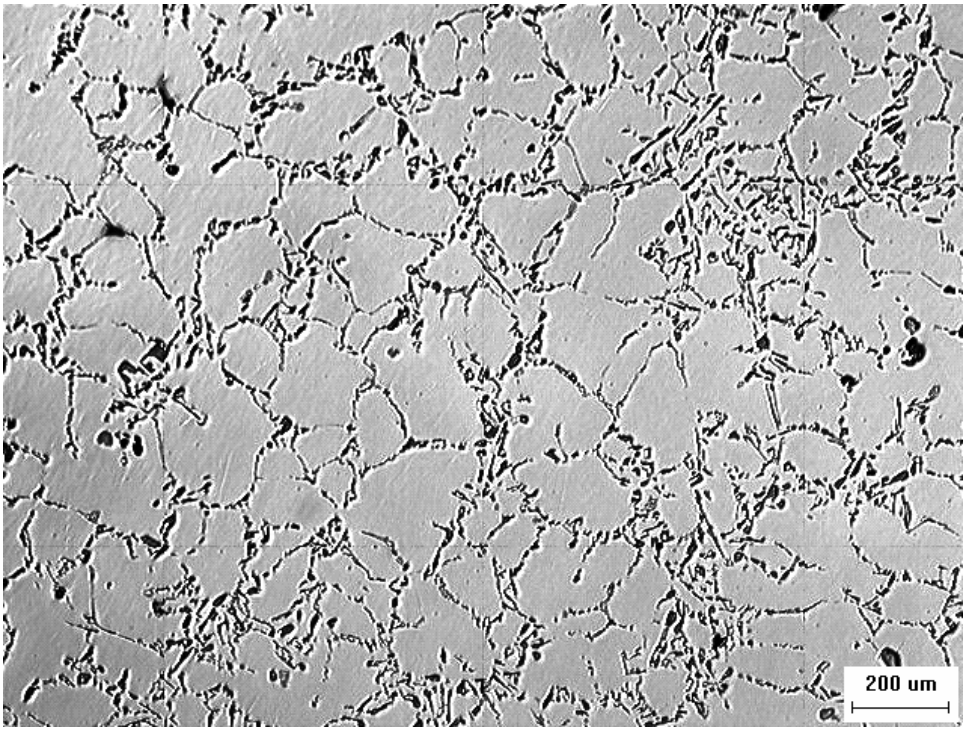

(a)

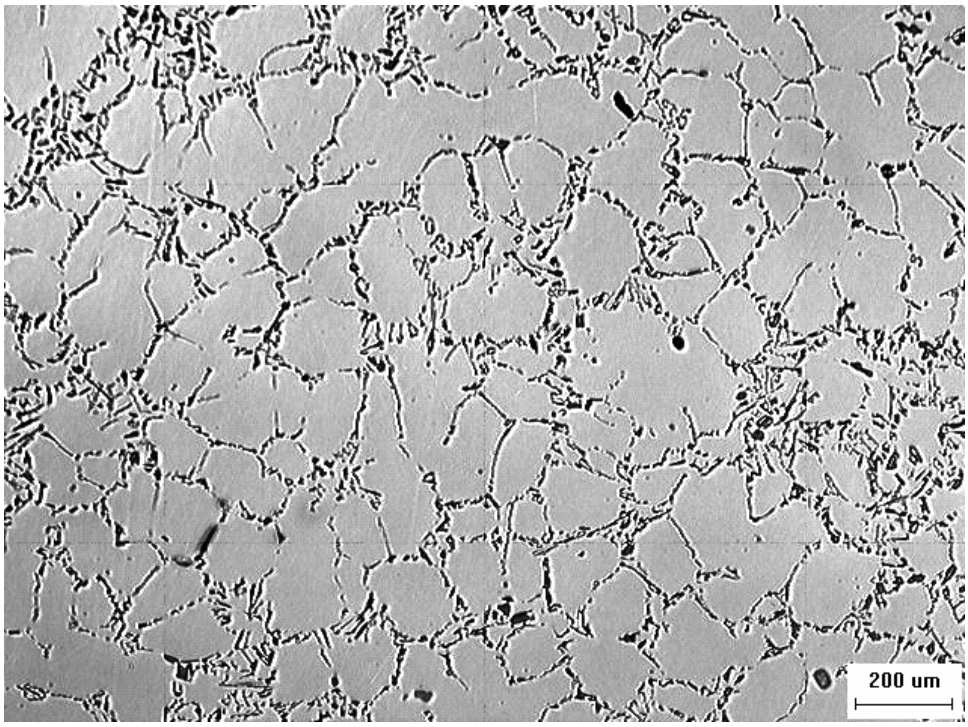

(b)

Figure 4.11: The microstructures of specimens subject to ultrasonic vibration for 20 s under isothermal processing conditions at (a) 614 °C and (b) 610 °C.

occur at a frequency of 20 kHz, which may be too fast for dendrite fragmentation. Some limited dendrite fragmentation occurred in our experiments, since the grain size is reduced with acoustic vibration. The limited dendrite fragmentation can be related to the acoustic streaming in the slurry, which promotes mass transfer and thus the remelting of dendrites at their roots.

Since dendrite fragmentation does not appear to affect the formation of globular, nondendrite microstructure in the acoustically processed melt, the dominant mechanism for the formation of a globular microstructure seems to be acoustically induced heterogeneous nucleation.

When ultrasonic vibration is applied to a melt, cavitation occurs, forming a large number of tiny discontinuities or cavities. These cavities expand and collapse essentially instantaneously. During the expansion stage, the temperature of the cavity surface drops. As a result, undercooling occurs on the cavity surfaces and results in the formation of solid phase nuclei. The nuclei thus formed can be distributed throughout the melt by acoustically induced streaming. A large number of nuclei can be produced during the expansion stage, resulting in the formation of globular grains.

Ultrasonic vibration induces heterogeneous nucleation right after pouring, while dendrite fragmentation takes place after solidification begins (at a temperature lower than the liquidus). The discussion above suggests that cavitation-induced heterogeneous nucleation is the dominant mechanism for globular grain formation in specimens processed using acoustic vibration [119].

Having established the mechanism of globular grain formation in an alloy under ultrasonic vibration, we now discuss the effect of processing parameters, such as ultrasonic intensity and casting temperature on the resultant microstructure of the ultrasonically processed alloy.

4.2.2. Ultrasonic intensity

To examine the effect of acoustic energy on grain structure, experiments that involved adjusting the ultrasonic amplitude were carried out, since the intensity of acoustic energy injected into the melt is proportional to the square of ultrasonic amplitude. The amplitude

of the ultrasonic unit is adjustable from 30% to 100%, or 24.5 μm to 81.6 μm (with booster), or 16.4 μm to 55 μm (without booster). Four amplitudes were used during the experiments: 0% (without ultrasound), 30%, 50%, and 70%. The casting temperature was 640°C, and the vibration duration was 60 s. A copper mold holding up to 250 g of molten aluminum was used.

Experimental results are shown in Figure 4.12, and the quantitative analysis of the effect of ultrasonic amplitude is shown in Figure 4.13. When no acoustic vibration was used (Figure 4.12a), Aluminum dendrites were fully developed. One branch of a primary dendrite shown in the middle of figure is about 800 μm in length, indicating that the grain size is in the range of many millimeters since one equiaxed grain usually contains six primary dendrite arms.

The intensity of the acoustic energy injected into the melt is proportional to the square of ultrasonic amplitude. As shown in Figure 4.12 b–d, with increasing ultrasonic amplitude, the primary aluminum grains become less dendritic and more spherical. High acoustic intensity favors the formation of small, spherical primary aluminum grains. This is because ultrasonically induced cavitation will be enhanced at high intensities, resulting in more heterogeneous nucleation embryos in the melt.

4.2.3. Casting temperature

Experiments were also conducted to determine the optimum casting temperature with ultrasonic vibration. The results are shown in Figure 4.14. Quantitative analysis of the effect of ultrasonic amplitude is shown in Figure 4.15. It can be seen in Figure 4.14 b-d that the size of the primary aluminum grain decreases with decreasing casting temperature, reaches a minimum size at 630°C, and then increases slightly with slightly decreasing casting temperature.

Figure 4.14 and Figure 4.15 indicate that the grain size decreases with decreasing temperature, reaches a minimum at 630°C, and then increases with decreasing temperature. This may be explained by the survival of the ultrasonically induced embryos in the melt. Since these embryos are not thermodynamically stable (only formed at the interfaces of the cavitation bubble and the melt during the expansion stage of the

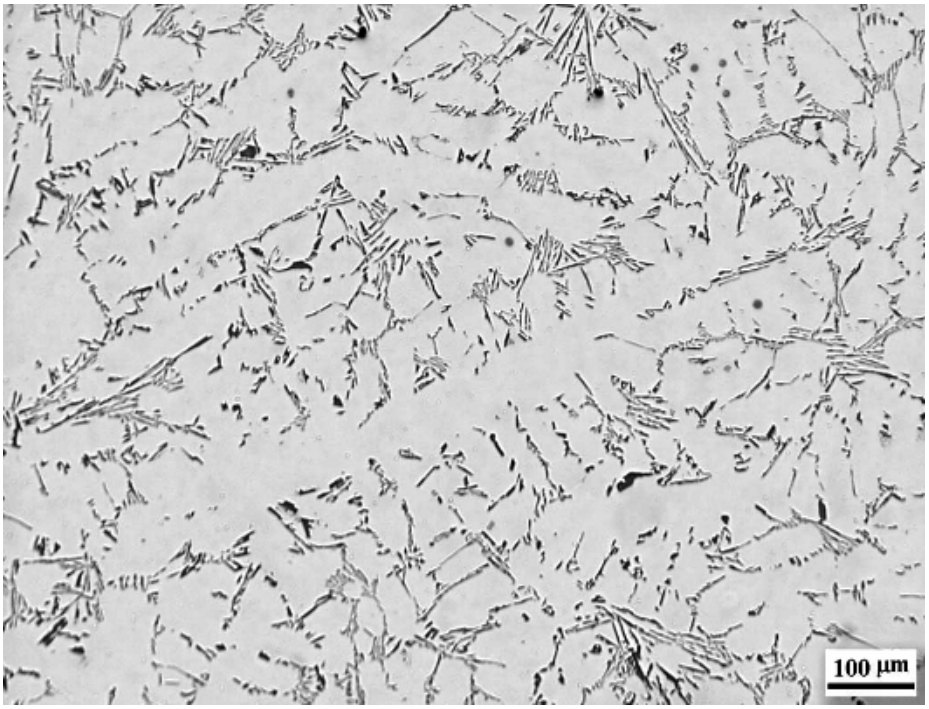

(a)

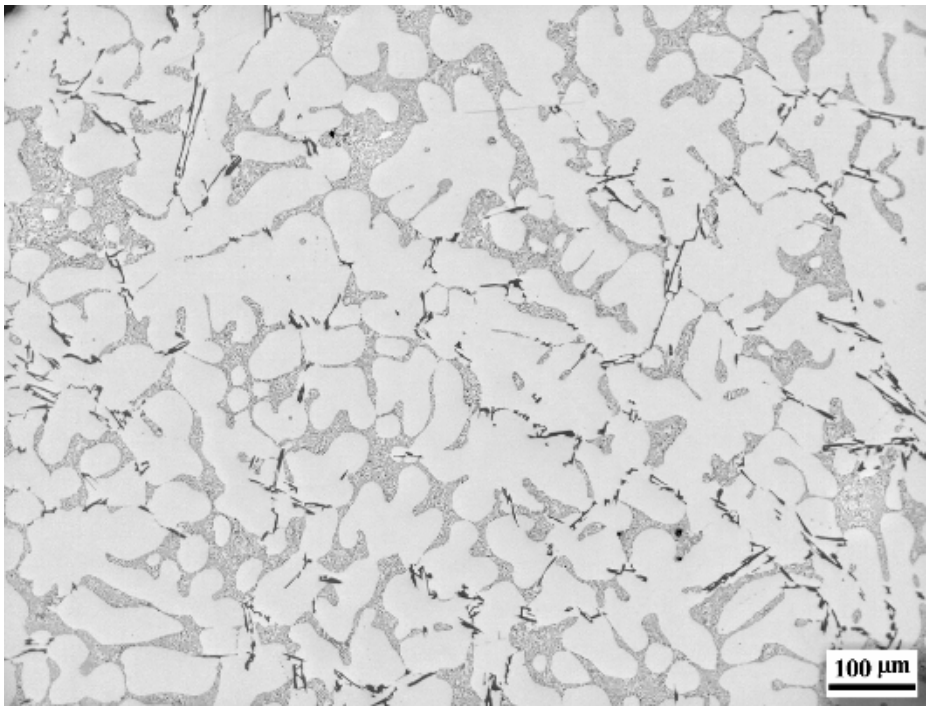

(b)

Figure 4.12: Microstructure of aluminum alloy A356 processed with varying ultrasonic amplitudes (a) 0% (No vibration), (b) 30%, (c) 50%, and (d) 70%. The casting temperature was 640°C. The specimens were vibrated for 60 s during solidification at ultrasonic amplitude of 0–70%. (Continued on the next page)

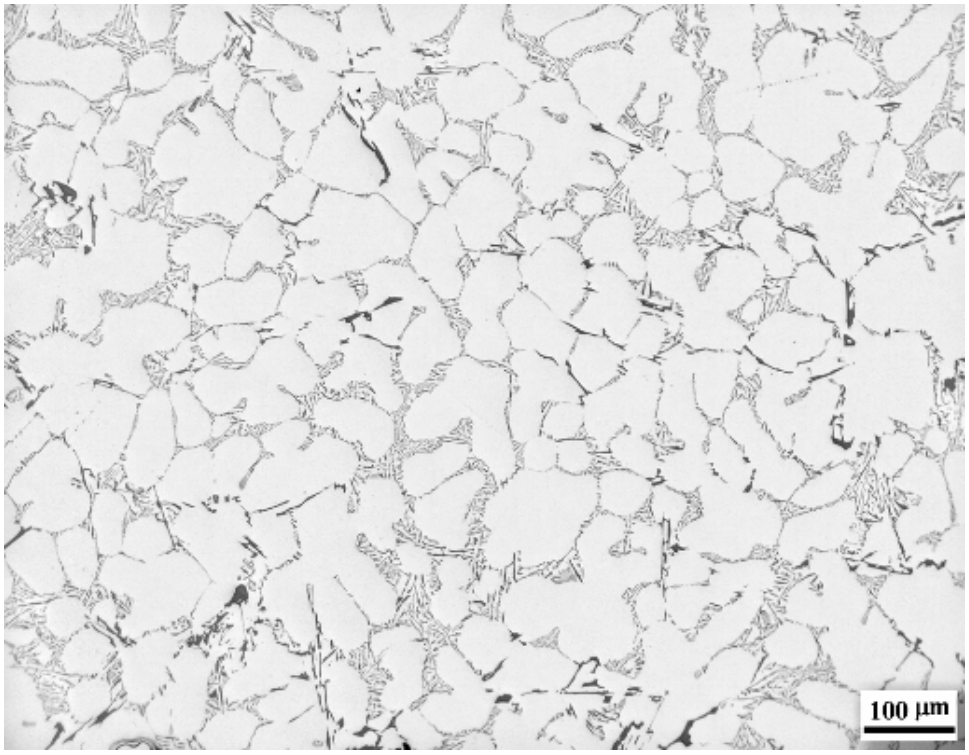

(c)

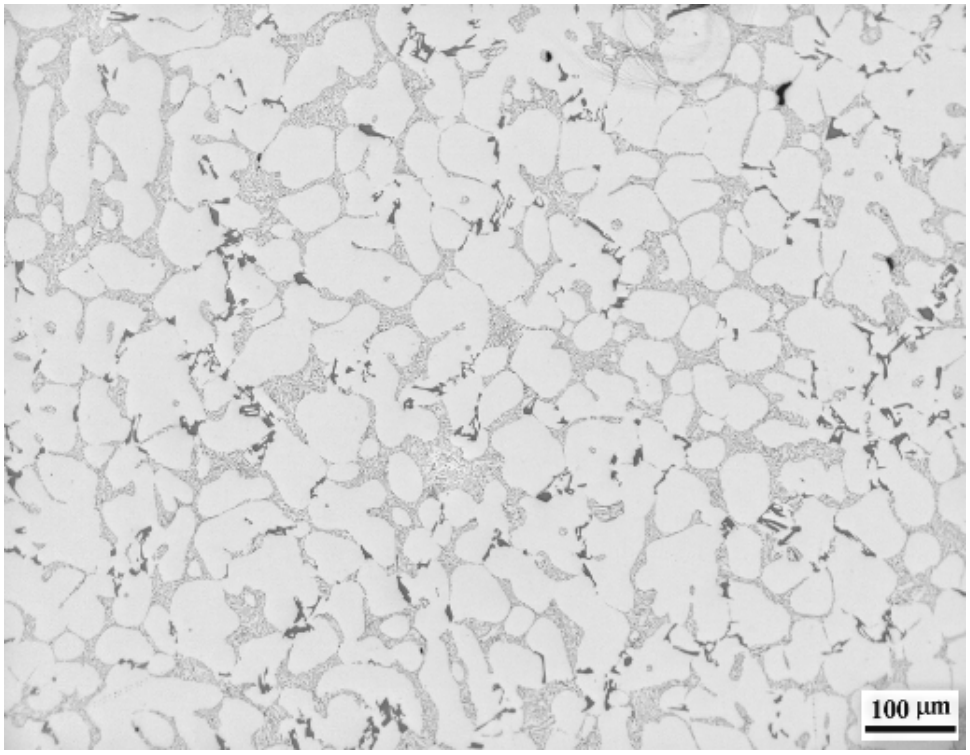

(d)

Figure 4.12 (Continued)

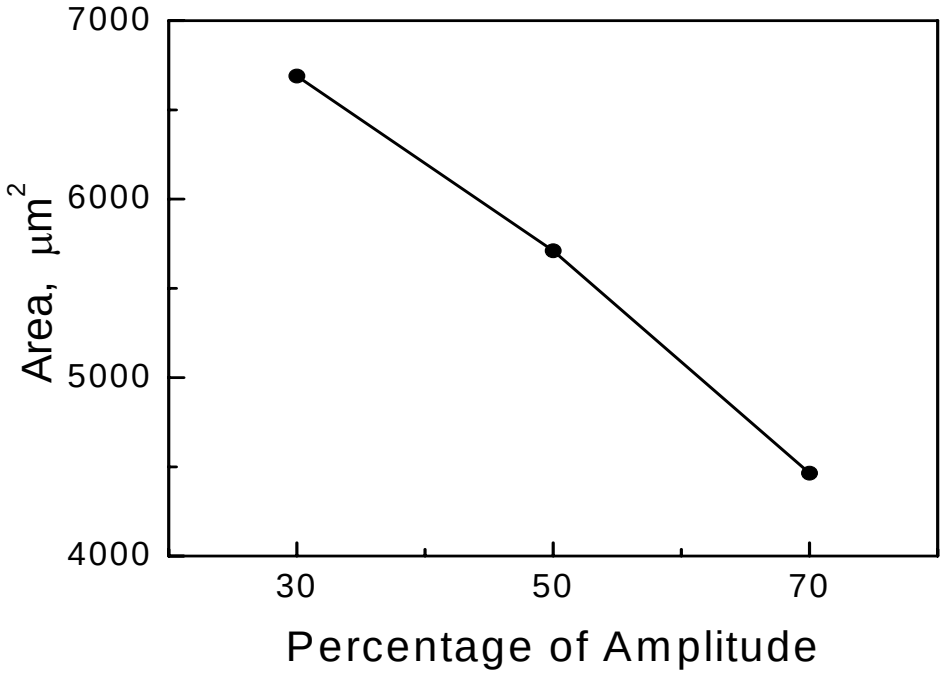

(a)

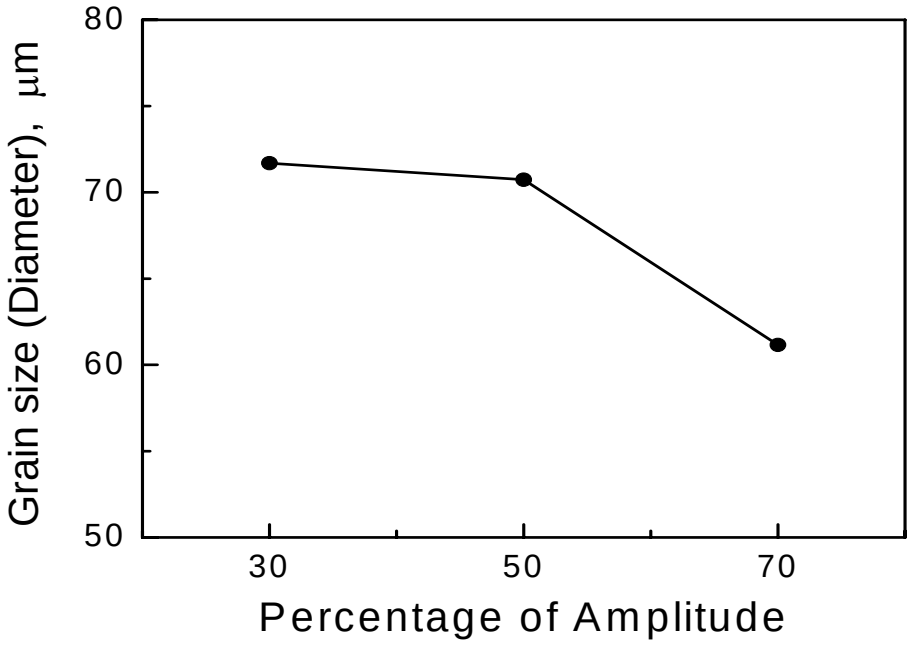

(b)

Figure 4.13: Quantitative analysis of the effect of ultrasonic amplitude on (a) primary grain area and (b) primary grain size. The casting temperature was 640°C. The grain size decreases with increasing amplitude of ultrasonic vibrations.

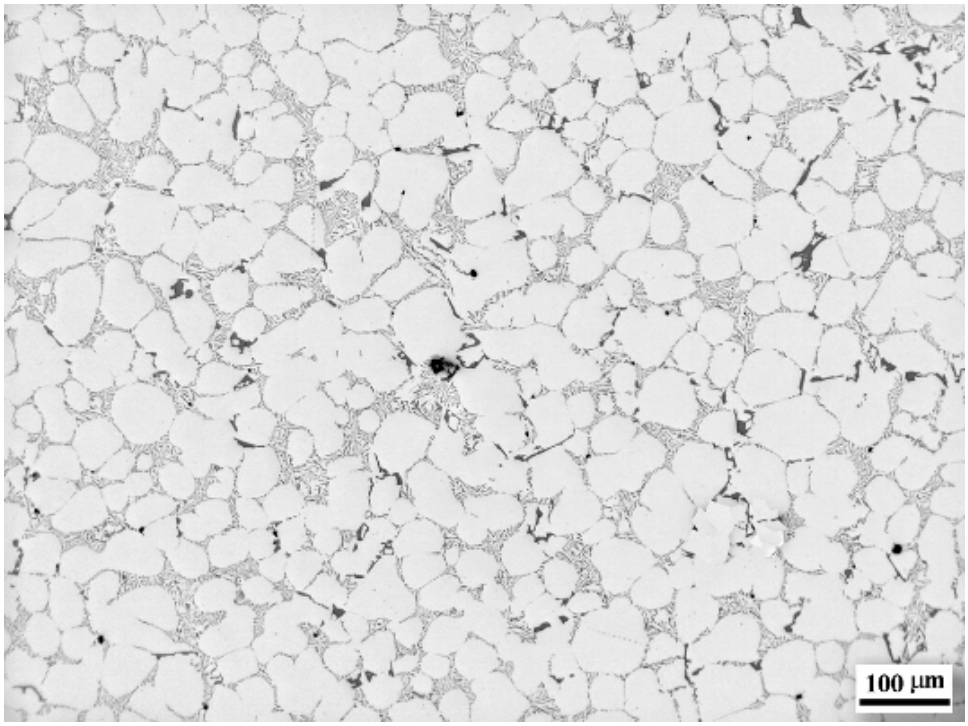

(a)

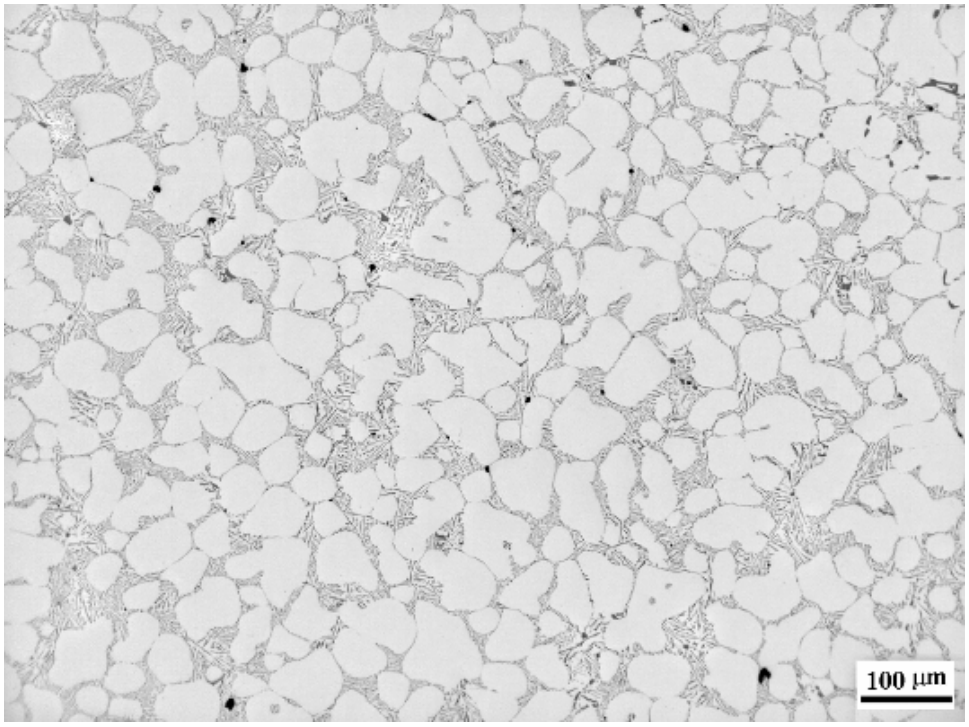

(b)

Figure 4.14: Effect of casting temperature on as-cast microstructure of A356 alloy with ultrasonic vibration at 70% amplitude for 60 s (a) 620 °C, (b) 630 °C, (c) 640 °C, and (d) 650 °C. The average grain size is smaller at lower casting temperatures. (Continued on the next page)

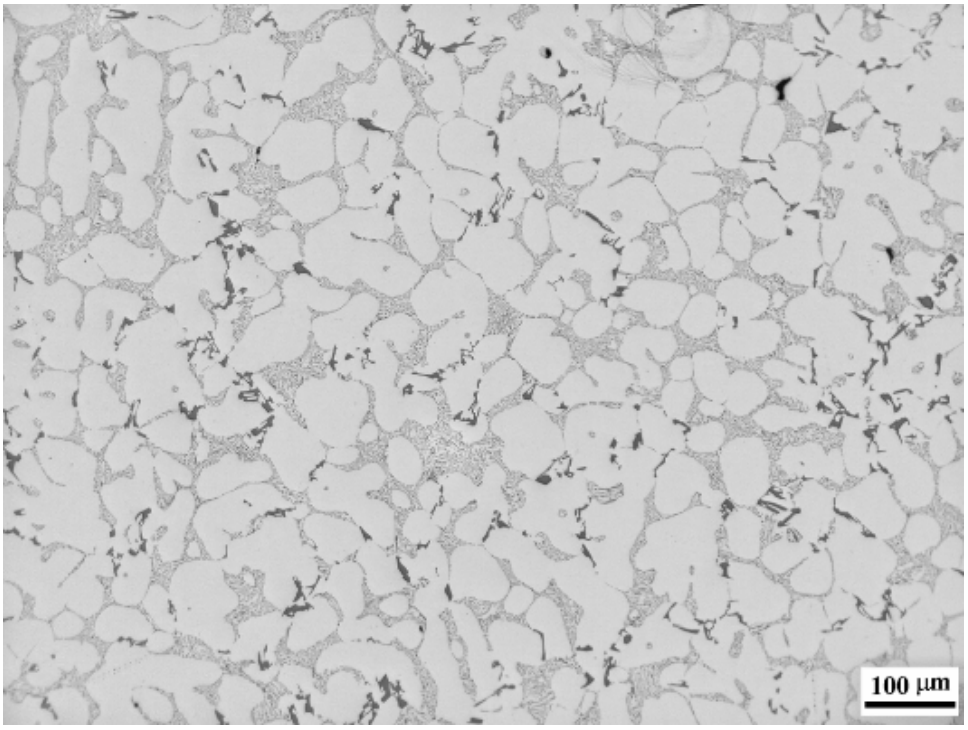

(c)

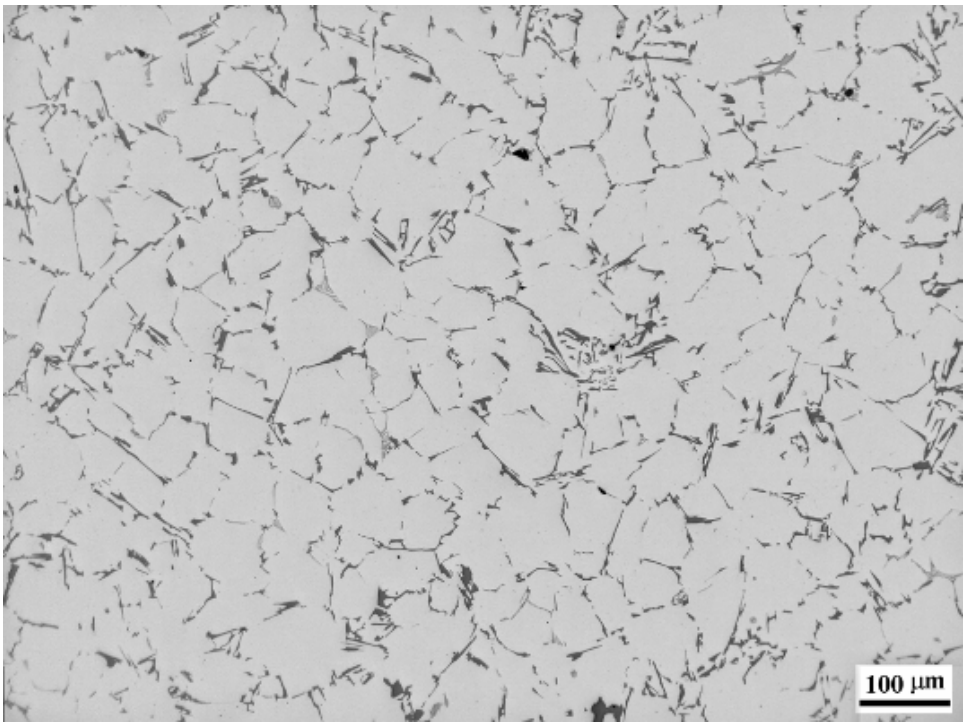

(d)

Figure 4.14 (Continued)

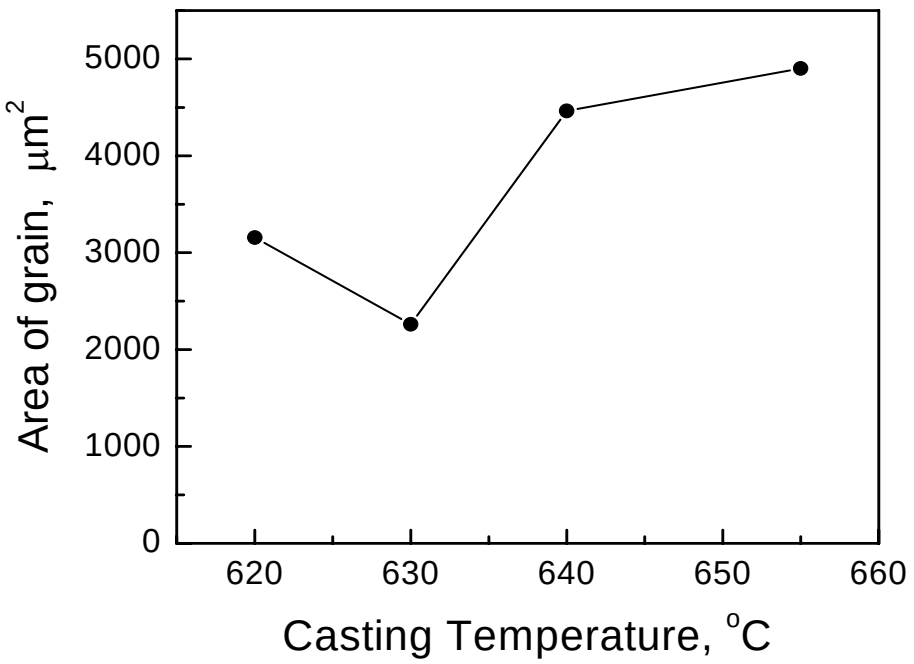

(a)

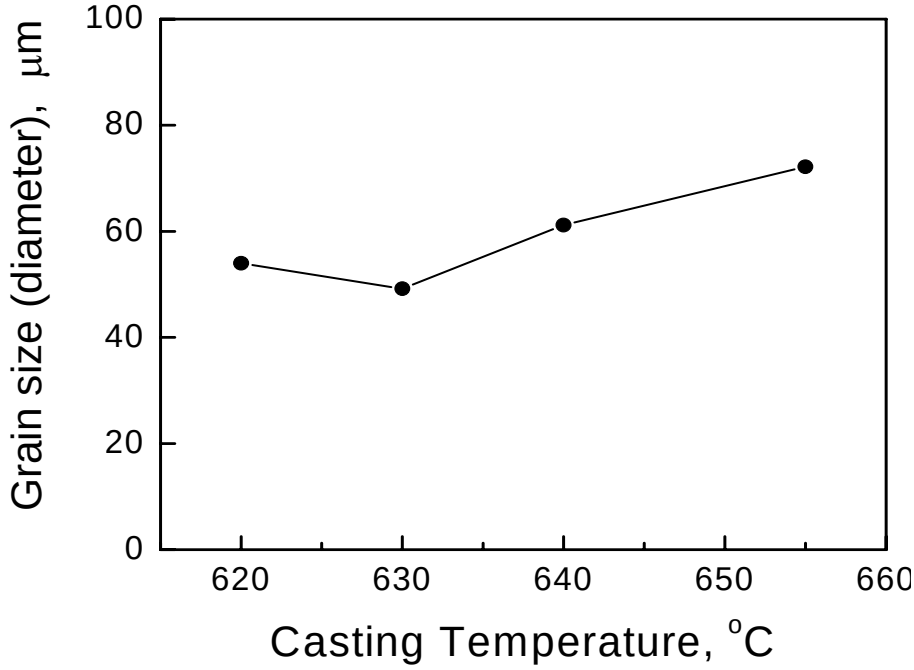

(b)

Figure 4.15: Quantitative analysis of the effect of casting temperature with ultrasonic vibration of 70% amplitude, (a) average area and (b) average size. The grain sizes are smaller at lower casting temperatures but the grain sizes are smallest at a casting temperature of 630°C.

cavitation bubbles), they will be dissolved after the cavitation bubbles are collapsed in the melt. The higher the temperature of the melt, the shorter survival time is for those embryos. As a result, fewer embryos will survive to grow into a grain at higher casting temperatures than at lower casting temperatures. When the casting temperature is closer to the liquidus temperature, the melt will be more viscous so the formation of cavitation bubbles is more difficult, resulting in less formation of embryos than at higher temperatures. This accounts for the larger grain size obtained at both higher and lower casting temperatures. The final grain size is determined by the creation and the survival of the embryos in the melt induced by the high-intensity ultrasonic vibrations.

4.2.4. Distance from the radiator

In addition to the previously mentioned factors affecting the resultant grain size, in our experiments, it is observed, for the first time, that the resultant localized primary aluminum grain size in a casting also varies with increasing distance from the acoustic radiator.

Figure 4.16 shows the primary fcc aluminum grains presented in the three zones and their transition regions of A356 alloy with ultrasonic treatment. In zone I (Figure 4.16(a)), the primary fcc aluminum grains are mostly very fine equiaxed globular grains with primary polyhedric silicon located on boundaries. Eutectic or independent colonies are rarely seen in this region. In the area between zone I and II (Figure 4.16 (b)), a clear, continuous interface is observed. Zone II differs from zone I mainly in the presence of eutectic or independent eutectic colonies, and less primary polyhedric silicon, which can be seen in Figure 4.16 and the right side of Figure 4.16(b). In zone III (Figure 4.16(e)), however, the primary fcc aluminum grains are basically fine globular grains encompassed by a continuous eutectic. Primary polyhedric silicon no longer exists in this region. Figure 4.16(d) shows that the interface between zone III and II is less clear than that between zone II and I in that less primary polyhedric silicon present in the region close to the interface than in the central region of zone II.

Accordingly the mean size and size distribution of primary fcc aluminum grains in the three zones are shown in Figure 4.17 and Figure 4.18. In the untreated A356 alloy,

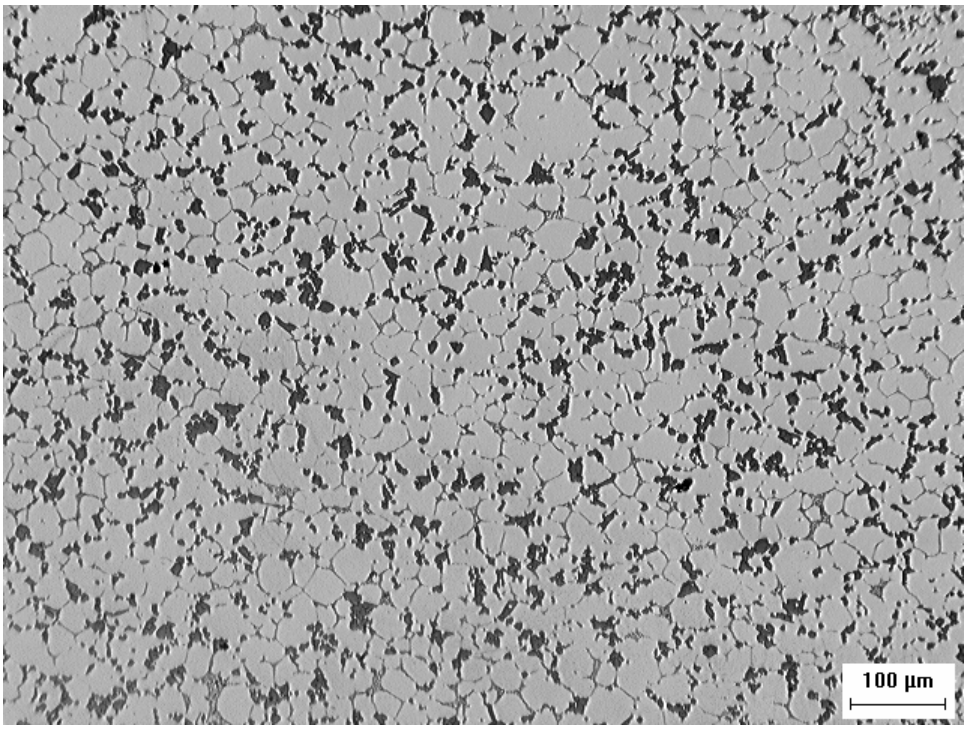

(a) Zone I

Figure 4.16: Primary fcc aluminum grains present in the three zones and their transitions of the sample with ultrasonic treatment, at position (a) Zone I; (b) Transition between zone I and II; (c) Zone II; (d) Transition between zone II and III; (e) Zone III. as illustrated in Figure 3.5 (Continued on the next page).

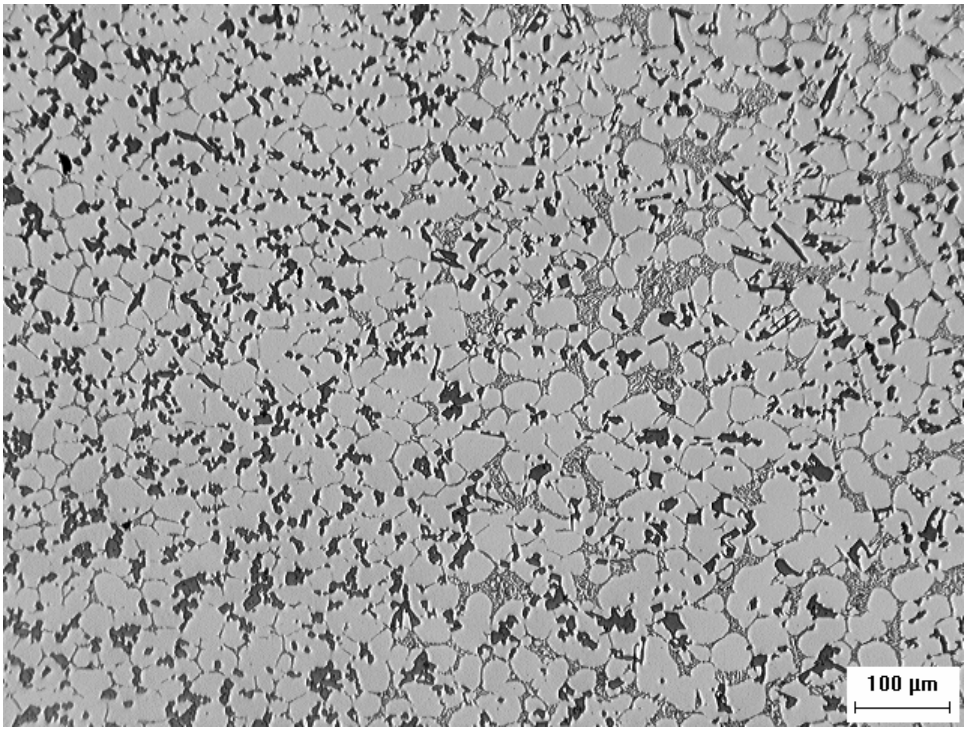

(b) Transition between zone I and II;

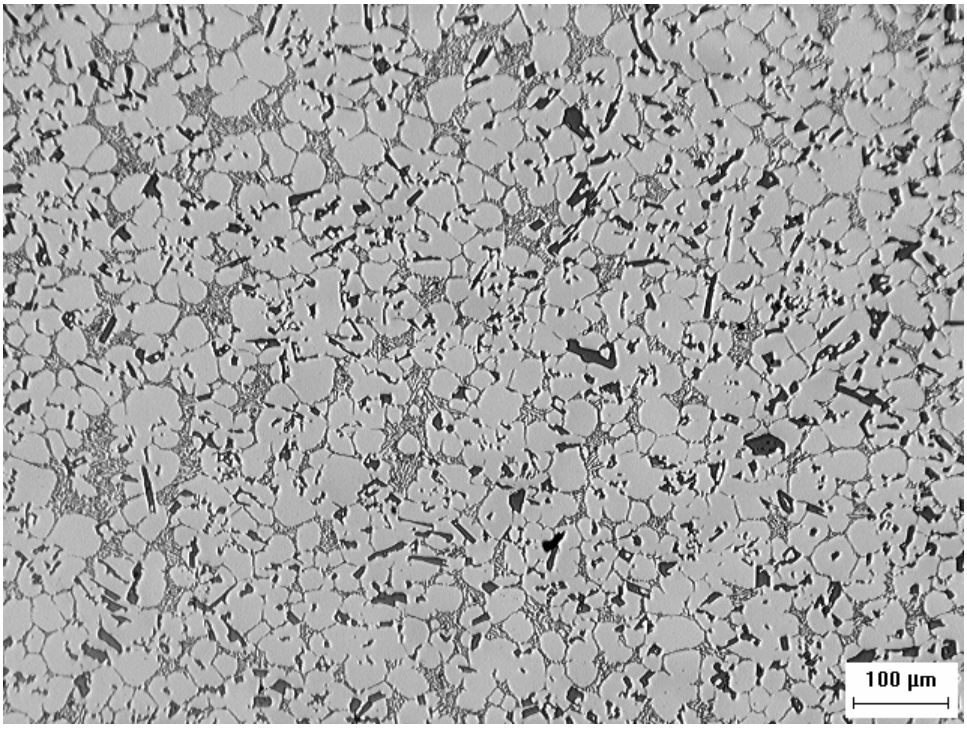

(c) Zone II.

(Continued)

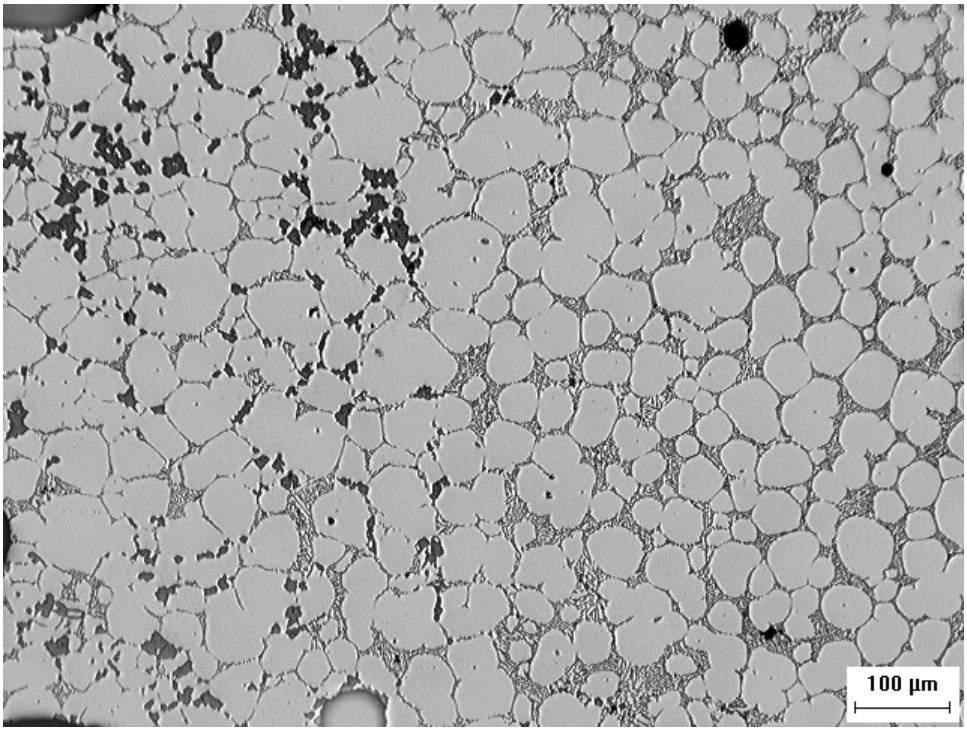

(d) Transition between zone II and III;

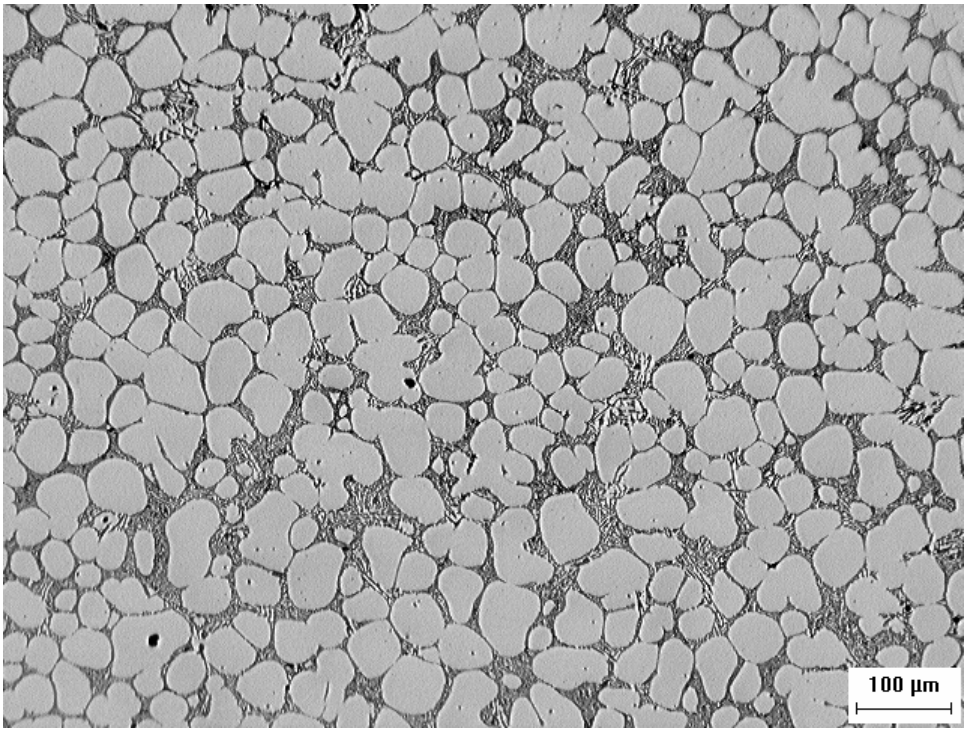

(e) Zone III.

(Continued)

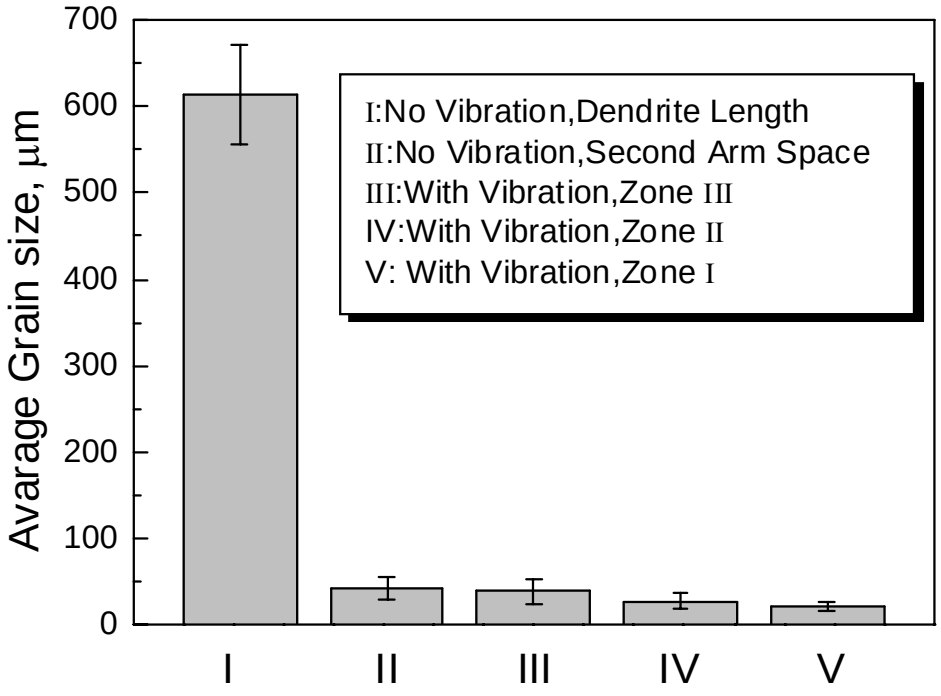

Figure 4.17: Comparison of primary fcc aluminum grain size of the samples without and with ultrasonic treatment

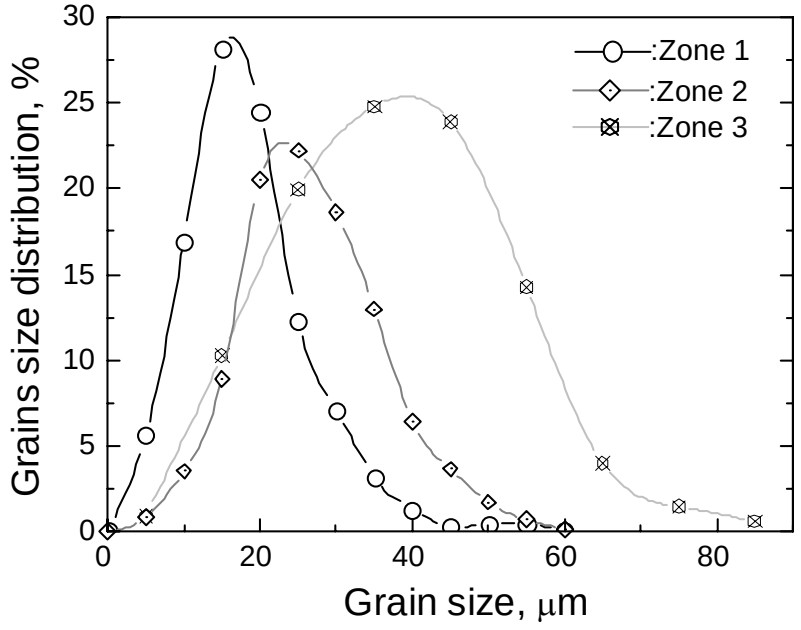

Figure 4.18: Size distribution of primary fcc aluminum grain in the three zones of the sample with ultrasonic treatment.

the mean length of the dendritic branches is about 600 μm, and the mean secondary arm space (SAS) about 45 μm. While in the ultrasonically treated A356 alloy, the grain size falls mainly in the range of 25 – 55 μm in zone III, and 15 – 35 μm in zone II, and 15 – 25 μm in zone I. and the average size (mean diameter) decreases from about 40 μm in zone III to about 28 μm in zone II, then to about 20 μm in zone I. It is evident that ultrasonic treatment not only changes the nature of primary fcc aluminum grains, but also refines the said grains. The refinement is better in the area closer to the ultrasonic radiator.

In general, the mechanisms for the effect of ultrasonic vibration on solidification have been discussed. It is shows that:

(1) Grain refinement was obtained in the experiments with continuous, intermittent and isothermal ultrasonic processing. However globular grains are difficult to achieve using the isothermal method.

(2) It is suggested that cavitation-induced heterogeneous nucleation is the dominant mechanism for globular grain formation in specimens processed using acoustic vibration

(3) High acoustic amplitude/intensity favors the formation of small, spherical primary aluminum grains.

(4) The casting temperature of 630°C brings about best grain refinement result.

(5) The primary aluminum grain size in a casting increases with the increasing distance from the acoustic radiator.

4.3 Grain refinement of A356 alloy for SSM processing

Semisolid material processing (SSM) offers distinct advantages over other near-net-shape manufacturing processes. However the high cost has been a drawback for its commercial utilization. The purpose of this investigation was to explore the use of ultrasonic vibration for semi-solid material processing to produce non-dendritic grains. An experimental apparatus has been designed and built for this purpose. Experiments were carried out using a steel mold suitable for industrial scale SSM processing to obtain grain refinement with the aid of ultrasonic vibration. Initial experimental results show that ultrasonic

vibration can be used in the SSM process, and has the potential advantages of more cost effective, energy efficient, and operationally robust than the other existing technologies for semi-solid material processing.

4.3.1. Introduction

Semisolid material processing (SSM) is an emerging technology that offers distinct advantages over other near-net-shape manufacturing processes, such as more homogeneous microstructure, improved die filling during processing, less oxide formation, less porosity and segregation, improved mechanical properties, and less die wear [120]. A semisolid material exhibits both solid-like and liquid-like behavior. As a "liquid," the material flows with relative ease under the application of shear [121]; as a "solid," the material maintains its structural integrity and can be handled like a solid during processing. SSM processing is ideally suited for die casting and a number of automotive components.

However, traditional SSM processing techniques such as thixocasting [122 - 125] and rheocasting [126 - 128] are encountering problems like high cost, metal waste, and/or large grains. Another approach that involves using electromagnetic stirring brings about too much oxidation and porosity formation that is not suitable for processing aluminum alloys. The purpose of this study is to develop a novel method for semi-solid materials processing using ultrasonic vibrations, which combines the advantages of both thixocasting and rheocasting. By incorporating ultrasonic vibration into SSM processing, this technology will have unique features such as cost effective, energy efficient, small capital investment required, much larger processing window for SSM processing than the other rheocasting methods, applicable to alloys difficult for conventional semi-solid processing, and less formed oxide than that of the other rheocasting methods.

4.3.2. Experimental conditions

Commercial aluminum A356 alloy was used in this study.

Based on the idea of incorporating ultrasonic vibration into the SSM processing, an experimental apparatus has been designed and built, as shown in Figure 4.19. The critical task for the experimental apparatus is the design of the ultrasonic vibrator/metal

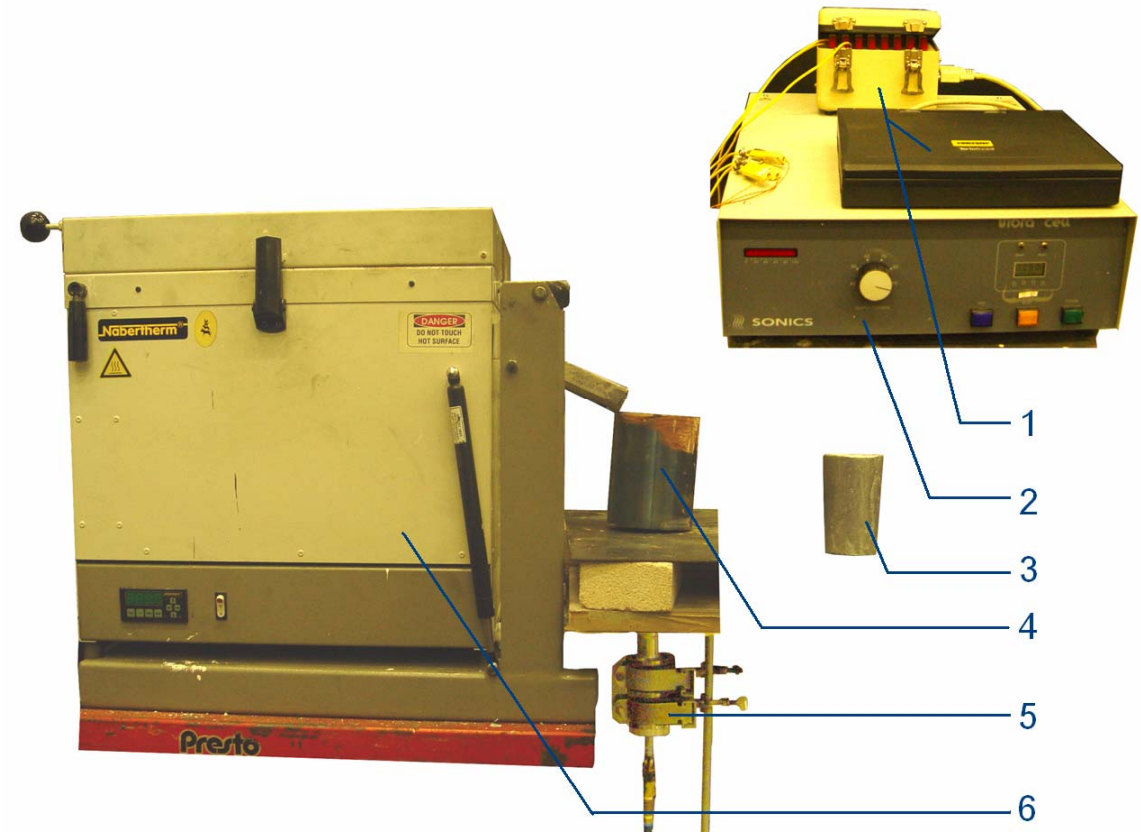

(1) Temperature recording unit; (2) High intensity RF power supply; (3) Billet; (4) Mild steel mold (cylindrical); (5) Ultrasonic processor; (6) Electric furnace.

Figure 4.19 Experimental apparatus for ultrasonic processing of molten aluminum alloy billet suitable for industrial scale SSM processing

injection assembly at the bottom of the metal mold. The assembly consists of an ultrasonic radiator/horn that injects ultrasonic energy into the molten metal, an ultrasonic transducer, a ram that connects to a piston to push the semi-solid billet out of the mold. The size of the billet is 3 inches in diameter and 5 inches in length, which is produced by the steel mold shown in the figure.

Two groups of experiments were carried out. The first one is the casting of A356 alloy with no grain refiner additions, without and with ultrasonic vibration at an amplitude of 56.7 μm during the solidification. The second one is the casting of A356 alloy with the addition of 0.28% 5Ti-B grain refiner, without and with ultrasonic vibration at an amplitude of 56.7 μm during the solidification. The addition of 0.28% Ti-B (5:1) has been reported as the best grain refinement practice [129].

After experiments, the samples were polished and etched using 0.5% HF water solution to a mild agitation, then subjected to optical microscopy observation and digital image analysis for the quantitative grain size and roundness.

4.3.3. Results and discussion

4.3.3.1 Ultrasonic processing of billet suit for SSM

From the above analyses, it is obvious that a casting temperature near the liquidus and high acoustic intensity favor the formation of small and spherical primary fcc aluminum grains. The casting of A356 alloy into the steel mold (3” in diameter by 5” in length) without and with ultrasonic vibration were carried out using the setup shown in Figure 4.19. The experimental conditions are: (1) casting temperature: 630 ^{o}C; (2) ultrasonic amplitude: 100%; and (3) vibration time: 60 seconds. Without ultrasonic vibration, the typical microstructure is fully developed long or rosette dendrites (Figure 4.20a). With the application of ultrasonic vibration, the primary fcc aluminum grains turn out to be much smaller and more globular (Figure 4.20 b -d). It is consistent with the result from small mold casting. The quantitative analytic results are shown in Figure 4.21. It can be seen that in most of the area, the grains are greatly refined. It is also observed that in the areas with a distance from the radiator (transversely or longitudinal) the grain size increases. This is consistent with the result obtained in Chapter 4 section 4.2.4. It proves

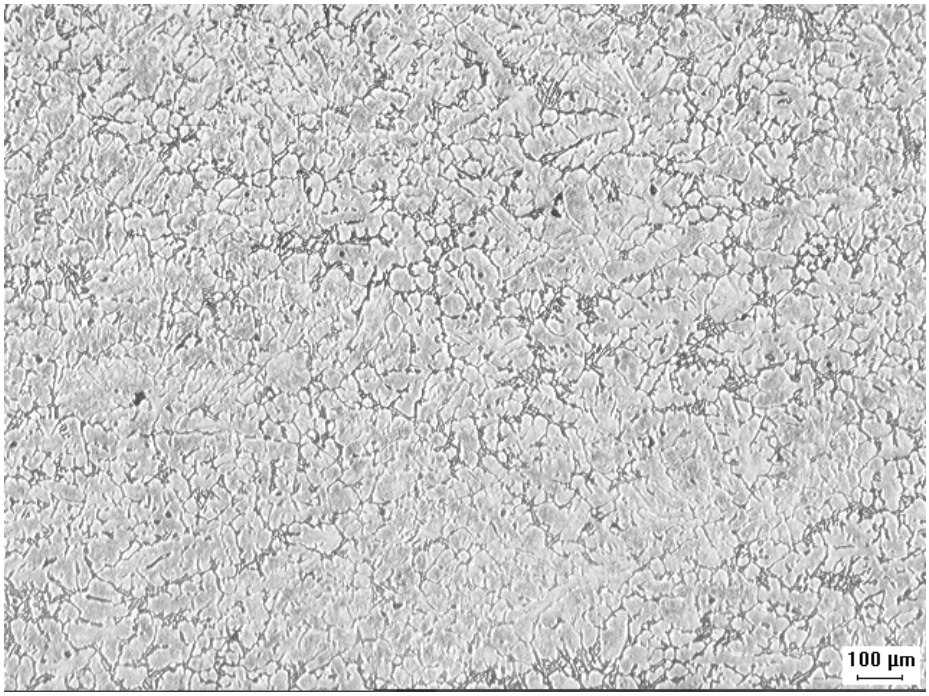

(a) Typical area

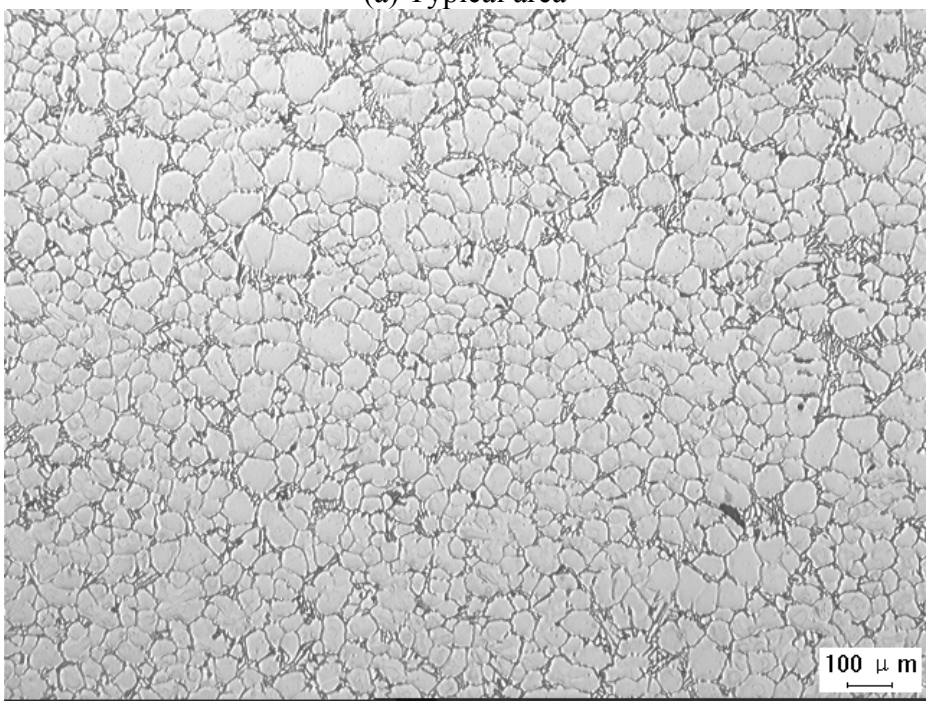

(b)10mm from the bottom

Figure 4.20: Casting of 2 kg billet of A356 alloy without (a) and with ultrasonic vibration at different location in the casting (b~d). The casting temperature was 630 ^{o}C, and amplitude 100%, vibration time 60 seconds. The ultrasonic radiator is located at the bottom in the center of the billet (Continue in the next page).

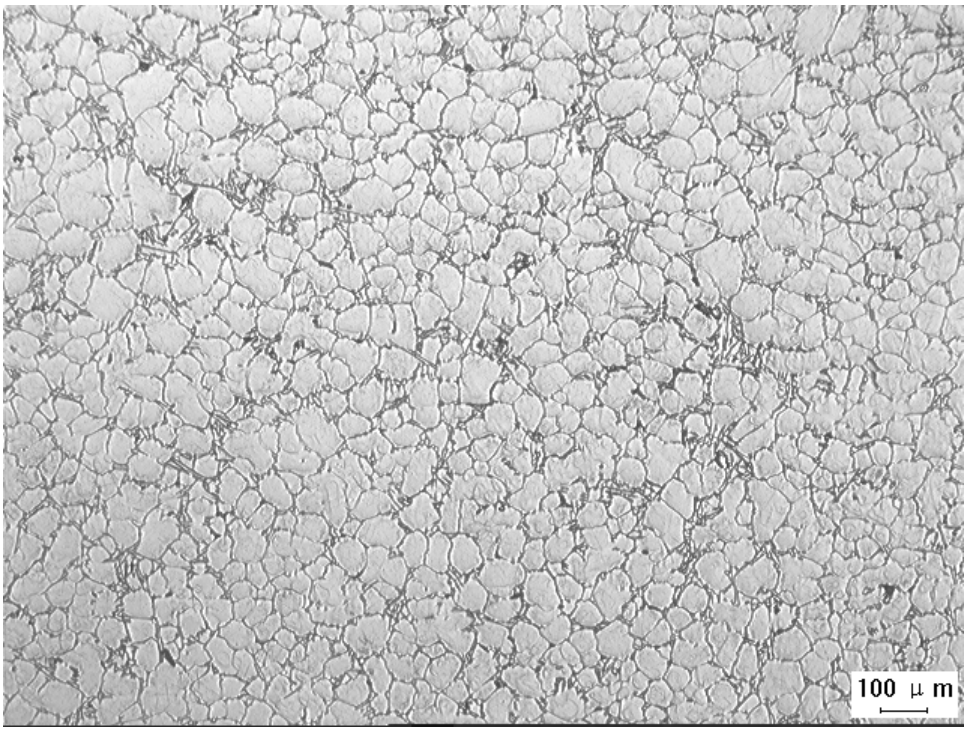

(c) 60mm from the bottom

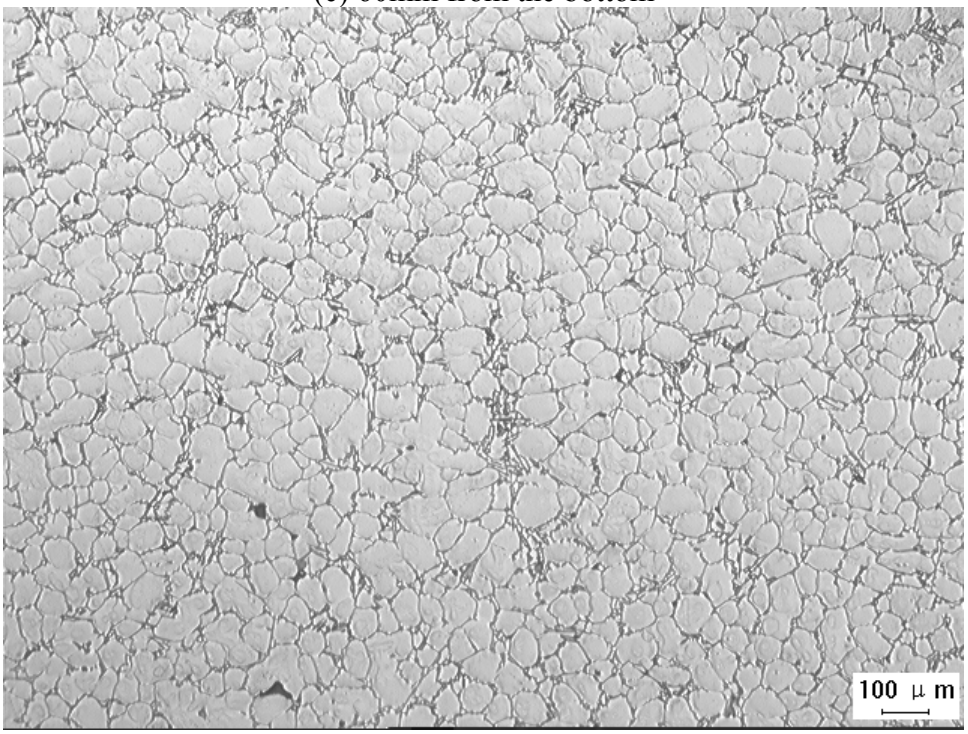

(d) 120mm from the bottom

(Continued)

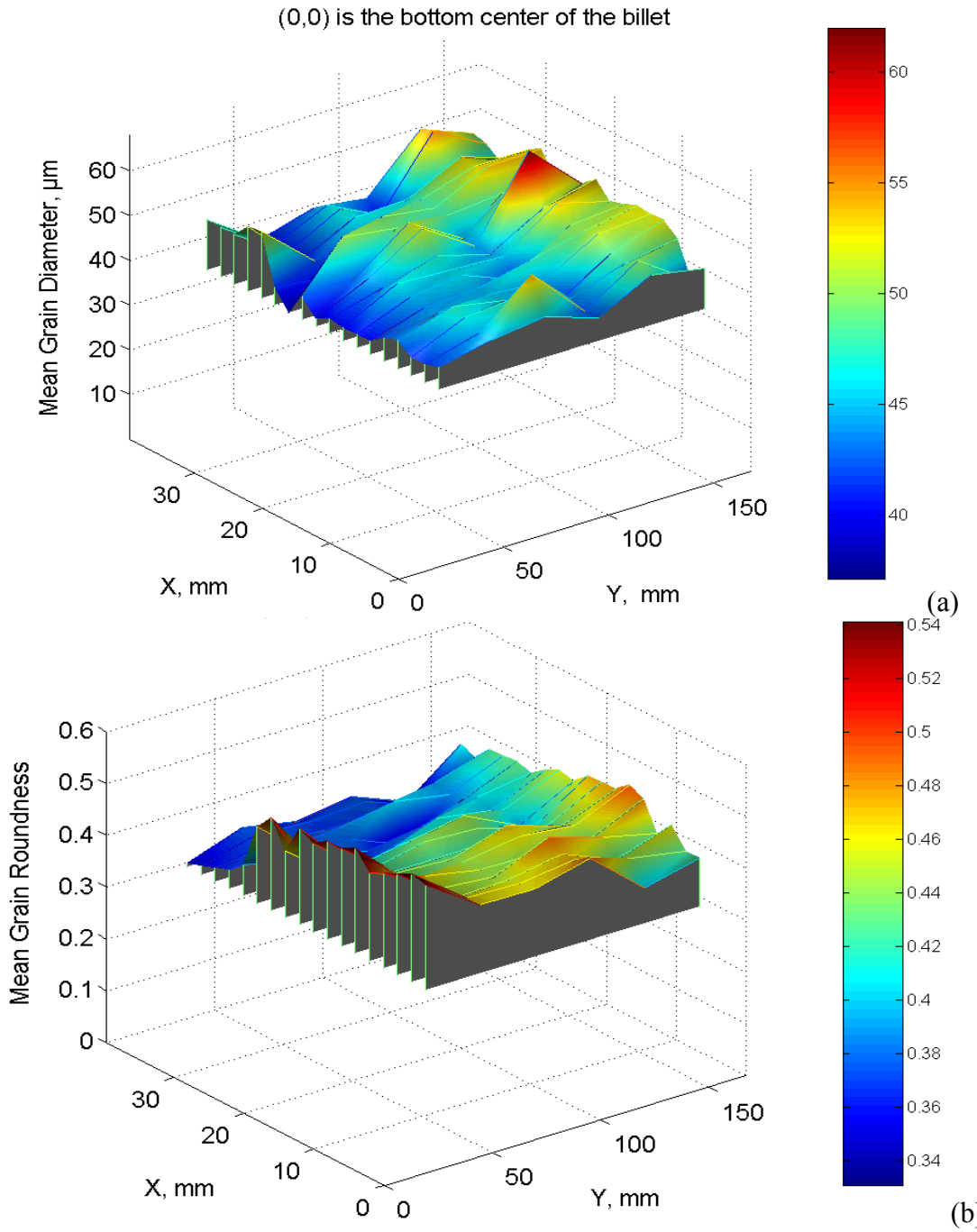

Figure 4.21: Quantitative analysis results showing the resultant 3-dimensional distribution of (a) average fcc grain size and (b) average roundness on the 2 kg billet with ultrasonic vibration. The ultrasonic radiator is located at (0, 0), where x is the distance from the center, and y is the distance from the bottom of the billet.

that ultrasonic vibration is suitable for high volume (SSM) processing.

4.3.3.2 Ultrasonic processing of billet suitable for SSM with the addition of grain refiner

The application of grain refiners in SSM has been studied elsewhere [130]. The resultant grain structures are somehow rosette dendrites, or even globular grains, with the grain size as small as 100 μm [130]. The effect of combining grain refiner and ultrasonic vibration on A356 alloy structure has been investigated. The results are shown in Figure 4.22, Table 4.4, and Table 4.5. With the application of both grain refiner and ultrasonic vibration, the mean grain size of the primary fcc aluminum grains can be even smaller than that of applied grain refiners with no vibration. It suggests that grain refiners can further refine the A356 alloy structure, with the combination of ultrasonic vibration.

To summarize when a high intensity ultrasonic vibration was applied in casting high volume (suitable for SSM process) A356 alloy, the following was observed:

(1) With ultrasonic vibration, the solidification structure is significantly modified. Non-dendritic/globular grains have been obtained in specimens solidified under ultrasonic vibration. The mean grain size of the primary fcc aluminum grains can be as small as 30 μm in specimens with ultrasonic vibration while the grain size is as large as a few millimeters without ultrasonic vibration. The roundness was also increased significantly.

Table 4.4: Quantitative analysis of effect of grain refiner on average grain size (μm)

	Bottom		Top	
	mean	std. dev	mean	std. dev
No vibration	169.3	123.7	156.1	104.6
With vibration	72.5	34.7	66.4	26.3

Table 4.5: Quantitative analysis of effect of grain refiner on average grain roundness

	Bottom		Top	
	mean	std. dev	mean	std. dev
No vibration	0.044	0.0333	0.028	0.021
With vibration	0.4	0.52	0.42	0.733

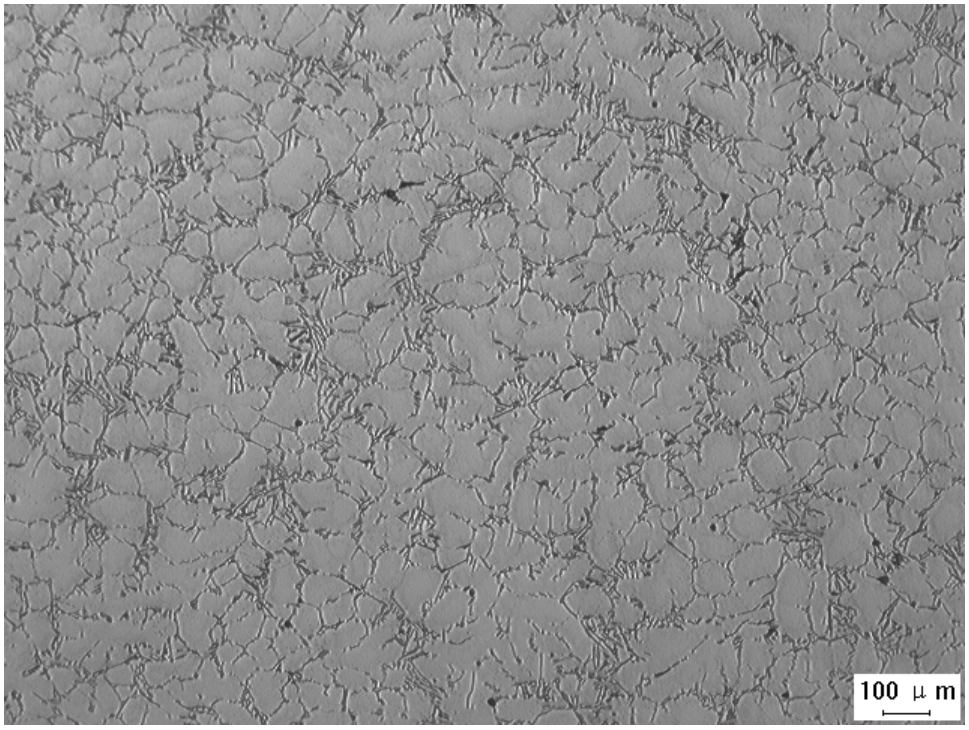

(a) Bottom

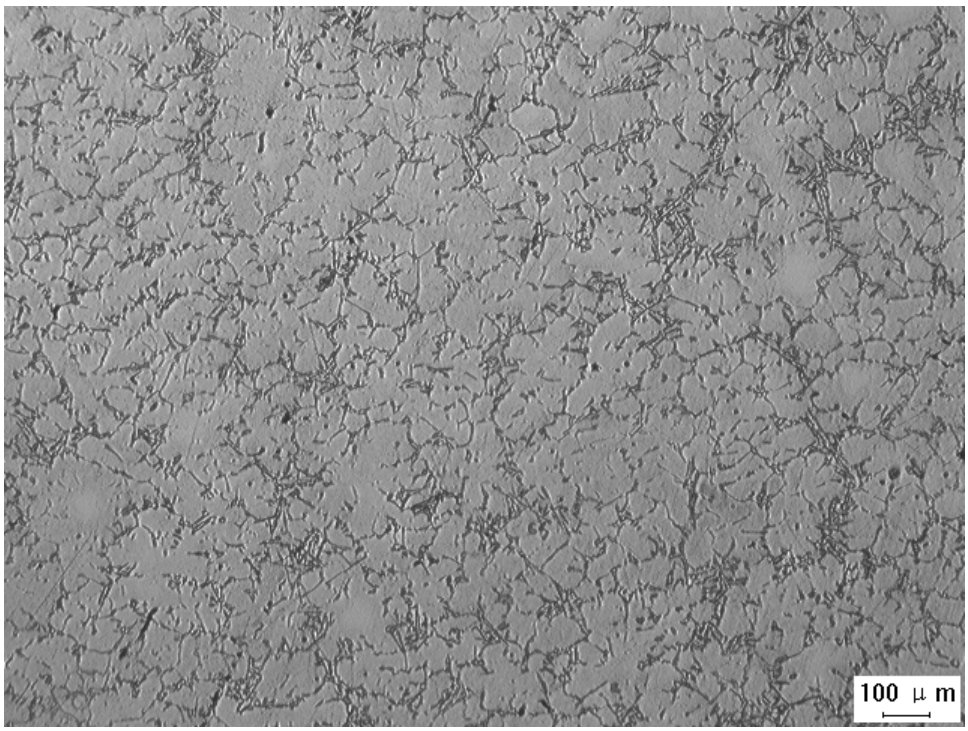

(b) Top

Figure 4.22: The effect of grain refiner on the 2 kg billet as-cast microstructure of A356 alloy without (a, b) and with (c, d) ultrasonic vibration under condition of 630 ^{o}C casting temperature, 100% amplitude, and 60 seconds vibration time.

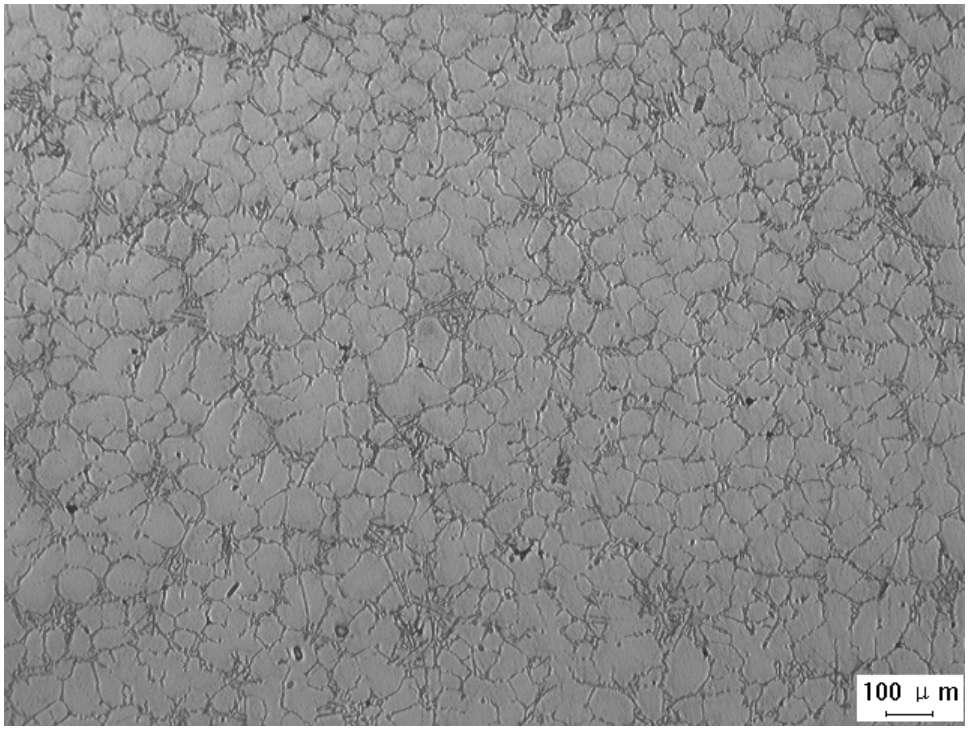

(c) Bottom

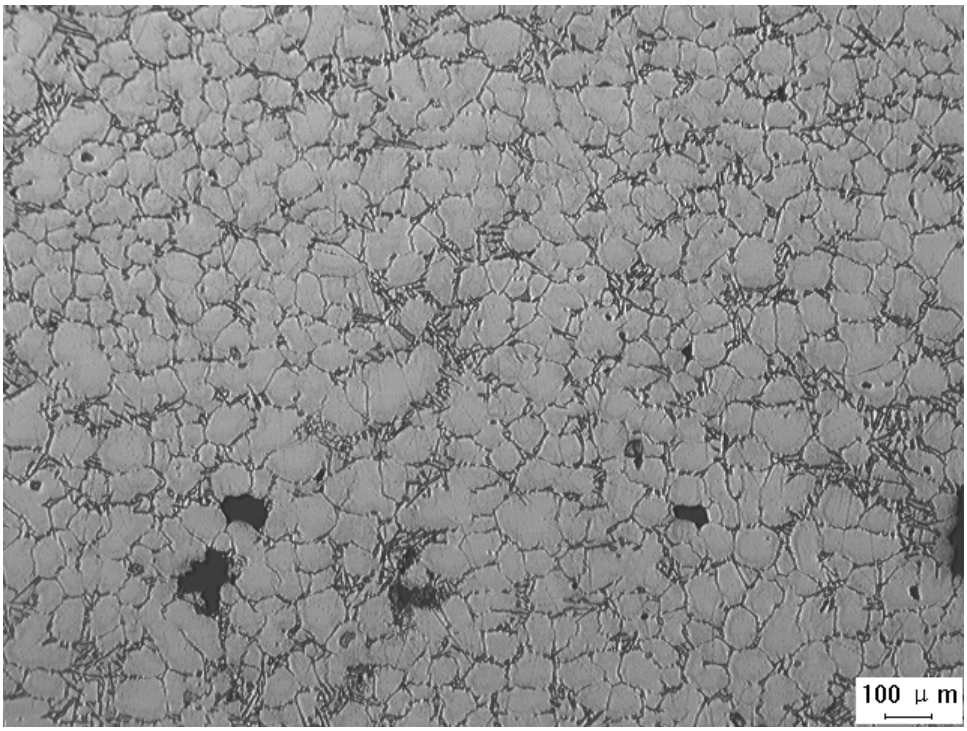

(d) Top

Figure 4.22: (continued)

(2) With the increasing distance from the radiator (transversely or longitudinal), the effectiveness of ultrasonic vibration on grain refinement weakens.

(3) The use of grain refiner breaks up the dendrites, results in smaller primary fcc aluminum grains (about 100 ~ 200 μm) when there is no vibration. With the application of both grain refiner and ultrasonic vibration, the mean grain size of the primary fcc aluminum grains can be even smaller than that of applied grain refiners with no vibration. It suggests that grain refiners can further refine A356 alloy structure, with the combination of ultrasonic vibration.

4.4 Grain refinement in other aluminum alloys

Experiments were also carried out on some other aluminum alloys, i.e., 6061 alloy, 6063 alloy, 319 alloy, 354 alloy, besides A356 alloy. In all cases, grain refinement was obtained in the castings of all alloys treated with high-intensity ultrasonic vibration during the solidification process.

4.4.1. 6061 alloy

Thermodynamic simulations indicated that the melting point of aluminum alloy 6061 is about 653°C. The experiments that involved ultrasonic processing of the solid part of the solidifying specimen were performed under a number of conditions, such as varying the casting temperature from 660 to 720°C. The vibrational amplitude was 100%, and vibration duration time was 60 s.

The resultant microstructures in castings without and with ultrasonic vibration are shown in Figure 4.23 and Figure 4.24, respectively. Without ultrasonic vibration at a casting temperature of 690 ºC, fully developed dendrites were obtained in the casting with averaging size of some millimeters (as shown in Figure 4.23). When exposed to ultrasonic vibration, the columnar/dendritic microstructure was completely removed and fine globular grains were obtained in the castings at different casting temperatures (as shown in Figure 4.24),. It is obvious that ultrasonic vibration is very effective in the grain refinement of this alloy.

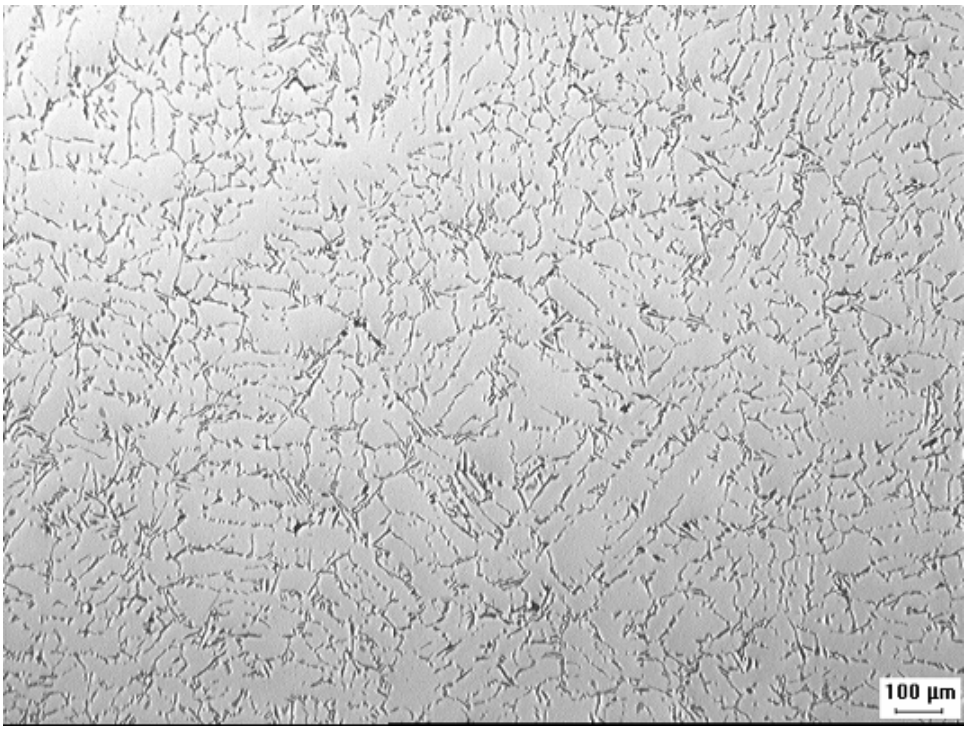

Figure 4.23: Microstructure of 6061 alloy without ultrasonic vibration at a casting temperature of 690 ºC. Fully developed dendrites were obtained with average size of some millimeters.

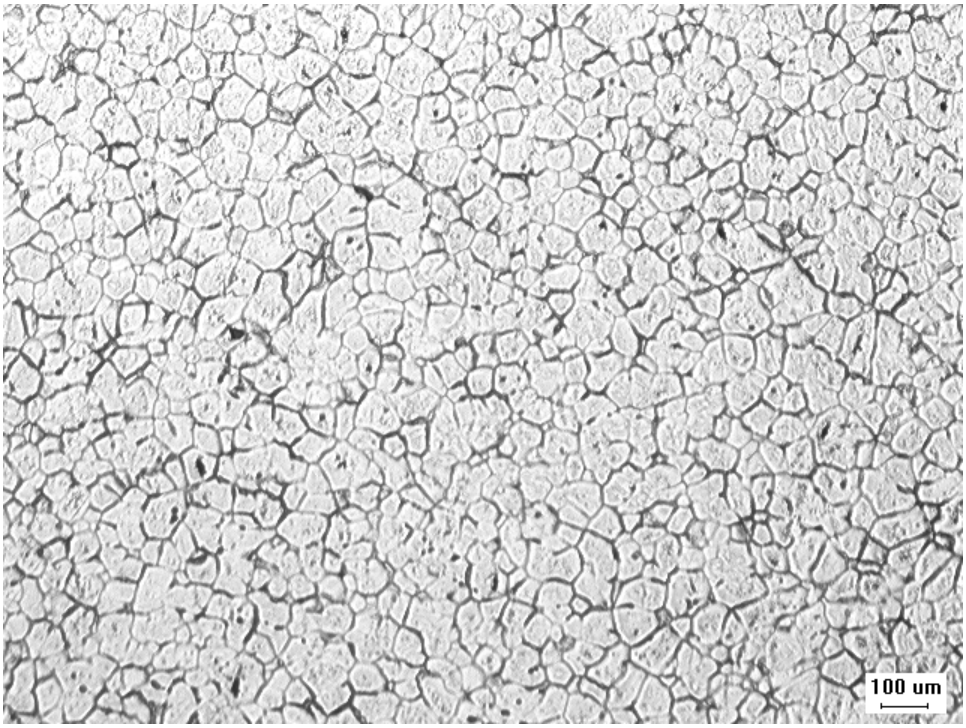

(a)

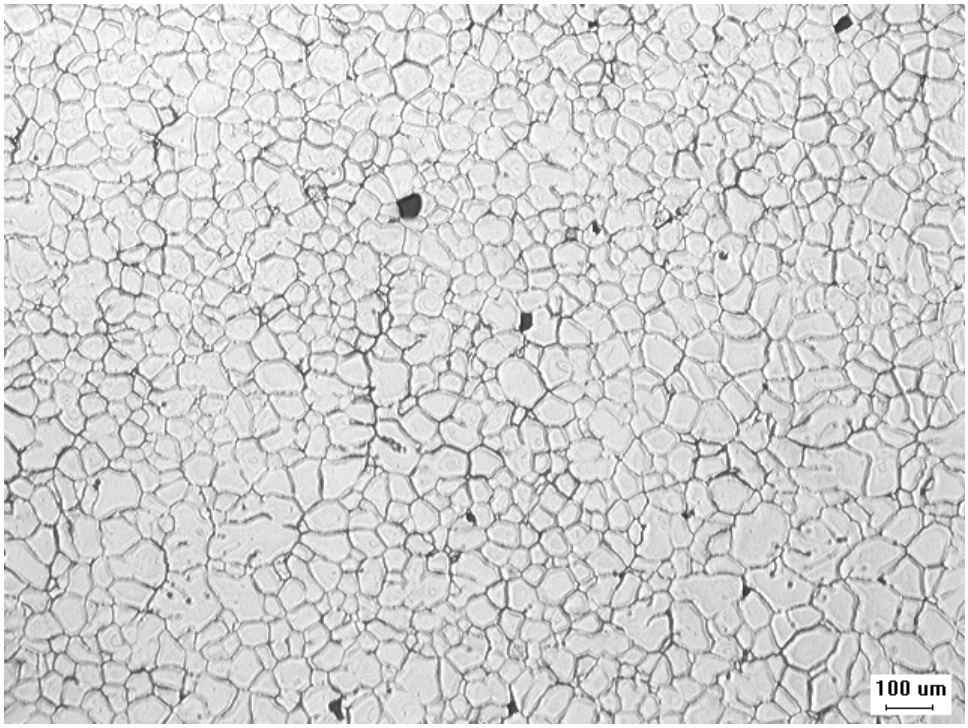

(b)

Figure 4.24: Microstructure of 6061 alloy with ultrasonic vibration at a casting temperature of (a) 700 ºC and (a) 720 ºC. Upon ultrasonic processing, fully developed dendrites were completely removed and fine globular grains were obtained.

4.4.2. 6063 alloy

Thermodynamic simulation indicated that the melting point of this alloy is about 657°C. The experiments to acoustically vibrate the solid part of the solidifying specimens were performed under a number of conditions, including varying the casting temperature from 670 to 730°C. The vibration amplitude was 100%, and vibration duration time was 60 s. Results are shown in Figure 4.25 and Figure 4.26. Dendrites are fully developed in the untreated specimen. However, in the two specimens treated ultrasonically, dendrites do not appear and the microstructure seems to be fine and globular. It is obvious that ultrasonic vibration is very effective in the grain refinement of this alloy.

4.4.3. 319 alloy

Aluminum alloy 319 was cast either in copper or graphite molds under ultrasonic vibration at different casting temperatures. Alloy 319 is of interest commercially for making automotive components; however, grain refinement is difficult to achieve with this material (the normal grain size is in millimeters). Experiments were conducted in order to investigate grain refinement via ultrasonic processing. The applied ultrasonic amplitude was set at 100% and the processing time was 60 seconds. Figure 4.27 shows the measured cooling curve of 319 alloy without ultrasonic vibration. Figure 4.28 shows an untreated specimen and ultrasonically treated specimens cast at different temperatures. As the figure indicates, ultrasonic processing greatly improved the microstructure of the alloy. The grain size decreased from >1 mm (without vibration) to <20 μm, and even to <10 μm under some conditions.

4.4.4. A354 alloy

Aluminum alloy A354 was cast without and with ultrasonic processing in both a 250-g metal mold and a 2-kg metal mold under conditions derived from the thermodynamic simulation. Ultrasonic vibration started right before the casting began. The ultrasonic amplitude was 100%, and the output power was 10–15% of full power. Processing time was 60 s.

Figure 4.29 (a) shows the microstructure of a specimen of the A354 alloy

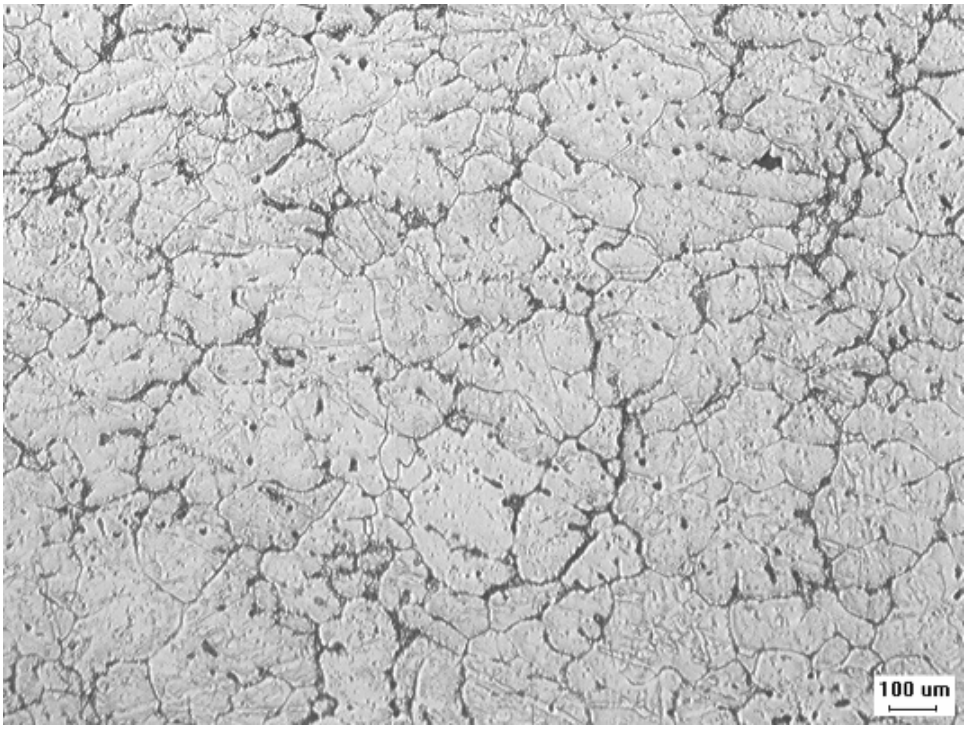

Figure 4.25: Microstructure of 6063 alloy without ultrasonic vibration at a casting temperature of 690 ºC. Fully developed dendrites were obtained with average size of some millimeters.

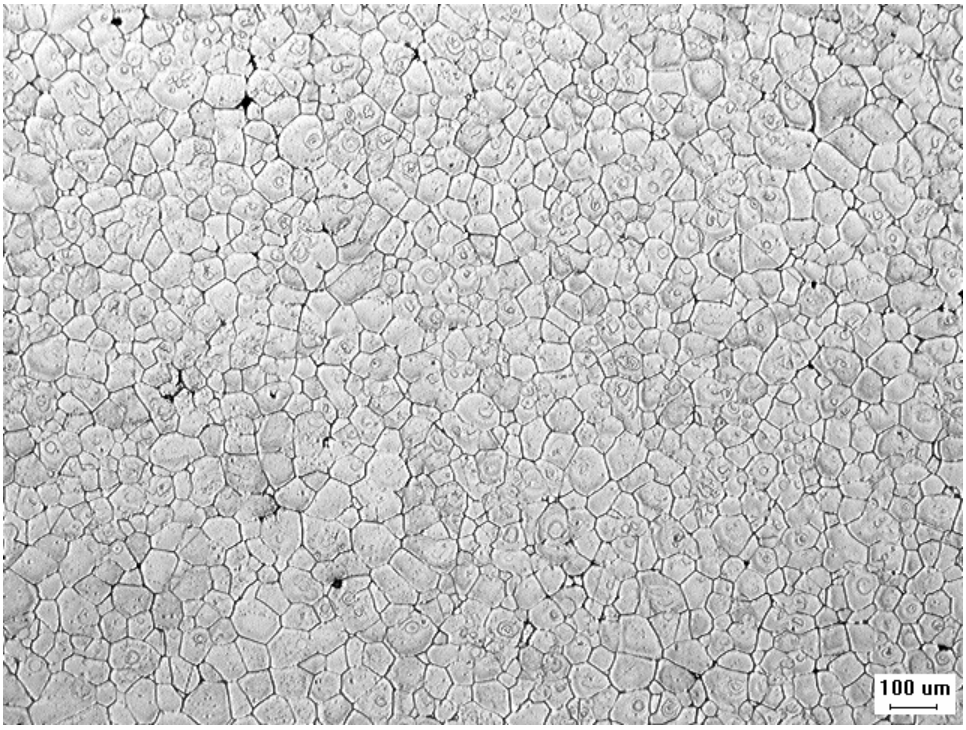

(a)

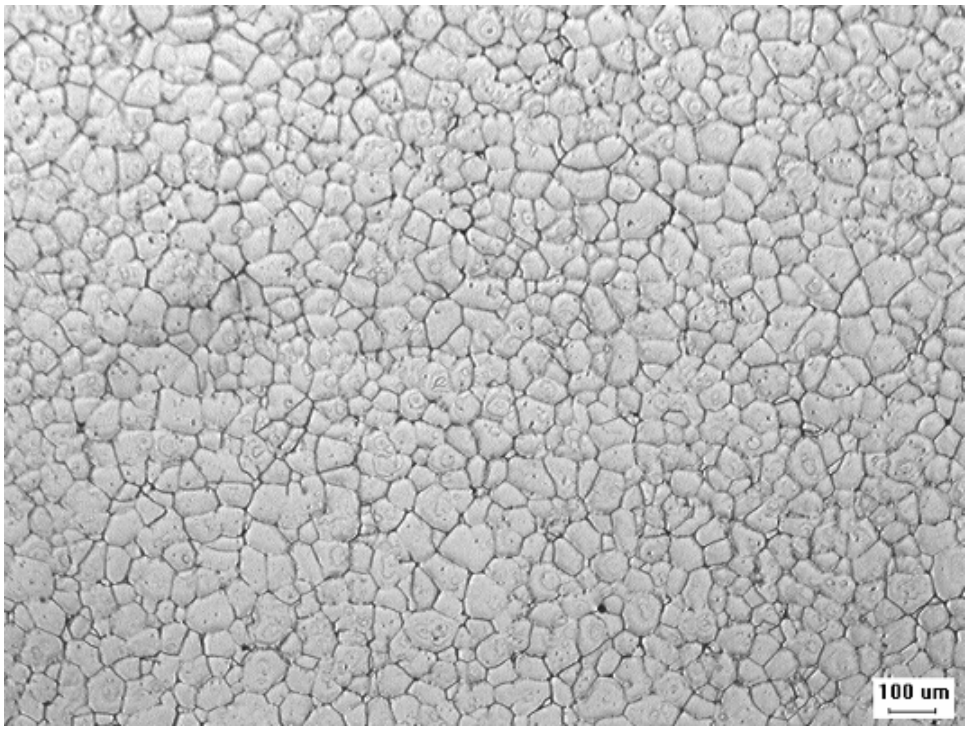

(b)

Figure 4.26: Microstructure of 6063 alloy with ultrasonic vibration at a casting temperature of (a) 700 ºC and (a) 730 ºC. Upon ultrasonic processing, globular grains were obtained. Again ultrasonic processing was proven to be efficient in obtaining small globular grains in this aluminum-silicon-magnesium wrought alloy.

Figure 4.27: Microstructure of 319 alloy without ultrasonic vibration at a casting temperature of 650 ºC. Dendritic microstructure was obtained.

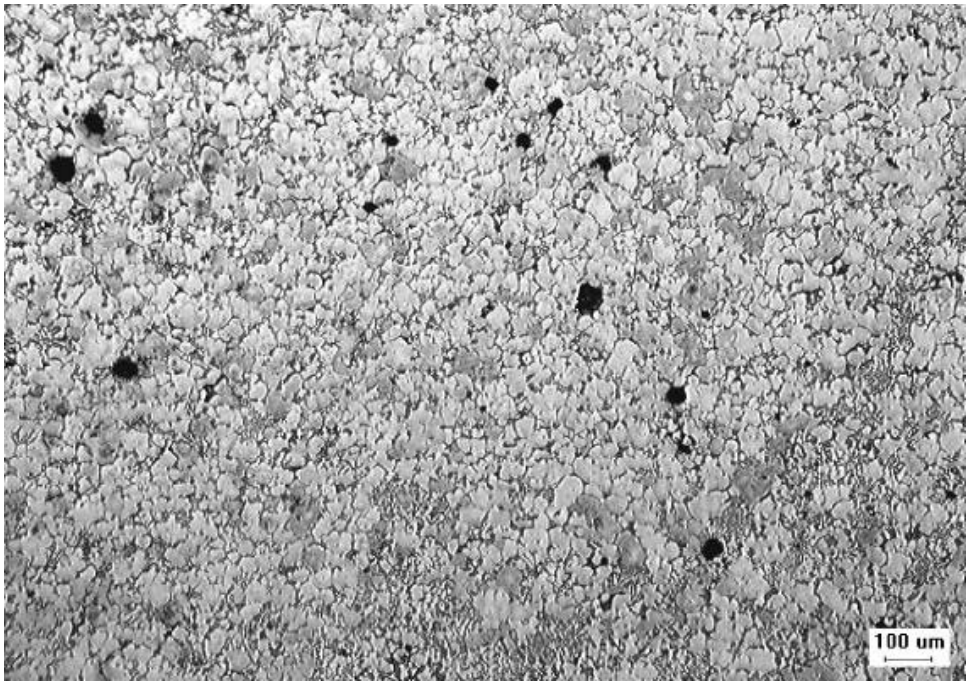

(a)

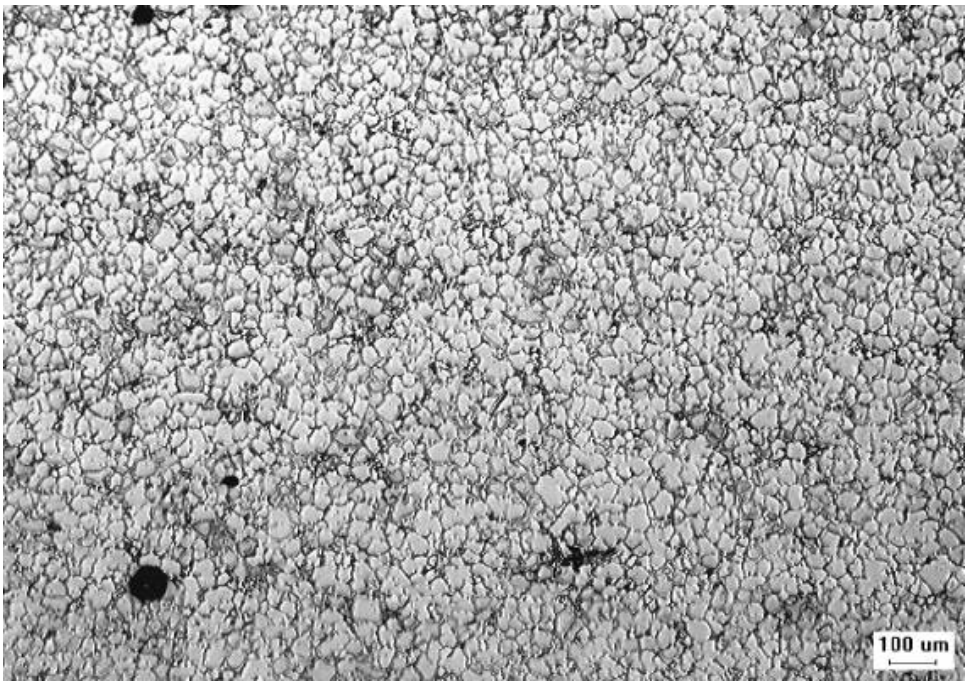

(b)

Figure 4.28: Microstructure of 319 alloy with ultrasonic vibration at a casting temperature of (a) 640 ºC and (a) 650 ºC. Upon ultrasonic processing, globular grains were obtained. Again ultrasonic processing was proven to be efficient in obtaining small globular grains in this aluminum-silicon-magnesium foundry alloy.

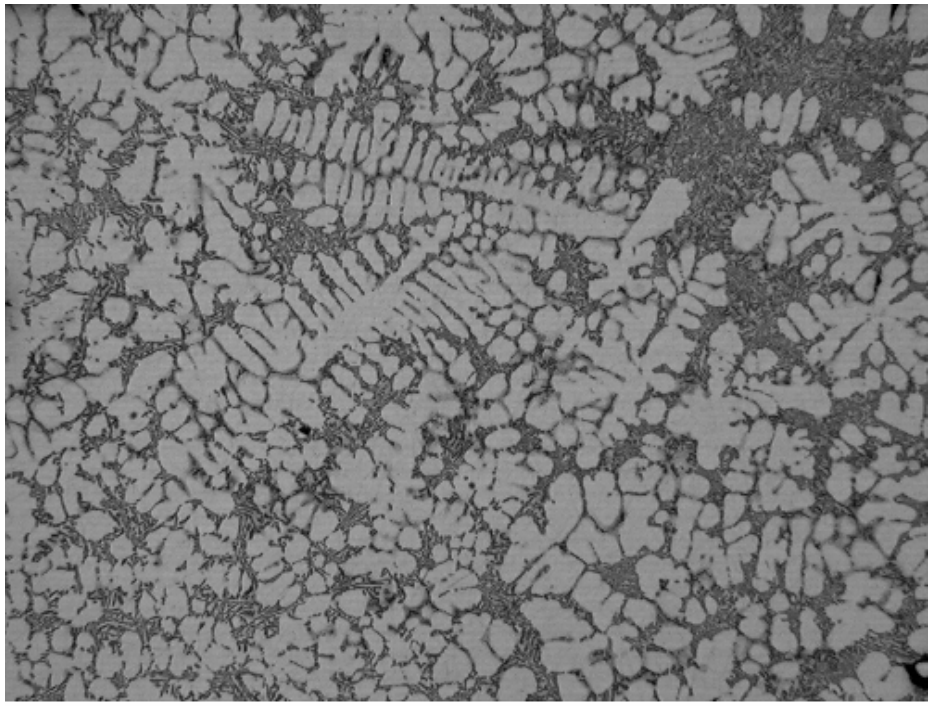

(a)

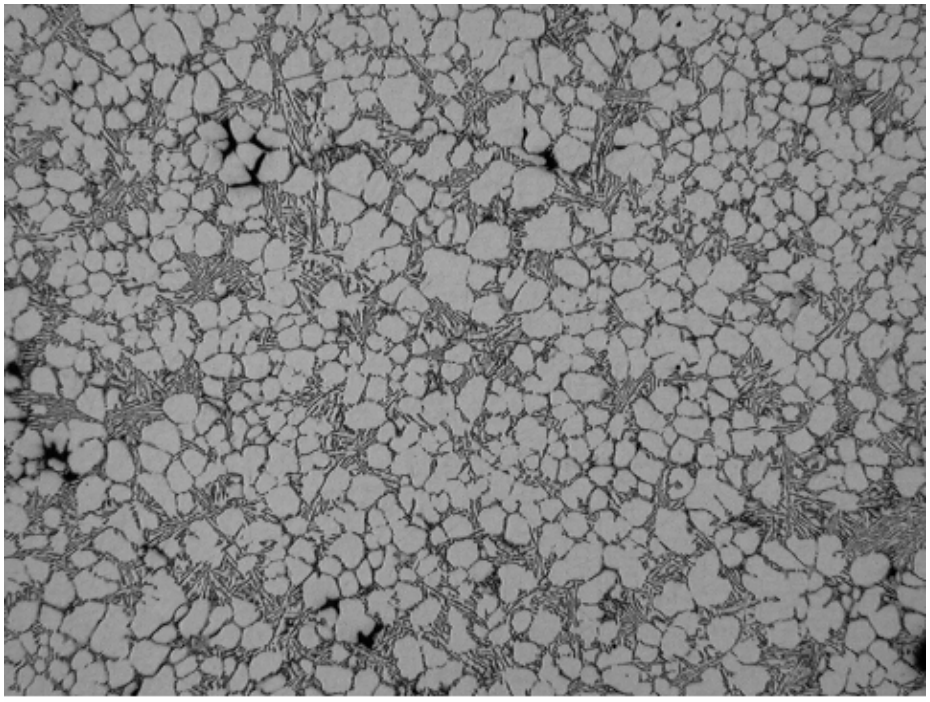

(b)

Figure 4.29: Microstructure of A354 alloy (a) without and (b) with ultrasonic processing. It is clearly seen that with ultrasonic vibration the dendrites were removed. Fine globular primary aluminum grains were obtained and eutectic silicon phase was also refined.

processed without ultrasound, while Figure 4.29 (b) shows the microstructures resulting from exposure to ultrasonic energy.

It can be seen that upon ultrasonic vibration, the dendritic primary face-centered cubic (fcc) aluminum was broken into fine, globular grains, while the morphology of second phases was also modified. The A354 aluminum alloy is used mainly in the aerospace industry, where outstanding strength characteristics are required. In general, a fine as-cast microstructure improves mechanical properties owing to the increased yield strength as well as toughness. Fine second phases such as eutectic silicon enhance toughness properties, especially ductility and fatigue toughness. The enhanced microstructure will also lead to reduced scrap rate of casting, resulting in energy and cost savings

4.4.5. 2618 alloy

Aluminum 2618 alloy is a wrought alloy commonly used in the forging industry. It is therefore of great interest to refine this alloy before the final forging and shape-forming process. Experiments were conducted in attempting to find the optimum casting temperature for grain refinement with the aid of ultrasonic processing for the industry application purpose. The thermodynamical simulation result shows that the solidus of this alloy is 638 °C. Accordingly the alloy was melted and held at a temperature of 750 °C before being cast into the steel mold prepared by Queen City Forging CO. Six casting temperatures, i.e., 640 °C, 650 °C, 660 °C, 670 °C, 680 °C, and 690 °C, have been tried in the experiments. The applied ultrasonic amplitude was set at 100% and the processing time was 60 seconds. Subsequently the samples were polished and etched with Graff and Sargent Reagent (84mL water, 15.5 mL HNO_3, 0.5 mL HF, 3 g CrO_3) especially for revealing grain size of 2xxx wrought alloys. The samples were immersed 20 s in this etchant with mild agitation then immersed in 0.5% HF water-solution for 3 s.

Figure 4.30 shows the microstructure of 2618 alloy casting without ultrasonic vibration at the magnifications (a) 50 x and (b) 400 x. Typical dendritic grains can be seen in either photos. While Figure 4.31 - Figure 4.34 display the resultant microstructure at the casting temperatures of 680 °C, 670 °C, 660 °C, 650 °C, respectively, with

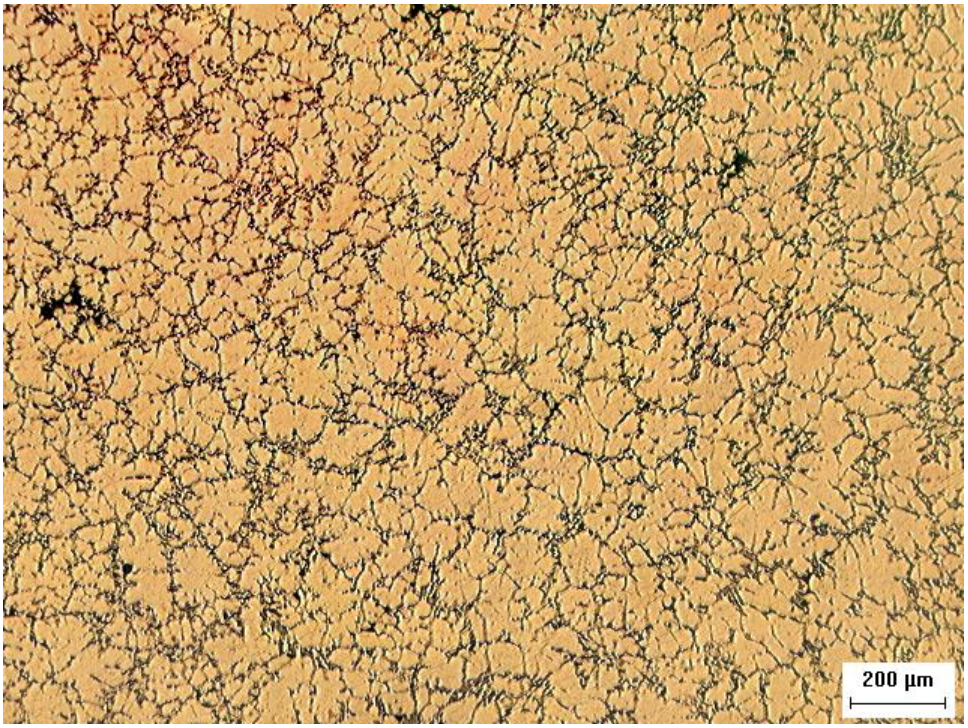

(a)

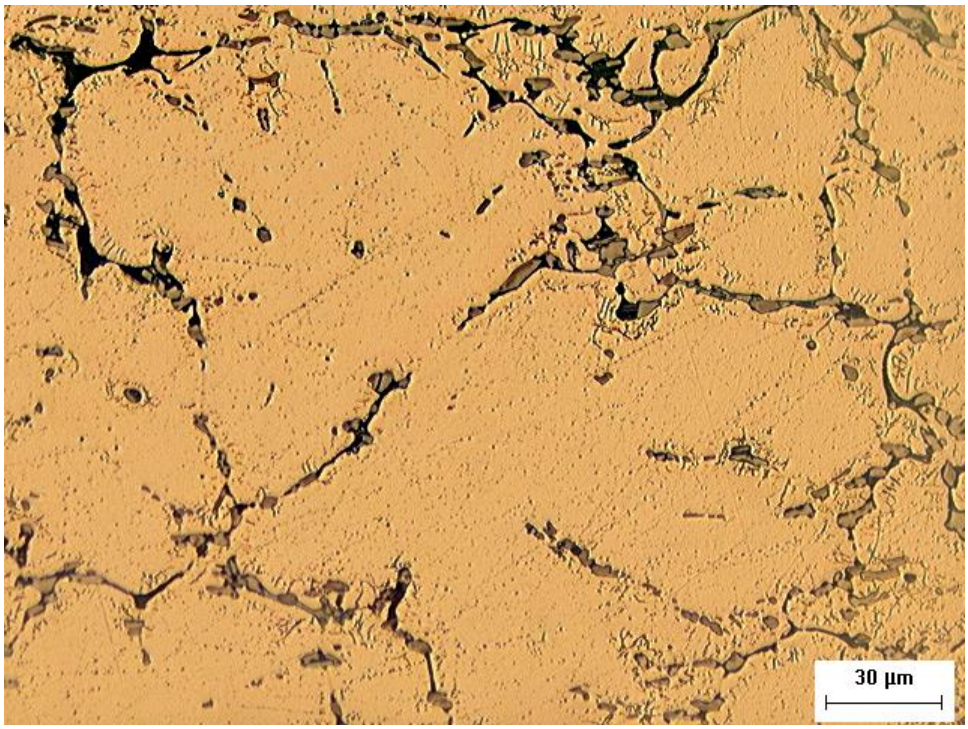

(b)

Figure 4.30: Microstructure of 2618 alloy casting without ultrasonic vibration at the magnifications (a) 50 x and (b) 400 x. Typical dendritic grains can be seen in either photos.

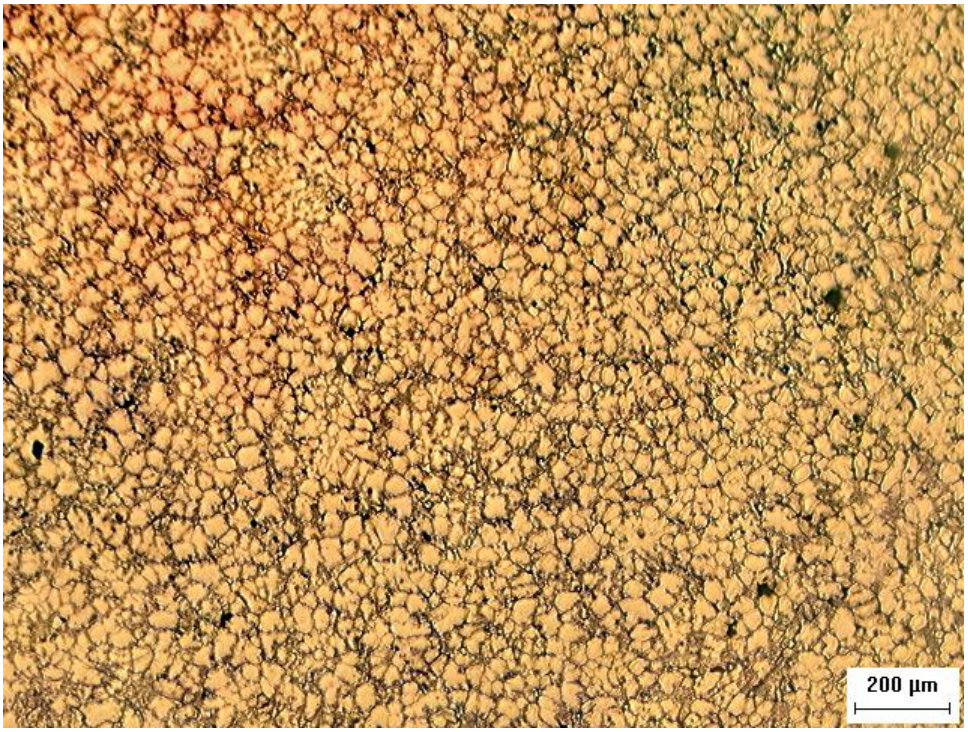

(a)

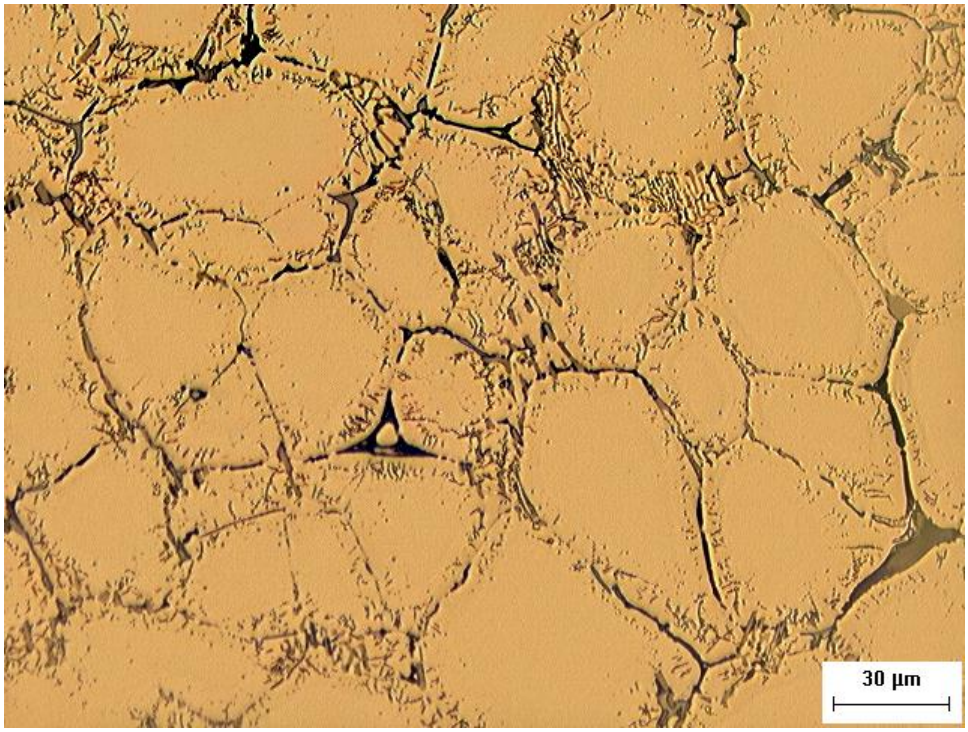

(b)

Figure 4.31: Microstructure of 2618 alloy casting at the casting temperature of 680 °C with ultrasonic vibration at the magnifications (a) 50 x and (b) 400 x. Fine globular grains were obtained.

(a)

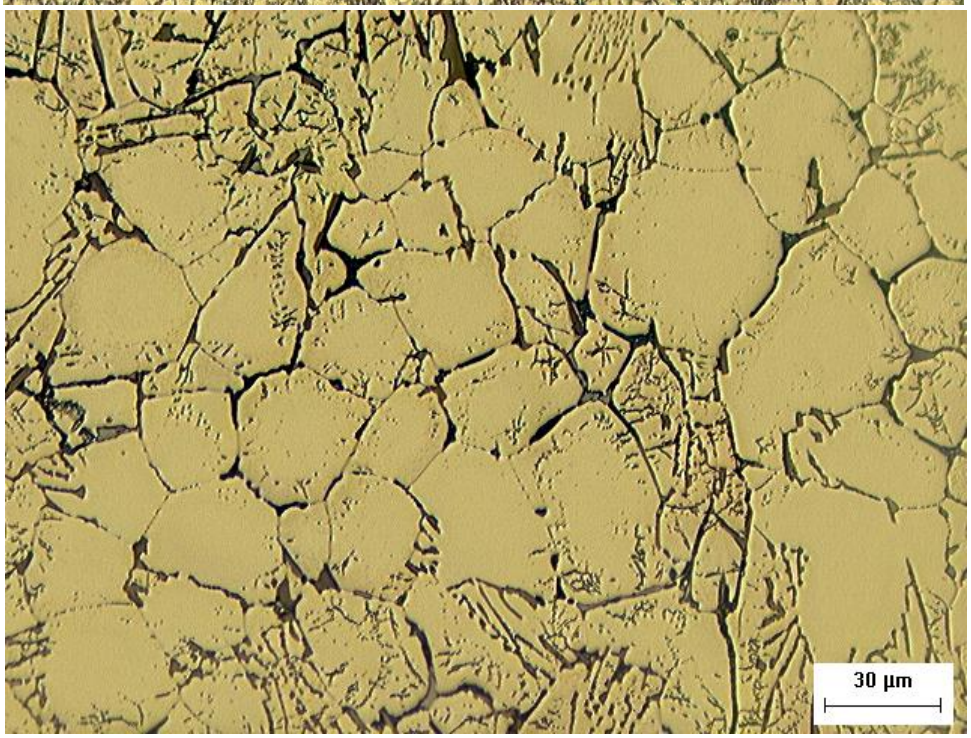

(b)

Figure 4.32: Microstructure of 2618 alloy casting at the casting temperature of 670 °C with ultrasonic vibration at the magnifications (a) 50 x and (b) 400 x. Extremely fine globular grains were obtained.

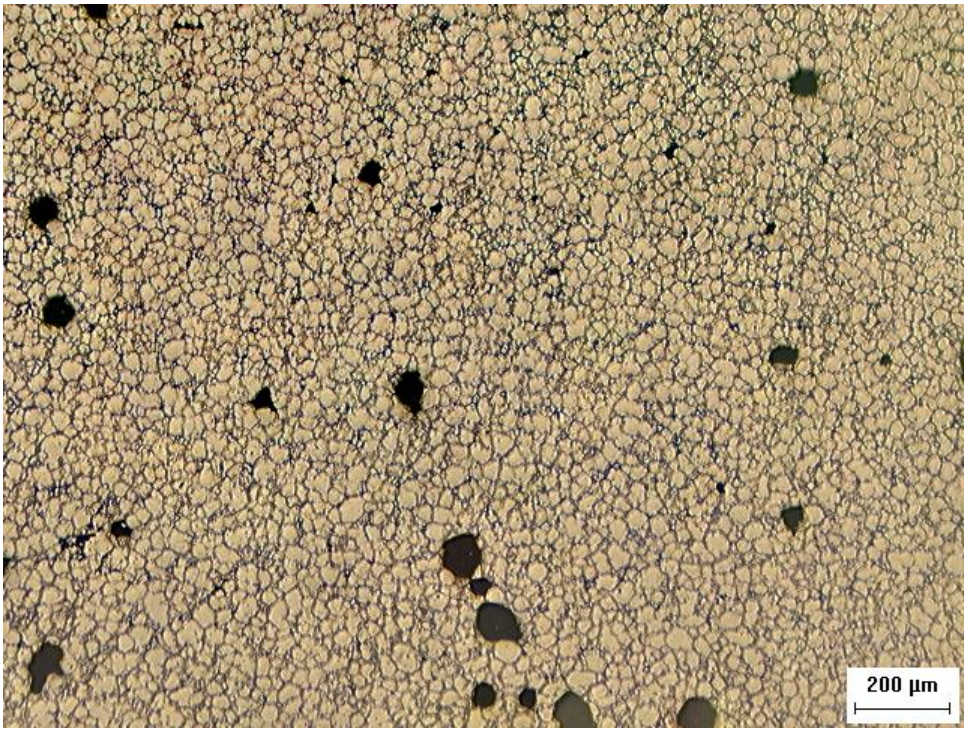

(a)

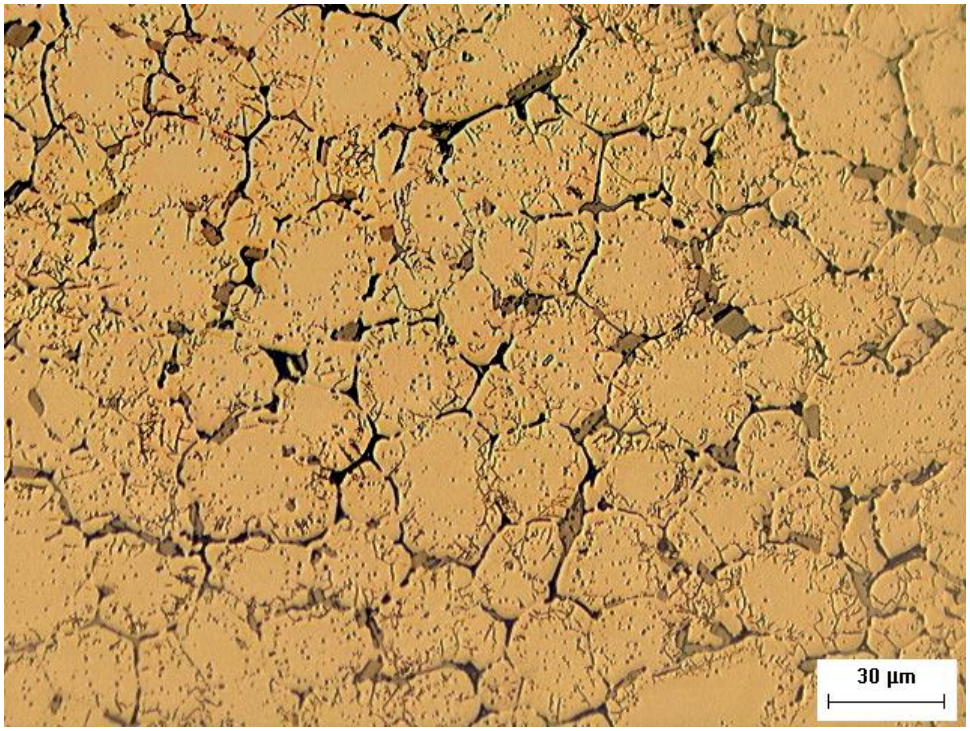

(b)

Figure 4.33: Microstructure of 2618 alloy casting at the casting temperature of 660 °C with ultrasonic vibration at the magnifications (a) 50 x and (b) 400 x. Fine globular grains were obtained.

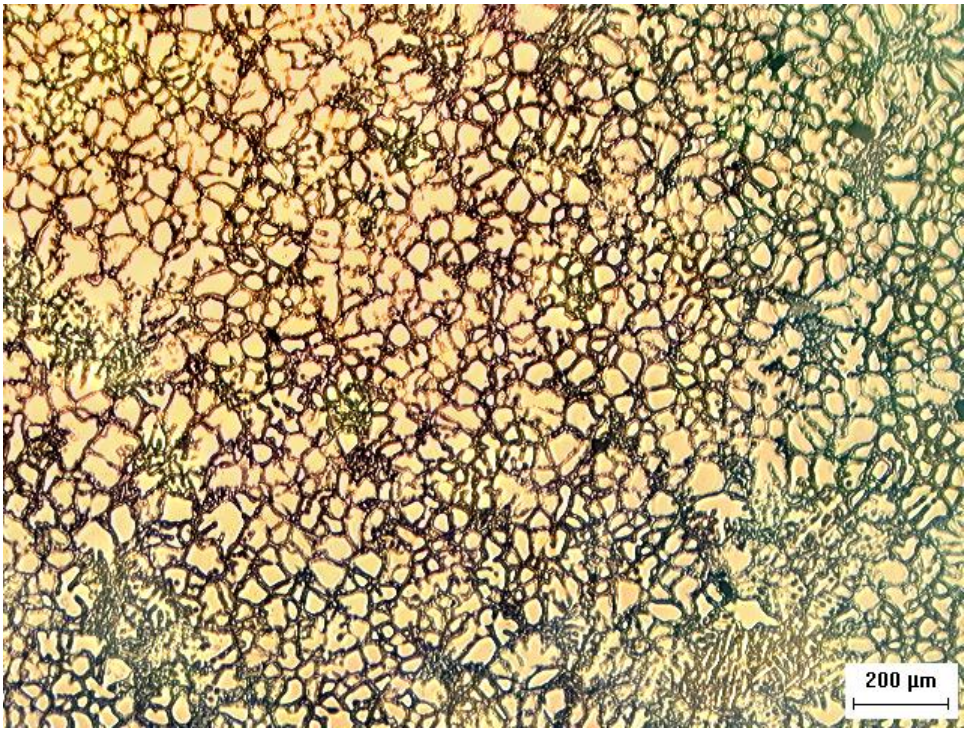

(a)

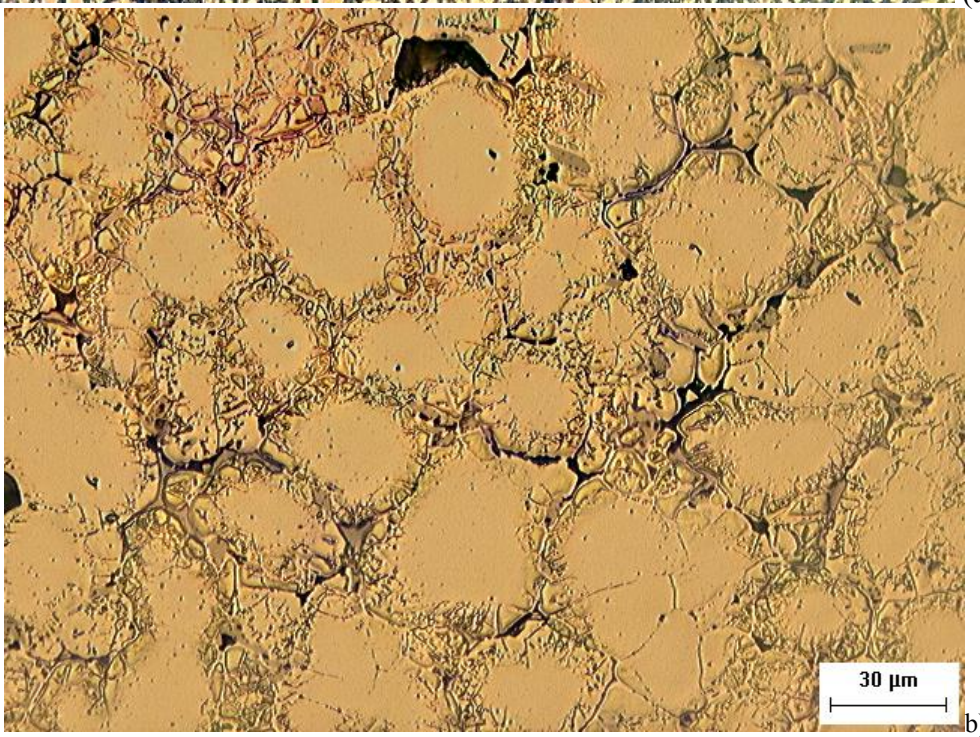

b)

Figure 4.34: Microstructure of 2618 alloy casting at the casting temperature of 650 °C with ultrasonic vibration at the magnifications (a) 50 x and (b) 400 x. The alloy was refined to some extent however the dendritic structure can be observed in the photos.

ultrasonic vibration at the magnifications (a) 50 x and (b) 400 x. As the figures indicate, ultrasonic processing greatly improved the microstructure of the alloy. At the casting temperature of 670 °C, extremely fine globular grains were obtained. While larger but still fine globular grains were obtained in the castings at the casting temperature of 680 °C and 660 °C. However, at the casting temperature of 650 °C, the alloy was refined to some extent; however, the dendritic structure can be observed in the photos.

Quantitative analysis was carried out on the grain size without ultrasonic vibration and with ultrasonic vibration at various casting temperatures. The results are drawn in Figure 4.35. From the figure, it is obvious that the casting temperature of 670 °C is the optimum temperature for grain refinement with the aid of ultrasonic vibration.

To summarize when ultrasonic energy is introduced into various metal melts, the following is observed:

(1) Fine globular grains were obtained in various aluminum alloys, including A354, 319, 6063, 6061, 2618 alloys.

(2) 670 °C is the optimum casting temperature for grain refinement of 2618 wrought alloy with the aid of ultrasonic vibration.

4.5 Eutectic modification of an Al – Si based alloy

The eutectic silicon in A356 alloy can be refined and modified using either chemical, quench, or superheating modification. We observed, for the first time, that the eutectic silicon can also be significantly refined using high-intensity ultrasonic vibration. Rosette-like eutectic silicon is formed during solidification of the specimen treated with high-intensity ultrasonic vibration.

4.5.1. Introduction

Aluminum A356 alloy is one of the widely used casting aluminum alloys because of its good mechanical strength, ductility, hardness, fatigue strength, pressure tightness, fluidity, and machinability [143]. The A356 alloy contains about 50 vol% primary fcc aluminum and 50 vol% eutectic phases. Fine as-cast primary fcc grain structure improves mechanical properties owing to the increased yield strength as well as toughness. With fine second phases, the eutectic silicon morphology, enhances properties especially the

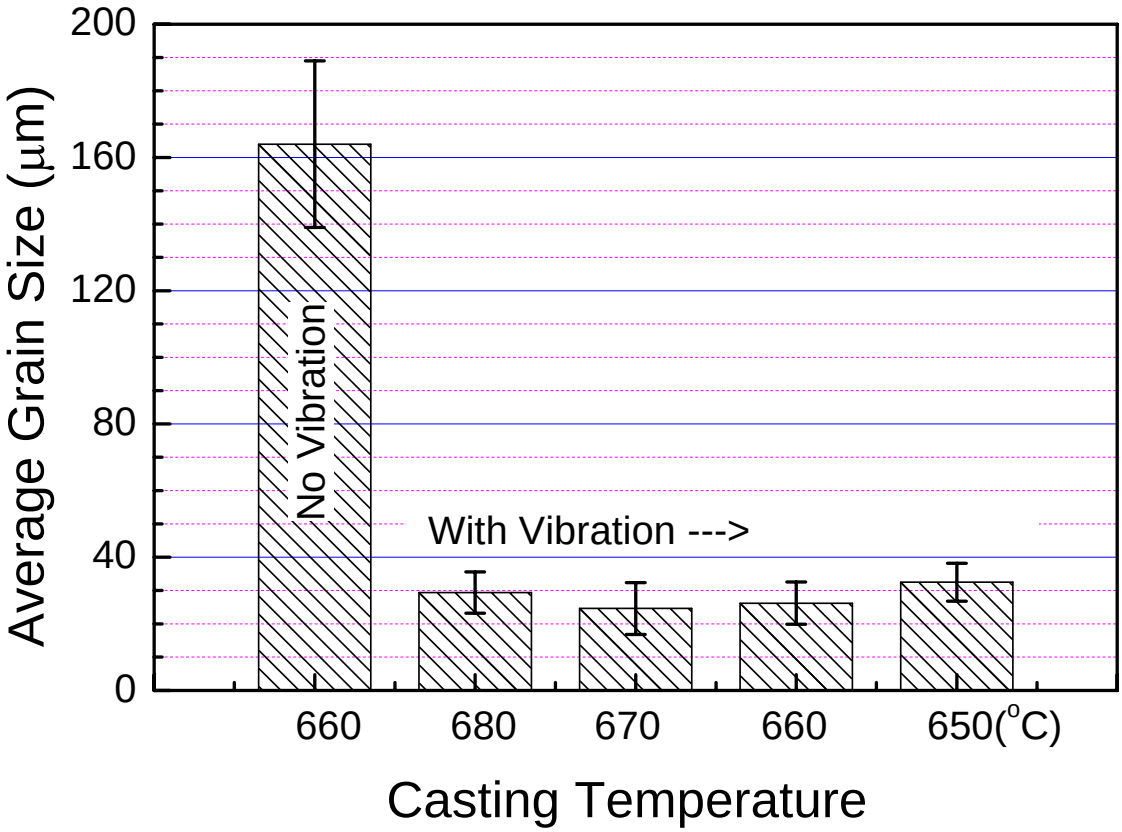

Figure 4.35: Grain size calculation for 2618 alloy with and without ultrasonic vibration. It is obvious that the casting temperature of 670 °C is the optimum temperature for grain refinement with the aid of ultrasonic vibration

ductility and prevents defects [144]. It is of interests to modify its microstructure, to control not only the size of dendrites, but also the eutectic mixture of the two coprecipitating phases.

The final microstructure of A356 is largely determined by the eutectic reaction. Due to its diamond cubic crystal structure which predominantly grows in the <112> directions on (111) planes, silicon is a faceted phase with strongly anisotropic growth thus it is difficult to change the growth direction [145, 146]. In unmodified A356 alloy, the main eutectic reaction occurs at 574 °C as a binary reaction, which results in coarse irregular plate-like silicon. The modification of eutectic silicon is of general interests since fine eutectic silicon along with fine primary aluminum grains improve mechanical properties and ductility [147].

Three well known eutectic modification methods have been developed thus far, namely 1) chemical modification [145-152], which produces a fine fibrous silicon structure through the addition with trace-levels of several elements, such as sodium, antimony, potassium, calcium, strontium, and barium; 2) quench modification [146, 153], which results in silicon forming an exceedingly fine form when compared to the unquenched silicon, through high cooling rates and rapid solidification in the growth rate ranging from 400 to 1000 μm per second; and 3) superheating modification, which requires the presence of magnesium in the alloy [154] to obtain fibrous silicon by heating up the melt from the usual pouring temperature (for example, 680 °C) to a temperature of 850 – 900 °C and held for about 15 – 30 minutes, then quickly cooled to the pouring temperature before casting. The chemical modification has been widely used in industry for producing A356 alloy with fine and fibrous eutectic silicon phase, and thus improved mechanical properties.

This section describes experimental results on the modification of the eutectic silicon phase using high intensity ultrasonic vibration. Similar results have never been published by other researchers.

4.5.2. Experimental conditions

Commercial aluminum A356 alloy was used in this study. The primary aluminum dendrites start to form at 614°C and the binary Al-Si eutectic at 574°C. The tertiary eutectics and complex intermetallics form at the late stage of solidification [155].

An experimental setup described in Figure 3.4 was used. The power output of the unit was variable within a maximum of 1500 watts by adjusting the output acoustic amplitude from 24.3 – 81 μm, or 30% to 100% of the unit's upper limit. The ultrasonic radiator was placed at the bottom of a copper mold which held up to 250 grams of molten aluminum.

Ultrasonic vibration with an amplitude of 56.7 μm was started right before the melt was poured into the copper mold. For comparison reasons, samples were also made without ultrasonic vibration. These untreated castings were hemispherical in shape with a diameter of 5 cm and weight of 200 g.

The as-polished samples were characterized using an optical microscope with the capability of quantitative metallographic analysis. They were then lightly etched using a 0.5% HF – water solution and further examined using a Hitachi S-4700 scanning electron microscope (SEM) with a light element EDS X-ray detector. Finally the samples were deep etched in a 0.5% HF – water solution for two hours in order to reveal the three-dimensional morphology of the eutectic silicon phase.

4.5.3. Results and discussion

The optical micrographs (100x) of the samples from castings made with and without high-intensity ultrasonic vibration are shown in Figure 4.36. Casting sample made without ultrasonic vibration exhibited coarse acicular eutectic silicon dispersed among the fully developed primary aluminum dendrites. The eutectic silicon was about 100 μm in length. In addition, one branch of a primary dendrite shown in the middle of Figure 4.36 (a) was about 800 μm in length, indicating that the grain size was in the range of a few millimeters since one equiaxed grain usually contained six primary dendrite arms. In contrast, the ultrasonically treated A356 alloy displayed a microstructure of continuous very fine Al-Si eutectic interspersed with fine globular primary aluminum grains (

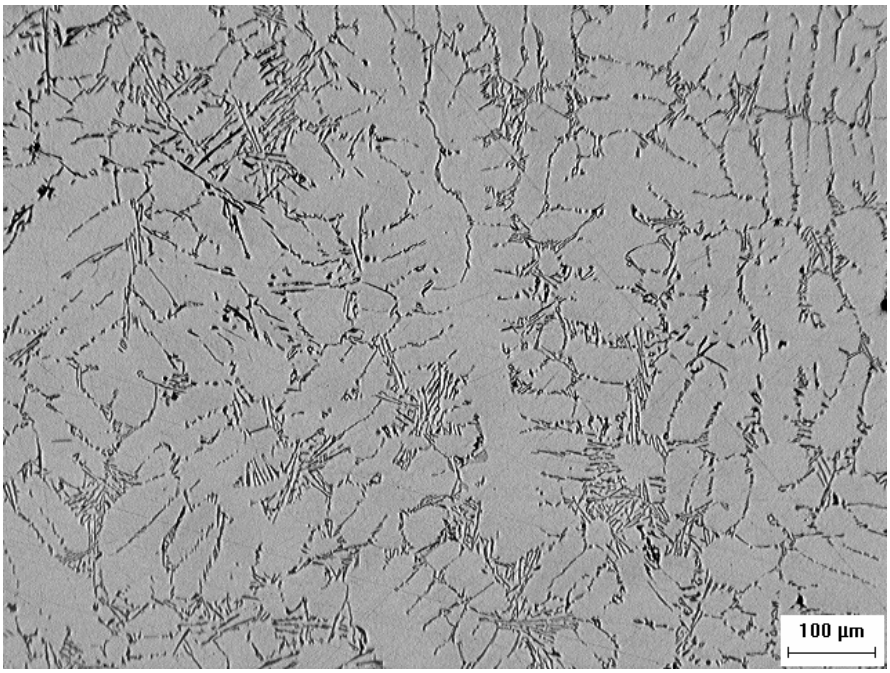

(a)

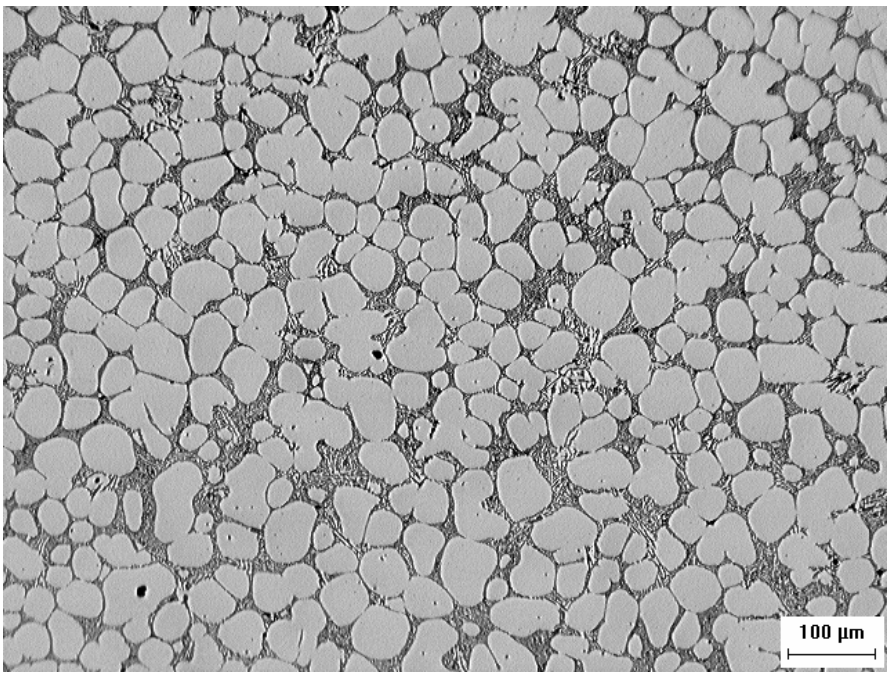

(b)

Figure 4.36: Eutectic modification observed by optical metallurgical microscopy at low magnification, (a) without ultrasonic treatment and (b) with ultrasonic treatment.

Figure 4.36(b)). The shape and size of individual eutectic silicon grains could not be resolved at such a magnification. The formation of a spherical primary aluminum phase has been reported elsewhere [154].

Both samples were characterized with SEM at a high magnification of 2000 X, as shown in Figure 4.37. The coarse acicular eutectic silicon observed on the untreated A356 alloy agreed with that of low magnification observation. While with ultrasonic treatment, very fine eutectic silicon was observed, which was finer than that in strontium modified A356 alloy of similar casting condition [156]. The EDS X-ray analysis verified that those particles shown in the eutectic areas were mainly elemental silicon, rather than intermetallic phases or inclusions.

Results of quantitative metallographic analysis of silicon morphology are illustrated in Figure 4.38. Without ultrasonic treatment, the average length of eutectic silicon was about 26 μm, and the average width 2.7 μm. The aspect ratio was slightly less than 10. While with ultrasonic treatment, the average length and width were respectively about 2 μm and 0.6 μm, with an aspect ratio of slightly less than 3. A comparison of the aspect ratio of the untreated (about 9.8) and ultrasonically treated (about 2.8) A356 alloy suggests that the silicon morphology in ultrasonically modified A356 alloy is not just an exceedingly fine form of the silicon in the unmodified alloy.

Figure 4.39 shows the comparison of the 3-dimensional morphology of eutectic silicon observed by SEM on the deep-etched samples. The eutectic silicon without ultrasonic treatment exhibited a typical coarse plate-like form (Figure 4 (a)); whereas it had a rosette-like form with ultrasonic treatment (Figure 4.39 (b)). The result again suggested that the modified eutectic silicon is not simply a finer form of the unmodified A356 alloy. The mechanism by which the finer eutectic silicon phase forms under ultrasonic treatment is not clear at the moment. However, the rosette-like structure of the silicon phase shown in Figure 4.39 (b) is an indication that the eutectic cells were nucleated in the remaining liquid among dendrites during eutectic solidification. The center of the rosette could be the center of a eutectic cell. The untreated specimen exhibited plate-like structure which was most likely due to the nucleation and the

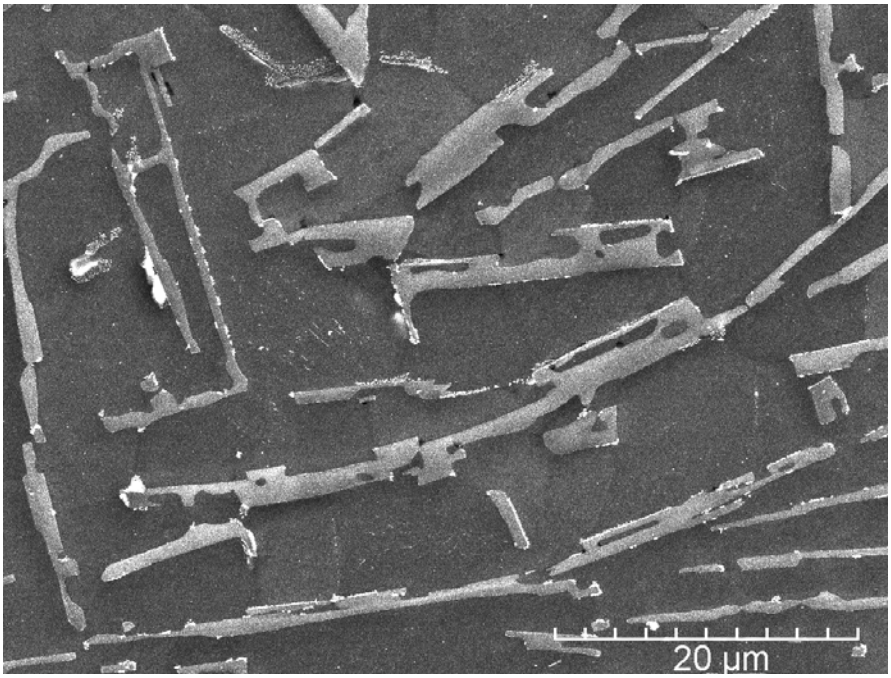

(a)

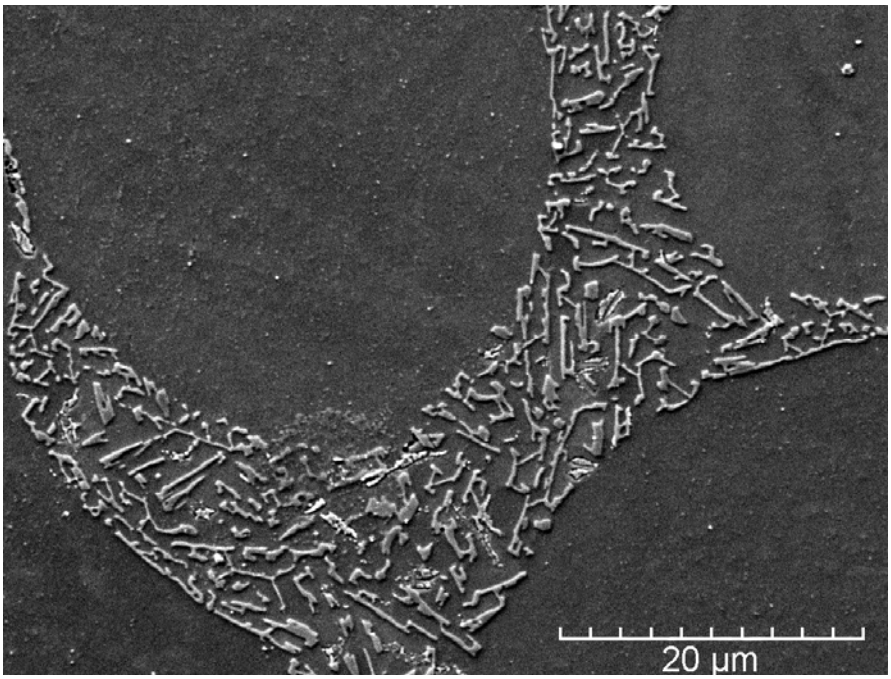

(b)

Figure 4.37: Eutectic modification observed by SEM at 2000X magnification, (a) without ultrasonic vibration and (b) with ultrasonic vibration.

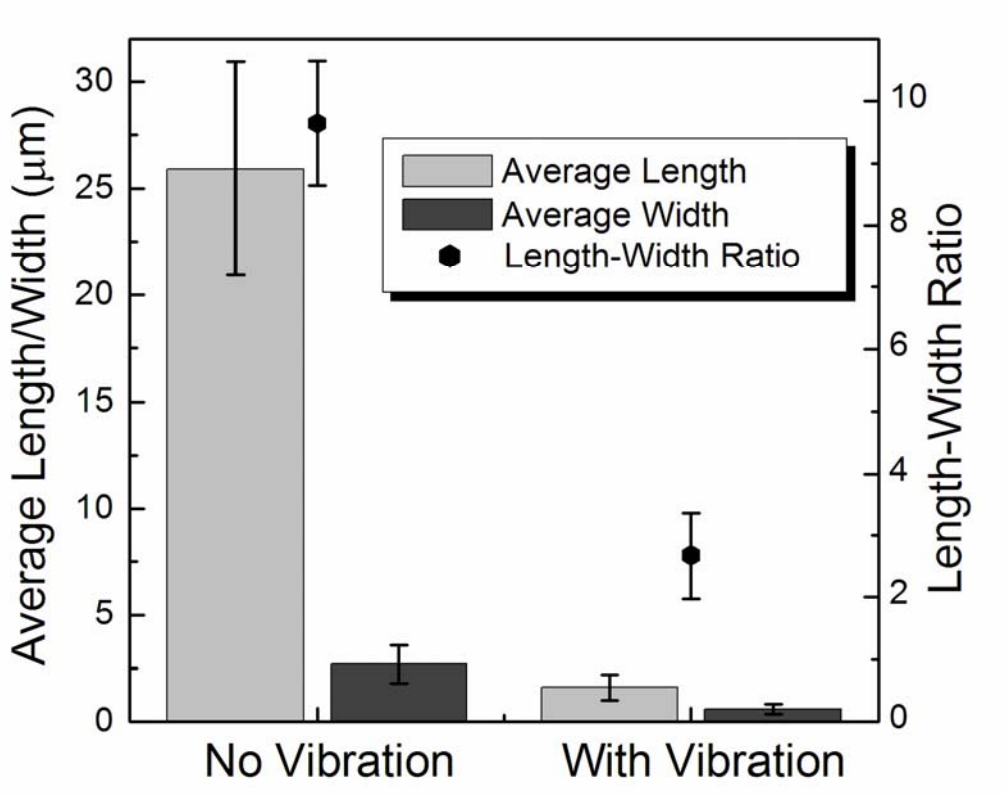

Figure 4.38: Silicon morphological analyses of A356 alloy without and with ultrasonic treatment.

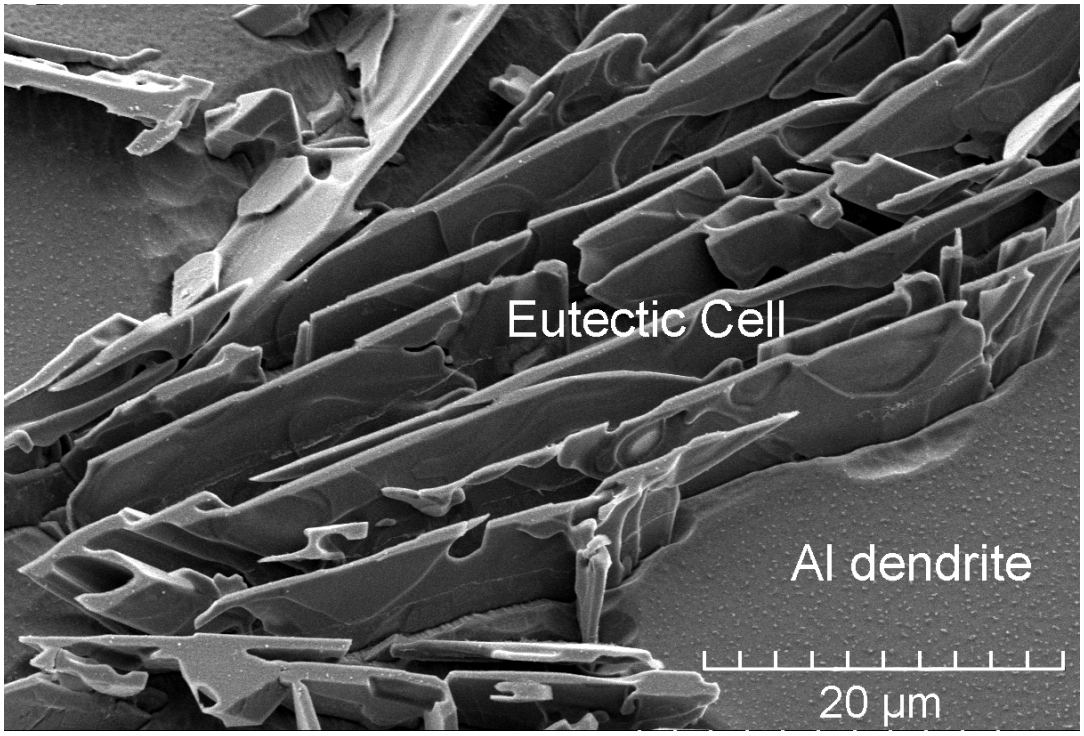

(a)

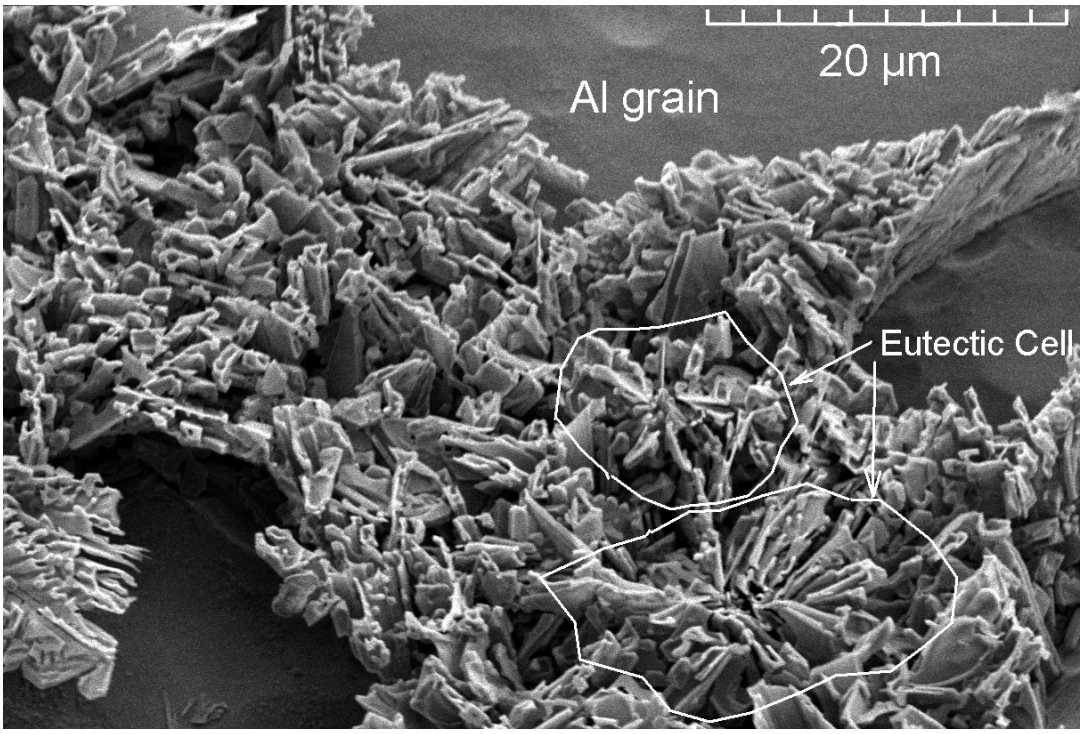

(b)

Figure 4.39: Three-dimensional eutectic morphology observed using SEM at 2000X magnification, (a) without ultrasonic treatment and (b) with ultrasonic treatment.

subsequent growth of the eutectic cells on the existing aluminum dendrites (shown schematically in Figure 4.40 (a)), rather than the independent nucleation and growth of the eutectic cells in the liquid (Figure 4.40 (b)). This suggests that ultrasonic treatment increases the probability of eutectic nucleation occurring within the interdendritic liquid compared to on the primary Al dendrites.

To summarize when ultrasonic energy of 20 KHz frequency is introduced into A356 alloy as it is cast into a metal mold at a temperature of 630 °C, the following is observed:

(1) The morphology of eutectic silicon was modified from a coarse acicular plate-like form when no ultrasonic vibration was used, to a finely dispersed rosette-like form when ultrasonic treatment was employed.

(2) Ultrasonic treatment reduced the size of eutectic silicon from 26 μm to 2 μm in length, which is over an order of magnitude, and width from 2.7 μm to 0.6 μm. The aspect ratio was also reduced by ultrasonic treatment from slightly less than 10 to slightly less than 3.

4.6 Microstructure modification in the magnesium AM60B alloy

In the past decades, several grain-refining techniques have been reported for magnesium – aluminum based alloys, such as superheating, carbon inoculation, and the Elfinal process. This section describes the modification of the solidification structure of the magnesium AM60B alloy using high intensity ultrasonic vibrations. Ultrasonic energy up to 1500 W was injected into the alloy during its solidification. Casting temperature was varied in order to obtain the optimal effect on grain refinement. The experimental results indicate that grain refinement was readily achievable for this alloy with ultrasonic vibrations. When the casting temperature was 675 °C, globular grains were obtained. The grain size can be as small as 30 to 40 μm, which was over an order of magnitude smaller than the dendritic grains obtained without using ultrasonic vibrations. On the other hand, the morphology of eutectic phases was modified from a mainly fully divorced blocky morphology dispersed among dendrite arms when no ultrasonic vibration was used, to a

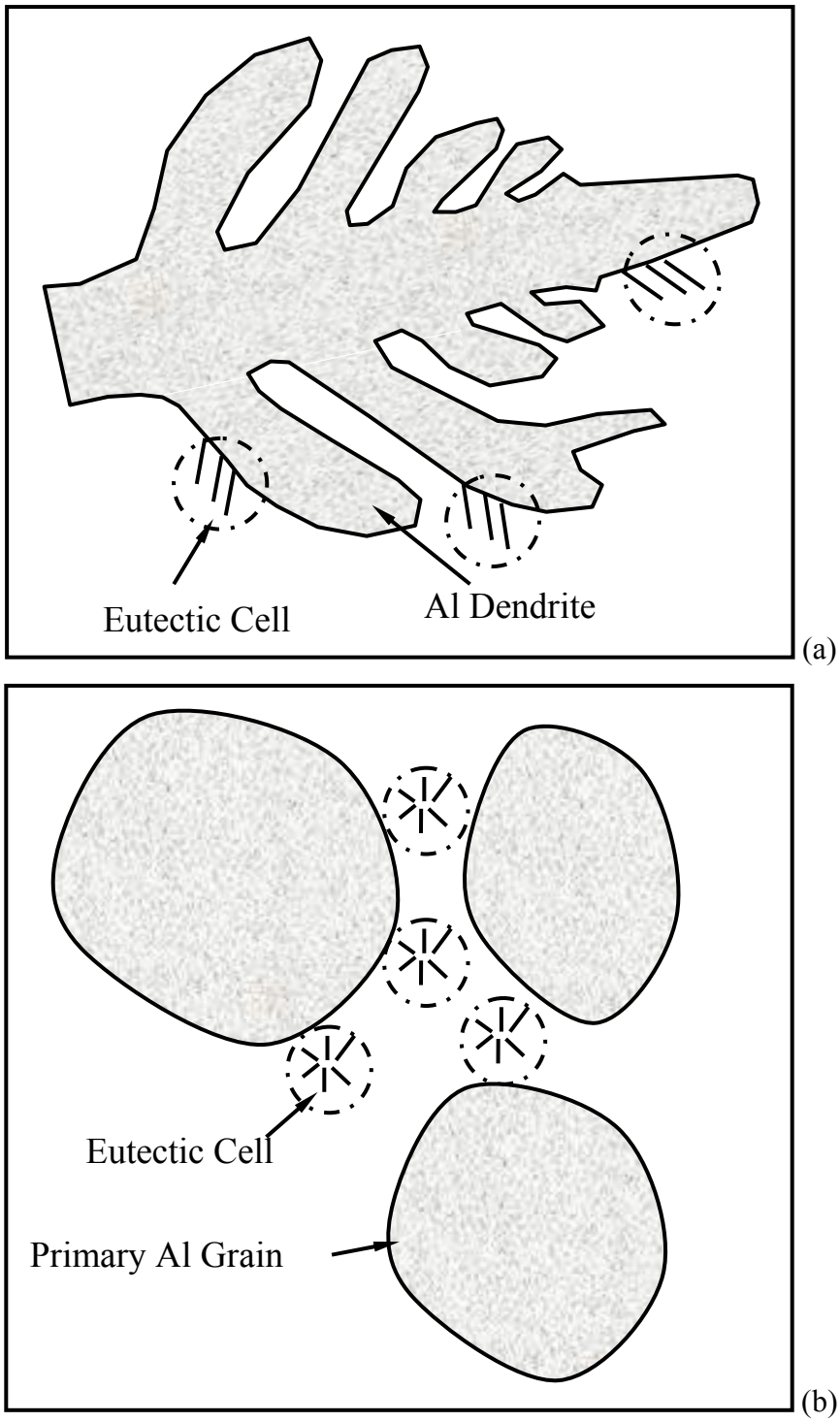

Figure 4.40: Formation of eutectic cells among the aluminum grains (a) the eutectic cells form on the dendrite and grow in the remaining liquid in the mushy zone, (b) the eutectic cells nucleated independently in the liquid among the dendrites.

mainly lamellar/script morphology across the grain boundaries when ultrasonic treatment was employed. Furthermore, the volume fraction of the eutectic morphology is less than that of without ultrasonic vibration. Both of these two aspects suggest that the modification to the eutectic phases by ultrasonic vibration will benefit the creep resistance of magnesium – aluminum based alloys.

4.6.1. Introduction

In the post-energy crisis era, magnesium alloys have caught the attention of the automotive industry [157] due to their unique combination of higher strength-density ratios compared with steel and aluminum, and higher temperature capabilities and improved crash worthiness over plastics. They are already reducing the mass of vehicles and thus improving fuel efficiency [158]. Currently, casting is the primary method to manufacture magnesium alloy parts and magnesium-aluminum based alloys are mostly commercially available because of their relatively cheap price, readily castable, and good mechanical properties. The addition of manganese to form ternary alloys with preferable corrosion resistance, ductility and impact strength, for example, AM60B alloy, is a common practice.

For the purpose of improving the mechanical properties, grain refinement of magnesium – aluminum based alloys has been studied extensively since 1930s [159-176]. Some grain refining technologies have been developed, such as superheating treatment [163, 164], carbon inoculation method [162], Elfinal process [161,165], and the addition of other additives, such as Mn, Sr, Re, Th, Si, Ca, B, AlN, MgO, TiB_2, and TiC.[169, 171-173] . Superheating treatment involves rising the melt to a temperature of 150 – 260 °C above the equilibrium liquidus and hold for a short time, then rapid cool down the melt to a predetermined casting temperature [163, 164]. This method has the disadvantage of high cost during the elevated operating temperature. The Elfinal process considers the grain refinement through the supplement of anhydrous ferritic chloride ($FeCl_3$) to magnesium-Al-Mn based alloys melt. The degraded corrosion resistance by Fe is a hindrance to the application of this technology. Carbon inoculation involves the addition of carbon (in the form of carbon-containing agents such as C_2Cl_6; CCl_4, SiC

particles [176], and carbonaceous gases) into the melt to produce grain refinement. The major advantages of this method, such as less-fading effect and lower operating temperature, have made it the major industrial grain refinement technique. Recently, a native grain refinement phenomenon was proposed [174], which states that high purity magnesium–Al type alloys have a naturally finer grain size than that of commercial purity alloys with the same basic compositions. Table 4.6 lists the grain refinement results of those grain refining technologies.

A comparison of the results shown in Table 4.6 shows that the grain refinement of those existing technologies is far from satisfactory: either the gain factor of grain refinement is too small (not much improvement) or the resultant grain size is still too large (dendritic). In addition, those grain refining technologies involve, more or less, disadvantages such as high cost and difficulties in operation. Therefore, in a commercial sense, none of the available grain refiners for magnesium-Al alloys is satisfactory [176]. Thus it is of general interests to search for a suitable solution for the grain refinement problem of magnesium-Al alloys, through an existing process with significantly improved efficacy, a new chemical addition, or a new technology.

On the other hand, recent research has indicated that the secondary phases precipitated from magnesium – aluminum based alloys, such as β-$Mg_{17}Al_{12}$, are to some extent related to magnesium – aluminum based alloys' creep resistance [177, 178]. Stress test shows a highly non-uniform stress distribution between the primary magnesium

Table 4.6: Comparison of existing grain refining technologies of Mg-Al alloys

Grain Refining Method		Average Grain Size (μM)		Gain Factor: D_{normal} / $D_{refined}$	Reference
		Normal	Refined		
Elfinal process	$FeCl_3$ added to Mg -3% Al	~310	~120	2.5	162
Superheating Method	Mg - 6.8% Al, heated to 850 °C	104	81	1.28	164,165
Carbon inoculation	C_2Cl_6 added to Mg -3% Al	400	120	3.33	169
	0.5 wt.% Al_4C_3-SiC/Al master alloy added into Mg -6 % Al	300	200	1.5	166
	0.8 Al_4C_3 % added to AZ31	4000	~800	5	168
Mn	0.2 % Mn added to AZ31	650	270	2.4	169
Native refinement	Commercial/high purity Mg-5% Al	~350	~230	1.52	175

phase and the eutectic phase. A reduction of eutectic phase volume fraction tends to increase the creep resistance of magnesium alloys [177].

The present work on the grain refinement and microstructural modification of aluminum alloys by high-intensity ultrasonic vibration caused the introduction of high-intensity ultrasonic vibration to the investigation of microstructural modification of magnesium-aluminum based alloys. This section describes initial results on microstructural modification of both the primary magnesium grains and eutectic phases (α-Mg and β-$Mg_{17}Al_{12}$) using ultrasonic vibration.

4.6.2. Experiment

Commercial AM60B alloy was used in this study. Experimental details are described in Chapter 3, section 3.5.

4.6.3. Results and discussion

4.6.3.1 Effect of ultrasonic treatment on primary α-Mg grain size

Figure 4.41 shows the typical dendritic microstructure in an AM60B alloy copper-mold casting without ultrasonic treatment. The casting temperature was 675 ºC. The magnesium dendrites have a characteristic six-fold symmetric shape. The white oval phase among the dendrite arms is eutectic α-Mg and secondary phase β-$Mg_{17}Al_{12}$. The dendrite shown in this picture is about 767 μm in diameter (2-dimensional).

Figure 4.42~Figure 4.45 exhibit the typical microstructure in an AM60B alloy copper-mold casting with ultrasonic treatment at different positions in the casting (as illustrated in Figure 3.5). Compared with the sample without ultrasonic vibration, the influence of ultrasonic vibration is obvious, which displays a much finer primary α-Mg grain throughout the casting, either at the bottom (near the acoustic radiator) or at the top (about 40 mm away from the radiator).The grain size demonstrated an evolution of continuous increase in size and decrease in globularity with increasing distance from the radiator, from position I (Figure 4.42), through position II and III (Figure 4.43 and Figure 4.44, respectively), to the top of the casting (Figure 4.45). At position I, extremely fine globular grains were obtained. At position II (5 mm from the radiator), the grains became

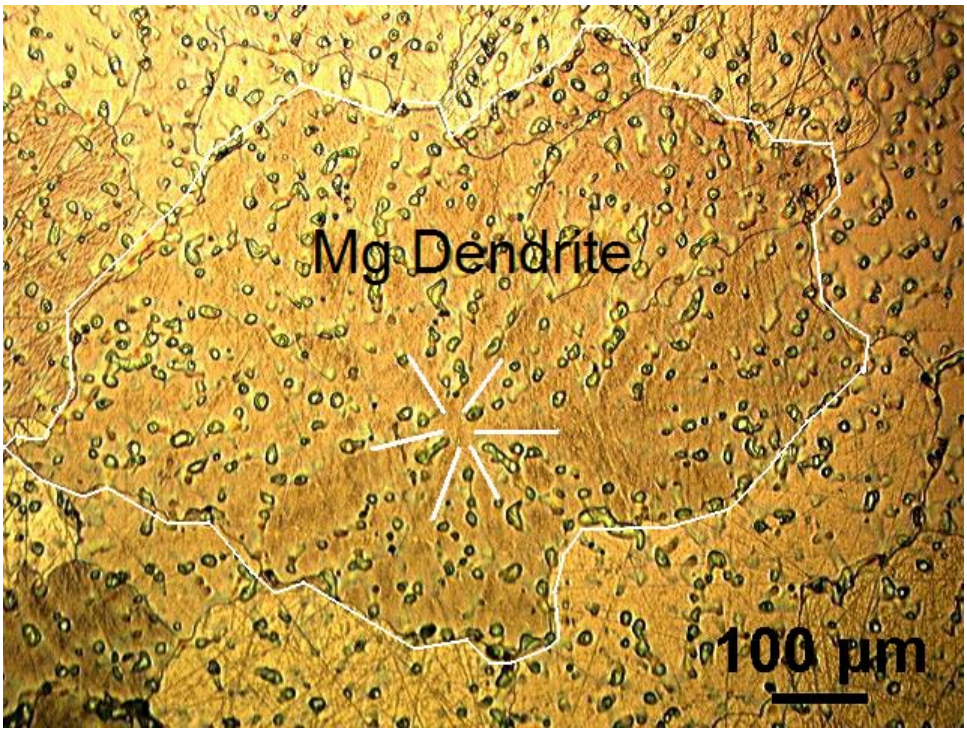

Figure 4.41: Dendritic microstructure in an AM60B alloy copper-mold casting without ultrasonic treatment. The casting temperature was 675 °C. The magnesium dendrites have a characteristic sixfold symmetric shape. The dendrite shown in this picture is about 767 µm in diameter. The white phase between the dendrites is secondary eutectic phase $Mg_{17}Al_{12}$.

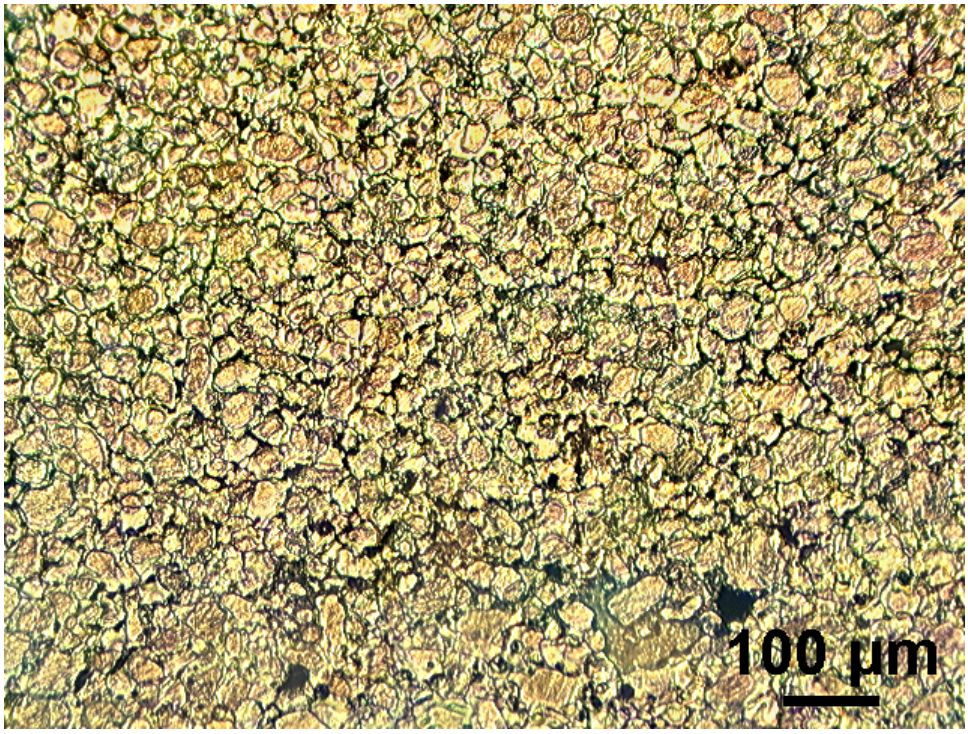

X100

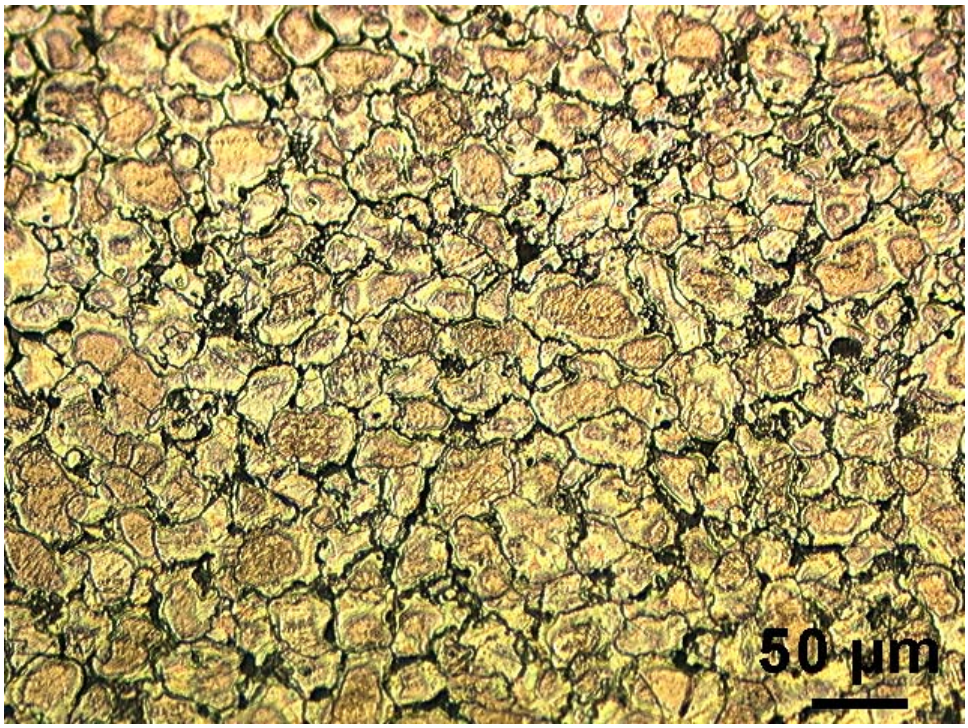

X200

Figure 4.42: Fine globular grains in an AM60B alloy copper-mold casting with ultrasonic treatment, at position I as illustrated in Figure 3.5. The casting temperature was 675 °C. The average grain size was about 25 µm.

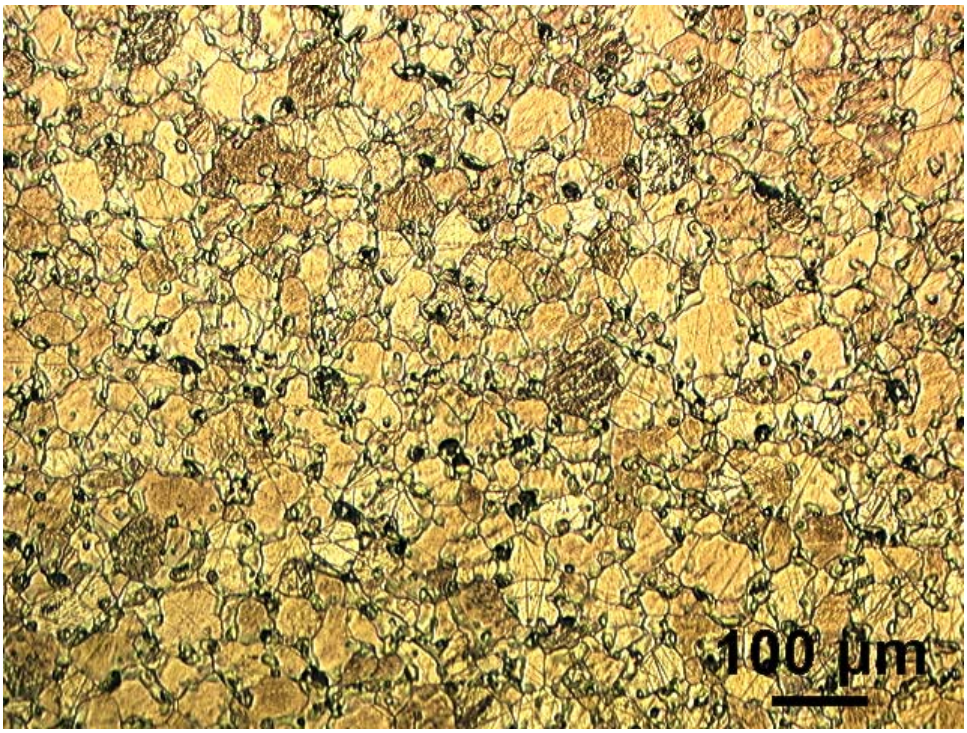

Figure 4.43: Small grains in same sample as shown in Figure 4.42, from position II (5mm from the radiator). The grains were less globular and larger with an average size of about 42 µm, compared with that of position I.

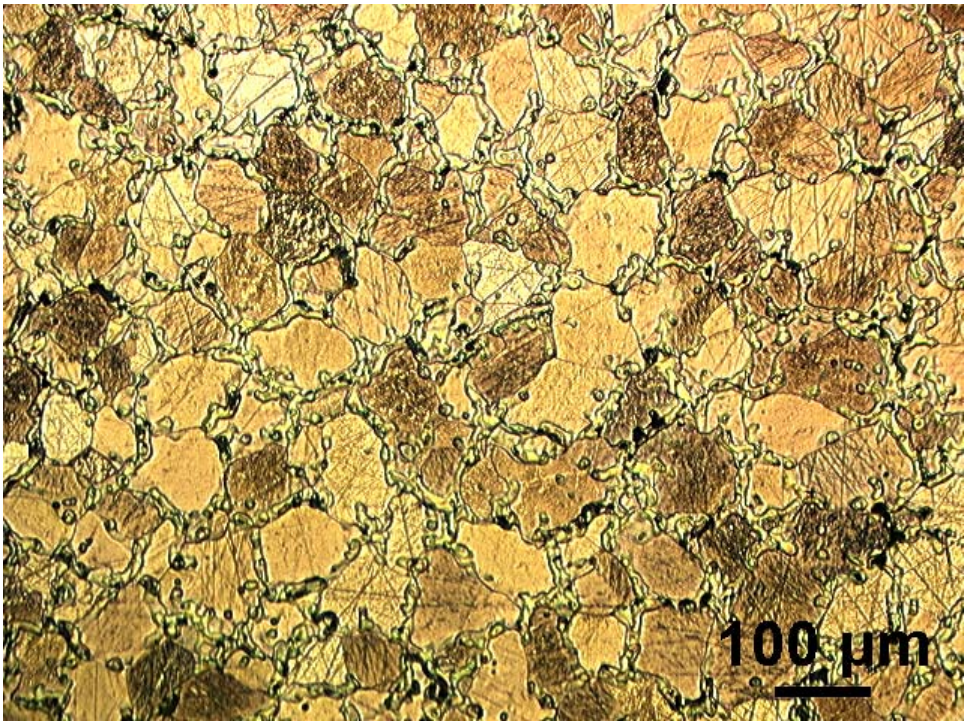

(a)

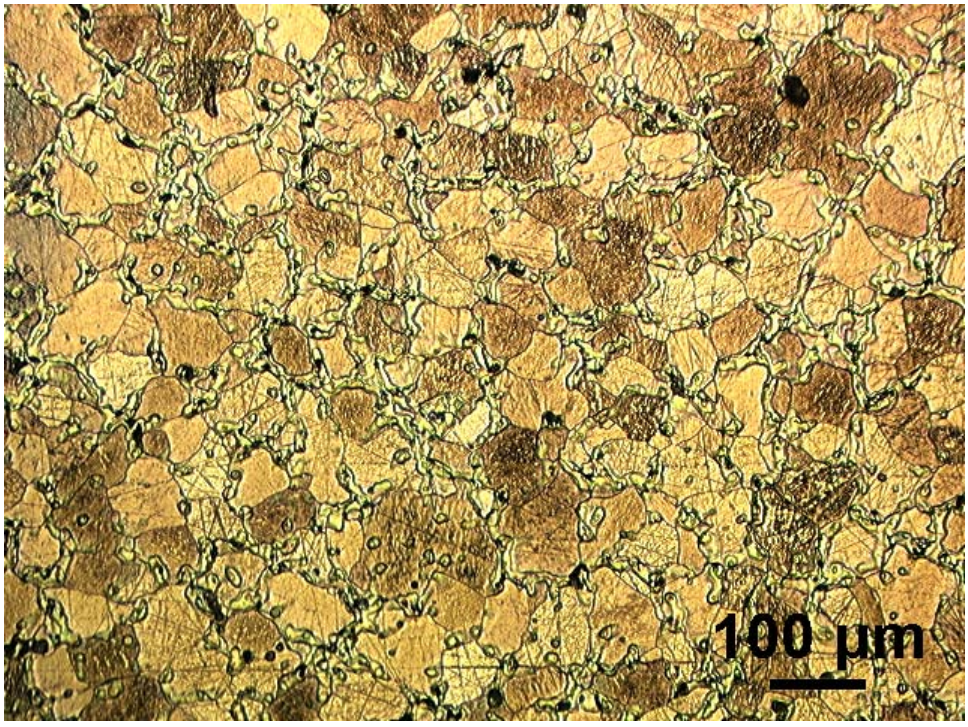

(b)

Figure 4.44: Small grains in same sample as shown in Figure 4.42, from position III (a) 15mm from the radiator; (b) 30 mm from the radiator. The grains were larger and not globular compared with that of position II, averaging 64 (a) and 54 µm (b) in diameter.

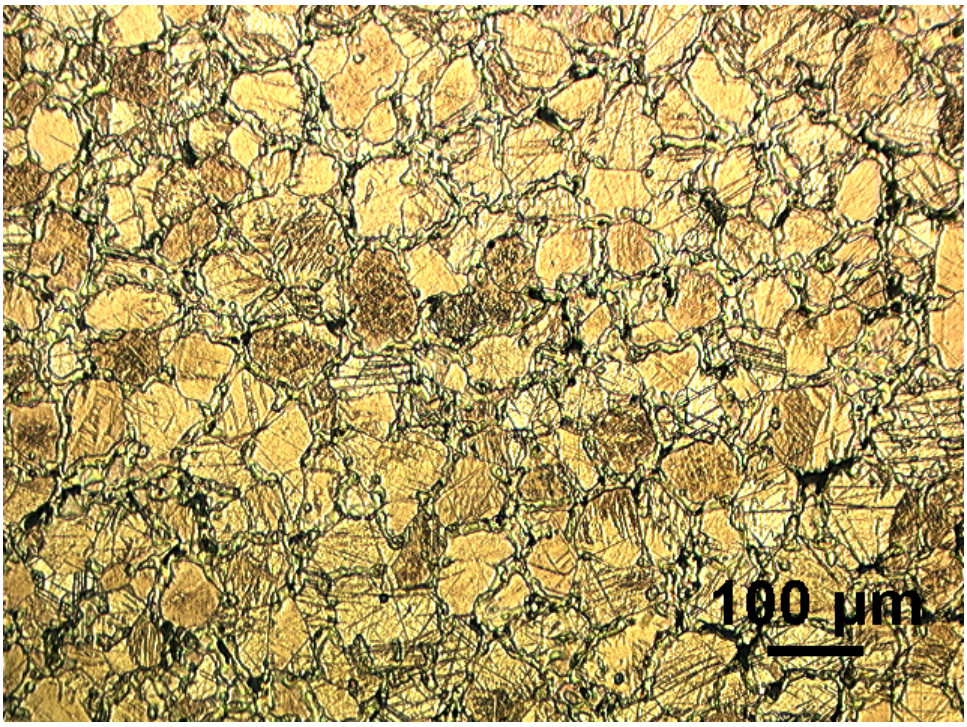

Figure 4.45: Small grains in same sample as shown in Figure 4.42, from position IV (top of the sample). The grains were a little smaller compared with that of position III, averaging 57 µm in diameter.

less globular and grow larger. At position III, The grains first reached the largest size (15 mm from the radiator) then decrease a little in size and became less globular compared with that of position II. In the areas near the top, the primary α-Mg grains were similar to those of 30 mm from the radiator.

Due to scatter and absorption, ultrasonic intensity attenuates with the distance it travels. In the casting with ultrasonic vibration, the ultrasonic intensity reaches a maximum in the area near the radiator, and the minimum at the top. Combine this argument and the result shown above, it can be seen that high acoustic power density favors the formation of fine and spherical α-Mg grains. This is in accordance with the conclusion made in previous research [132].

The quantitative analysis of the grain sizes of the AM60B alloy casting with and without ultrasonic treatment is illustrated in Figure 4.46. It again proves the effectiveness of ultrasonic vibration on grain size of AM60B alloy. Without vibration, the average dendrites are about 760 μm in diameter. While with vibration, the grain size is as small as 25 μm in the area near the radiator, where the gain factor of grain refinement is about 30.4; and about 50 μm in the bulk area, where the gain factor is about 15.8.

The most effective grain refinement method listed in Table 4.6 is the Carbon inoculation method, with 0.8 Al_4C_3 % added to AZ31 alloy and a gain factor of 5. A comparison of the gain factors by ultrasonic vibration and other traditional methods listed in Table 4.6 indicates that ultrasonic vibration is far more effective than all others for the grain refinement of magnesium – aluminum based alloys. Furthermore, the ultrasonic vibration method has the advantage of lower energy consumption and more operational convenience due to lower operational temperature involved, lower cost due to no additions required for the grain refinement, and no detrimental effect on other properties such as corrosion resistance, when compared with other grain refinement methods for magnesium – aluminum based alloys.

4.6.3.2 Effect of ultrasonic treatment on eutectic morphology

Figure 4.47 shows the eutectic morphology in an AM60B alloy casting without ultrasonic treatment. From previous work done by Han [119, 179], it is determined that the blocky

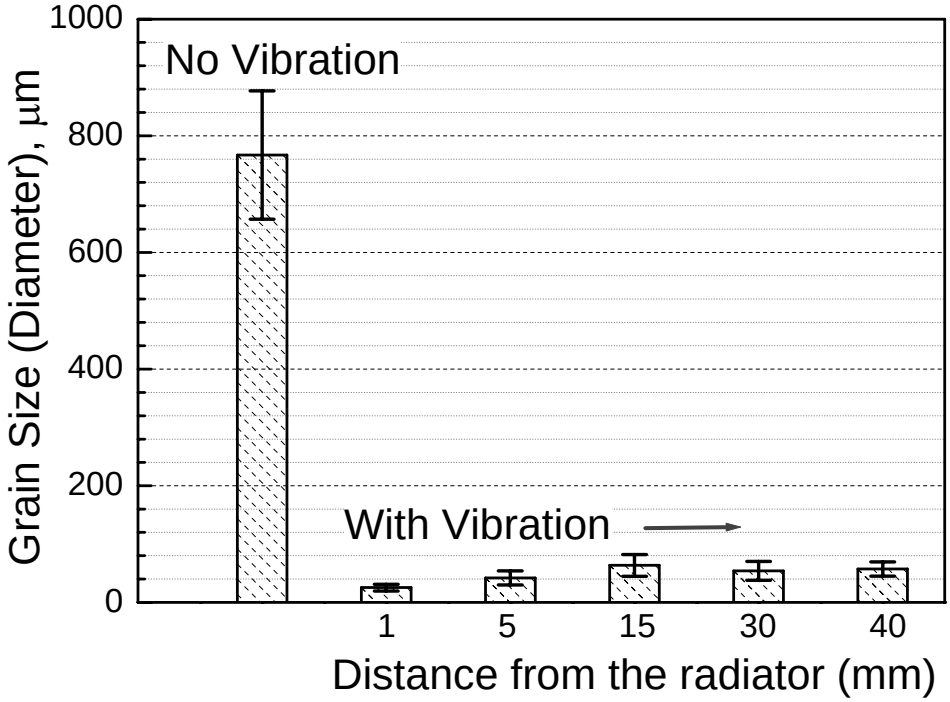

Figure 4.46: Comparison of primary magnesium grain size in an AM60B alloy copper-mold casting with and without ultrasonic treatment. Without vibration, the dendrites are about 760 μm in diameter. In contrast, the grain size is much smaller with vibration.

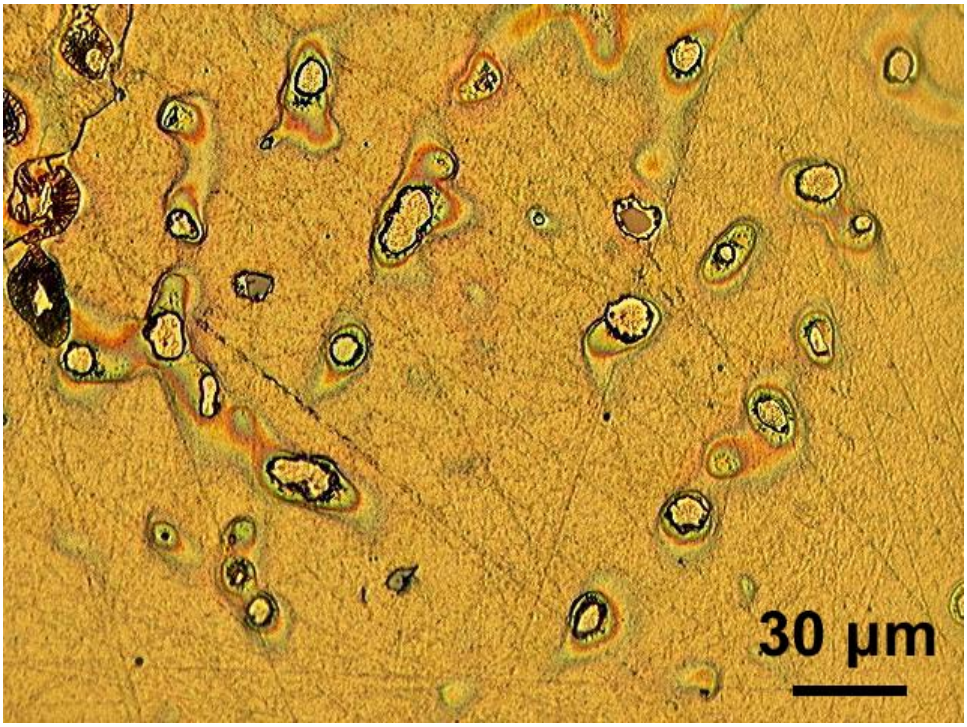

(a)

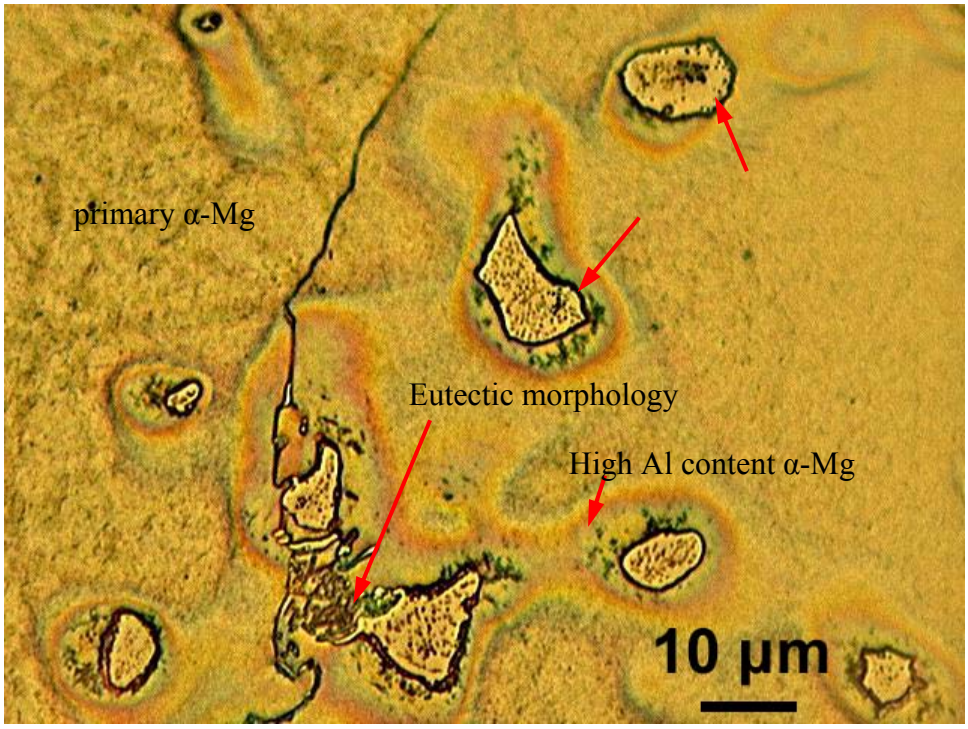

(b)

Figure 4.47: Secondary phase in the same sample shown in Figure 4.41. It shows the major secondary phase is divorced morphology in this casting, and the coring from the low Al content areas near the centers of their arms (yellow) to the high Al content areas near the edges of their arms (golden).

particles shown in Figure 4.47 are fully divorced β-$Mg_{17}Al_{12}$, which developed from a continuous precipitation from the liquid; the dark lamellar/script areas are eutectic morphologies, which result from a discontinuous precipitation from the liquid; the golden areas surrounding the divorced β-$Mg_{17}Al_{12}$ particles are high Al content α-Mg (Figure 4.47); and the yellow areas are primary α-Mg dendrites. A coring can be clearly seen between the low Al content areas near the centers of their arms (yellow) and the high Al content areas near the edges of their arms (golden) (Figure 4.47). Figure 4.47 displays mainly fully divorced β-$Mg_{17}Al_{12}$ dispersed among dendrite arms. This is in accordance with the observation in Figure 4.41. It suggests that the major eutectic phase is divorced morphology in this casting.

However, a significantly different eutectic morphology may be observed on an AM60B alloy casting with ultrasonic treatment, as shown in Figure 4.48Figure 4.51. At position I (Figure 4.48), the secondary phase displays a morphology of mainly lamellar/script eutectic morphology across the grain boundaries, and free of divorced blocky β-$Mg_{17}Al_{12}$ particles. At position II (5 mm from the radiator, as shown in Figure 4.49), the secondary phase still displays a morphology of mainly lamellar/script eutectic morphology across the grain boundaries, however some small divorced blocky β-$Mg_{17}Al_{12}$ particles are seen. At position III (Figure 4.50), more divorced blocky β-$Mg_{17}Al_{12}$ particles than that of position II are seen. At position IV (Figure 4.51), the secondary phase contains partly blocky β-$Mg_{17}Al_{12}$ particles, and partly lamellar/script eutectic morphology across the grain boundaries.

It can be seen that with ultrasonic vibration, the eutectic phase is mainly lamellar/script morphology across the grain boundaries and the volume fraction of the eutectic morphology is less than that of without ultrasonic vibration. A coring can be seen between the center of the low Al content primary α-Mg grains (yellow) and the high Al content areas near the grain boundaries (golden). Furthermore, the fully divorced blocky β-$Mg_{17}Al_{12}$ particles are both smaller and less than that of without ultrasonic vibration.

The morphology of the eutectic phases plays an important role in determining the creep resistance of magnesium – aluminum based alloy. Divorced blocky β-$Mg_{17}Al_{12}$ phase is notoriously known to be responsible for the poor creep resistance of magnesium

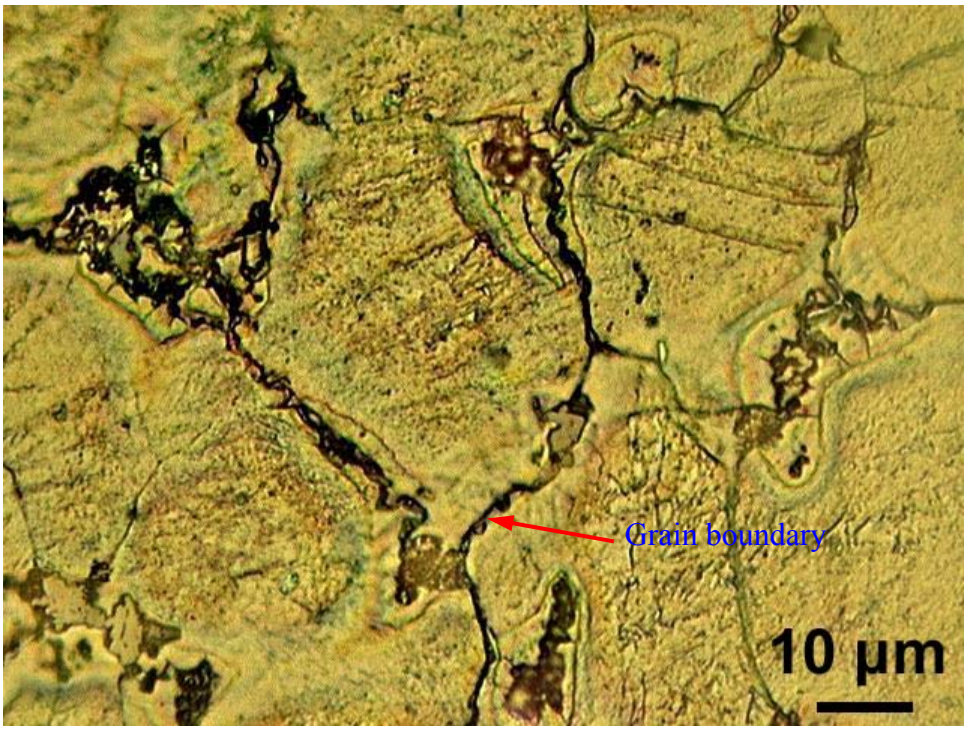

Figure 4.48: Secondary phase from position I in the same sample shown in Figure 4.42. It shows free of divorced β-$Mg_{17}Al_{12}$ particles, and the major secondary phase in a lamellar/script eutectic morphology across the grain boundaries.

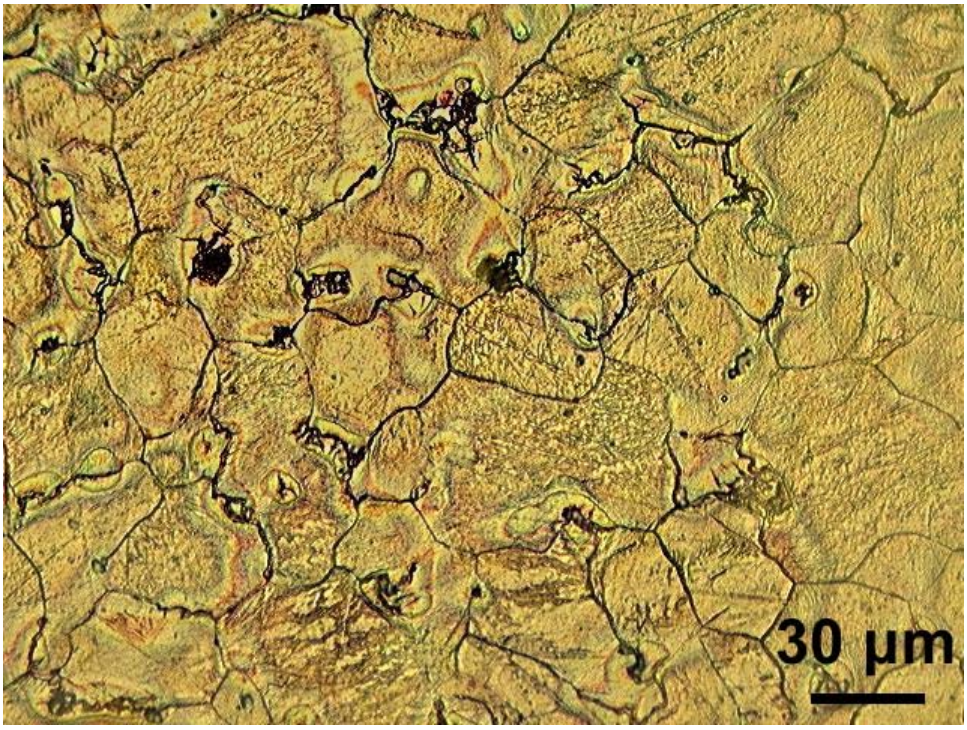

(a)

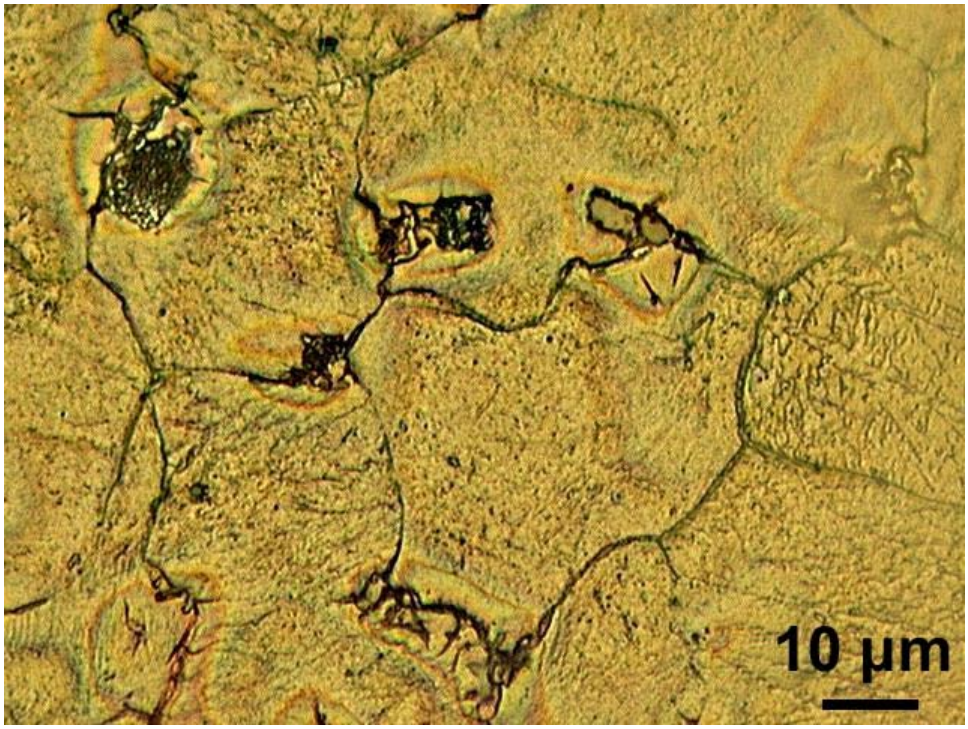

(b)

Figure 4.49: Secondary phase from position II in the same sample shown in Figure 4.42 at different magnification (a) 400 X and (b) 1000 X. It shows the major secondary phase in a lamellar/script eutectic morphology and some divorced β-$Mg_{17}Al_{12}$ particles, both located across the grain boundaries.

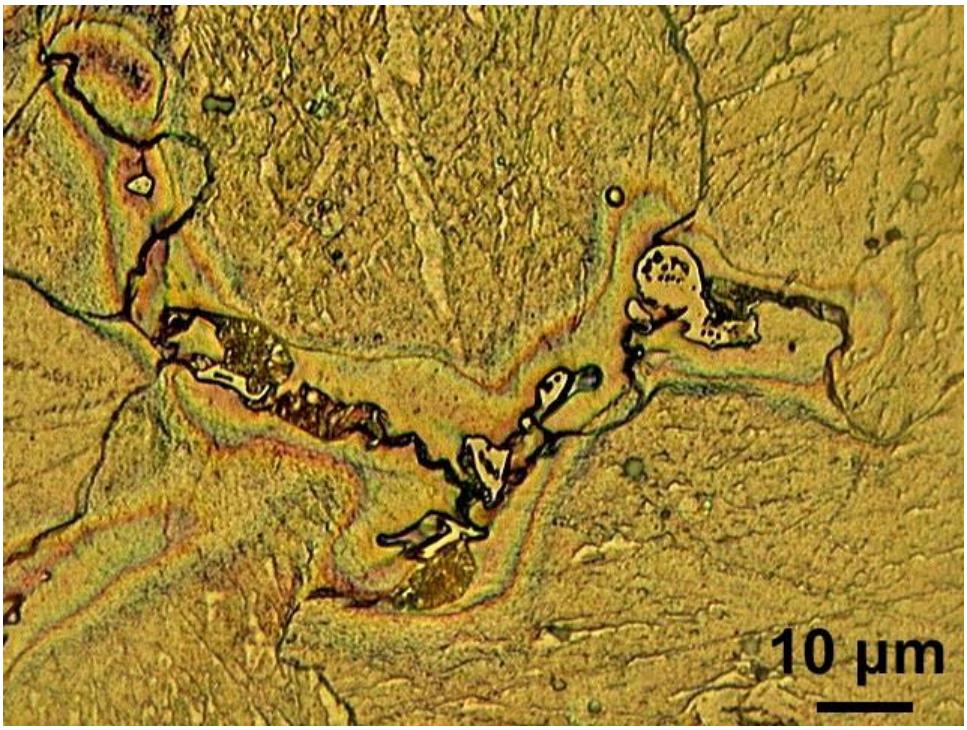

(a)

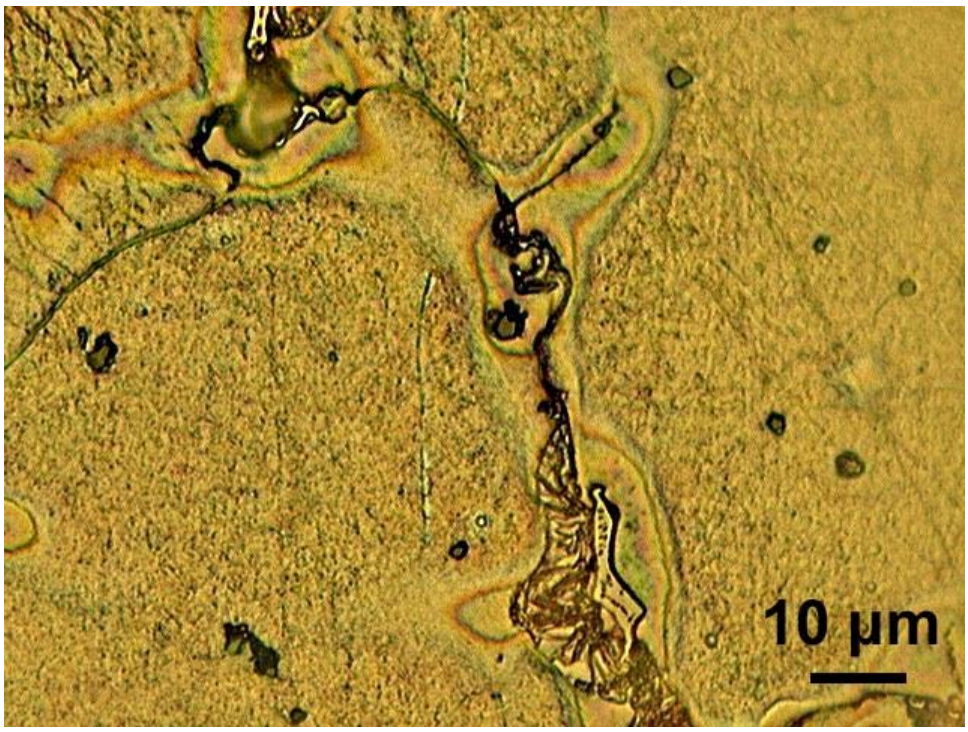

(b)

Figure 4.50: Secondary phase in position III in the same sample shown in Figure 4.42. a) 20 mm and (b) 30 mm from the radiator, showing increased tendency of forming divorced β-$Mg_{17}Al_{12}$ particles, however still much smaller than that of without ultrasonic treatment.

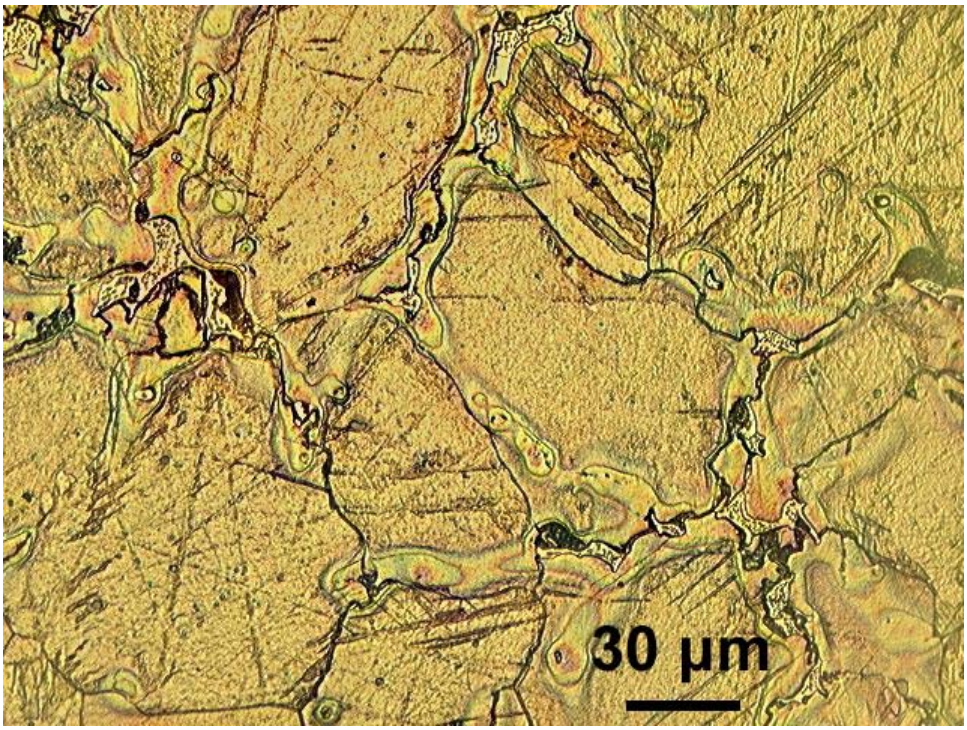

(a)

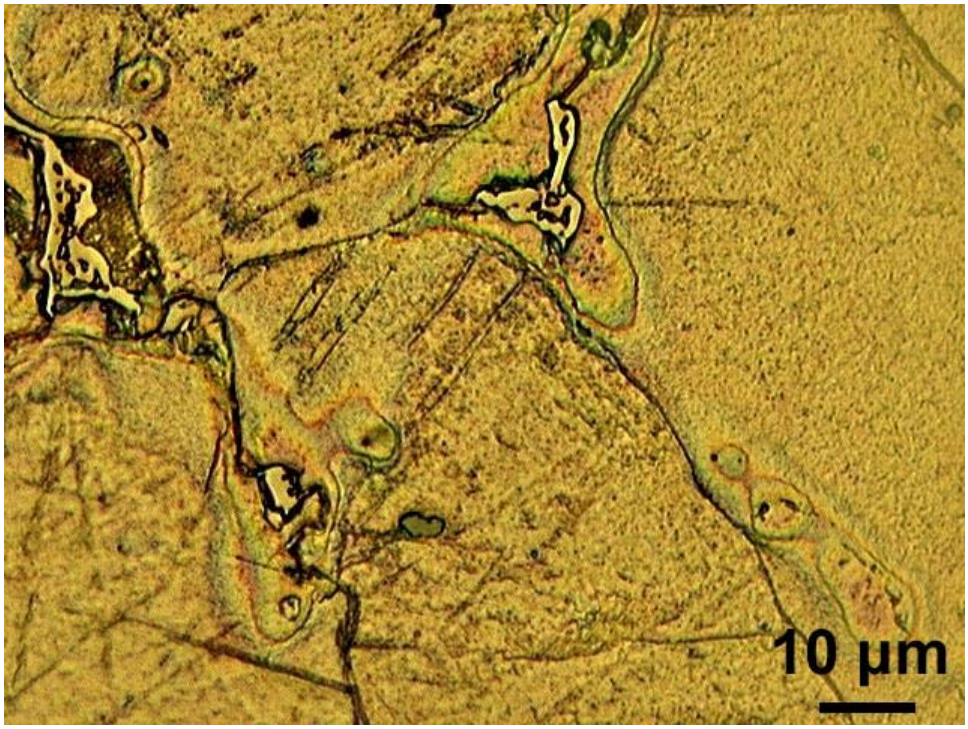

(b)

Figure 4.51: Secondary phase in position IV (40 mm from the radiator) in the same sample shown in Figure 4.42 at a) 400 X and (b) 1000 X, showing the secondary phases as partly divorced β-$Mg_{17}Al_{12}$ particles and l lamellar/script eutectic morphology.

– aluminum based AZ91D alloy, while the laminar/rosette-like/script secondary phase is suggested to be beneficial to the good creep resistance in magnesium – aluminum based AE42 and AS41 alloy [178]. It suggests that the modification to the eutectic morphology by ultrasonic vibration will increase the creep resistance of AM60B alloy.

The creep resistance of magnesium – aluminum alloy is likely to decrease with increasing volume fraction of eutectic phase. So the decrease of volume fraction of eutectic phase observed in the AM60B alloy casting with ultrasonic vibration is another potential beneficial factor for the creep resistance of this alloy.

Both the primary α-Mg grain size and eutectic morphology are greatly improved by ultrasonic vibration. It implies that ultrasonic vibration is a potent candidate in a commercial sense to refine the grains and to improve the mechanical properties, especially creep resistance, of magnesium - Al alloy castings.

To summarize when ultrasonic vibration at 20 KHz was introduced into AM60B alloy as it was cast into a permanent copper – mold at the temperature of 675 °C, the following is observed:

(1) Ultrasonic treatment reduced the size of primary α-Mg grains from 760 μm to about 25~48 μm in diameter. The maximum gain factor for grain refinement is 30.4 (near the radiator); the gain factor for grain refinement in the bulk area is 15.8. Both results are much greater than 5, or the best result from traditional grain refinement method.

(2) The morphology of eutectic phases was modified from a mainly fully divorced blocky morphology dispersed among dendrite arms when no ultrasonic vibration was used, to a mainly lamellar/script morphology across the grain boundaries when ultrasonic treatment was employed. Furthermore, the volume fraction of the eutectic morphology is less than that without ultrasonic vibration. Both of these two aspects suggest that the modification to the eutectic phases by ultrasonic vibration will benefit the creep resistance of magnesium – aluminum based alloys.

(3) The suggested improvement in both creep resistance (through eutectic modification) and other mechanical properties (through grain refinement) by ultrasonic vibration implies that ultrasonic vibration is a potent candidate in a commercial sense.

Chapter 5

Summary

5.1 Conclusions

The following main results have been described in this dissertation:

(1) The thermal analysis results show that, with ultrasonic vibration, the steady growth temperature and the minimum supercooling temperature have been elevated; the recalescence time decreased, which indicates a much slower growth rate of primary fcc aluminum grains; the difference between dendrites nucleation/growth and thickening is not significant, which might suggest dendrite formation might not be present in this solidification process.

(2) Grain refinement was obtained in the experiments with continuous, intermittent and isothermal ultrasonic processing. However globular grains are difficult to achieve using the isothermal method. It is suggested that cavitation-induced heterogeneous nucleation is the dominant mechanism for globular grain formation in specimens processed using acoustic vibration.

(3) High acoustic amplitude/intensity favors the formation of small, spherical primary aluminum grains. The casting temperature of 630°C brings about the best grain refinement result. The primary aluminum grain size in a casting increases with the increasing distance from the acoustic radiator.

(4) High intensity ultrasonic vibration has been applied in casting high volume (suitable for SSM process) A356 alloy. Non-dendritic/globular grains have been obtained. The use of a grain refiner can further refine the A356 alloy structure, with the combination of ultrasonic vibration.

(5) Fine globular grains were obtained in various aluminum alloys, including A354, 319, 6063, 6061, 2618 alloys. The temperature of 670 °C is the optimum casting temperature for grain refinement of 2618 with the aid of ultrasonic vibration.

(6) The introduction of ultrasonic vibration into A356 alloy modified the morphology of eutectic silicon from a coarse acicular plate-like form to a finely dispersed rosette-like form. The size of eutectic silicon reduced from 26 μm to 2 μm in length; the width reduced from 2.7 μm to 0.6 μm; and the aspect ratio was also reduced by ultrasonic treatment from slightly less than 10 to slightly less than 3.

(7) With ultrasonic vibration, the AM60B alloy experienced a reduction in size of the primary α-Mg grains from 760 μm to about 25~48 μm in diameter, which is much better than other traditional grain refinement methods. The morphology of eutectic phases was modified from a mainly fully divorced blocky morphology dispersed among dendrite arms, to a mainly lamellar/script morphology across the grain boundaries. Furthermore, the volume fraction of the eutectic morphology is less.

5.2 Suggestions for future work

Future studies should include an investigation of the primary mechanism of ultrasonic vibration on the eutectic structures in aluminum alloys. It is highly recommended that the research reported in this study be continued with the application and commercialization of this technology.

This technology may have a number of applications. Incorporating ultrasonic vibration into a die casting machine would dramatically increase the integrity and properties of die castings. Ultrasonic vibration may be used for producing semisolid feedstock directly from molten metal. Ultrasonic techniques can also find applications in the forging industry for processing alloys that are difficult to cast.

The investigation has shown that the ultrasonic vibration is suitable for SSM process. It has the potential for scaling up for the production of critical metal components for transportation and defense applications, leading to cost reduction, energy savings, and many other benefits.

Bibliography

1. "Metal Casting Census Index," Foundry Management and Technology, Penton Publishing (1987).
2. Brent Haight, "Advanced Technologies are opening doors for new materials," Automotive Industries, 2003, 4.
3. Turnbull, D., and Fisher, J. C.: J. Chem. Phys., 17:71 (1949).
4. Turnbull, D.: "Thermodynamics in Metallurgy," American Society for Metals, Metals Park, Ohio, 1949.
5. Hillig, W. B., and Turnbull, D.: J. Chem. Phys., 24:914 (1956).
6. Frank, F. C.: Discussions Faraday Soc., 5:48 (1949).
7. Wagner, R. S.: Acta Met., 8:57 (1960).
8. Hamilton, D. R., and Seidensticker, R. G.: J. Appl. Phys., 31: 1165 (1960).
9. Scheil, E. "Bemerkungen zur schichtkristallbildung", Z. Metallk., 34:70 (1942).
10. Gulliver, G. H.: "Metallic Alloys" (Appendix), Charles Griffin & Co., Ltd., London, 1922.
11. Tiller, W. A., Jackson, K. A., Rutter, J. W., and Chalmers, B.: Acta Met., 1:428 (1953).
12. Radhakrishna, K., S. Seshan and M. R. Seshadri. "Dendrite Arm Spacing in Aluminum Alloy Casting," AFS Transactions, 88 (1980), pp 695-702.
13. Kubota, M. and S. Kitaoka. "Solidification Behavior and Hot Tearing Tendency of Aluminum Casting Alloys," AFS Transactions, 81 (1973) pp. 424-427.
14. Entwistle, R. A., J. E. Gruzleski and P. M. Thomas. "Development of Porosity in Aluminum-based Alloys," Solidification and Casting of Metals, The Metals Society, Publication 192 (1979) pp 345-349.
15. Kennerknecht, S. "Metallurgical Aspects of Quality Control in the Production of Premium Quality Aluminum Investment Castings for the Aerospace Industry," Advanced Casting Technology, AGARD Conference Proceedings No. 325.
16. Achenbach K, Nipper HA, Piwowarsky E. Giesserei 1939;26:597-621.
17. Emley EF. Priciples of magnesium technology. Oxford: Pergamon Press; 1966. p. 200–3, 231.

18. Qinglin Jin, etc.: “Grain refining mechanism of a carbon addition method in a Mg–Al magnesium alloy”, Scripta Materialia 49 (2003) 1129–1132.
19. Ma Qian a, P. Cao.: “Discussions on grain refinement of magnesium alloys by carbon inoculation,” Scripta Materialia 52 (2005) 415–419.
20. Nelson CE. Trans Am Found Soc 1948;56:1.
21. Wood RT. Foundryman 1953;46:98.
22. Qian M, St. John DH, Frost MT. Scripta Mater 2004;50:1115.
23. Saunders WP, Strieter FP. Trans Am Found Soc 1952;60:581.
24. Lu SZ, Hellawell A. Journal of Crystal Growth 1985; 73: 316-328.
25. Hanna MD, Lu SZ, Hellawell A. Metall Trans A1984; 15A:459.
26. Heiberg G, Nogita K, Dahle AK, Arnberg L. Acta Materialia 2002; 50:2537.
27. Jenkinson DC, Hogan LM. Journal of Crystal Growth 1975; 28: 171.
28. Nogita K., et al. Mater Trans 2001; 42:1981.
29. Lu SZ, Hellawell A. Metall Trans A1987; 18A:1721.
30. Jie W, Chen Z, Reif W, Muller K. Met Mat Trans A 2003; 34A:799.
31. O. V. Abramov: High-intensity ultrasonic: theory and industrial applications, Gordon and Breach Science Publishers, Amsterdam, The Netherlands, 1998.
32. C. Liu, Y. Pan, and S. Aoyama, Proceedings of the 5th International Conference on Semi-Solid Processing of Alloys and Composites, Ed.: A. K. Bhasin, J. J. Moore, K. P. Young, and S. Midson, Colorado School of Mines, Golden, CO (1998), pp 439-447.
33. Chernov, D; Reports of the Imperial Russian Metallurgical Society 1878.
34. Boyle, R. W.: Trans. Roy. Soc. Canada, 1922, 3(16), 157.
35. Taylor, G. B., Sproule, D. O.: Trans. Roy. Soc. Canada, 1929, 3(23), 91.
36. Wood, R. W., Loomis, A. L.: Phil. Mag., 1927 7(4), 417.
37. Sokolov, S. Ya.: Zh. Tekh. Fiz., 1936, 3, 176.
38. Seemann, H. J.: Metallforschung mit Ultraschall, Metallwirt., 1936, 15, 1067.
39. Schmid, G., Ehret, L.: Zt. Elektrochem., 1937, 43, 869.

40. Danilov, V. I., Chedzhenov, G. Ch. Problems in Metal Science and Physics of Metals, 1955, Issue 4 of Collected Papers of Central Research Institute of Pure Materials, 152.
41. Danilov, V. I.: Structure and Solidification of Liquids, 1955, Kiev, Izd, AN USSR.
42. Kapustin, A. P.: Effect of Ultrasound on the Kinetics of Solidification, Moscow: Izd. AN USSR, 1962.
43. Teumin, I. I.: Tekhn. Inform. Bull. OKB-UVU, 1962, 1 (19), 9.
44. O. V. Abramov: The growth and imperfections of metallic crystals, Metallurgiya, Moscow, 1966.
45. Abramov, O. V. et al.: Sov. Phys. Acoust., 1967, 14(2) 141-149.
46. O. V. Abramov and I. I. Teumin: The physical principles of ultrasonic manufacturing. Nauka, Moscow, 1970.
47. O. V. Abramov: Crystallization of metals in ultrasonic field, 1972.
48. Polotskii, I. G.: Primenenie ultrazuvkovykh kolebanii dlya issledovaniya svoistv, kontrolya kachestva I obrabotki metallov I splavov, Kiev: Izd. AN USSR, 1960.
49. G. I. Eskin, H. G. Flynn: J. Acoust. Soc. Amer., 1965, 37, 3, 493.
50. G. I. Eskin: Ultrasonic treatment of light alloy melts, 1998.
51. G. I. Eskin: Ultrasonic treatment of molten Al, 2nd edition, 1988.
52. G. I. Eskin, et al: Advanced performance materials, 1995, 2, 43.
53. O. V. Abramov: High-intensity ultrasonic: theory and industrial applications, Gordon and Breach Science Publishers, Amsterdam, The Netherlands, 1998.
54. O. V. Abramov: Ultrasound in liquid and solid metals, 1994.
55. Lane, D. H.; Cunningham, J. W.; Tiller, W. A. Application of ultrasonic energy to ingot solidification. I. Transactions of the American Institute of Mining, Metallurgical and Petroleum Engineers, 1960, 218, 985-90.
56. G. Rai, E, Lavernia and NJ Grant: Powder Size Distribution in Ultrasonic Gas Atomization. Journal of Metals, 1985, 8, 22.
57. Furukawa, Minoru; Miura, Yasuhiro; Nemoto, Minoru. Effects of aging on the acoustic emission and ductility of aluminum-lithium alloys. Nippon Kinzoku Gakkaishi, 1987, 51(11), 994-1002.

58. Nakanishi, H., Tsanekawa, Y., and Mohri, N.: Met. Abstr. Light Metal Alloys, Osaka, 1993, 26, 141.
59. Bergmann, L.: Ultraschall und seine Anwendung in Wissenschaft und Technik, Stuttgart, S. Hirzel, 1954.
60. Matauschek, J.: Einfuhrung in die Ultraschalltechnik, Berlin Verlag Technik, 1959.
61. Herrmann, E., Hoffmann, D.: Handbook on Continuous Casting, Dusseldorf: Aluminum Verlag, 1980.
62. Pohlman, R., Heisler, K., Cichos, M.: Ultrasonics, 1974, 1, 11.
63. Seemann, H. J., Buxmann, K.: Metallwiss Techn., 1972, 1, 1.
64. Seemann, H. J., Dorr, W.: Met. Techn., 1976, 1, 1029.
65. Crawford, A. E: Ultrasonic Engineering with references to High Power Applications, Butterworths, London, 1955.
66. Mason, T. J., Ahmad, J., Bacon, M., Sterritt, A.: "Improving Light Alloy Castings with Power Ultrasound," Metallurgia, 1994, 61, 224.
67. T.J.Mason and M.Bacon, Improved Castings and Enhanced Energy Efficiency with Power Ultrasound, Future Practice R&D Profile No 55, Energy Efficiency Office, 1995.
68. T.J.Mason, J.P.Lorimer, L.Paniwnyk, B.Pollet and Y.Zhao, "Ultrasound starts quiet revolution in materials science," Materials World, 1999, 7, 69-71.
69. Angelov, G. Izv. Vissho Mash. Elektrotekn. Inst., 1970, 24, 1, 143.
70. Kratky, J.: Trend VUMA, 1979, 10(1), 33.
71. Lin, Chun Mao: ULI, 1979, 8(5), 467.
72. Eskin, G. I.: Ultrasonic Treatment of molten Aluminum, Moscow, Metallurgiya, 1965.
73. L.D. Rozenberg (ed.), Sources of High-Intensity Ultrasound, Vol. 1 and 2, Plenum Press, New York, 1969.
74. L. D. Rozenberg (ed.), Physical Principles of Ultrasonic Technology – vol. 2, Plenum Press, New York 1973.
75. Balandin, G. F.: Formation of Crystalline Structure of Ingots, Moscow, Mashinostroyenie, 1973.

76. I. Campbell: Intern. Met. Rev., 1981, 2, 71-108.
77. R. W. Wood and A. L. Loomis: Phil. Mag., 1927, 4(22), 417.
78. O. K. Eknadiosyants: The physical principles of ultrasonic manufacturing, Nauka, Moscow, 1970.
79. O. V. Abramov, et al: in Transactions 20th international conference on acoustics, Prague, 1981.
80. W. Eisenmenger: Acoustica, 1965, 9 (4), 327.
81. M. Kornfeld: Elasticity and Strength of Liquids (Russian translation), GINTL, Moscow, Leningrad, 1951.
82. D. Y. Hsieh and M. S. Plesset, J. Acoust. Soc. Am., 1961, 33, 206.
83. M. Strasberg: J. Acoust. Soc. Am. , 1961, 33, 359L.
84. G. Flinn: Acoustic Principles and Methods, Vol. 1, Methods and Devices, Part B, W. P. Mason Ed., Academic Press, New York, 1964.
85. R. H. Cole: Underwater Explosions, Princeton University Press, Princeton, N. J., 1948.
86. G. Flinn: Acoustic Principles and Methods, Vol. 1, Methods and Devices, Part B, W. P. Mason Ed., Academic Press, New York, 1964.
87. O. V. Abramov, et al: Tekhnologiya Sudostroeniya, 1976, 1, 111-113.
88. O. V. Abramov, et al: Metallurgiya, Moscow, 1974.
89. E. Kikuchi: Fourth International Congress on Acoustics, Tokyo, 1968, Report NH-5-6.
90. R. B Dean: J. Appl. Phys., 1944, 15, 446-451.
91. J. D. Hunt and K. A. Jackson: J. Appl. Phys., 1966, 37(1), 254-257.
92. M. J. Berger and W. Rostoker: Foundry, July 1953, 81, 100-105, 260.
93. J. D. Hunt and K. A. Jackson: J. Appl. Phys., 1968, 1, 247-257.
94. K. Buxmann and W. Dorr: Ann. Univ. Sarav. Math. Naturwise. Fak., 1970, (8), 62-77.
95. H. J. Seeman and K. Buxmann: Metalwises. Technik, 1972, 26 (1), 1-9.
96. R. S. Richards and W. Rostoker: ASM Trans., 1956, 48, 884-903.
97. R. T. Southin: J. Inst. Met., 1966, 94, 401-407.

98. J. J. Frawley and W. J. Childs: Trans. AIME, 1968, 242, (2), 256-263.
99. A. Cibula: J. Inst. Metals, 1967, 95 (2), 159.
100. J. D. Hunt and K. A. Jackson: J. Appl. Phys., 1966, 37(1), 254-257.
101. Danilov, V. I., Teverovskii, B. M.: Crystallization of Organic Substances in an Ultrasonic Field, Zh. Eksp. Teor. Fiz., 1940, 10(11), 1305.
102. F. S. Gorskii: Izvesiya Akad. Nauk .BSSR, 1950.
103. O. V. Abramov: Ultrasound in liquid and solid metals, 1994, 107.
104. M. Warmuzek, Aluminum-Silicon Casting Alloys: Atlas of Microfractographs, ASM International, Ohio, USA, 2004, 2.
105. ASM Handbook Committee, Alloy Phase Diagrams, ASM International, Ohio, USA, 1992.
106. Shabestari, S. G.; Malekan, M. Thermal analysis study of the effect of the cooling rate on the microstructure and solidification parameters of 319 aluminum alloy, Canadian Metallurgical Quarterly (2005), 44(3), 305-312.
107. Emadi, D.; Whiting, L. V.; Nafisi, S.; Ghomashchi, R. Applications of thermal analysis in quality control of solidification processes. Journal of Thermal Analysis and Calorimetry (2005), 81(1), 235-242.
108. Cetin, A.; Kalkanli, A. Evaluation of latent heat of solidification of gray cast iron from cooling curves. Canadian Metallurgical Quarterly (2005), 44(1), 1-6.
109. Baez, J. C.; Gonzalez, C.; Chavez, M. R.; Castro, M.; Juarez, J. Fourier thermal analysis of the solidification kinetics in A356/SiCp cast composites. Journal of Materials Processing Technology (2004), 153-154 531-536.
110. Van Rooyen, M.; Maartensdijk, J. A. Sinte; Mittemeijer, E. J. Precipitation of Guinier-Preston zones in aluminum-magnesium; A calorimetric analysis of liquid-quenched and solid-quenched alloys. Metallurgical Transactions A: Physical Metallurgy and Materials Science (1988), 19A(10), 2433-43.
111. Zhang, Jingguo; Cai, Xinxing; Huang, Weili; Yan, Shouping; Ke, Jun. Computer simulation of rapid solidification in self-quenching. Rapidly Solidified Mater., Proc. Int. Conf. (1985), 23-8.

112. Krajewski, Witold. DTA examinations of the solidification course of medium-aluminium zinc alloys modified with Ti. Metallurgy and Foundry Engineering (2000), 26(2), 143-147.
113. Ekpoom, U.; Heine, R. W. Thermal analysis by differential heat analysis (DHA) of cast iron. Transactions of the American Foundrymen's Society (1981), 89 27-38.
114. Battezzati, L.; Baricco, M.; Marongiu, F.; Serramoglia, G.; Bergesio, D. Melting and solidification studies by advanced thermal analysis. Semi-Solid Processing of Alloys and Composites, International Conference, 6th, Turin, Italy, Sept. 27-29, 2000 (2000), 411-416.
115. Jeng, Shih Chang; Chen, Sinn Wen. Determination of the solidification characteristics of the A356..2 aluminum alloy. Materials Science Forum (1996), 217-222(Pt. 1, Aluminium Alloys, Pt. 1), 283-288.
116. Chen, S-W. and Huang, C-C., Solidification curves of Al-Cu, Al-Mg and Al-Cu-Mg alloys, Acta Materialia, 1996, 44(5), 1955.
117. Lennart Backerud, Guocai Cai, Jarmo Tamminen, Solidification Characteristics of Aluminum Alloys, volume 1, Skanaluminum, Oslo, Norway, 1986.
118. Lennart Backerud, Guocai Cai, Jarmo Tamminen, Solidification Characteristics of Aluminum Alloys, volume 2: Foundry Alloys, AFS/Skanaluminum, Des Plaines, IL, 1990.
119. Lennart Backerud, Guocai Cai, Jarmo Tamminen, Solidification Characteristics of Aluminum Alloys, volume 3: Wrought Alloys, AFS/Skanaluminum, Des Plaines, IL, 1990.
120. M.C. Flemings, Metall. Metaer. Trans., 22A, (1991), pp. 957-981.
121. M.C. Flemings, R.G. Riek, and K.P. Young, Materials Science and Engineering, 25, (1976), pp. 103-117.
122. M. Garat, S. Blais, C. Pluchon, W.R. Loué, Proceedings 5th International Conference on Semi-Solid Processing of Alloys and Composites, (Eds Bhasin, A.K., Moore, J.J., Young, K.P., and Midson, S., Golden, Colorado, June 23-25), 1998, pp.xvii-xxxi.
123. Q. Han, and J.D. Hunt, Journal of Crystal Growth, 140, (1994), pp.398-405.

124. Q. Han, and J.D. Hunt, Special edition of the Japanese Journal of Metals, ISIJ International, 35, (1995), pp.221-227.
125. D.H. Kirkwood, International Materials Reviews, 39, (5), (1994), pp.173-189.
126. R. Sebus, and G. Henneberger, Proccedings 5th International Conference on Semi-Solid Processing of Alloys and Composites, (Eds Bhasin, A.K., Moore, J.J., Young, K.P., and Midson, S., Golden, Colorado, June 23-25), 1998, pp. 481-487.
127. D.B. Spencer, R. Mehrabian, and M.C. Flemings, Metall. Trans., 3, (1972), pp.1925-1932.
128. B. Wolfe, Madison-Kipp, Private communication, 2000.
129. Saha, Deepak; Apelian, Diran; Musser, Mark A.; Killingsworth, Dayne; Brown, Zach. Semisolid casting process of Al-Si alloys with a TiB grain refiner. PCT Int. Appl. (2004), 18 pp.
130. Q. Y. Pan, et al, AFS Transactions, AFS, (2004), Paper 04-053(2).
131. X. Jian, H. Xu, T. Meek, Q. Han, "Effect of Power Ultrasound on Solidification of Aluminum A356 Alloy", Materials Letters, 2005; 59 (2-3):190.
132. X. Jian, C. Xu, T. Meek, Q. Han. "The Effect of Ultrasonic Vibration on the Solidification Structure of A356 Alloy", AFS Transaction 2005; article 05-085.
133. O. V. Abramov, Action of high intensity ultrasound on solidifying metal, Ultrasonics 1987: 25(2), 73-82.
134. G. Brodova, P. S. Popel and G. I. Eskin, Liquid Metal Processing (Taylor & Francis Inc, New York, 2002).
135. V. O. Abramov, O. V. Abramov, F. Sommer, D. Orlov, Properties of Al-Pb base alloys applying electromagnetic forces and ultrasonic vibration during casting, Materials Letters, 1995: 23 (1-3), 17-20.
136. G. I. Eskin, Broad prospects for commercial application of the ultrasonic (cavitation) melt treatment of light alloys, Ultrasonics Sonochemistry 2001: 8(3), 319-325.
137. G. I. Eskin and D. G. Eskin, Production of natural and synthesized aluminum-based composite materials with the aid of ultrasonic (cavitation) treatment of the melt, Ultrasonics Sonochemistry 2003: 10 (4-5), 297-301.

138. G. I. Eskin, Influence of cavitation treatment of melts on the processes of nucleation and growth of crystals during solidification of ingots and castings from light alloys, Ultrasonics Sonochemistry 1994: 1 (1), S59-63.
139. V. Abramov, O. Abramov, V. Bulgakov, F. Sommer, Solidification of aluminium alloys under ultrasonic irradiation using water-cooled resonator, Materials Letters 1998: 37 (1-2), 27-34.
140. E. D. Manson-Whitton, I. C. Stone, J. R. Jones, P. S. Grant, and B. Cantor, "Isothermal Grain Coarsening of Spray Formed Alloys in the Semi-Solid State," *Acta Materialia* 50, no. 10 (June 2002): 2517–2535.
141. D. Brabazon, D. J. Browne, and A. J. Carr, "Mechanical Stir Casting of Aluminium Alloys from the Mushy State: Process, Microstructure, and Mechanical Properties," *Materials Science and Engineering A* 326, no. 2 (2002): 370–381.
142. Weimin Mao, Yanjun Li, Aimin Zhao, and Xueyou Zhong, "The Formation Mechanism of Non-dendritic Primary α-Al Phase in Semi-Solid AlSi7Mg Alloy," *Science and Technology of Advanced Materials* 2, no. 1 (March 2001): 97–99.
143. Sigworth, G. K., "Theoretical and Practical Aspects of the Modification of Al-Si Alloys", AFS Transactions, 91(1983), 7-15.
144. Laslaz G., "Macrostructure in hypoeutectic Al-Si alloys, dendrites and eutectic grains. Its effects on shrinkage behavior", Fourth international conference on molten aluminum processing, Orland, Florida, Nov 1995, 459-480.
145. Gruzleski J E, Closet BM. The treatment of liquid aluminum-silicon alloys. Desplaines: American Foundrymen's Society, Inc; 1990. p. 17.
146. Lu SZ, Hellawell A. Journal of Crystal Growth 1985; 73: 316-328.
147. Hanna MD, Lu SZ, Hellawell A. Metall Trans A1984; 15A:459.
148. Heiberg G, Nogita K, Dahle AK, Arnberg L. Acta Materialia 2002; 50:2537.
149. Nogita K, Dahle AK. Scripta Materialia 2003; 48:307.
150. Jenkinson DC, Hogan LM. Journal of Crystal Growth 1975; 28: 171.
151. Dahle AK, et al. Metall Mater Trans A 2001; 32:949.
152. Nogita K., et al. Mater Trans 2001; 42:1981.
153. Lu SZ, Hellawell A. Metall Trans A1987; 18A:1721.

154. Jie W, Chen Z, Reif W, Muller K. Met Mat Trans A 2003; 34A:799.
155. Han Q, Viswanathan S. Materials Science and Engineering A 2004; 364(1 – 2):48.
156. Nogita K, Dahle AK. Materials characterization 2001; 46:305.
157. Lou,A., Renaud, J., Nakatsugawa, I., and Plourde, J., 1995, JOM, 47, 28.
158. Brent Haight, "Advanced Technologies are opening doors for new materials," Automotive Industries, 2003, 4.
159. Achenbach K, Nipper HA, Piwowarsky E. Giesserei 1939; 26:597-621.
160. Emley EF. Principles of magnesium technology. Oxford: Pergamon Press; 1966. p 200-3, 231.
161. P. Cao, Ma Qian, D. StJohn, Effect of iron on grain refinement of high-purity Mg-Al alloys, Scripta Materialia, 2004, 51, 125-129.
162. Qinglin Jin, et al. Grain refining mechanism of a carbon addition method in a Mg-Al magnesium alloy, Scripta Materialia, 2003: 49, 1129-1132.
163. Cao, Peng; Qian, Ma; St. John, David. Grain refinement of commercial purity Mg-9% Al alloys by superheating. Magnesium Technology 2005, Proceedings of the Symposium held during the TMS Annual Meeting, San Francisco, CA, United States, Feb. 13-17, 2005 (2005), 297-302.
164. Motegi, Tetsuichi; Yano, Eiji; Tamura, Yosuke; Sato, Eiichiro. Clarification of grain refining mechanisms of superheat-treated Mg-Al-Zn alloy castings. Materials Science Forum (2000), 350-351(Magnesium Alloys 2000), 191-198.
165. Liu, Yanhui; Liu, Xiangfa; Bian, Xiufang, Grain refinement of Mg-Al alloys with Al4C3-SiC/Al master alloy, Materials Letters (2004), 58(7-8), 1282-1287.
166. E.F. Emley: Principles of Magnesium Technology, Pergamon Press, Oxford, United Kingdom, 1966, pp. 206-23.
167. Wood, Robert T. Grain refinement of magnesium castings, Foundry, 1953, 81(n 2), 98-99.
168. Feng Xue, Wenwen Du, Yangshan Sun; Microstructure Refinement of Magnesium Based Alloy, Materials Science Forum, 2005, vols 488-489, 143-146.

169. Peng Cao, David H. StJohn, Ma Qian; The Effect of Manganese on the Grain Size of Commercial AZ31 Alloy, Materials Science Forum, 2005, vols 488-489, 139-142.
170. Nelson CE. Trans AFS 1948, 56, 1.
171. S. Boily and M. Blouin: Canadian Patent 2,327,950, 2002.
172. N. Nishino, H. Kawahara, Y. Shimizu, and H. Iwahori: in Magnesium Alloys and Their Applications, K.U. Kainer, ed., Wiley-VCH, New York, NY, 2000, pp. 59-64.
173. Y.C. LEE, A.K. DAHLE, and D.H. StJOHN, The Role of Solute in Grain Refinement of Magnesium, Metallurgical And Materials Transactions A, 2000, vol 31 (11), 2895-2906.
174. Peng Cao, Ma Qian, David H. StJohn, Native grain refinement of magnesium alloys, Scripta Materialia 53 (2005), 841–844.
175. Wallace, J. F.; Schwam, D.; Zhu, Y., The influence of potential grain refiners on magnesium foundry alloys, Transactions of the American Foundry Society (2003), 111, 1061-1075.
176. DAVID H. StJOHN, Grain Refinement of Magnesium Alloys, Metallurgical And Materials Transactions A, 2005, vol 36 (7), 1669-1679.
177. Q. Han, B. Kad, S. Viswanathan, Design perspectives for creep-resistant magnesium die-casting alloys, Philosophical Magazine, 2004, 84 (36), 3843-3860.
178. E. Payzant, S. Agnew, Q. Han, S. Viswanthan, Mg17Al12 Phase Precipitation in Die Casting Alloys AZ91D and AM60B, Magnesium Technology 2001, edited by J. Hryn, TMS, 183-187.
179. Q. Han, E. Kenik, S. Agnew, and S. Viswanathan, Solidification Behavior of Commerical Magnesium Alloys, Magnesium Technology 2001, Edited by J. Hryn, TMS, 2001.
180. I. I. Teumin, High-Power Ultrasonic Generators (in Russian), Nauka, Moscow, 1967, p207.
181. J. J. Connor, C. A. Brebbia, Finite Element Techniques for Fluid Flow, Newnes-Butterworth, London-Boston (1977).

182. A.E. Crawford, Industrial Ultrasonics, Loughborough University of Technology, 1969, 1.
183. E. A. Neppiras, Acustica, 1963, 5(13), 368-370.
184. E. A. Neppiras, Ultrasonics International Conference Proceedings, 1977, 96.
185. E. A, Neppiras, Ultrasonic measurements in liquids. Ultrasonics (1965), 3, 201-2.
186. Neppiras, E. A.. Measurements in liquids at medium and high ultrasonic intensities. Ultrasonics (1965), 3, 9-17.
187. A.E. Kolesnikov, Ultrasonic Measurements, Izd. Standartov, Moscow, 1970.
188. S. P. Alekseev, A. M. Kazakov, and N. N. Kolotilov, Noice and Vibration Measurements in Mechanical Engineering, Mashinostroenie, Moscow, 1970.
189. L.O. Makarov, Acoustic Measurements in Ultrasoinc Technology, Mashinoenie, Moscow, 1983.
190. J. Rayleigh and Lord, Theory of Sound, MacMillan & Co., London, 1. 252 et seq, 1926.
191. J. Weber, R. Stefens, Absorption in Liquids, in Ultrasonics in Quantum and Solid-State Physics, Mir, Moscow, 1970, 75.
192. R. Truel, C. Elbaum, B. Chick, Ultrasonics in Solid-State Physics, Mir, Moscow, 1972.

Appendices

Appendix A

Ultrasonic Processing System

A.1 Ultrasonic vibration unit

The requirement for processing materials has need of high intensity with a specified frequency ultrasonic system. Such a system is often comprised of a power supply (energy source), a transducer (also called converter, electroacoustical or mechanoacoustical), an acoustic horn (other names: waveguide, booster or resonator set), a replaceable tip or extender. The processed materials form the load of the system.

Power supplies

The power supplies are often connected with specific converters. Motor-driven, vacuum tube and solid-state generators are power supplies often employed to produce high frequency ultrasound. Most industrial processes use low frequency (up to 50 KHz) ultrasound, ranging from 0.025~25KW.

Motor-driven generator consists of an AC motor and an AC generator. It has the advantages of high efficiency, reliability and easy maintenance and disadvantage of hard to maintain the working frequency. Vacuum tube and solid-state generators have the virtue of independent excitation or self-excitation, electrical or acoustic automatic frequency control and output stabilization.

Transducers

Mechanoacoustical converters include gas dynamic converters, sirens (dynamic/rotary and pulsating) and hydrodynamic converters.

Electroacoustical converters can be broken down into magnetostriction and piezoelectric. The magnetostriction converter owes its life to the behavior of magnetostrictive materials in an alternating magnetic field. Today piezoelectric converters are more often used in industry.

Acoustic horn

The use of an acoustic horn/waveguide/booster is to provide a connection between the transducer and the load, pass vibration parameters and match the mechanical impedances of the load and the transducer. Certain requirements should be met for a horn to successfully pass a specific type of ultrasound wave. For the case of longitudinal wave, the diameter of a uniform-section waveguide should satisfy [180]:

$$0.05 < \frac{d}{\lambda} < 0.5 \quad \text{Equation A.1}$$

When a round or rectangular waveguide's acoustic parameters, like E, ρ and cross-section, are constants along the length, it is called a homogeneous waveguide. Otherwise it becomes an inhomogeneous waveguide. The booster is a familiar inhomogeneous waveguide of which shape changes along the length. Owing its special designed shape, a booster can serve as matching transducer and load, or amplifying the oscillation displacement and speed, while keeping the wave type and intensity. Boosters are often characterized by an amplification factor k_y, conversion factor k_c, mismatch factor k, area coefficient N, form factor φ, which are given by the following equations [181-184]:

$$k_y = \frac{\xi_1}{\xi_0} = \frac{v_1}{v_0} = \frac{\sigma_1}{\sigma_0}; \quad k_c = \frac{S_0}{S_l}; \quad k = \frac{R_{in} S_l}{R_{out} S_0}; \quad k_y = \sqrt{k_c} = \sqrt{\frac{S_0}{S_l}} \quad \text{Equation A.2}$$

$$N = \sqrt{\frac{S_0}{S_l}} \quad \text{Equation A.3}$$

$$\varphi = \frac{1}{c} \frac{v_m}{\in_m} \quad \text{Equation A.4}$$

Here the subscripts 0 and l denote the head and the end of the booster. Technologically the mismatch factor k ranges from 10 to 15. For most waveguides the form factor φ≈1.

In order to efficiently transmit ultrasound into the melt with a certain vibration pressure and velocity, the horn should satisfy requirements of 1) a common shape, like conical, exponential, catenoidal, stepped and Gaussian; 2) the length of 1, 2 or 3 half-wave (to match the converter load).

A.2 Measurement of acoustic parameters

Reliable measurement of acoustic parameters is beneficial to the application of ultrasonic system to a load of high temperature, chemical caustic, non linear or time dependent. The metrological problems can fall into three groups [185 -189].

Energy exchange efficiency from the converter to the horn

Many electronic wattmeters can serve for the measurement. The efficiency of magnetostrictive transducers can be obtained from the converter's frequency dependence to the load or the circular diagrams of input resistance. The measured efficiency may be applied to estimate the acoustic intensity in the horn.

Parameters for ultrasound transmitted to the horn

Such parameters include the amplitude, velocity, acceleration, strain and the wave distribution in the horn. Those parameters can be obtained by contact measurements or noncontact measurements. In contact measurements the sensor is connected to the vibrating unit(s). Several traditional vibrometric methods belong to this category. In order to have acceptable accuracy the sensor should be comparatively small and sequentially light weight. The noncontact measurements of vibrational velocity and amplitude include light sensors (light microscope, laser interferometers, holographic interferometry, fiber optics), electromagnetic sensors and electrodynamic sensors.

Parameters for ultrasound transferred to the load

The estimation of acoustic power pass to the load can be obtained by

$$Na = \frac{1}{2}\xi_e^2\omega^2 R_1$$ .... Equation A.5

Where ξ_e is the amplitude, ω is the frequency, R_1 is the radius of the resonator, *Na* is the ultrasonic intensity in the horn. Suppose there is no loss in the horn.

When ultrasound is applied to a load, the acoustic parameters vary with the state of the load (such as solid, liquid and gas), so different sensors are used in different loads. Hydrophones are often used in liquid media, whereas electrostatic, electrodynamic receivers or piezoelectric microphones in gaseous media, and load cell in solid.

A.3 Elastic wave and ultrasound

The classification of elastic wave

The main principles of classical acoustics were established by Galilei, Mersenne, Euler, Weber and Helmholtz. *Theory of Sound* written by Rayleigh established classical acoustics [190]. According to basic acoustic literature, the wave can break down into two types: mechanical wave and electromagnetic wave. Mechanical wave is the repetitive alterations of position and velocity of a body or its parts. When mechanical wave propagates in elastic medium, it becomes elastic wave. Ultrasound belongs to the category of elastic wave. It can be seen from Table A.1.

Basic parameters of ultrasound

Physically, elastic waves are common in nature, no matter what frequency they are. When propagating through a medium, the ultrasonic characteristics depend on the vibration parameters and properties of the medium. For instance, at a given temperature, the velocity of ultrasonic longitudinal wave in a solid is governed by:

$$c = \sqrt{\frac{E(1-\mu)}{\rho(1+\mu)(1-2\mu)}} \quad \text{Equation A.6}$$

Where E is young's modulus; μ, Poisson's ratio; ρ, solid density.

Table A.1: Classification of elastic wave

Name		Frequency, Hz	Typical wavelength, inches	
			In water	In steel
Infrasound		0 ~ 16	0.292×10^{3}	1.15×10^{3}
Audio sound (Sonic)		16 Hz ~ 16 K	0.584×10^{2}	2.3×10^{3}
Ultrasound	Common UPM*	16 K ~ 1 M	0.292×10^{1}	1.15×10^{1}
	Common NDT*	1M~ 20 M	0.584×10^{-2}	2.3×10^{-2}
Hypersound or microwave		10G ~	0.584×10^{-6}	2.3×10^{-6}
Crystal lattice vibrations		> 1000G	0.584×10^{-8}	2.3×10^{-8}

*UPM: Ultrasonic processing of materials

*NDT: Nondestructive Testing

When in a liquid, where elastic properties depend upon compression, the wave speed becomes:

$$c = \sqrt{\frac{1}{\beta_{ad}\rho}} \quad \text{Equation A.7}$$

Where β_{ad} is adiabatic compressibility; ρ, liquid density.

For gas, the wave speed is:

$$c = \sqrt{\frac{\gamma P_o}{\rho}} \quad \text{Equation A.8}$$

Where βad is adiabatic compressibility; ρ, gas density.

Often the ultrasonic wave is described by the form of a harmonic wave,

$$A = A_0 \sin(\omega t - \omega x / c) \quad \text{Equation A.9}$$

Where ω=2πf is the cycle frequency and x/c is the phase factor.

And respective magnitudes of the vibrating velocity (v), acceleration (j), sound pressure (P_A), and intensity (I) will be given by:

$$v = A\omega,\ j = -A\omega^2,\ P_A = \rho c A\omega,\ I = \frac{1}{2}\rho c (A\omega)^2 \quad \text{Equation A.10}$$

Acoustic calculations usually use relative levels of sound energy, intensity, and pressure expressed in decibels (dB). That is, use a logarithmic scale.

Relative energy

$$L_W = 10\log\frac{W}{W_0} \quad \text{Equation A.11}$$

Relative intensity

$$L_I = 10\log\frac{I}{I_0} \quad \text{Equation A.12}$$

Relative pressure

$$L_P = 10\log(\frac{P}{P_0})^2 = 20\log\frac{P}{P_0} \quad \text{Equation A.13}$$

Another often used unit for sound intensity is Napiers (Np), its relationship with decibel is:

$$1Np = 8.686dB \quad \text{Equation A.14}$$

Table A.2 and Table A.3 show the characteristic intensities of various sonic sources and acoustic parameters, including velocity and acoustic resistance/acoustic impedance, or the product of density (p) and acoustic velocity (V) of that material.

Table A.2: Sounds and their intensity

Various sonic or ultrasonic	Typical intensity / [W/m^2]	Intensity level [dB]	# times greater than Threshold of Hearing
Threshold of Hearing (TOH)	1×10^{-12}	0	10^0
Whisper	1×10^{-10}	20	10^2
Normal Conversation	1×10^{-6}	60	10^6
Chamber-music orchestra	1.6×10^{-2}	100	10^6
Front Rows of Rock Concert	1×10^{-1}	110	10^{11}
Airplane	1.0	120	10^6
Threshold of Pain	1×10^1	130	10^{13}
Instant Perforation of Eardrum	1×10^4	160	10^{16}
Low-intensity ultrasound	1×10^4	160	No feeling/10^{16}
Middle-intensity ultrasound	1×10^5	170	No feeling/10^{17}
High-intensity ultrasound	1×10^6	180	No feeling/10^{18}

Table A.3: Acoustic impedance of some materials

Material	Longitudinal Velocity(m/s)	Shear Velocity (m/s)	Density g/cm^3	Acoustic Impedance g/cm^2-sec x10^5
Aluminum	6320	3130	2.70	17.10
Iron, Cast	4800	2400	7.80	37.44
Molybdenum	6290	3350	10.2	64.16
Steel, 4340	5850	1280	7.80	45.63
Titanium	6070	3310	4.50	27.32
Titanium Carbide	8270	5160	5.15	42.59
Alumina	9810	*N/A*	2.60	25.5
Glass Quartz	5570	3430	2.60	14.5
Silica (fused)	5960	*N/A*	2.20	13.1
Water (20° C)	1480	*N/A*	1.00	1.483
Nitrogen (20° C)	350	*N/A*	1.16 x 10^{-3}	.000406
Oxygen (20° C)	328	*N/A*	1.32 x 10^{-3}	.000433
PZT-5A	4350	*N/A*	7.75	33.7

Provided that there is identical external force, systems with greater impedance will vibrate at a slower rate than those with smaller impedance. The calculation of acoustic impedance and its value in some typical materials are shown below.

$$Z = \rho c \quad \text{.....Equation A.15}$$

Acoustic impedance is important in:

1) The determination of acoustic transmission and reflection at the boundary of two materials having different acoustic impedance
2) The design of ultrasonic transducers.
3) Assessing absorption of sound in a medium.

Ultrasonic waves are reflected at boundaries where there are differences in acoustic impedance, Z. This is commonly referred to as impedance mismatch. The fraction of the incident-wave intensity in reflected waves can be derived because particle velocity and local particle pressures are required to be continuous across the boundary between materials. Formulation for acoustic reflection and transmission coefficients (pressure) are shown below.

$$R = \left[\frac{Z_2 - Z_1}{Z_2 + Z_1}\right]^2 \text{, T=1-R.....Equation A.16}$$

Note that Transmitted Sound Energy + Reflected Sound Energy = 1

If being loaded, the vibrating system generates both standing and traveling waves. A coefficient named the traveling wave ratio describes their relative amplitudes. In melts, emission of standing waves usually is neglectable, and the transducer face emits mainly traveling waves toward the melts.

Attenuation of Sound Waves [191, 192]

It is well known that sound energy decreases with distance traveled. Attenuation is the decrease of sound intensity with distance. In natural materials, the combined effect of scattering and absorption on ultrasound is attenuation. Natural properties and loading conditions can be related to attenuation. Attenuation often serves as a measurement tool that leads to the formation of theories to explain physical or chemical phenomenon.

Ultrasonic attenuation is the decay rate of mechanical radiation at ultrasonic frequency as it propagates through material. A decaying plane wave is expressed as:

$$A = A_0 e^{-ax} e^{i(\omega \cdot x - kx)} ; I = I_0 e^{-2ax} e^{i(\omega \cdot x - kx)}$$ .....…..…Equation A.17

Where a is the attenuation of the wave, z is the traveling direction, $k = 2\pi/\lambda$, λ is the wavelength; ω is the wave's angular frequency.

The absorption of ultrasound is controlled by viscosity, thermal conductivity, and so on. The attenuation comes from liquid viscosity can be obtained by

$$a_f = \frac{\omega^2}{2\rho_0 c_0^3}(\frac{4}{3}\eta + \eta')$$ ….....….....….. ..…Equation A.18

And from heat conduction:

$$a_T = \frac{\omega^2}{2\rho_0 c_0^3}\kappa_t(\frac{1}{c_v} - \frac{1}{c_p}')$$ …..... .....….. ..…Equation A.19

Appendix B

Grain Refinement of 4340 Steel

Steel alloy 4340 was melted in an induction furnace, and poured into a graphite mold with 20 kHz acoustic energy applied onto the outside surface of the mold. Acoustic energy was applied for 120 s. The melt was then allowed to cool very quickly. Results show a significant difference between the conventionally processed specimens and those to which acoustic energy was applied. Fully developed dendrites were developed on the specimen without ultrasonic processing, while fine globular grains were obtained on the specimens ultrasonically processed at both temperatures. The result shown here indicates that if applied in the steel industry, this technology will lead to a considerable energy saving during the subsequent heat treating operations of these fine grained materials. This is because it will take much shorter time and lower temperature to heat treat the fine grained steels.

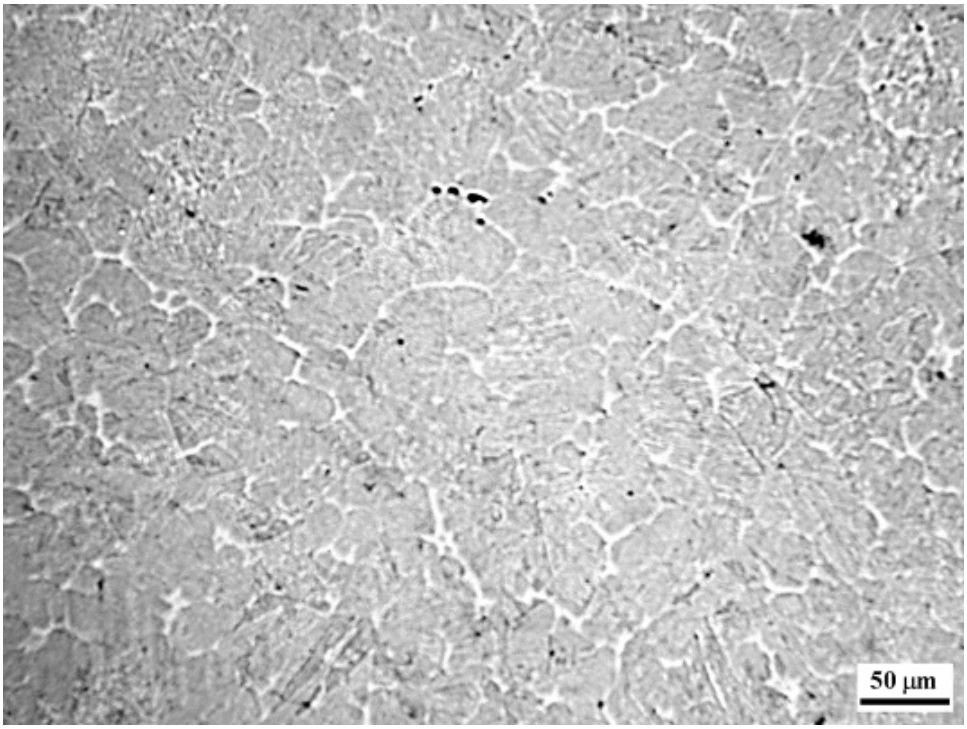

Figure B.1: Microstructure of 4340 steel without ultrasonic vibration casting temperature, 1525°C. Fully developed dendrites were observed on the specimen.

(a)

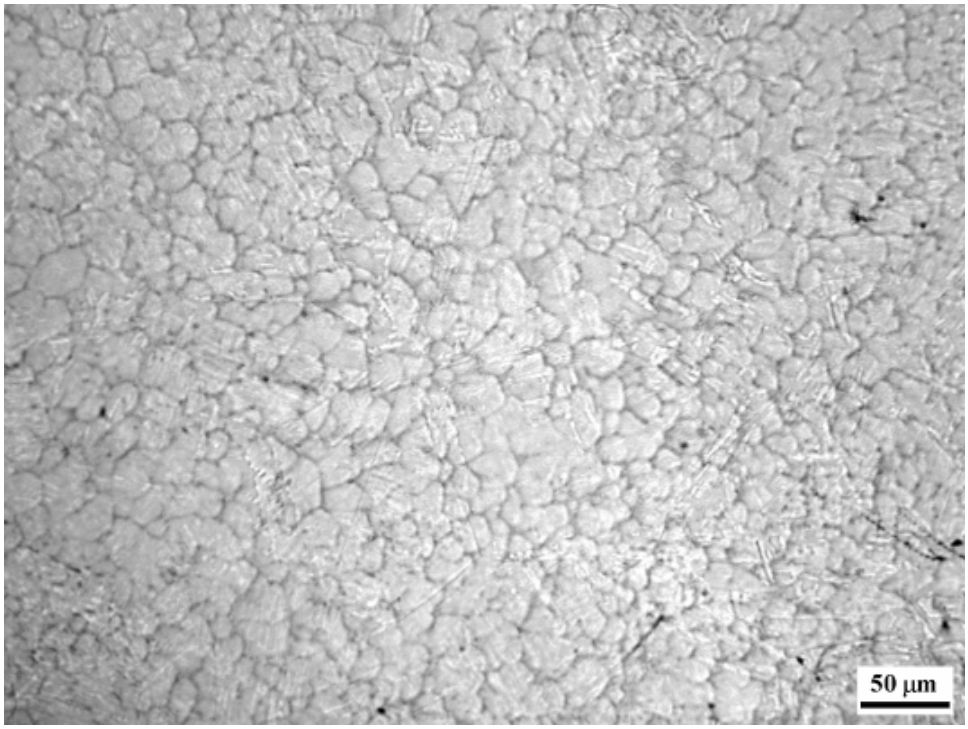

(b)

Figure B.2: Microstructure of 4340 steel with 100% ultrasonic amplitude and 120 second exposure time (a) Casting temperature 1548°C (b) Casting temperature 1516°C. Fine globular grains were obtained in both castings.

Appendix C

Grain Refinement of Bismuth-Tin Alloy Using High Frequency Ultrasonic Vibration

A bismuth/tin alloy specimen was melted at 150°C. During the solidification process, ultrasonic vibration of 400 kHz was introduced into the top of the melt for 20 s. The results are shown in Figure C.1. A comparison between photos (a) and (b) of the figure shows that ultrasonic vibration produced finer grains. Figure C.2 also shows that the grain size increases with the increase of distance from the ultrasonic radiator.

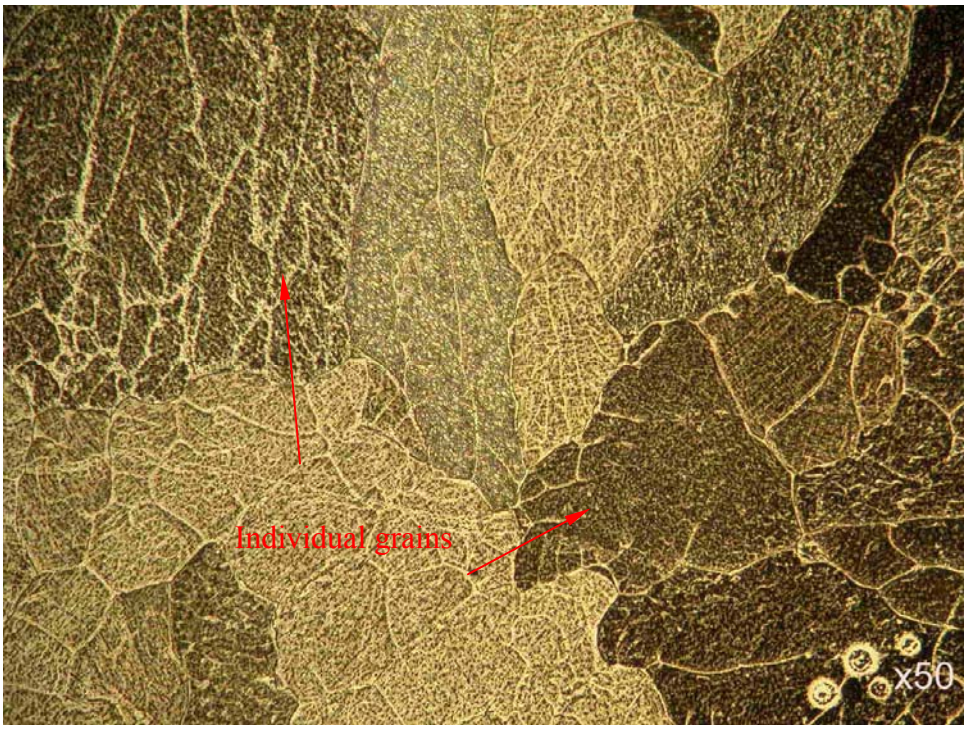

Figure C.1: Microstructure of bismuth/tin alloy without ultrasonic vibration. Fully developed dendrites were observed on the specimen.

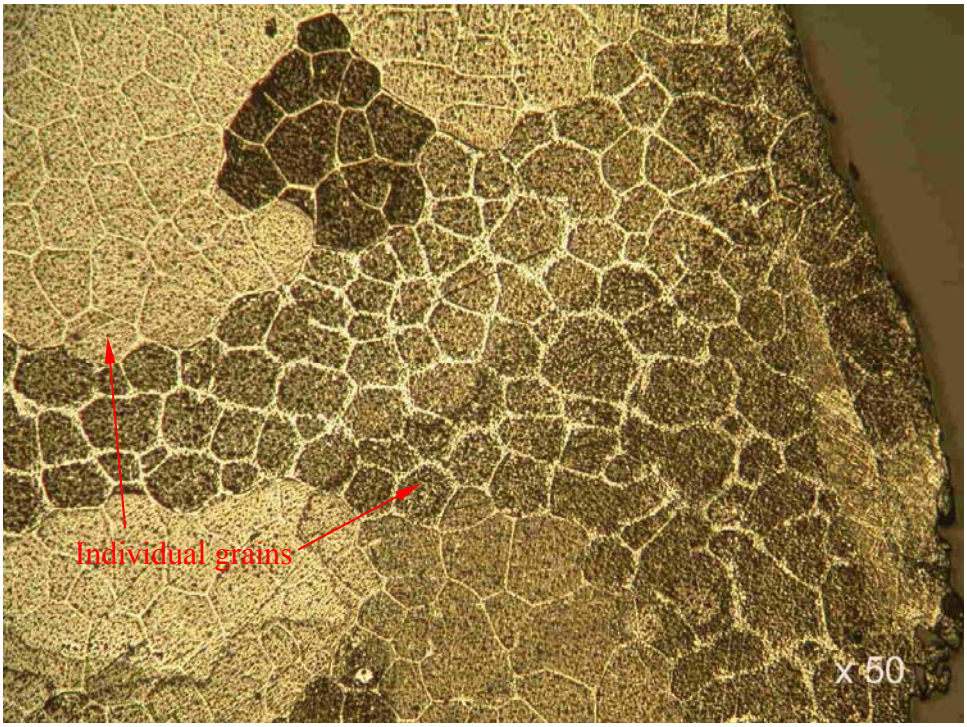

Figure C.2: Microstructure of bismuth/tin alloy with 400-kHz vibration and varying ultrasonic amplitude. It is clearly seen that grain refinement was obtained upon high frequency ultrasonic processing.

Vita

Xiaogang Jian was born in Xinyu, the People's Republic of China on June 10, 1973. For the next eighteen years he attended Tongchun Elementary School, Fushan Middle School, and No. 1 Xinyu High School. He entered Nanchang University in the fall of 1992 and began work on his undergraduate degree in Chemical Engineering. After struggling with the financial difficulties, he completed his undergraduate degree in the summer of 1996 graduating with honors. In the fall of 1996, he entered the graduate school of the Institute of Metal Research, the Chinese Academy of Sciences after a success in the National Graduate Entrance Examination. He changed his major to Material Sciences and Engineering when pursuing his Master Degree. After two and a half years successful study and research entitled "The effect of magnetic field on the friction and wear of ferromagnetic materials," he earned his master's degree in the spring of 1999. Then he adventured his life in Shanghai, the biggest city in south-eastern China till the call from the University of Tennessee, Knoxville for a higher level study. At the last day of 2001 he came to the United States and began the pursuit of a Ph.D. degree in the university. He did most of the research at Oak Ridge National Laboratory. He graduated from the University of Tennessee with a Ph.D. in Materials Science and Engineering in December of 2005.

Xiaogang Jian's work during Ph.D. study

PATENT APPLICATIONS (With ORNL)

- Method and Apparatus for Semi-Solid Material Processing
- Method of Producing Nanostructured Metals Using High-Intensity Ultrasonic Vibration
- Production of Functional Gradient Materials (FGMS) Using Ultrasonic Vibration
- Ultrasonically Assisted Bonding between Reinforcement and Casting Using the Cast-In Method
- Localized Grain Refinement Using Ultrasonic Vibration

JOURNAL AND PROCEEDING ARTICLES

1. X. Jian, Q. Han, T. Meek, Eutectic Modification of Aluminum A356 Alloy by Ultrasonic Vibration, Scripta Materialia (accepted)
2. X. Jian, T. Meek, T. Geer, Q. Han, Grain Refinement of Magnesium AM60B Alloy Using Ultrasonic Vibration, Magnesium Technology 2006
3. X. Jian, T. Meek, Q. Han, The Refinement of As-Cast Microstructure of Aluminum 319 Alloy by High Intensity Ultrasonic Vibration, TMS Annual Meeting 2006
4. X. Jian, C. Xu, T. Meek, Q. Han, The Effect of Ultrasonic Vibration on the Solidification Structure of A356 Alloy, AFS Transaction 2005, paper 05-085
5. X. Jian, H. Xu, T.T. Meek and Q. Han, Effect of power ultrasound on solidification of aluminum A356 alloy, Materials Letters, Volume 59, Issues 2-3, February 2005, Pages 190-193
6. X. Jian, H. Xu, T.T. Meek, Q. Han, S. Viswanathan; Solidification Of Aluminum Alloy A356 Under Ultrasonic Vibration; Solidification of Aluminum alloys, Edited by M.G. Chu, D.A. Granger and Q. Han; TMS (The Minerals, Metals & Materials Society), 2004 3, Pages 73-79
7. X. Jian, Q. Han, T. Meek, Mechanism of the Formation of Globular Grains by Ultrasonic Vibration, in submitting
8. X. Jian, S. Zhang, Q. Han, T. Meek, Thermal Analysis of Ultrasonic Processing of Aluminum A356, in submitting
9. X. Jian, Q. Han, T. Meek, Microstructure Modification of Magnesium AM60B Alloy Using High-Intensity Ultrasonic Vibration, submitted to Acta Materialia
10. X. Jian, T. Meek, Q. Han, Formation of Superfine Globular Grains in the Aluminum A356 Alloy by Ultrasonic Processing, in preparation
11. Hanbing Xu, Xiaogang Jian, Thomas T. Meek, and Qingyou Han, Degassing of molten aluminum A356 alloy using ultrasonic vibration, Materials Letters, Volume 58, Issue 29, November 2004, Pages 3669-3673
12. H. Xu, X. Jian, T.T. Meek and Q. Han, Ultrasonic Degassing In Aluminum A356 Alloy, LiMAT-2003, Edited by W. E. Frazier, Y. D. Han, N. J. Kim, and E. W. Lee, Center for Advanced Aerospace Materials, POSTECH, 2004, Pages 456 – 464
13. H. Xu, X. Jian, T.T. Meek and Q. Han, Investigation of Ultrasonic Degassing in Molten Aluminum A356 Alloy, Light Metals 2004, Edited by Alton T. Tabereaux, Pages 731-735
14. X. Jian, H. Xu, T.T. Meek, Q. Han; Ultrasonic Solidification of Aluminum Alloy A356; Presented in LiMat 2003, November 2003, Hawaii